Gerson Shigeru Kobayashi

Investigação da etiologia de malformações craniofaciais com uso de células derivadas de crista neural

Investigating craniofacial malformations with the use of neural crest-derived cell models

São Paulo

2016

Gerson Shigeru Kobayashi

Investigação da etiologia de malformações craniofaciais com uso de células derivadas de crista neural

Investigating craniofacial malformations with the use of neural crest-derived cell models

Tese apresentada ao Instituto de Biociências da Universidade de São Paulo, para a obtenção de Título de Doutor em Ciências, na Área de Biologia/Genética.

Orientadora: Maria Rita dos Santos e Passos-Bueno

São Paulo

2016

Ficha Catalográfica

Kobayashi, Gerson

Investigação da etiologia de malformações craniofaciais com uso de células derivadas de crista neural

169 páginas

Tese (Doutorado) - Instituto de Biociências da Universidade de São Paulo. Departamento de Genética e Biologia Evolutiva.

1. Modelagem *in vitro* 2. Crista neural 3. Célula-tronco I. Universidade de São Paulo. Instituto de Biociências. Departamento de Genética e Biologia Evolutiva.

Comissão Julgadora:

Prof(a). Dr(a)._____ Prof(a). Dr(a)._____

Prof(a). Dr(a)._____ Prof(a). Dr(a)._____

Profa. Dra. Maria Rita dos Santos e Passos-Bueno

Orientadora

Agradecimentos

Agradeço primeiramente à minha orientadora, Rita, por toda a preocupação com nossa formação e bem-estar, por estimular um ambiente de colaboração entre os alunos do laboratório e de fora, e por estar sempre presente. Agradeço também pela grande confiança depositada em mim durante este período de doutorado. Também agradeço a todos os coautores dos trabalhos expostos nesta tese, em especial aos integrantes do nosso grupo - Lucas, Felipe, Camila Musso, Robs, Karina, e Jéssica (Andressa) – e de outros laboratórios (Ernesto e Luiz, Leonardo).

Expresso grande gratidão também pelos membros de nosso laboratório, que, apesar da bagunça e barulho, propiciam um ambiente amigável e agradável para trabalhar. Obrigado especialmente à May, Danielle (Criatura), Luciano, Naila, Simone, Jéssica, Meire, Suzaninha. Agradeço aos Professores, colaboradores ou não, e seus alunos; especialmente ao pessoal do Keith, Mayana, Mariz, Luis Netto e Menck. Agradeço ao pessoal da secretaria de pós-graduação e da Genética, além da Vanessa Sato, Wagner, ao pessoal do serviço - que aguenta a nossa desorganização, e aos funcionários do Genoma – que aguentam a nossa bagunça.

Por fim, agradeço aos companheiros Andrews, Camila, Heman, Elaine, Fábio, Joice, Atique, Carol, Maneco, Mel, e especialmente ao Chuchu, que me apoiou bastante nos momentos difíceis. Obrigado também ao meu irmão Mauro, meus familiares, e aos pacientes, sem os quais não poderíamos realizar este trabalho.

Este doutorado contou com auxílio da CNPq, FAPESP/CEPID, MCT e CAPES.

Preface

This doctoral thesis includes three original works developed between 2011 and 2016 at the Laboratory of Developmental Genetics within the Human Genome and Stem Cell Research Center, Institute of Biosciences University of São Paulo, Brazil (*Centro de Estudos sobre o Genoma Humano e Células-Tronco, Instituto de Biociências, Universidade de São Paulo*).

The aforementioned works are presented as the core chapters of this thesis (chapters II – IV), and include one published journal article and two unpublished articles. These chapters are preceded by a general introduction (chapter I), and they are followed by the general discussion and conclusions (chapter V). Additional co-authored material was assigned to an appendix section comprising one review article, four journal articles, and one book chapter. These publications are not a direct result of the main work of this thesis, so they have been added as attachments without supplementary material.

Index

Chapter I

INTRODUCTION AND OBJECTIVES

1. Overview: craniofacial malformations

Craniofacial malformations (CFMs) comprise a large and heterogeneous group of disorders in which tissues of the skull and face are affected. These disorders are largely considered to arise from disturbances in craniofacial morphogenesis during embryonic development, and they collectively represent over one-third of all congenital birth defects, or 0.3% of all stillbirths. CFMs can affect different craniofacial components with or without association with other clinical manifestations, including intellectual disability, limb defects, and others. Therefore, CFMs can be part of a clinically distinguishable syndrome, or they may emerge isolated, as is often the case for cleft lip and palate (Gorlin et al., 2001).

The development of craniofacial skeletal and connective tissues is particularly affected in CFMs. Craniosynostoses, for example, are determined by premature ossification of cranial sutures, resulting in abnormal skull shape and facial features, cranial growth restriction and increased intracranial pressure (Gorlin, 2001; Governale, 2015). Other craniofacial components are also compromised in CFMs, such as in facial dysostoses, which may involve hypoplasia of maxillary, mandibular, and zygomatic bones, in addition to ear anomalies (Trainor & Andrews, 2013). In the orofacial region, embryonically adjacent structures may fail to fuse, resulting in orofacial clefts that frequently consist of a gap affecting bone, muscle, and other tissues (De Mey et al., 1989; Wijayaweera et al., 2000; Farronato et al., 2014). By affecting a large variety of craniofacial tissues, CFMs ensue significant functional impairment and morbidity to patients, which often suffer from airway obstruction, feeding difficulties, and other problems (Trainor & Andrews, 2013).

CFMs entail significant burden to patients and health care systems. Since not only facial appearance is changed but also craniofacial tissues can be functionally affected, patients with CFMs face important psychological outcomes and require extensive treatment

throughout several years of life. Functional rehabilitation and social integration of patients frequently involves diverse health professionals, such as otorhinolaryngologists, psychologists, surgeons, dentists, among others (Hamm & Robin, 2015). Considering these facts and the high incidence of CFMs, understanding the aetiology of these disorders is of great importance, as it may lead to the development or improvement of preventive and therapeutic strategies in the future.

2. Development of the face and head

2.1 The neural crest

Craniofacial development is a spatio-temporally coordinated multi-stage process that begins with the emergence of the cranial neural crest (CNC) cells. Neural crest cells are transient cell populations that originate along the neuraxis, at the interface between the neural plate and non-neural ectoderm in the dorsal side of the embryo, around the time of neurulation (The ectodermal cells in this region, in response to molecular cues majorly determined by WNT, FGF and BMP signalling, undergo transdifferentiation through epithelial-mesenchymal transition (EMT) and migrate to colonise several sites within the embryonic body (Gong, 2014). In the foremost portion of the neuraxis, CNC cells migrate from the forebrain, the midbrain and hindbrain regions to populate the mesenchyme of the developing craniofacial complex. CNC cells emigrating from the forebrain and rostral midbrain colonise the frontonasal region, while those arising from the caudal midbrain populate the first pharyngeal arch; CNC cells from the hindbrain region emigrating from rhombomeres 1-6 populate the first, second, and third pharyngeal arches (Gong, 2014; Trainor, 2014; Fig. 1A). After migration, the CNC cell-derived mesenchyme within these structures undergoes intense proliferation to give rise to the facial prominences. Ultimately, differentiation of CNC-derived mesenchymal cells contributes to a range of craniofacial structures and cells, such as cartilage, pericytes, teeth, and most of the cranioskeleton (Szabo-Rogers et al., 2010; Twigg & Wilkie, 2015; Choe et al., 2014; Moody, 2015; Fig. 1A).

2.2 Craniofacial CNC cell derivatives

The facial prominences are subject to finely orchestrated morphogenetic events in order to make up the human face. The first pharyngeal arch originates the maxillary and

mandibular prominences, which arise bilaterally and will constitute the upper and lower jaw tissues of the embryo. The maxillary prominences grow latero-medially and fuse with the frontonasal prominence-derived medial and lateral nasal prominences, constituting the upper lip region, maxilla, and primary palate (Fig. 1B). Likewise, inside the developing oral cavity, bilaterally arranged extensions of the maxillary prominences (called palatine shelves) must also undergo re-orientation, growth and fusion to originate the secondary palate (Fig. 1B'). The fusion events taking place during orofacial development are reliant upon EMT and apoptosis of the epithelial cells lining the facial prominences to establish a seamless and continuum mesenchyme. CNC-derived mesenchymal cells within the maxillary prominences differentiate to create the zygomatic, maxillary, and palatine bones; the mandibular prominences, also derived from the first pharyngeal arch, develop into the lower jaw portion of the head, constituting the mandible, lower lip, and parts of the tongue (Fig. 1A, B). Akin to the maxillary prominences, the mandibular prominences must grow latero-medially and fuse through EMT; however, this process occurs prior to fusion of all the other facial prominences. During mandible development, CNC-derived mesenchymal cells differentiate into the Meckel's cartilage, a transient structure that supports the lower jaw. As the mandibular prominences fuse, the distal ends of the Meckel's cartilage also fuse, forming the mandibular symphysis, which undergoes ossification only after birth. As CNC-derived mesenchymal cells undergo osteogenic differentiation, the Meckel's cartilage is replaced by bone tissue to originate the mandible. Finally, CNC-derived cells within the remaining pharyngeal arches contribute to internal ear elements and the hyoid bone (Gong, 2014; Moody, 2015)

The series of morphogenetic events leading to the full assembly of the craniofacial structures is particularly sensitive to perturbations. Hence, insults to migration, growth, differentiation and fusion of cells or tissues that compose the facial prominences generate a variety of defects, in accordance with the high incidence of CFMs. Remarkably, the majority of cellular constituents of tissues taking part in these processes are of neural crest origin, further evidencing the pivotal role of these cells in the aetiology of CFMs.

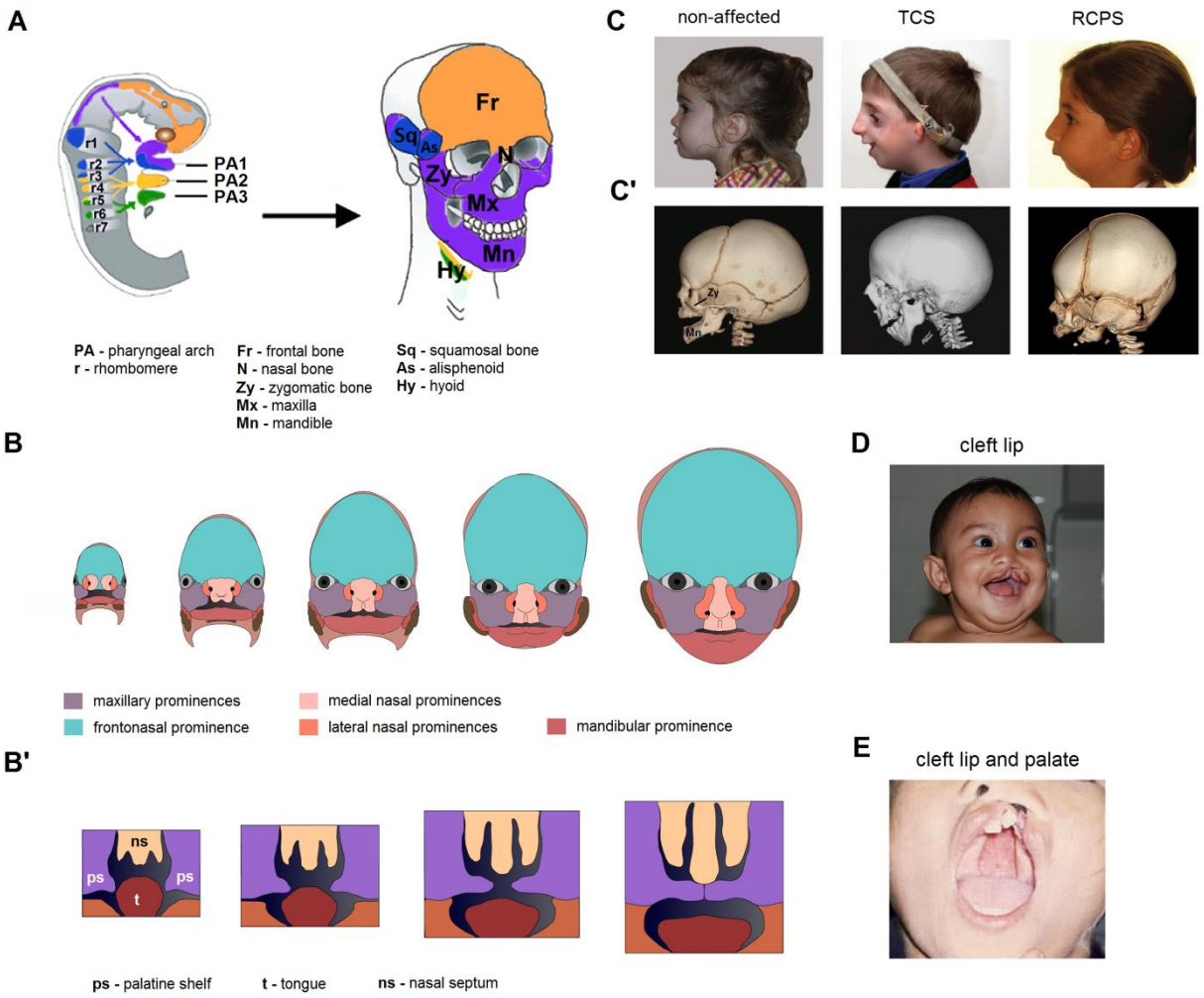

Figure 1: Craniofacial development and congenital malformations; **A)** Cranial neural crest migration streams and their skeletal fates; **B and B')** Orofacial development (left to right), showing **(B)** frontal view of the developing facial prominences during assembly of the maxillary (including upper lip) region, and **(B')** sagittal section of the developing secondary palate inside the oral cavity; **C and C')** Examples of craniofacial malformations and their respective cranioskeletal outcomes; subjects are shown in gross lateral view and lateral 3D computed tomography scans; **C)** Subjects affected by Treacher Collins syndrome (TCS) and Richieri-Costa-Pereira syndrome; **C')** Cranial CT scans; note zygomatic and mandibular bone hypoplasia (TCS), and mandibular agenesis (RCPS). The RCPS subjects in the CT scan and in the photograph are not the same; **D)** Subject with unilateral cleft lip; **E)** Subject with unilateral cleft lip and cleft palate. Modified from Gong, 2014; Clouthier et al., 2013; Raskin et al., 2013; Lehalle et al., 2015; Dixon et al., 2011; http://www.indiana.edu/~anat550/hnanim/face/face.html.

3. Aetiology of CFMs

As stated above, the underlying causes of congenital CFMs can be traced back to disturbances during embryonic craniofacial development. These disturbances are thought to be exerted by genetic or environmental factors, acting separately in different cases, or in conjunction. Examples of environmental causes include maternal alcohol intake, smoking and nutritional deficiencies, which have been associated with several congenital malformations, including foetal alcohol syndrome and cleft lip/palate (Krapels et al., 2006; Smith et al., 2014;

Sabbagh et al., 2015). Amongst genetic factors, chromosomal alterations and monogenic variants are usually implicated in craniofacial syndromes or isolated CFMs segregating in a Mendelian fashion, whilst the interplay between environmental factors and susceptibility variants in different *loci* has been associated with multifactorial CFMs, such as non-syndromic cleft lip/palate (Brito et al., 2012). Considering the myriad of disorders affecting craniofacial tissues, only three types of CFMs have been selected to illustrate different aetiological mechanisms behind CFMs; these disorders are further explored in the core chapters of this work, and are briefly described below:

3.1 Facial dysostoses: Richieri-Costa-Pereira syndrome and Treacher Collins syndrome

Facial dysostoses are a heterogeneous group of CFMs in which tissues derived from the first and second pharyngeal arches are compromised. They can be classified into mandibulofacial dysostoses, presenting with normal extremities, and acrofacial dysostoses, when limb anomalies manifest in addition to CFMs (Wieczorek, 2013). Both groups of disorders are thought to originate from disturbances in development of CNC cells or CNC cell-derived tissues.

Richieri-Costa-Pereira syndrome (RCPS) is a rare acrofacial dysostosis characterised by midline mandibular cleft, mandibular hypoplasia, Robin sequence (micrognathia, glossoptosis, and cleft palate), radial and tibial defects, among other clinical findings (Favaro et al., 2011; Fig. 1C). So far, RCPS has only been diagnosed in Brazilian families and one French subject. It is caused by repeat expansions in the 5'UTR of the gene *EIF4A3*, leading to loss of function of the encoded protein eIF4AIII (Favaro et al., 2014). This protein plays important roles in RNA metabolism, including nonsense mRNA decay, splicing and translation (Chan et al., 2004; Singh et al., 2013; Wang et al., 2014). Currently, it is unclear how eIF4AII loss of function affects CNC cell development, resulting in the clinical manifestations of RCPS.

The mandibulofacial dysostosis Treacher Collins syndrome (TCS) is another rare condition, present in 1:50,000 live births. The main clinical findings in TCS include underdevelopment of facial bones, particularly the zygomatic bones and the mandible, external ear anomalies and conductive hearing loss (Gorlin, 2001; Fig. 1C). Mutations in *TCOF1* are responsible for the majority of TCS cases (Splendore et al., 2000) and lead to haploinsufficiency of the protein treacle, which is known to participate in ribosome biogenesis (Gonzales et al., 2005). Studies in animal models have shown that insufficient ribosome

production leads to proliferative stress and apoptosis of pre-migratory CNC cells at the neuroepithelial region of the embryo, reducing the amount of CNC cells migrating into the pharyngeal arches (Dixon et al., 2006; Weiner et al., 2012); such deficit of CNC-derived mesenchymal cells is thought to result in hypoplasia of the facial structures affected in the syndrome. However, it remains to be determined if this is the sole cause of TCS, as the functional consequences of treacle haploinsufficiency in post-migratory CNC cells have not been thoroughly investigated.

3.2 Non-syndromic cleft lip/palate

Non-syndromic cleft lip/palate (NSCL/P) is a multifactorial CFM in which clefts of the upper lip accompanied or not by cleft palate are the sole clinical finding in affected subjects (Fig. 1D, E). It is a prevalent congenital disorder, with incidences ranging between 3.4 and 22.9 per 10,000 births world-wide, depending upon factors such as ethnic background, geographical location, and socio-economic status (Mossey et al., 2009). Development, growth and fusion of the facial prominences and palatine shelves are reliant upon cell migration, proliferation, transdifferentiation and apoptosis; therefore, susceptibility factors acting on these processes are thought to be the underlying causes of NSCL/P (Jiang et al., 2006; Yu et al., 2009; Greene & Pisano, 2010). Although several susceptibility *loci* (e.g. 8q24, 10q25, *IRF6*; Brito et al., 2012a; Brito et al., 2012b; Ludwig et al., 2012) have been identified mainly through genetic association studies, the functional effects exerted on craniofacial development by the majority of them and how they interact with environmental factors remain poorly understood. Further, these variants do not explain the high heritability estimated for NSCL/P (45-85%) for several populations, including the Brazilian (Brito et al., 2011).

RCPS, TCS and NSCL/P are examples of how disruption of basic cellular mechanisms imparts such drastic outcomes in craniofacial development. The mechanisms through which genetic and/or environmental insults affect such important developmental pathways have yet to be completely dissected for most CFMs. Although genetic variants and environmental factors possibly involved in CFMs can be identified through various approaches (e.g. association studies, gene mapping, and next-generation sequencing), their biological effects must still be demonstrated through functional studies. In this regard, cellular and animal models are of great use to perform these analyses, having so far provided important contributions to the understanding of craniofacial development and the pathogenesis of a number of CFMs.

4. Investigating the pathogenesis of CFMs with the use of in vivo and in vitro models

4.1 Animal models

Animal models have greatly contributed to our understanding of normal and abnormal craniofacial development. By targeting specific genes involved in CFMs, it is possible to examine the outcomes in craniofacial morphogenesis of developing embryos. This approach includes the use of dominant-negative constructs, RNA interference and anti-sense morpholinos particularly in *Xenopus*, zebrafish, and chick embryos (Barriga et al., 2015). Since mice are presumptively more likely to reflect mammalian development, they are considered to be more appropriate to model human disorders, and gene targeting/loss-of-function approaches in this organism have also led to important advances in understanding human CFMs such as TCS, 22q11.2 deletion syndrome, an craniosynostoses (Dixon et al., 2006; Jones et al., 2008; Holmes, 2012; Trainor and Andrews, 2013; He and Soriano, 2013; Fantauzzo and Soriano, 2014; Meechan et al., 2015). Recent technical advances in genome editing have enabled the production of improved knockout animals or animals harbouring specific mutations, opening new possibilities for disease modelling (Seruggia & Montoliu, 2014).

Despite being thoroughly explored as a mammalian model for craniofacial development, the mouse embryo may not completely represent embryonic development across species. Knockout mice for important genes involved in neural crest development often do not show results comparable to other model organisms, sometimes turning out without any detectable phenotype. This discrepancy has been attributed to technical limitations in generating mutant mouse lines or species-specific differences within the neural crest gene regulatory network (Thyagarajan et al., 2003; Barriga et al., 2015). Despite these limitations, the mouse model still stands as an important tool to investigate human craniofacial phenotypes, and, in conjunction with non-mammalian models and human cell culture systems, it holds great potential for discovery.

4.2 Cellular models

Cell culture systems offer a unique opportunity to study cellular phenotypes and pathways involved in human disease. Given that a genetic defect or disorder does not necessarily produce symptoms in animal models, cell cultures from human tissues are the most appropriate complement to *in vivo* studies. Furthermore, the phenotype of patients' cells

carrying disease-specific genomic elements can be examined under culture conditions that can be controlled and experimentally manipulated *in vitro* (Unternaehrer & Daley, 2011; Srijaya et al., 2012; Sterneckert et al., 2014). However, access to disease-relevant primary cells is hindered for conditions in which embryonic tissues are primarily affected, such as in craniofacial and neurodevelopmental disorders. Circumventing this drawback, stem cells have emerged as a promising instrument with which to conduct functional studies.

4.2.1 Stem cells from human exfoliated deciduous teeth

Stem cells from human exfoliated deciduous teeth (SHED) are an easily accessible, multipotent stem cell population (Miura et al., 2003). These cells possess osteogenic, chondrogenic, adipogenic, myogenic and dentinogenic capacity, which can be studied *in vitro* if these differentiation properties are of interest to the disease under investigation. More importantly, SHED comprise CNC-derived mesenchymal cells, and therefore they share the same origin with the mesenchymal cells within the embryonic craniofacial structures affected in many CFMs (Cordero et al., 2011; Janebodin et al., 2011; Komada et al., 2012).

SHED have been successfully employed to identify altered cellular pathways involved in developmental disorders, including NSCL/P (Bueno et al., 2011; Kobayashi et al., 2013; Grisei-Oliveira et al., 2013; Suzuki et al., 2014). In 2011, our group performed transcriptome profiling of SHED from NSCL/P patients, identifying dysregulation of co-expressed gene networks involved in DNA damage response and repair. These networks displayed aberrant expression of key genes involved in these cellular processes, including *BRCA1*, *MSH2*, and *RAD51*, which were predicted to be regulated by transcription factor E2F1 (Kobayashi, 2011). These dysregulation patterns are in accordance with the proposed aetiological overlap between cleft lip/palate and several types of cancer, which frequently co-occur in patients and families (Zhu et al., 2002; Bille et al., 2005; Taioli et al., 2010; Vieira et al., 2012); also, these findings raised the possibility that susceptibility to DNA damage in addition to environmental insults during embryonic development could lead to alterations in lip and palate development. If that hypothesis is true, DNA repair gene networks must be important for proper craniofacial development, and tissues from NSCL/P subjects should display increased DNA damage when exposed to genotoxic factors, in comparison to controls.

4.2.2 Induced pluripotent stem cell-derived neural crest cells

Induced pluripotent stem cells (iPSCs) are an invaluable asset to study human disorders. iPSCs can be generated from somatic cells by forced expression of pluripotency-associated factors (Takahashi et al., 2007), and differentiated into a multitude of cell types. With this technology, it is possible to isolate patients' cells, induce pluripotency, and generate the specific cell type afflicted with the disease.

This possibility has recently embraced craniofacial diseases, as directed generation of neural crest cells (NCCs) from iPSCs is now attainable. iPSC-derived NCCs express several neural crest markers and are able to migrate under appropriate cues *in vitro* and *in vivo* (Kreitzer et al., 2013; Menendez et al., 2013). Moreover, akin to their embryonic counterparts, they are able to generate multipotent mesenchymal progenitors that can be differentiated into craniofacial cell types affected in CFMs, thus expanding possibilities for investigating disease-related phenotypes (Menendez et al., 2013; Fukuta et al., 2014, Matsumoto et al., 2015). Albeit methods for differentiation of NCCs from pluripotent cells have existed since 2007 (Lee et al., 2007), they required laborious procedures involving embryoid body and neural rosette cultures, often resulting in only a small proportion of NCCs (Menendez et al., 2011; Trainor, 2014). Recent approaches for differentiation of NCCs from iPSCs rely on WNT pathway activation and TGF-β pathway blockade with the use of small molecules, producing more homogeneous NCC populations (Menendez et al., 2011; Menendez et al., 2013; Fukuta et al., 2014). Given the novelty of this approach, so far only mesenchymal, non-craniofacial phenotypes of fibrodysplasia ossificans progressiva have been modelled with these cells (Matsumoto et al., 2015; Hino et al., 2015), and reports exploring the properties of iPSC-derived NCCs to unravel the pathogenesis of CFMs are still scarce.

5. Objectives

In face of the necessity to better understand the pathogenesis of CFMs, in this work we proposed functional studies to investigate three selected disorders: NSCL/P, RCPS, and TCS. These studies were conducted in neural crest-derived cell cultures from affected patients, as a means to assess disease-specific phenotypes in a cell type presumptively affected in these disorders. The main objectives of this thesis were as follows:

a) To perform functional studies in SHED from NSCL/P patients in order to evaluate if the dysregulated patterns of expression previously observed (Kobayashi, 2011) result in observable cellular phenotypes and ;

b) To produce patient-specific RCPS and TCS iPSCs and differentiate them into NCCs through standardisation of current differentiation methodology;

c) To identify a possible pathogenetic mechanism responsible for RCPS by screening for altered cellular phenotypes in iPSC-derived NCCs from affected subjects;

d) To evaluate if Treacle haploinsufficiency in post-migratory CNC derivatives could play a role in the aetiology of TCS, through investigation of cellular properties of NCC-derived mesenchymal cells.

REFERENCES

Barriga, E. H., P. A. Trainor, et al. Animal models for studying neural crest development: is the mouse different? Development, v.142, n.9, May 1, p.1555-60. 2015.

Bille, C., J. F. Winther, et al. Cancer risk in persons with oral cleft--a population-based study of 8,093 cases. Am J Epidemiol, v.161, n.11, Jun 1, p.1047-55. 2005.

Brito, L. A., C. F. Bassi, et al. IRF6 is a risk factor for nonsyndromic cleft lip in the Brazilian population. Am J Med Genet A, v.158A, n.9, Sep, p.2170-5. 2012.

Brito, L. A., L. A. Cruz, et al. Genetic contribution for non-syndromic cleft lip with or without cleft palate (NS CL/P) in different regions of Brazil and implications for association studies. Am J Med Genet A, v.155A, n.7, Jul, p.1581-7. 2011.

Brito, L. A., J. G. Meira, et al. Genetics and management of the patient with orofacial cleft. Plast Surg Int, v.2012, p.782821. 2012.

Brito, L. A., L. M. Paranaiba, et al. Region 8q24 is a susceptibility locus for nonsyndromic oral clefting in Brazil. Birth Defects Res A Clin Mol Teratol, v.94, n.6, Jun, p.464-8. 2012.

Bueno, D. F., D. Y. Sunaga, et al. Human stem cell cultures from cleft lip/palate patients show enrichment of transcripts involved in extracellular matrix modeling by comparison to controls. Stem Cell Rev, v.7, n.2, Jun, p.446-57. 2011.

Chan, C. C., J. Dostie, et al. eIF4A3 is a novel component of the exon junction complex. RNA, v.10, n.2, Feb, p.200-9. 2004.

Choe, Y., K. S. Zarbalis, et al. Neural crest-derived mesenchymal cells require Wnt signaling for their development and drive invagination of the telencephalic midline. PLoS One, v.9, n.2, p.e86025. 2014.

Clouthier, D. E., M. R. Passos-Bueno, et al. Understanding the basis of auriculocondylar syndrome: Insights from human, mouse and zebrafish genetic studies. Am J Med Genet C Semin Med Genet, v.163C, n.4, Nov, p.306-17. 2013.

Cordero, D. R., S. Brugmann, et al. Cranial neural crest cells on the move: their roles in craniofacial development. Am J Med Genet A, v.155A, n.2, Feb, p.270-9. 2011.

De Mey, A., I. Van Hoof, et al. Anatomy of the orbicularis oris muscle in cleft lip. Br J Plast Surg, v.42, n.6, Nov, p.710-4. 1989.

Dixon, J., N. C. Jones, et al. Tcof1/Treacle is required for neural crest cell formation and proliferation deficiencies that cause craniofacial abnormalities. Proc Natl Acad Sci U S A, v.103, n.36, Sep 5, p.13403-8. 2006.

Dixon, M. J., M. L. Marazita, et al. Cleft lip and palate: understanding genetic and environmental influences. Nat Rev Genet, v.12, n.3, Mar, p.167-78. 2011.

Fantauzzo, K. A. e P. Soriano. PI3K-mediated PDGFRalpha signaling regulates survival and proliferation in skeletal development through p53-dependent intracellular pathways. Genes Dev, v.28, n.9, May 1, p.1005-17. 2014.

Farronato, G., P. Cannalire, et al. Cleft lip and/or palate: review. Minerva Stomatol, v.63, n.4, Apr, p.111-26. 2014.

Favaro, F. P., L. Alvizi, et al. A noncoding expansion in EIF4A3 causes Richieri-Costa-Pereira syndrome, a craniofacial disorder associated with limb defects. Am J Hum Genet, v.94, n.1, Jan 2, p.120-8. 2014.

Favaro, F. P., R. M. Zechi-Ceide, et al. Richieri-Costa-Pereira syndrome: a unique acrofacial dysostosis type. An overview of the Brazilian cases. Am J Med Genet A, v.155A, n.2, Feb, p.322-31. 2011.

Fukuta, M., Y. Nakai, et al. Derivation of mesenchymal stromal cells from pluripotent stem cells through a neural crest lineage using small molecule compounds with defined media. PLoS One, v.9, n.12, p.e112291. 2014.

Gong, S. G. Cranial neural crest: migratory cell behavior and regulatory networks. Exp Cell Res, v.325, n.2, Jul 15, p.90-5. 2014.

Gonzales, B., D. Henning, et al. The Treacher Collins syndrome (TCOF1) gene product is involved in pre-rRNA methylation. Hum Mol Genet, v.14, n.14, Jul 15, p.2035-43. 2005.

Gorlin, R. J. e M. M. H. Cohen Jr., R. C. M. Syndromes of the Head and Neck. New York, NY, US: Oxford University Press. 2001. 905-907 p.

Governale, L. S. Craniosynostosis. Pediatr Neurol, v.53, n.5, Nov, p.394-401.

Greene, R. M. e M. M. Pisano. Palate morphogenesis: Current understanding and future directions. Birth Defects Res C Embryo Today, v.90, n.2, Jun, p.133-54. 2010.

Griesi-Oliveira, K., D. Y. Sunaga, et al. Stem cells as a good tool to investigate dysregulated biological systems in autism spectrum disorders. Autism Res, v.6, n.5, Oct, p.354-61. 2013.

Hamm, J. A. e N. H. Robin. Newborn craniofacial malformations: orofacial clefting and craniosynostosis. Clin Perinatol, v.42, n.2, Jun, p.321-36, viii. 2015.

He, F. e P. Soriano. A critical role for PDGFRalpha signaling in medial nasal process development. PLoS Genet, v.9, n.9, p.e1003851. 2013.

Hino, K., M. Ikeya, et al. Neofunction of ACVR1 in fibrodysplasia ossificans progressiva. Proc Natl Acad Sci U S A, v.112, n.50, Dec 15, p.15438-43. 2015.

Holmes, G. Mouse models of Apert syndrome. Childs Nerv Syst, v.28, n.9, Sep, p.1505-10. 2012.

Janebodin, K., O. V. Horst, et al. Isolation and characterization of neural crest-derived stem cells from dental pulp of neonatal mice. PLoS One, v.6, n.11, p.e27526. 2011.

Jiang, R., J. O. Bush, et al. Development of the upper lip: morphogenetic and molecular mechanisms. Dev Dyn, v.235, n.5, May, p.1152-66. 2006.

Jones, N. C., M. L. Lynn, et al. Prevention of the neurocristopathy Treacher Collins syndrome through inhibition of p53 function. Nat Med, v.14, n.2, Feb, p.125-33. 2008.

Kobayashi, G. S. Transcriptome analysis of mesenchymal stem cells to investigate the aetiology of non-syndromic cleft lip and palate. (Dissertation). Instituto de Biociências, Universidade de São Paulo, São Paulo, 2011. 93 p.

Kobayashi, G. S., L. Alvizi, et al. Susceptibility to DNA damage as a molecular mechanism for non-syndromic cleft lip and palate. PLoS One, v.8, n.6, p.e65677. 2013.

Komada, Y., T. Yamane, et al. Origins and properties of dental, thymic, and bone marrow mesenchymal cells and their stem cells. PLoS One, v.7, n.11, p.e46436. 2012.

Krapels, I. P., G. A. Zielhuis, et al. Periconceptional health and lifestyle factors of both parents affect the risk of live-born children with orofacial clefts. Birth Defects Res A Clin Mol Teratol, v.76, n.8, Aug, p.613-20. 2006.

Kreitzer, F. R., N. Salomonis, et al. A robust method to derive functional neural crest cells from human pluripotent stem cells. Am J Stem Cells, v.2, n.2, p.119-31. 2013.

Lee, G., H. Kim, et al. Isolation and directed differentiation of neural crest stem cells derived from human embryonic stem cells. Nat Biotechnol, v.25, n.12, Dec, p.1468-75. 2007.

Lehalle, D., D. Wieczorek, et al. A review of craniofacial disorders caused by spliceosomal defects. Clin Genet, v.88, n.5, Nov, p.405-15. 2015.

Ludwig, K. U., E. Mangold, et al. Genome-wide meta-analyses of nonsyndromic cleft lip with or without cleft palate identify six new risk loci. Nat Genet, v.44, n.9, Sep, p.968-71. 2012.

Matsumoto, Y., M. Ikeya, et al. New Protocol to Optimize iPS Cells for Genome Analysis of Fibrodysplasia Ossificans Progressiva. Stem Cells, v.33, n.6, Jun, p.1730-42. 2015.

Meechan, D. W., T. M. Maynard, et al. Modeling a model: Mouse genetics, 22q11.2 Deletion Syndrome, and disorders of cortical circuit development. Prog Neurobiol, v.130, Jul, p.1-28. 2015.

Menendez, L., M. J. Kulik, et al. Directed differentiation of human pluripotent cells to neural crest stem cells. Nat Protoc, v.8, n.1, Jan, p.203-12. 2013.

Menendez, L., T. A. Yatskievych, et al. Wnt signaling and a Smad pathway blockade direct the differentiation of human pluripotent stem cells to multipotent neural crest cells. Proc Natl Acad Sci U S A, v.108, n.48, Nov 29, p.19240-5. 2011.

Miura, M., S. Gronthos, et al. SHED: stem cells from human exfoliated deciduous teeth. Proc Natl Acad Sci U S A, v.100, n.10, May 13, p.5807-12. 2003.

Moody, S. Principles of Developmental Genetics: Publisher: Academic Press, v.1. 2015. 784 p.

Mossey, P. A., J. Little, et al. Cleft lip and palate. Lancet, v.374, n.9703, Nov 21, p.1773-85. 2009.

Raskin, S., M. Souza, et al. Richieri-costa and Pereira syndrome: severe phenotype. Am J Med Genet A, v.161A, n.8, Aug, p.1999-2003. 2013.

Sabbagh, H. J., M. H. Hassan, et al. Passive smoking in the etiology of non-syndromic orofacial clefts: a systematic review and meta-analysis. PLoS One, v.10, n.3, p.e0116963. 2015.

Seruggia, D. e L. Montoliu. The new CRISPR-Cas system: RNA-guided genome engineering to efficiently produce any desired genetic alteration in animals. Transgenic Res, v.23, n.5, Oct, p.707-16. 2014.

Singh, K. K., L. Wachsmuth, et al. Two mammalian MAGOH genes contribute to exon junction complex composition and nonsense-mediated decay. RNA Biol, v.10, n.8, Aug, p.1291-8. 2013.

Smith, S. M., A. Garic, et al. Neural crest development in fetal alcohol syndrome. Birth Defects Res C Embryo Today, v.102, n.3, Sep, p.210-20. 2014.

Splendore, A., E. O. Silva, et al. High mutation detection rate in TCOF1 among Treacher Collins syndrome patients reveals clustering of mutations and 16 novel pathogenic changes. Hum Mutat, v.16, n.4, Oct, p.315-22. 2000.

Srijaya, T. C., P. J. Pradeep, et al. The promise of human induced pluripotent stem cells in dental research. Stem Cells Int, v.2012, p.423868. 2012.

Sterneckert, J. L., P. Reinhardt, et al. Investigating human disease using stem cell models. Nat Rev Genet, v.15, n.9, Sep, p.625-39. 2014.

Suzuki, A. M., K. Griesi-Oliveira, et al. Altered mTORC1 signaling in multipotent stem cells from nearly 25% of patients with nonsyndromic autism spectrum disorders. Mol Psychiatry, Jan 13. 2015.

Szabo-Rogers, H. L., L. E. Smithers, et al. New directions in craniofacial morphogenesis. Dev Biol, v.341, n.1, May 1, p.84-94. 2010.

Taioli, E., C. Ragin, et al. Cleft lip and palate in family members of cancer survivors. Cancer Invest, v.28, n.9, Nov, p.958-62. 2010.

Takahashi, K., K. Tanabe, et al. Induction of pluripotent stem cells from adult human fibroblasts by defined factors. Cell, v.131, n.5, Nov 30, p.861-72. 2007.

Thyagarajan, T., S. Totey, et al. Genetically altered mouse models: the good, the bad, and the ugly. Crit Rev Oral Biol Med, v.14, n.3, p.154-74. 2003.

Trainor, P. Neural Crest Cells: Evolution, Development and Disease: Academic Press; 1 edition, v.1. 2014. 488 p.

Trainor, P. A. e B. T. Andrews. Facial dysostoses: Etiology, pathogenesis and management. Am J Med Genet C Semin Med Genet, v.163C, n.4, Nov, p.283-94. 2013.

Twigg, S. R. e A. O. Wilkie. New insights into craniofacial malformations. Hum Mol Genet, Jun 17. 2015.

Unternaehrer, J. J. e G. Q. Daley. Induced pluripotent stem cells for modelling human diseases. Philos Trans R Soc Lond B Biol Sci, v.366, n.1575, Aug 12, p.2274-85. 2011.

Vieira, A. R., S. Khaliq, et al. Risk of cancer in relatives of children born with isolated cleft lip and palate. Am J Med Genet A, v.158A, n.6, Jun, p.1503-4. 2012.

Wang, Z., V. Murigneux, et al. Transcriptome-wide modulation of splicing by the exon junction complex. Genome Biol, v.15, n.12, p.551. 2014.

Weiner, A. M., N. L. Scampoli, et al. Fishing the molecular bases of Treacher Collins syndrome. PLoS One, v.7, n.1, p.e29574. 2012.

Wieczorek, D. Human facial dysostoses. Clin Genet, v.83, n.6, Jun, p.499-510. 2013.

Wijayaweera, C. J., N. A. Amaratunga, et al. Arrangement of the orbicularis oris muscle in different types of cleft lips. J Craniofac Surg, v.11, n.3, May, p.232-5. 2000.

Yu, W., M. Serrano, et al. Cleft lip and palate genetics and application in early embryological development. Indian J Plast Surg, v.42 Suppl, Oct, p.S35-50. 2009.

Zhu, J. L., O. Basso, et al. Do parents of children with congenital malformations have a higher cancer risk? A nationwide study in Denmark. Br J Cancer, v.87, n.5, Aug 27, p.524-8. 2002.

Chapter II

Susceptibility to DNA damage as a molecular mechanism for non-syndromic cleft lip and palate

Gerson S. Kobayashi, Lucas Alvizi, Daniele Y. Sunaga, Philippa Francis-West, Anna Kuta, Bruno V. P. Almada, Simone G. Ferreira, Leonardo C. de Andrade-Lima, Daniela F. Bueno, Cássio E. Raposo-Amaral, Carlos F. Menck and Maria Rita Passos-Bueno.

Abstract

Non-syndromic cleft lip/palate (NSCL/P) is a complex, frequent congenital malformation, determined by the interplay between genetic and environmental factors during embryonic development. Previous findings have appointed an aetiological overlap between NSCL/P and cancer, and alterations in similar biological pathways may underpin both conditions. Here, using a combination of transcriptomic profiling and functional approaches, we report that NSCL/P dental pulp stem cells exhibit dysregulation of a co-expressed gene network mainly associated with DNA double-strand break repair and cell cycle control ($p = 2.88\times10^{-2}$–5.02×10^{-9}). This network included important genes for these cellular processes, such as *BRCA1*, *RAD51*, and*MSH2*, which are predicted to be regulated by transcription factor E2F1. Functional assays support these findings, revealing that NSCL/P cells accumulate DNA double-strand breaks upon exposure to H_2O_2. Furthermore, we show that *E2f1*, *Brca1* and *Rad51* are co-expressed in the developing embryonic orofacial primordia, and may act as a molecular hub playing a role in lip and palate morphogenesis. In conclusion, we show for the first time that cellular defences against DNA damage may take part in determining the susceptibility to NSCL/P. These results are in accordance with the hypothesis of aetiological overlap between this malformation and cancer, and suggest a new pathogenic mechanism for the disease.

Published Article: Kobayashi GS, Alvizi L, Sunaga DY, Francis-West P, Kuta A, et al. (2013) Susceptibility to DNA Damage as a Molecular Mechanism for Non-Syndromic Cleft Lip and Palate. PLoS ONE 8(6): e65677. doi: 10.1371/journal.pone.0065677

Author's notes: Preliminary transcriptomics analyses had been previously carried out (Kobayashi, 2011); its full analysis and all functional studies were carried out during the period encompassed by this doctoral thesis.

OPEN ACCESS Freely available online

PLOS ONE

Susceptibility to DNA Damage as a Molecular Mechanism for Non-Syndromic Cleft Lip and Palate

Gerson Shigeru Kobayashi[1☯], Lucas Alvizi[1☯], Daniele Yumi Sunaga[1], Philippa Francis-West[2], Anna Kuta[2], Bruno Vinícius Pimenta Almada[1], Simone Gomes Ferreira[1], Leonardo Carmo de Andrade-Lima[3], Daniela Franco Bueno[1,4], Cássio Eduardo Raposo-Amaral[4], Carlos Frederico Menck[3], Maria Rita Passos-Bueno[1]*

1 Human Genome Research Center, Institute for Biosciences, University of São Paulo, São Paulo, Brazil, **2** Dental Institute, Department of Craniofacial Development and Stem Cell Biology, King's College London, London, United Kingdom, **3** Institute of Biomedical Sciences, University of São Paulo, São Paulo, Brazil, **4** SOBRAPAR Institute, Campinas, São Paulo, Brazil

Abstract

Non-syndromic cleft lip/palate (NSCL/P) is a complex, frequent congenital malformation, determined by the interplay between genetic and environmental factors during embryonic development. Previous findings have appointed an aetiological overlap between NSCL/P and cancer, and alterations in similar biological pathways may underpin both conditions. Here, using a combination of transcriptomic profiling and functional approaches, we report that NSCL/P dental pulp stem cells exhibit dysregulation of a co-expressed gene network mainly associated with DNA double-strand break repair and cell cycle control ($p = 2.88\times10^{-2}$–5.02×10^{-9}). This network included important genes for these cellular processes, such as *BRCA1*, *RAD51*, and *MSH2*, which are predicted to be regulated by transcription factor E2F1. Functional assays support these findings, revealing that NSCL/P cells accumulate DNA double-strand breaks upon exposure to H_2O_2. Furthermore, we show that *E2f1*, *Brca1* and *Rad51* are co-expressed in the developing embryonic orofacial primordia, and may act as a molecular hub playing a role in lip and palate morphogenesis. In conclusion, we show for the first time that cellular defences against DNA damage may take part in determining the susceptibility to NSCL/P. These results are in accordance with the hypothesis of aetiological overlap between this malformation and cancer, and suggest a new pathogenic mechanism for the disease.

Citation: Kobayashi GS, Alvizi L, Sunaga DY, Francis-West P, Kuta A, et al. (2013) Susceptibility to DNA Damage as a Molecular Mechanism for Non-Syndromic Cleft Lip and Palate. PLoS ONE 8(6): e65677. doi:10.1371/journal.pone.0065677

Editor: Dale J. Hedges, University of Miami, United States of America

Received December 20, 2012; **Accepted** April 26, 2013; **Published** June 12, 2013

Funding: This work is funded by CNPq (National Counsel of Technological and Scientific Development), FAPESP (São Paulo Research Foundation), CAPES (Higher Education Co-Ordination Agency) and MCT (Ministry of Science, Technology and Innovation). The funders had no role in study design, data collection and analysis, decision to publish, or preparation of the manuscript.

Competing Interests: The authors have declared that no competing interests exist.

* E-mail: passos@ib.usp.br

☯ These authors contributed equally to this work.

Introduction

Non-syndromic cleft lip with or without cleft palate (NSCL/P [OMIM %119530]) is one of the most common congenital defects. Its birth prevalence is variable, ranging from 3.4 to 22.9 per 10,000 births world-wide, depending upon factors such as ethnic background, geographical location, and socio-economic status [1].

The interplay between genetic and environmental factors during embryonic development is thought to be determinant in the aetiology of NSCL/P. Genome-wide association studies (GWAS) have enabled the consistent identification of several candidate *loci*. However, the low attributed risk for each variant fails to explain the estimated heritability for NSCL/P (as high as 85% in some populations [2]), and little is known about their functional role in the pathogenesis of the disease. The fact that non-coding genomic regions harbour many of these variants (which include an enhancer upstream of *IRF6*, and intronic and intergenic regions [3,4,5,6] is indicative that they might play a transcriptional regulatory role in the embryo, in agreement with the idea that alterations in gene expression may be a relevant mechanism underlying susceptibility to complex diseases [7]. Therefore, if disease susceptibility is shaped by transcriptional anomalies, which in turn are driven by the individual's genetic constitution, a feasible approach to investigate the aetiology of NSCL/P is the gene expression analysis of cells from affected individuals. This strategy not only allows the screening of candidate biological pathways contributing to the disease, but also enables the investigation of environmental agents and how they affect these pathways. Previous data derived from fibroblasts and mesenchymal stem cells support this rationale, as they revealed alterations in gene networks functionally relevant for orofacial development, such as collagen metabolism and extracellular matrix remodelling [8,9,10,11].

NSCL/P is thought to arise from anomalies in cell migration, proliferation, transdifferentiation and apoptosis [12,13,14], all of which are known to be involved in cancer progression. The relationship between orofacial clefts and cancer is subject of debate; however, several studies have reported co-occurrence of orofacial clefts and a variety of cancer types. [15,16,17,18]. Accordingly, alterations in genes that are known to play diverse roles during carcinogenesis, such as *CDH1*, *TP63*, *NBS* and *AXIN2*, have been related to both syndromic and non-syndromic

cleft lip/palate [19,20,21,22,23,24]. Moreover, both are common diseases with significant genetic heterogeneity; therefore, an aetiological overlap is more likely to occur when compared to other diseases. Given these observations, similar biological pathways may be underpinning susceptibility to both conditions.

Thus, our objective was to search for dysregulated gene networks associated with tumourigenesis, using NSCL/P and control dental pulp stem cell cultures. We chose this cell source because it comprises populations of mesodermal and neural crest-derived cells, and therefore it shares the same origin with the cells that populate the mesenchyme of the craniofacial structures involved in lip and palate morphogenesis [25,26,27]; in addition, we have previously demonstrated the applicability of using these cells in detecting gene networks important for NSCL/P aetiology [9]. We expect that the results will not only assist in elucidating the aetiology of NSCL/P, but also provide more information on the mechanisms through which it relates to cancer.

Results

Overview of the Differentially Expressed Genes (DEGs)

By comparing the microarray expression data from NSCL/P (n = 7) and control (n = 6) dental pulp stem cell cultures, we obtained 126 and 211 DEGs using the SAM (Significance Analysis of Microarrays) and Rank Products algorithms, respectively. Combining these two gene sets, we observed an overlap of 109 genes from both methodologies, with a final number of 228 DEGs (72 up-regulated, 156 down-regulated; Table S1), which were submitted to the subsequent analyses.

A Transcriptional Network Associated with Response to DNA Damage and Cell Cycle Control is Dysregulated in NSCL/P Cells

To functionally characterise the DEGs and to determine possible interactions between them, an IPA analysis (Interactive pathways analysis of complex 'omics data; Ingenuity Systems) was performed. The highest-scoring network assembled by IPA (score = 61) harboured DEGs associated with the following functions: Cell Cycle; DNA Replication, Recombination, and Repair; and Cellular Compromise ($p = 2.88\times10^{-2}$–5.02×10^{-9}; Table S2), in which the gene *BRCA1* occupied a central node, functionally connected to a variety of other molecules associated with DNA repair and cell cycle regulation (e.g. *MSH2*, *BLM*, *RAD51*, *CDC6*, *CLSPN*; Fig. 1A). Moreover, the top canonical pathway enriched in our gene set was 'Role of BRCA1 in DNA Damage Response' (p-value = 3.92×10^{-8}; Fig. 1B and 1C). Taken together, the results indicated that NSCL/P cells feature transcriptional dysregulation of genes involved in cell cycle control and DNA damage repair mediated by BRCA1. This motivated us to further investigate this molecule and its relationship with the remaining DEGs.

Assuming that co-expressed genes may partake in the same biological process, we performed a similarity-based clustering analysis, based on *BRCA1* transcript levels. We obtained a highly homogeneous cluster harbouring 30 genes of similar expression patterns across samples (average homogeneity = 0.974, Fig. 2A), including several genes pertaining to the IPA interaction network and BRCA1-mediated DNA repair canonical pathway, such as *MSH2*, *RAD51*, and *BLM*. In accordance with the observations derived from IPA, this cluster exhibited Gene Ontology enrichment for attributes related to the DNA repair machinery and regulation of cell cycle (p = 0.001; Fig. 2B). Subsequent transcription factor binding site enrichment analysis revealed E2F1 as a putative regulator for this co-expression cluster ($p<0.05$; Fig. 2B). To corroborate this result, we used ChIP-chip information available on the FANTOM4 (Functional ANnoTation of the Mammalian genome) database, demonstrating that E2F1 is experimentally proven to interact with 23 out of all 30 clustered genes (Fig. 2C).

Validation of the Microarray Assays using Quantitative Real Time PCR (qRT-PCR)

We carried out the qRT-PCR validation using RNA extracted from independent cell cultures from the same individuals submitted to the microarray assays. We applied this strategy as an attempt to avoid biased interpretation of the transcriptomic data, as the expression of many of the genes detected is cell-cycle dependent and therefore may be subject to fluctuations in asynchronous cultures.

Twenty-four DEGs, including 10 genes present in the *BRCA1* similarity cluster, were submitted to validation by qRT-PCR. We observed that one NSCL/P sample (F4243.1) exhibited a discordant expression pattern for 15 out of the 24 genes as compared to the rest of the NSCL/P group, with expression values distant at least 3 standard deviations from the mean (data not shown). Based on this observation and the fact that RNA aliquots did not correspond to the original samples hybridised on the microarray chips, we classified this sample as an outlier and excluded it from the subsequent analyses. Differences in expression values between NSCL/P and control samples were tested for statistical significance, which revealed that mRNA levels for 17 out of the 24 DEGs selected for validation were significantly different between groups ($p<0.05$). Moreover, we confirmed the differential expression of all genes that were submitted to validation and that also pertained to the *BRCA1* similarity cluster (Table S3).

NSCL/P Cells Accumulate Double-strand Breaks (DSBs) upon Exposure to H_2O_2

In the presence of DNA double-strand breaks (DSBs), the BRCA1 pathway is responsible for cell cycle checkpoint regulation, DNA damage sensor signalling, and participates in DNA repair through homologous recombination [28]. Moreover, oxidative stress plays a major role in carcinogenesis and in teratogen-induced congenital malformations through DSBs induced by reactive oxygen species [29]. Based on the microarray results, we asked if the transcriptional dysregulation of the DSB response system would result in observable cellular phenotypes in NSCL/P cells upon oxidatively generated DNA damage. By flow cytometry quantitation of γ-H2AX (phospho-histone H2AX), we assessed DSB formation in cell cultures exposed to H_2O_2, using 7 NSCL/P and 5 control samples. We observed that a significantly greater proportion of NSCL/P cells were positively stained for γ-H2AX (γ-H2AX$^+$ cells; quantitated in relation to untreated cells for each individual) after 6 and 24 hours of H_2O_2 treatment, when compared to controls ($p<0.05$; Fig. 3A, smaller graph). In fact, NSCL/P samples exhibited a heterogeneous response to H_2O_2 treatment, which could be divided into three subgroups: some individuals exhibited a very high percentage of γ-H2AX$^+$cells after 6 hours (subgroup I - F4243.1, F4245.1, F4293.1); a second subgroup maintained a higher frequency of γ-H2AX$^+$ for longer (24 hours; subgroup II - F4244.1 and F4293.1); and a third subgroup exhibited a lower frequency of γ-H2AX$^+$ cells, similar to the control cells (subgroup III - F4294.1, F4311.1 and F4388.1), as shown in figure 3A and 3B. For subgroup II, we observed an accumulation of γ-H2AX$^+$ cells in G1 and early S that coincided with the still elevated γ-H2AX staining at 24 hours. This subgroup also exhibited a significant increment

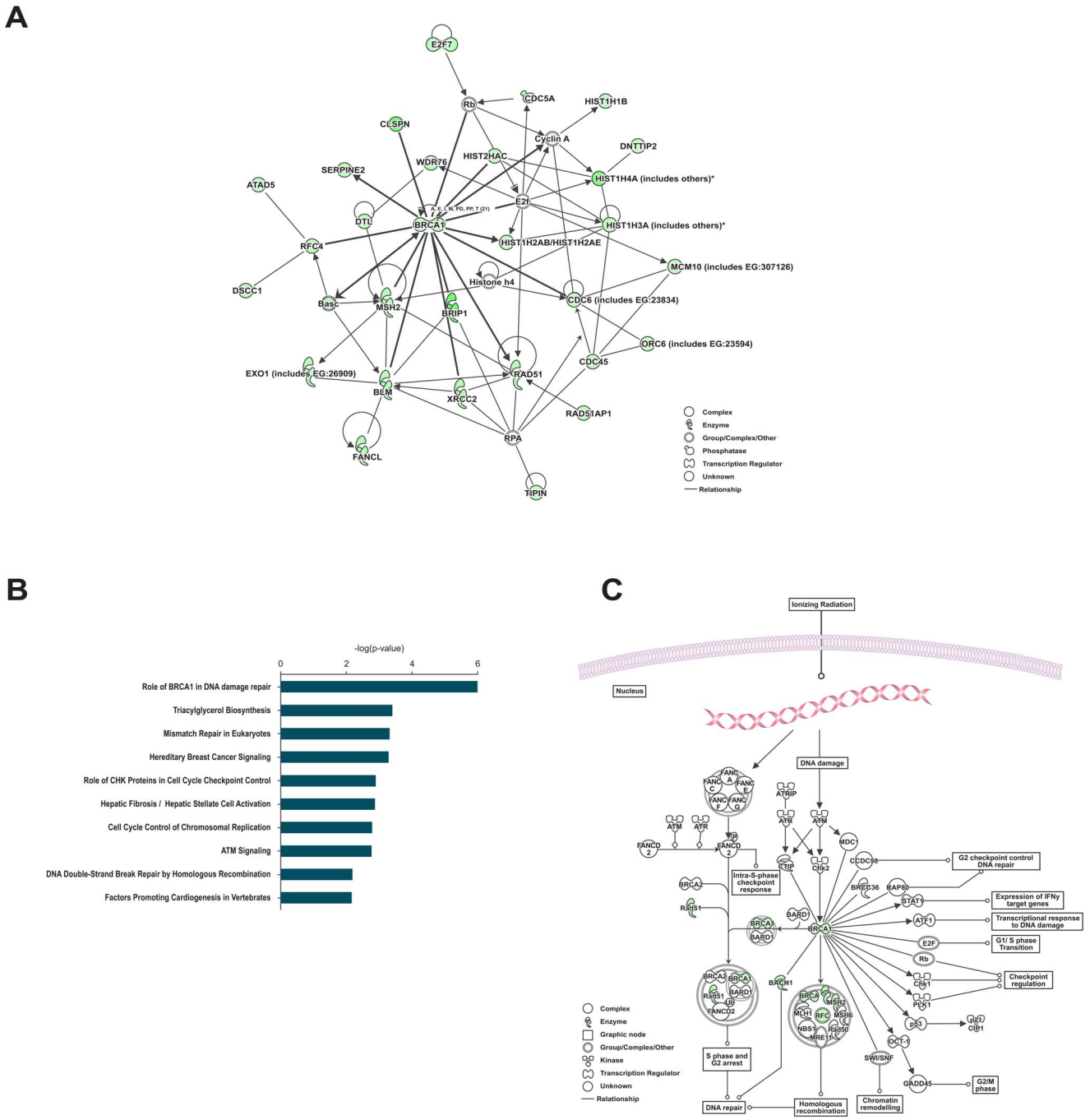

Figure 1. NSCL/P cells exhibit a gene expression profile associated with dysregulation of DNA repair and cell cycle control. (A) IPA network. DEGs were used to assemble a functional interaction map. Lines with arrowheads represent that one molecule acts on another, while regular lines represent protein interactions. Down-regulated genes are shown as green nodes, whereas genes without differential expression are shown as blank nodes. (B) Top 10 Canonical Pathways significantly enriched among the 228 DEGs (Fisher's Exact Test, p-value <0.01). (C) 'Role of BRCA1 in DNA Damage Response' Canonical Pathway.
doi:10.1371/journal.pone.0065677.g001

of sub-G1 cells in this time point, compared to controls and the other subgroups ($p<0.005$; Fig. 3C). Therefore, subgroup II had problems to resume the cycle even at 24 hours, and these cellular responses to H_2O_2 treatment indicate that at least part of the NSCL/P cells (subgroup II) presents a defective repair of DSBs, and this leads to increased cell death.

Next, using an expanded sample of NSCL/P ($n = 11$) and control ($n = 10$) cells, we performed qRT-PCR experiments to assess if exposure to H_2O_2 affects the transcriptional behaviour of DEGs related to cell cycle control and DNA repair that were co-expressed with *BRCA1*, and also the putative upstream regulator *E2F1*. We found that after 6 hours of treatment *E2F1*, *CDC6*, *BRCA1*, *BRIP1*, *RAD51*, *RAD51AP1*and *BLM* did not exhibit significant differences in fold-expression compared to untreated samples, for both NSCL/P and control groups. These genes were transcriptionally repressed at 24 hours, possibly as a cellular

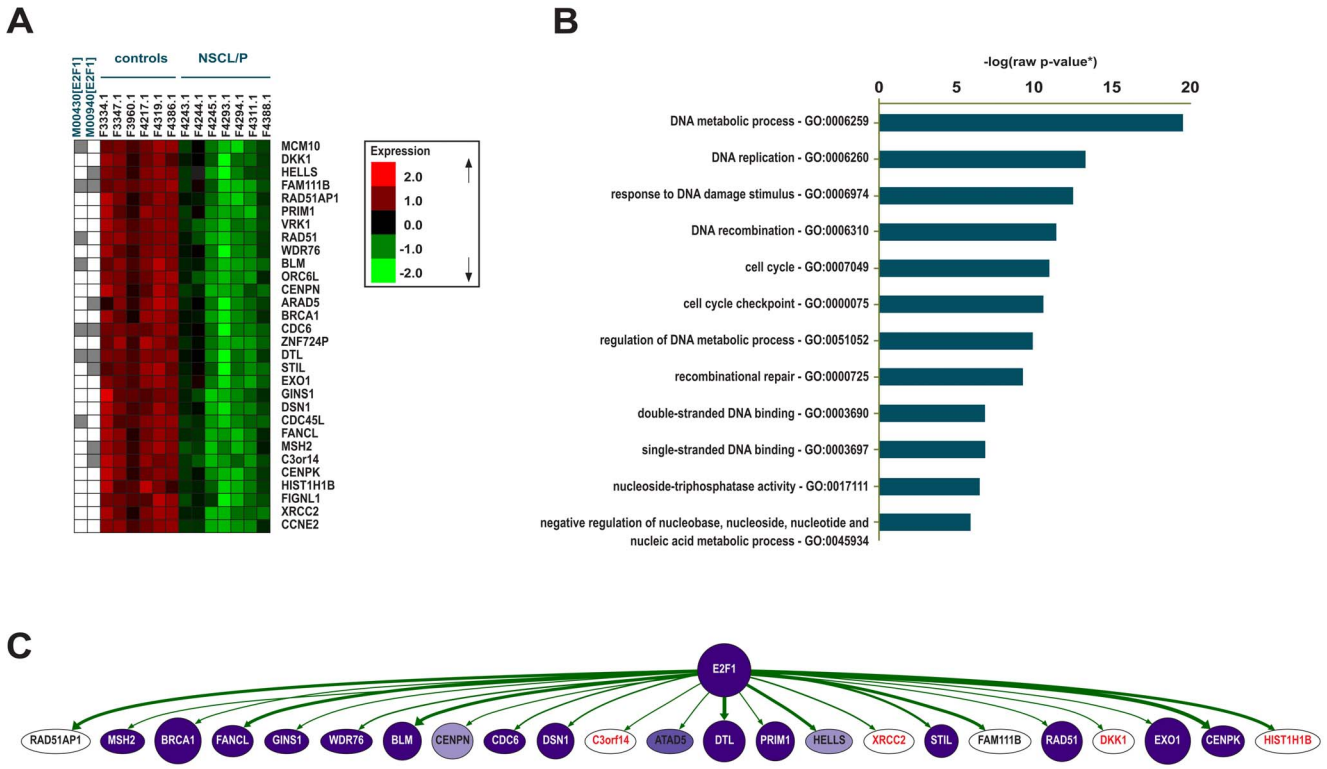

Figure 2. NSCL/P patterns of co-expression are associated with DNA repair, and suggest E2F1 as a regulator. (A) Supervised similarity cluster based on *BRCA1* expression (avg. homogeneity = 0.974). Transcription factor binding sites significantly over-represented in the cluster are marked in grey, for each motif identified (Bonferroni-adjusted p-value <0.05). (B) GO attributes enriched in the similarity cluster and their respective representation among the 30 clustered genes, expressed in percentages ([*] Bootstrap-adjusted p-values = 0.001, raw p-values were used in the chart). (C) Analysis of transcription factor-gene interactions. ChIP-chip data from FANTOM4 were used to validate the interaction between E2F1 and 23 out of the 30 genes of the similarity cluster. The thickness of the arrows indicates how often the interaction has been experimentally detected; node colours represent the level of expression in the cell lines used to assemble the database, from low (light) to high (dark).
doi:10.1371/journal.pone.0065677.g002

response to the treatment. On the other hand, *CDC45L*, which is essential for new DNA synthesis, was more expressed in control cells after 6 hours and 24 hours when compared to NSCL/P cells ($p<0.05$, Fig. 3D).

In light of these findings, we proposed that NSCL/P cells also feature abnormalities in the response to oxidatively generated DNA damage. Therefore, we went back to the transcriptomic data and searched for DEGs related to oxidative stress and subsequent steps of oxidatively generated DNA damage repair. We found differential expression of several molecules directly or indirectly related to these processes, including genes involved in oxidative stress (*GSTM2* [30], *NOX4* [31], *PTGS2* [32], *SMAD3* [33], *BRCA1* [33]), stabilisation of the replication fork (*CLSPN* [34], *TIPIN* [34]), regulation of base-excision repair (*BRCA1* [35]), and new DNA synthesis during homologous recombination repair (*CDC45L* [36], *GINS1* [36], *MCM10* [37]; Table S4), in addition to those already found to be involved in homologous recombination (e.g. *RAD51*, *MSH2*, BLM; Table S1 and Fig. 1C).

Murine Palatal Shelves Express DNA Damage Repair Genes

As the transcriptome analysis and functional assays were conducted in adult stem cells, we considered it crucial to verify if genes involved in DNA repair and cell cycle regulation are expressed in the embryonic structures important for lip and palate morphogenesis. Hence, using qRT-PCR, we first assessed expression of some of these genes, namely *Brca1*, *Brip1*, *Msh2*, *Rad51*, *Rad51ap1*, and *Blm*, in murine palatal shelves extracted at E11.5 (n = 2), E14.5 (n = 3), and E17.5 (n = 3). We observed a positive expression during palatal shelf growth, followed by a trend towards down-regulation of these genes after palate formation had been completed (E17.5), albeit with statistical significance only for *Rad51ap1* ($p<0.05$; Fig. S1), probably due to sample size.

We also analysed *Brca1*, *Rad51*, and *E2f1* expression by whole-mount RNA *in situ* hybridisation of E10.5–E13.5 murine embryos. This revealed that *Brca1*, *Rad51* and *E2f1* transcripts are expressed in the mesenchyme of all the facial primordia (Fig. 4A-C and data not shown). Analysis of E11.5 embryos showed that all 3 genes are expressed in similar domains within the mesenchyme of the maxillary primordia, lateral and medial nasal processes which contribute to the development of the upper lip. Low levels of expression were also detected in the ectoderm at the point of fusion. At E12.5 and E13.5, *Brca1*, *Rad51* and *E2f1* transcripts were clearly co-expressed in the mesenchyme and in some regions of the ectoderm within the developing palatal shelves which arise in the maxillary primordia (Fig. 4E-F and data not shown). Negative sense hybridisation control showed no staining in the facial primordia (Figure S3).

Discussion

Orofacial morphogenesis is dependent upon tightly regulated spatio-temporal patterns of cell migration, proliferation, transdifferentiation, and apoptosis [12,13,14]. Dysregulation of biological pathways orchestrating these processes is thus presumed to play a

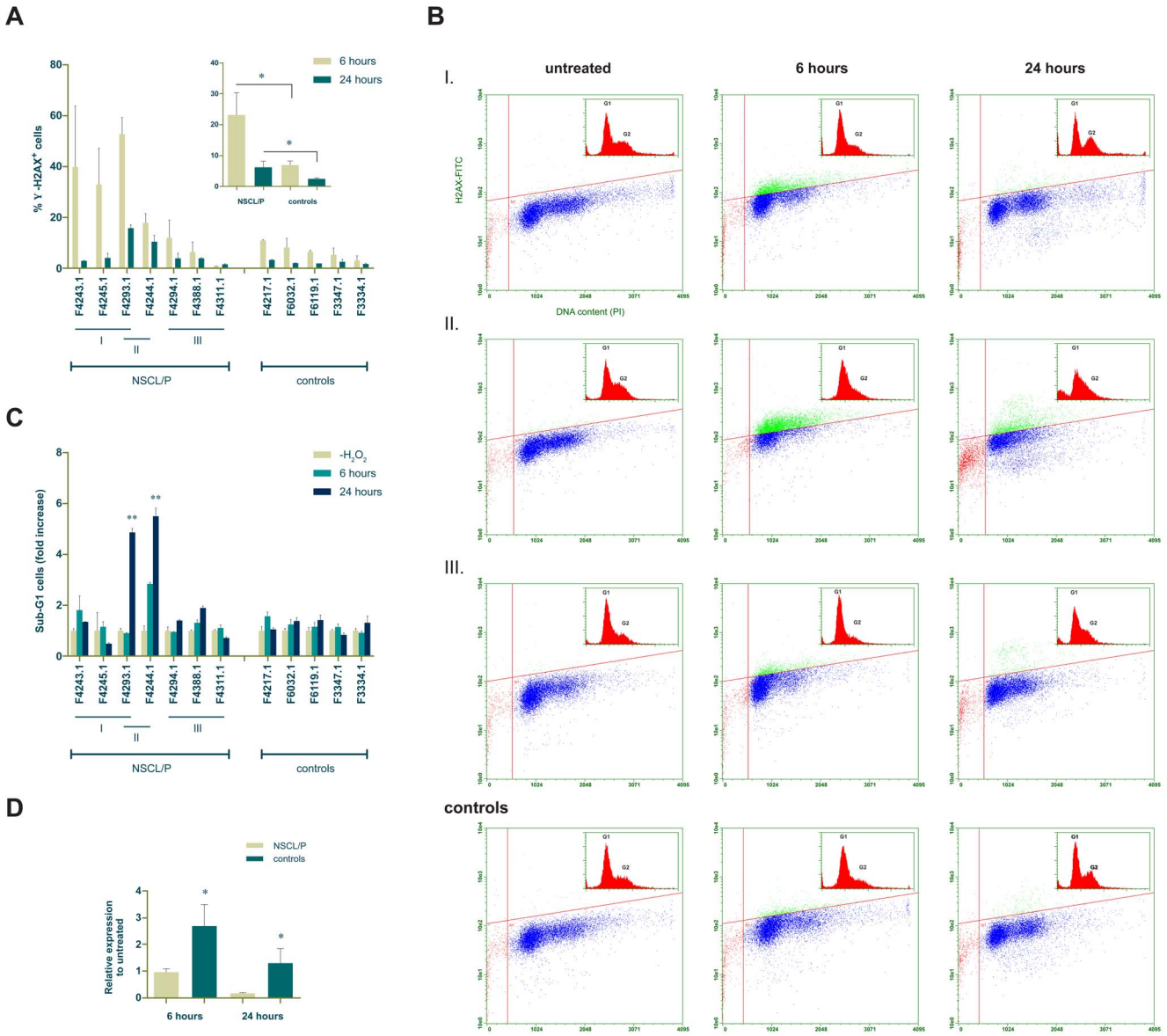

Figure 3. NSCL/P cells exhibit a heterogeneous response to H_2O_2, with distinct patterns of DSB accumulation. (A) Smaller graph - Comparison of the fraction of γ-H2AX$^+$cells between NSCL/P and control cells, at 6 and 24 hours of treatment with H_2O_2. Large graph – Individual quantitation of γ-H2AX$^+$ cells, revealing the subgroups (I–III) within the NSCL/P samples. (*) $p<0.05$. (B) Representative γ-H2AX and PI profiles depicting DSB and cell cycle distribution, for each NSCL/P subgroup and controls. (C) Quantitation of sub-G1 cells, revealing a significant increment in NSCL/P subgroup II, at 24 hours of treatment, as compared to the other subgroups and the controls. (**) $F = 6.04$; $p<0.005$. (D) Relative expression of *CDC45L* following treatment with H_2O_2, revealing a significant decrease in NSCL/P samples at both time points, by comparison to controls. (*) $p<0.05$.
doi:10.1371/journal.pone.0065677.g003

role in the pathogenesis of NSCL/P. Importantly, the identification of these pathways and how they interact with environmental agents will not only provide insight into the molecular basis of NSCL/P, but will also enable the development of more effective preventive strategies.

Using dental pulp stem cells from NSCL/P individuals, we identified a dysregulated transcriptional network mainly associated with response to DNA damage and cell cycle control. The functional interaction network assembled with the DEGs had a central node occupied by tumour suppressor *BRCA1* which, in combination with other key genes, plays a pivotal role in the cellular response to DNA damage and cell cycle control [38]. We confirmed that many genes found to be functionally connected to *BRCA1* in this network not only had a similar expression pattern, but also have well-established roles in the aforementioned cellular functions (e.g. *CDC6*, *CDC25A*, *MSH2*, *BLM*, *RAD51* [39,40]). E2F1, the putative upstream regulator identified for this dysregulation block, is a transcription factor that acts in conjunction with its repressor pRB (encoded by *RB1*) and is responsible for up-regulating a variety of genes necessary for the transition from G1 to S in the cell cycle, being essential for cell cycle progression and DNA damage response [41,42]. Also, it has been shown that E2F1 may play a role during murine palatogenesis [43]. Since *E2F1* and *RB1* were not differentially expressed in NSCL/P cells, we believe that disturbances at the protein level (i.e. affecting protein function but not necessarily the expression) could be responsible for altering

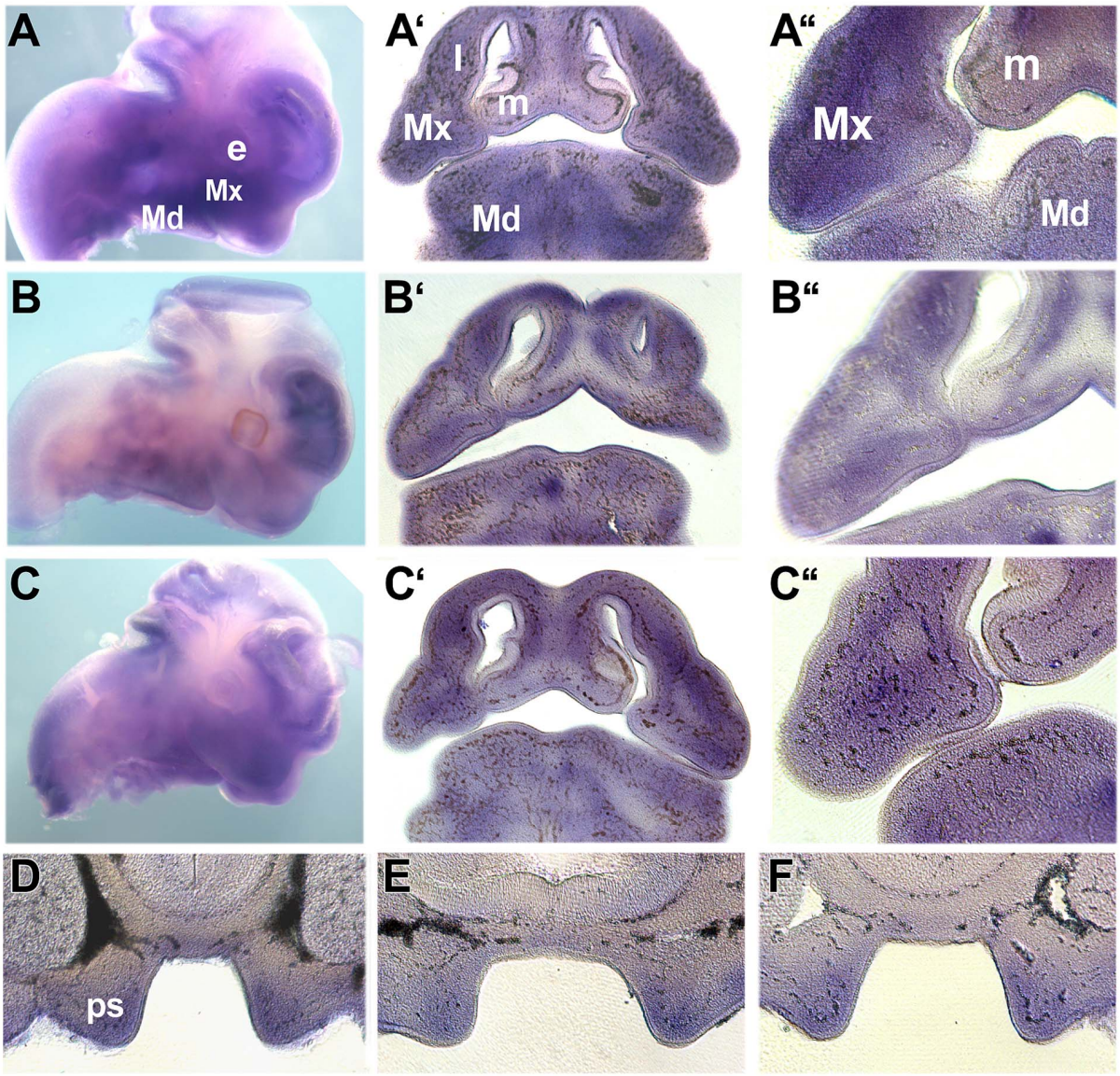

Figure 4. Expression of *Brca1*, *Rad51* and *E2f1* in the developing facial primordia. Whole-mount *in situ* hybridisation (A–F) showing the expression of *Brca1* (A, D), *Rad51* (B, E) and *E2F1* (C, F) in E11.5 (A–C) and E12.5 (D–F) embryos. Expression is indicated by the blue/purple staining. A–C are sagittal views of the developing head whilst A′–C′ are frontal sections through the embryos shown in A–C. A″–C″ show high power views through the developing maxillary primordia, lateral and medial nasal processes. E–F are frontal sections through the developing E12.5 palatal shelves. *e*, eye; *l*, lateral nasal process; *m*, medial nasal process; *Md*, mandibular primordia; *Mx*, maxillary primordia; *ps*, palatal shelves.
doi:10.1371/journal.pone.0065677.g004

the activity of these regulators, resulting in the expression patterns detected here.

The cellular functions attributed to the dysregulated gene network found here are strongly associated with tumourigenesis and risk of cancer [44]. Notably, mutations in BRCA1 have been implicated in risk of hereditary cancers, such as breast, ovarian, pancreatic, and prostate cancer [45], whereas reduced levels of BRCA1 mRNA and protein have also been associated with sporadic tumours [46,47,48]. Additionally, other types of cancer have been ascribed to alterations in many DEGs detected in our analysis, such as *CDC6*, *BLM*, *RAD51*, and *MSH2* [39,49,50,51]. These observations are in agreement with the proposed hypothesis of aetiological overlap between cancer and NSCL/P [15,16,17,18].

We showed that transcriptional dysregulation of BRCA1 and its co-operators is associated with an accumulation of DSBs in NSCL/P cells, compared to controls. NSCL/P samples exhibited a heterogeneous behaviour, in which we observed three cellular phenotypes: individuals with increased DSB formation but efficient repair (subgroup I); those with increased DSB formation and deficient repair (subgroup II); and those with a similar pattern to the one observed among controls (subgroup III), which did not exhibit significant changes in the DSB profile. To better understand this variation, the mechanism by which H_2O_2 induces DSBs has to be taken into account. One possibility is that H_2O_2 generates the hydroxyl free radical OH°, a highly reactive oxygen species that afterwards induces formation of DNA single-strand breaks (SSBs) which, in turn, result in DSBs upon collapse of the replication fork during the S phase of the cell cycle. In this

situation, cells accumulate one-ended DSBs, and repair likely occurs by homologous recombination [52,53,54,55]. The detection of DEGs associated with processes presumed to prevent the oxidative generation of this type of DNA lesion and ensure its repair (i.e., oxidative stress, SSB repair, stabilisation of the replication fork, and DSB sensor signalling and repair via homologous recombination) explain the accumulation of DSBs observed in some of the NSCL/P samples. Therefore, we propose that the concurrent accumulation of G1/early S cells and elevated DSB signals at 24 hours, observed in NSCL/P subgroup II, reflects the inability of these cells to undergo homology-directed DSB repair. This is supported by the observed H_2O_2-dependent increment in apoptotic cells in this subgroup, and by the fact that NSCL/P cells that are able to repair the DSBs (subgroup I) did not display such accumulation in G1 and early S after 24 hours of treatment, being able to progress past early S and further into later stages of the cell cycle. Accordingly, controls and NSCL/P subgroup III did not show appreciable changes in DSB signal nor cell cycle distribution in the presence of H_2O_2, possibly because these cells do not possess alterations in anti-oxidative response and repair of DNA lesions. The finding that *CDC45L* fails to undergo up-regulation in NSCL/P cells exposed to H_2O_2 further suggests that deficiency in this type of DNA repair could play a role in the manifestation of the observed NSCL/P cellular phenotypes, as this DEG is involved in new DNA synthesis during homologous recombination [36] repair. H_2O_2 can also directly induce DSBs irrespective of cell cycle phase; consequently, deficiency of other repair pathways, such as non-homologous end-joining in G1 and G2 [56], would also be important. Yet, this does not seem to be the case, as the contribution of H_2O_2 in direct DSB formation is low [57]. Unexpectedly, in H_2O_2-treated cells we did not detect expression differences for the other DSB repair-related genes neither at 6 or 24 hours. This may have occurred because their transcriptional modulation could be required before the time points investigated in our experiments; for example, BRCA1 is known to act as an early detector and mediator in response to DSBs, and RAD51 is required for homology searching before DNA repair takes place [52,58]. Nevertheless, we were able to confirm that NSCL/P cells display an impaired response to DNA damage, and the results suggest that oxidatively-generated DSBs may play an important role in this mechanism, providing a possible connection between this type of genotoxic insult and the aetiology of NSCL/P. Furthermore, the variation in response to H_2O_2 observed for the NSCL/P samples is in agreement with the genetic heterogeneity associated with the disease, indicating that these alterations are present in only some of the NSCL/P cases.

Previous research has reported a positive association between occurrence of NSCL/P and oxidative stress-initiating environmental factors [59]. Oxidative generation of DSBs and other types of DNA lesions have been reported to arise from many cleft-related environmental factors, such as maternal exposure to alcohol, nicotine, phenytoin, and valproic acid [59,60,61,62,63,64,65,66,67]. Among these, valproic acid has been reported to down-regulate homologous recombination DNA repair genes (e.g. *BRCA1*, *RAD51*, *BLM*) by decreasing E2F1 recruitment to its target promoters [68], which supports the hypothesis that this transcription factor could be at least in part responsible for dysregulating downstream genes through dysfunctional protein activity in the NSCL/P cells, as previously discussed. Moreover, folate deficiency has been related to orofacial clefts [69], and folate is essential for DNA biosynthesis, replication and repair [70,71]; accordingly, it has been shown that genes related to DNA repair and cell cycle regulation, many of which were detected in our analysis, are differentially expressed in response to this molecule [72]. Importantly, if orofacial clefts are related to oxidative/genotoxic factors, they must act during embryonic development and affect the structures responsible for lip and palate formation, where abnormal cellular responses to these environmental insults are expected to play an important role in shaping susceptibility to NSCL/P.

If appropriate transcriptional regulation of the genes detected by our analyses is critical for normal lip and palate development, spatially and temporally co-ordinated expression of these genes would be expected in the embryonic precursors of these structures. Indeed, RNA *in situ* hybridisation assays using mouse embryos confirmed that *Brca1*, *Rad51* and *E2f1* are co-expressed within the mesenchyme of the facial primordia that contribute to the lip and the developing palatal shelves. *Brca1*, *Rad51* and *E2f1* were also detected in small domains within the ectoderm where they may act together with *Irf6* which is expressed throughout the facial epithelium [73,74]. Therefore, *Brca1*, *Rad51* and *E2f1* are expressed during the critical stages of facial morphogenesis and dysregulation would be expected to impact on facial development. Their co-expression strongly supports the possibility that they function together as a molecular hub involved in facial growth and development. Another fact that supports this idea is that stem cells have increased DNA repair compared to differentiated cells [75]; thus, the decreased expression of these genes in NSCL/P cells may reflect problems during development. Furthermore, DNA repair and cell cycle-related genes are progressively down-regulated during orofacial morphogenesis, as suggested by the qRT-PCR experiments during palatogenesis here, and as reported in other works investigating the growth and fusion of facial prominences, and migrating neural crest cells [76,77]. If these cellular systems are more active prior to differentiation of the craniofacial tissue, they must be important in a context of intense cellular proliferation or migration during the establishment, growth, and fusion of the embryonic facial structures, before differentiation takes place. Consequently, these embryonic structures must be more susceptible to the action of environmental DNA-damaging agents, and the effects would be expected to be exacerbated if dysregulation of the biological DNA repair processes revealed by the transcriptomic and functional assays here are taken into account. Therefore, the combined effects of transcriptional dysregulation and of environmental factors must be critical in a tissue-and time-specific manner, which can explain why orofacial clefts have not been observed in knockout animal models for pivotal DNA repair genes, including *E2F1*. Under these circumstances, we hypothesise that the inability to appropriately deal with DNA damage would result in disturbances in cell proliferation and/or lead to apoptosis, disrupting lip and palate morphogenesis.

In conclusion, we report here that gene networks governing cellular defences against DNA damage may play a role in the aetiology of NSCL/P, in accordance with the idea that orofacial clefts and cancer may have overlapping aetiologies. The identification of E2F1 as a putative regulator behind the expression profiles detected in this work reinforces the existence of one or a few upstream elements underlying dysregulation in NSCL/P cells. It is not yet possible to determine if the few NSCL/P-associated variants previously identified through GWAS [3,4,5,6] can be accountable for dysregulating entire cellular functions as seen here; additionally, none of these variants are mapped to any of the DEGs identified in this work. Therefore, we speculate that alterations in a few unidentified upstream genetic or epigenetic regulators, combined with the effects of disease-associated variants, could be responsible for disturbances in regulatory or signalling events, such as those modulating activity of transcription factors like E2F1, or directly regulating entire pathways. Importantly, we

do not presuppose that dysregulation of the biological processes described here is fully responsible for the pathogenesis of NSCL/P; instead, we believe that they are part of a variety of mechanisms, such as perturbations in extracellular matrix biology [8,9], ultimately impairing orofacial morphogenesis. If regulatory anomalies are behind these disturbances, future research must focus on identifying such underlying genetic or epigenetic alterations that, upon interaction with environmental factors, result in cleft lip and palate. Consequently, a better understanding of the impact of these environmental agents, particularly those with genotoxic properties, will enable the development of preventive strategies in the future.

Materials and Methods

Ethics Statement

Ethical approval to extract stem cells from the dental pulp of deciduous teeth was obtained from the Biosciences Institute Research Ethics Committee (Protocol 037/2005) in the University of São Paulo. Samples were included only after signed informed consent by the parents or legal guardians. Those who declined to participate or otherwise did not participate were not disadvantaged in any way by not participating in the study. Care and use of mice were in compliance with the animal welfare guidelines approved by the Institute for Biosciences' Animal Care and Use Committee and the King's College Research Ethics Committee.

Cell Cultures

Deciduous teeth were non-invasively obtained from children in exfoliation period. Specimens were kept in DMEM/High Glucose supplemented with 1% penicillin-streptomycin solution (Life Technologies), and taken to the laboratory to be processed. Control teeth were obtained from donors attending odontopaediatric clinics in São Paulo, Brazil, while NSCL/P teeth were obtained from patients enrolled for surgical treatment at SOBRAPAR Institute, Campinas, Brazil. We considered an individual to be affected by NSCL/P if no malformations other than clefting of the upper lip with or without cleft palate were present. RNA extracted from cell cultures derived from a total of 6 controls and 7 NSCL/P patients was used for microarray assays and quantitative real-time PCR. The same 7 NSCL/P patients and 2 novel control cell cultures in addition to 3 of the 6 aforementioned control samples were submitted to flow cytometry quantitation of γ-H2AX. Additional 4 NSCL/P and 6 control samples were used for qRT-PCR during exposure to H_2O_2 (See Table S5 for more details regarding the samples).

Dental pulp stem cell cultures were established according to previously published protocols. The primary culture establishment protocols used in our laboratory are reproducible and consistent with regard to the immunophenotype and differentiation potential of the cell populations [9,78]. Cells were cultured in DMEM-F12 (Life Technologies) supplemented with 15% Foetal Bovine Serum (HyClone), 1% Non-essential aminoacids solution (Life Technologies), 1% penicillin-streptomycin solution (Life Technologies), in a humidified incubator at 37°C and 5% CO_2. For storage, cells were frozen in medium containing 90% FBS and 10% DMSO (LGC Biotecnologia). For RNA extraction, frozen cells were thawed and grown until 80% confluent in a 75 cm^2 culture flask. Microarray, qRT-PCR and flow cytometry experiments were conducted using cells between the 4^{th} and 8^{th} passage. During routine culture, cell populations exhibited spindle-shaped morphology and did not show significant morphological changes or cell death. We used asynchronous cells in all experiments.

In order to ensure that the transcriptional profiles were not biased by proliferative differences between controls and NSCL/P cells, 3 NSCL/P (F4243.1; F4244.1; F4293.1) and 3 control (F4217.1; F6119.1; F6032.1) samples were randomly chosen for proliferation assays. A total of 10^4 cells/cm^2 were seeded into 12-well plates (Corning). The following day, medium was changed and cells were harvested at days 0, 2, 3, 4, and 5 post-seeding, fixed in 1% paraformaldehyde, and counted using a flow cytometer (Guava). The results did not reveal significant differences between NSCL/P and controls (repeated measures two-way ANOVA, no interaction between factors; $F = 0.3701$, $p > 0.05$; Fig. S2).

RNA Extraction and Microarray Hybridisation

Total RNA isolation was performed with NucleoSpin RNA II kit (Macherey-Nagel), following manufacturer's recommendations. RNA quality and concentration were assessed using Nanodrop 1000 and agarose gel electrophoresis. Only RNA samples with absorbance ratio 260/280>1.8, preserved rRNA ratio (28S/18S) and no signs of degradation were used.

Expression measurements were performed using the Affymetrix Human Gene 1.0 ST array, which interrogates 28,869 transcripts, followed by RNA labelling and hybridisation protocols as recommended by the manufacturer. After array scanning, quality control was performed with the GCOS software (Affymetrix) according to the manufacturer's recommendations. Raw gene expression data are available at http://www.ncbi.nlm.nih.gov/geo/, under accession code GSE42589.

Microarray Data Processing and Mining

Gene expression values were obtained using the three-step Robust Multi-array Average (RMA) pre-processing method, implemented in the Affy package in R/Bioconductor [79]. DEGs were acquired using two algorithms: SAM and Rank Products both included in the MeV (MultiExperiment Viewer) software. SAM is a t-test based method in which mean and variance are taken into account in DEG selection [80]. In contrast, Rank Products is a ranking-based method, which enables the identification of consistent differences, even if only in a subgroup of samples under analysis [81]. Genes selected by Rank Products do not necessarily exhibit homogeneous expression levels within test and control groups, and therefore, this analysis is suitable for detecting differential expression in complex diseases [9,82]. Due to the complexity of the disease studied in this work, we decided to use both approaches in order to interrogate genes that are altered in all affected individuals analysed as well as genes altered in only a subgroup of them. Since SAM is a more conservative method, its p-value threshold was set at 0.05 while Rank Products' was set at 0.01. Both were adjusted for multiple testing with the FDR (False Discovery Rate) method [83]. As the fold change calculation differs between the SAM and Rank Products methods, we calculated it for each gene by subtracting the average of the (log) control values from the average of the (log) case values (Avg(cases)-Avg(controls)).

Transcriptome Analysis

We performed functional annotation and network analysis using IPA (http://www.ingenuity.com). We used the following parameters: Molecules per Network = 35; Networks per Analysis = 25; direct relationships only; "Ingenuity Expert Information" and "Ingenuity Supported Third Party Information" (including "miRNA-mRNA interactions", "protein-protein interactions", and "additional information") data sources.

Supervised clustering was performed using EXPANDER (EXpression Analyzer and DisplayER - http://acgt.cs.tau.ac.il/expander/).We selected the probe matching the BRCA1 gene and set "expected cluster size" to 30. Gene Ontology (GO) enrichment analysis was executed with TANGO (Tool for ANalysis of GO enrichment), with the whole genome as the background set, and bootstrap-adjusted p-value = 0.001. Transcription factor binding site enrichment analysis was carried out using PRIMA (PRomoter Integration in Microarray Analysis), avoiding coding regions, with hit range between –1000 and +200, all genes as background, and Bonferroni-adjusted p-value threshold <0.05. These tools are also available in the EXPANDER software.

FANTOM4 (http://fantom.gsc.riken.jp/4/) was used to validate transcription factor-gene interactions. The FANTOM4 database contains transcriptomic and deep-CAGE information of differentiating THP-1 cell lines, as well as other published data, such as ChIP-chip [84]. We searched only for ChIP-chip experimental data, at t = 0 hours of differentiation.

qRT-PCR Assays Performed on Cell Cultures

Two micrograms of total RNA extracted from each cell culture were converted into cDNA using Superscript II, according to the manufacturer's recommendations. qRT-PCR reactions were performed in duplicates with final volume of 25 µL, using 20 ng cDNA, 2X SYBR Green PCR Master Mix, and 50 nM –200 nM of each primer. Fluorescence was detected using ABI Prism 7500 Sequence Detection System, under standard temperature protocol. Primer pairs were designed with Primer-BLAST (http://www.ncbi.nlm.nih.gov/tools/primer-blast/; primer sequences in Table S6), and their amplification efficiencies (E) was determined by serial cDNA dilutions expressed in $\log_{10}$ in which $E = 10^{-1/\text{slope}}$. Expression of target genes was assessed relative to a calibrator cDNA (ΔCt). Finally, GeNorm v3.4 [85] was used to determine the most stable endogenous controls (among *GAPDH*, *HPRT1*, *SDHA*, *HMBS*), and calculate normalisation factors for each sample. The final expression values were determined based on a previous method [86], dividing $E^{-\Delta Ct}$ by the corresponding normalisation factor. To compare the expression between control and NSCL/P groups, we applied a Student's t-test with Welch's correction. Primers and reagents were supplied by Life Technologies.

DSB Quantitation and Assessment of Cell Cycle Distribution

NSCL/P and control cells were seeded into 6-well plates (Corning), in duplicates (10^4 cells/cm^2). The next day, cells were rinsed with PBS, and the culture medium was replaced by medium containing 100uM of freshly diluted H_2O_2 (Merck), followed by incubation for 6 and 24 hours in the dark, at 37°C/5% CO_2, to stimulate DSB formation. Cells were harvested by trypsin incubation and fixed in 4% paraformaldehyde on ice for 15 minutes, followed by fixation in 70% ethanol overnight at −20°C. DSB quantification was performed based on a previously published protocol [87]. After complete fixation, cells were double-stained with PI (Propidium Iodide) and anti-γ-H2AX (Anti-phospho-H2A.X Ser139 clone JBW301 FITC conjugate, Millipore), in order to ascertain cell cycle distribution and DSB formation, respectively. Appropriate calibrators were applied for each individual (unstained sample; PI-stained- and anti-γ-H2AX -stained-only samples), and at least 5000 events were acquired. Data were analysed with Guava Express PRO software (Millipore) and gated to remove debris and cell clumps. To sort cells positively stained for γ-H2AX, we established a threshold using untreated cells of the same individual, below which ~98% of the cells expressed γ-H2AX (intrinsic DSB formation); cells exposed to H_2O_2 and located above this threshold were considered positive for γ-H2AX. Sub-G1 events were quantified to estimate the number of apoptotic cells. H2AX profiles were compared using a Student's t-test with Welch's correction, whilst differences in sub-G1 cells were assessed using two-way ANOVA (subgroups×treatment) with Bonferroni post-tests for multiple comparisons.

qRT-PCR and RNA in situ Hybridisation Studies in Mouse Embryos

Palatal shelves were dissected from CD1 mouse embryos at different stages of development: E11.5 (initial growth), E14.5 (period of fusion), and E17.5 (after complete formation), and divided into pools which were submitted to RNA extraction and conversion to cDNA. Gene expression levels were assessed by qRT-PCR, using appropriate mouse endogenous controls for normalisation (*B2m*, *Tbp*, *Tubb5* and *Ywhaz*; primer sequences in Table S6). Procedures were carried out as previously described. One-way ANOVA with Bonferroni post-tests was applied to compare mean expression values.

Whole-mount *in situ* hybridisation studies were carried out to E10.5, E11.5, E12.5 and E13.5 CD1 strain mouse embryos as previously described [88]. At E12.5 and E13.5 the palatal shelves were isolated to increase probe penetration. The embryonic tissues were treated with 10 µg/mL proteinase K for 20 (E10.5), 30 (E11.5), 45 (E12.5) and 60 minutes (E13.5). Whole-mounted embryos were fixed, embedded in 20% gelatin and were vibratome-sectioned at 40 µm. 900bp-1kb cDNA templates for ribroprobe synthesis were generated by PCR using the following primers: *Brca1* (5′GTCCTCGGCGCTTGGAAGTACG3′, 5′AACGACAGGCAGGTTCCCAGC3′), *Rad51* (5′GTGAGGATTTGGCGGGATTTCC3′, 5′CACTACTCAGGGCGGGGAGAGC3′); *E2f1* (5′CGCTGGTAGCAGTGGGCCAT3′, 5′ACCCCACGAGGCCCTTGACT3′) and were cloned in the pCRII-TOPO Vector. Antisense ribroprobe transcripts were synthesised with either T7 (*E2f1*) or Sp6 (*Bcra1* and *Rad51*) RNA polymerases.

Supporting Information

Figure S1 DNA repair genes are expressed in the developing palatal shelves. Gene expression of key DNA repair genes was assessed in murine palatal shelves at various stages of development, using qRT-PCR. (*) $p<0.05$.
(TIF)

Figure S2 NSCL/P and control cells exhibit similar proliferation profiles. Proliferation assays were performed in 3 NSCL/P and 3 control cells, and revealed no significant differences (repeated measures two-way ANOVA, $p>0.05$).
(TIF)

Figure S3 Negative control for the *in situ* hybridisation studies. Sagittal views of negative sense controls performed on E11.5 and E12.5 mouse embryos, showing no staining.
(TIF)

Table S1 List of DEGs obtained by comparing NSCL/P and control cells. For DEGs selected by both SAM and Rank Products, the highest p-value between the two algorithms is shown. (*) Genes selected by SAM; (°) Genes selected by Rank Products. Information regarding probe sets lacking annotation are left blank.
(PDF)

Table S2 Top enriched functions in the IPA interaction network. Detailed list of the top functions enriched in the

highest-scoring IPA network. The significance values for each biological function is a measure of the likelihood of that function being associated with the genes in the network due to chance, calculated using a right-tailed Fisher's Exact Test.
(PDF)

Table S3 Validation of the microarray assays. Genes submitted to qRT-PCR to validate the microarray results, and their respective p-values. (*) Genes pertaining to the *BRCA1* similarity cluster.
(PDF)

Table S4 DEGs involved in the oxidative generation and repair of DSBs. Gene symbol, summarised function and literature reference of DEGs directly or indirectly involved in oxidative stress and homologous recombination repair of oxidatively-generated DSBs.
(PDF)

Table S5 Cell cultures used in the study. Laboratory code, gender, and clinical status of the samples used in the microarray assays and their validation by qRT-PCR, flow cytometry, and qRT-PCR during exposure to H_2O_2. (*) CL = Cleft Lip; CLP = Cleft Lip and Palate; UL = Unilateral Left; UR = Unilateral Right.
(PDF)

Table S6 Primer sequences used for qRT-PCR experiments.
(PDF)

Acknowledgments

The authors would like to express their gratitude to: Mrs. Constância Urbani, for secretarial assistance; Vanessa Sato and Wagner Falciano, for financial management; Prof. Luis Eduardo Soares Netto, PhD and Erika Yeh, PhD, for their suggestions regarding the manuscript; Angela May Suzuki, and André Veloso Rueda, MSc, for their assistance with flow cytometry and statistical analyses, respectively. Finally, Mrs. Regina Bueno for editing the figures.

Author Contributions

Conceived and designed the experiments: GSK LA DYS LCAL PFW CFM MRPB. Performed the experiments: GSK LA BVPA SGF AK PFW. Analyzed the data: GSK LA DYS PFW AK. Contributed reagents/materials/analysis tools: DFB CERA LCAL CFM. Wrote the paper: GSK LA PFW MRPB.

References

1. Mossey PA, Little J, Munger RG, Dixon MJ, Shaw WC (2009) Cleft lip and palate. Lancet 374: 1773–1785.
2. Brito LA, Cruz LA, Rocha KM, Barbara LK, Silva CB, et al. (2011) Genetic contribution for non-syndromic cleft lip with or without cleft palate (NS CL/P) in different regions of Brazil and implications for association studies. Am J Med Genet A 155A: 1581–1587.
3. Birnbaum S, Ludwig KU, Reutter H, Herms S, Steffens M, et al. (2009) Key susceptibility locus for nonsyndromic cleft lip with or without cleft palate on chromosome 8q24. Nat Genet 41: 473–477.
4. Grant SF, Wang K, Zhang H, Glaberson W, Annaiah K, et al. (2009) A genome-wide association study identifies a locus for nonsyndromic cleft lip with or without cleft palate on 8q24. J Pediatr 155: 909–913.
5. Mangold E, Ludwig KU, Birnbaum S, Baluardo C, Ferrian M, et al. (2009) Genome-wide association study identifies two susceptibility loci for nonsyndromic cleft lip with or without cleft palate. Nat Genet 42: 24–26.
6. Beaty TH, Murray JC, Marazita ML, Munger RG, Ruczinski I, et al. (2009) A genome-wide association study of cleft lip with and without cleft palate identifies risk variants near MAFB and ABCA4. Nat Genet 42: 525–529.
7. Cookson W, Liang L, Abecasis G, Moffatt M, Lathrop M (2009) Mapping complex disease traits with global gene expression. Nat Rev Genet 10: 184–194.
8. Baroni T, Bellucci C, Lilli C, Pezzetti F, Carinci F, et al. (2010) Human cleft lip and palate fibroblasts and normal nicotine-treated fibroblasts show altered in vitro expressions of genes related to molecular signaling pathways and extracellular matrix metabolism. J Cell Physiol 222: 748–756.
9. Bueno DF, Sunaga DY, Kobayashi GS, Aguena M, Raposo-Amaral CE, et al. (2010) Human stem cell cultures from cleft lip/palate patients show enrichment of transcripts involved in extracellular matrix modeling by comparison to controls. Stem Cell Rev 7: 446–457.
10. Marinucci L, Balloni S, Bodo M, Carinci F, Pezzetti F, et al. (2009) Patterns of some extracellular matrix gene expression are similar in cells from cleft lip-palate patients and in human palatal fibroblasts exposed to diazepam in culture. Toxicology 257: 10–16.
11. Pezzetti F, Carinci F, Palmieri A, Vizzotto L, Moscheni C, et al. (2009) Diphenylhydantoin plays a role in gene expression related to cytoskeleton and protein adhesion in human normal palate fibroblasts. Pathology 41: 261–268.
12. Jiang R, Bush JO, Lidral AC (2006) Development of the upper lip: morphogenetic and molecular mechanisms. Dev Dyn 235: 1152–1166.
13. Greene RM, Pisano MM (2010) Palate morphogenesis: Current understanding and future directions. Birth Defects Res C Embryo Today 90: 133–154.
14. Yu W, Serrano M, Miguel SS, Ruest LB, Svoboda KK (2009) Cleft lip and palate genetics and application in early embryological development. Indian J Plast Surg 42 Suppl: S35–50.
15. Zhu JL, Basso O, Hasle H, Winther JF, Olsen JH, et al. (2002) Do parents of children with congenital malformations have a higher cancer risk? A nationwide study in Denmark. Br J Cancer 87: 524–528.
16. Taioli E, Ragin C, Robertson L, Linkov F, Thurman NE, et al. (2010) Cleft lip and palate in family members of cancer survivors. Cancer Invest 28: 958–962.
17. Bille C, Winther JF, Bautz A, Murray JC, Olsen J, et al. (2005) Cancer risk in persons with oral cleft–a population-based study of 8,093 cases. Am J Epidemiol 161: 1047–1055.
18. Vieira AR, Khaliq S, Lace B (2012) Risk of cancer in relatives of children born with isolated cleft lip and palate. Am J Med Genet A 158A: 1503–1504.
19. Rinne T, Brunner HG, van Bokhoven H (2007) p63-associated disorders. Cell Cycle 6: 262–268.
20. Restivo G, Nguyen BC, Dziunycz P, Ristorcelli E, Ryan RJ, et al. (2011) IRF6 is a mediator of Notch pro-differentiation and tumour suppressive function in keratinocytes. EMBO J 30: 4571–4585.
21. Letra A, Bjork B, Cooper ME, Szabo-Rogers H, Deleyiannis FW, et al. (2012) Association of AXIN2 with non-syndromic oral clefts in multiple populations. J Dent Res 91: 473–478.
22. Krenzlin H, Demuth I, Salewsky B, Wessendorf P, Weidele K, et al. (2012) DNA damage in Nijmegen Breakage Syndrome cells leads to PARP hyperactivation and increased oxidative stress. PLoS Genet 8: e1002557.
23. Ferone G, Thomason HA, Antonini D, De Rosa L, Hu B, et al. (2012) Mutant p63 causes defective expansion of ectodermal progenitor cells and impaired FGF signalling in AEC syndrome. EMBO Mol Med 4: 192–205.
24. Vogelaar IP, Figueiredo J, van Rooij IA, Simoes-Correia J, van der Post RS, et al. (2013) Identification of germline mutations in the cancer predisposing gene CDH1 in patients with orofacial clefts. Hum Mol Genet 22: 919–926.
25. Cordero DR, Brugmann S, Chu Y, Bajpai R, Jame M, et al. (2011) Cranial neural crest cells on the move: their roles in craniofacial development. Am J Med Genet A 155A: 270–279.
26. Komada M (2012) Sonic hedgehog signaling coordinates the proliferation and differentiation of neural stem/progenitor cells by regulating cell cycle kinetics during development of the neocortex. Congenit Anom (Kyoto) 52: 72–77.
27. Janebodin K, Horst OV, Ieronimakis N, Balasundaram G, Reesukumal K, et al. (2011) Isolation and characterization of neural crest-derived stem cells from dental pulp of neonatal mice. PLoS One 6: e27526.
28. Yarden RI, Papa MZ (2006) BRCA1 at the crossroad of multiple cellular pathways: approaches for therapeutic interventions. Mol Cancer Ther 5: 1396–1404.
29. Wells PG, McCallum GP, Chen CS, Henderson JT, Lee CJ, et al. (2009) Oxidative stress in developmental origins of disease: teratogenesis, neurodevelopmental deficits, and cancer. Toxicol Sci 108: 4–18.
30. Sharma R, Yang Y, Sharma A, Awasthi S, Awasthi YC (2004) Antioxidant role of glutathione S-transferases: protection against oxidant toxicity and regulation of stress-mediated apoptosis. Antioxid Redox Signal 6: 289–300.
31. Weyemi U, Dupuy C (2012) The emerging role of ROS-generating NADPH oxidase NOX4 in DNA-damage responses. Mutat Res 751: 77–81.
32. Yu H, Liu Z, Zhou H, Dai W, Chen S, et al. (2012) JAK-STAT pathway modulates the roles of iNOS and COX-2 in the cytoprotection of early phase of hydrogen peroxide preconditioning against apoptosis induced by oxidative stress. Neurosci Lett 529: 166–171.
33. Li H, Sekine M, Seng S, Avraham S, Avraham HK (2009) BRCA1 interacts with Smad3 and regulates Smad3-mediated TGF-beta signaling during oxidative stress responses. PLoS One 4: e7091.
34. Uno S, Masai H (2011) Efficient expression and purification of human replication fork-stabilizing factor, Claspin, from mammalian cells: DNA-binding activity and novel protein interactions. Genes Cells 16: 842–856.
35. Saha T, Rih JK, Roy R, Ballal R, Rosen EM (2010) Transcriptional regulation of the base excision repair pathway by BRCA1. J Biol Chem 285: 19092–19105.
36. Lydeard JR, Lipkin-Moore Z, Sheu YJ, Stillman B, Burgers PM, et al. (2010) Break-induced replication requires all essential DNA replication factors except those specific for pre-RC assembly. Genes Dev 24: 1133–1144.

37. Maiorano D, Lutzmann M, Mechali M (2006) MCM proteins and DNA replication. Curr Opin Cell Biol 18: 130–136.
38. Linger RJ, Kruk PA (2010) BRCA1 16 years later: risk-associated BRCA1 mutations and their functional implications. FEBS J 277: 3086–3096.
39. Seifert M, Reichrath J (2006) The role of the human DNA mismatch repair gene hMSH2 in DNA repair, cell cycle control and apoptosis: implications for pathogenesis, progression and therapy of cancer. J Mol Histol 37: 301–307.
40. Yata K, Esashi F (2009) Dual role of CDKs in DNA repair: to be, or not to be. DNA Repair (Amst) 8: 6–18.
41. Biswas AK, Johnson DG (2011) Transcriptional and nontranscriptional functions of E2F1 in response to DNA damage. Cancer Res 72: 13–17.
42. Iaquinta PJ, Lees JA (2007) Life and death decisions by the E2F transcription factors. Curr Opin Cell Biol 19: 649–657.
43. Kusek JC, Greene RM, Nugent P, Pisano MM (2000) Expression of the E2F family of transcription factors during murine development. Int J Dev Biol 44: 267–277.
44. Dixon K, Kopras E (2004) Genetic alterations and DNA repair in human carcinogenesis. Semin Cancer Biol 14: 441–448.
45. Rosen EM, Fan S, Ma Y (2006) BRCA1 regulation of transcription. Cancer Lett 236: 175–185.
46. Thompson ME, Jensen RA, Obermiller PS, Page DL, Holt JT (1995) Decreased expression of BRCA1 accelerates growth and is often present during sporadic breast cancer progression. Nat Genet 9: 444–450.
47. Lee WY, Jin YT, Chang TW, Lin PW, Su IJ (1999) Immunolocalization of BRCA1 protein in normal breast tissue and sporadic invasive ductal carcinomas: a correlation with other biological parameters. Histopathology 34: 106–112.
48. Mueller CR, Roskelley CD (2003) Regulation of BRCA1 expression and its relationship to sporadic breast cancer. Breast Cancer Res 5: 45–52.
49. Calin G, Herlea V, Barbanti-Brodano G, Negrini M (1998) The coding region of the Bloom syndrome BLM gene and of the CBL proto-oncogene is mutated in genetically unstable sporadic gastrointestinal tumors. Cancer Res 58: 3777–3781.
50. Borlado LR, Mendez J (2008) CDC6: from DNA replication to cell cycle checkpoints and oncogenesis. Carcinogenesis 29: 237–243.
51. Gao LB, Pan XM, Li LJ, Liang WB, Zhu Y, et al. (2010) RAD51 135G/C polymorphism and breast cancer risk: a meta-analysis from 21 studies. Breast Cancer Res Treat 125: 827–835.
52. Helleday T, Lo J, van Gent DC, Engelward BP (2007) DNA double-strand break repair: from mechanistic understanding to cancer treatment. DNA Repair (Amst) 6: 923–935.
53. Llorente B, Smith CE, Symington LS (2008) Break-induced replication: what is it and what is it for? Cell Cycle 7: 859–864.
54. Pardo B, Gomez-Gonzalez B, Aguilera A (2009) DNA repair in mammalian cells: DNA double-strand break repair: how to fix a broken relationship. Cell Mol Life Sci 66: 1039–1056.
55. Langerak P, Russell P (2011) Regulatory networks integrating cell cycle control with DNA damage checkpoints and double-strand break repair. Philos Trans R Soc Lond B Biol Sci 366: 3562–3571.
56. Mao Z, Bozzella M, Seluanov A, Gorbunova V (2008) Comparison of nonhomologous end joining and homologous recombination in human cells. DNA Repair (Amst) 7: 1765–1771.
57. Letavayova L, Markova E, Hermanska K, Vlckova V, Vlasakova D, et al. (2006) Relative contribution of homologous recombination and non-homologous end-joining to DNA double-strand break repair after oxidative stress in Saccharomyces cerevisiae. DNA Repair (Amst) 5: 602–610.
58. Wang Y, Cortez D, Yazdi P, Neff N, Elledge SJ, et al. (2000) BASC, a super complex of BRCA1-associated proteins involved in the recognition and repair of aberrant DNA structures. Genes Dev 14: 927–939.
59. Bahado-Singh RO, Schenone M, Cordoba M, Shieh WS, Maulik D, et al. (2011) Male gender significantly increases risk of oxidative stress related congenital anomalies in the non-diabetic population. J Matern Fetal Neonatal Med 24: 687–691.
60. Nulman I, Scolnik D, Chitayat D, Farkas LD, Koren G (1997) Findings in children exposed in utero to phenytoin and carbamazepine monotherapy: independent effects of epilepsy and medications. Am J Med Genet 68: 18–24.
61. Winn LM, Kim PM, Nickoloff JA (2003) Oxidative stress-induced homologous recombination as a novel mechanism for phenytoin-initiated toxicity. J Pharmacol Exp Ther 306: 523–527.
62. Alsdorf R, Wyszynski DF (2005) Teratogenicity of sodium valproate. Expert Opin Drug Saf 4: 345–353.
63. DeRoo LA, Wilcox AJ, Drevon CA, Lie RT (2008) First-trimester maternal alcohol consumption and the risk of infant oral clefts in Norway: a population-based case-control study. Am J Epidemiol 168: 638–646.
64. Leite IC, Koifman S (2009) Oral clefts, consanguinity, parental tobacco and alcohol use: a case-control study in Rio de Janeiro, Brazil. Braz Oral Res 23: 31–37.
65. Sha K, Winn LM (2010) Characterization of valproic acid-initiated homologous recombination. Birth Defects Res B Dev Reprod Toxicol 89: 124–132.
66. Tung EW, Winn LM (2011) Valproic acid increases formation of reactive oxygen species and induces apoptosis in postimplantation embryos: a role for oxidative stress in valproic acid-induced neural tube defects. Mol Pharmacol 80: 979–987.
67. Park SC, Lim JY, Jeen YT, Keum B, Seo YS, et al. (2012) Ethanol-induced DNA damage and repair-related molecules in human intestinal epithelial Caco-2 cells. Mol Med Report 5: 1027–1032.
68. Kachhap SK, Rosmus N, Collis SJ, Kortenhorst MS, Wissing MD, et al. (2010) Downregulation of homologous recombination DNA repair genes by HDAC inhibition in prostate cancer is mediated through the E2F1 transcription factor. PLoS One 5: e11208.
69. Wehby GL, Murray JC (2010) Folic acid and orofacial clefts: a review of the evidence. Oral Dis 16: 11–19.
70. Joshi R, Adhikari S, Patro BS, Chattopadhyay S, Mukherjee T (2001) Free radical scavenging behavior of folic acid: evidence for possible antioxidant activity. Free Radic Biol Med 30: 1390–1399.
71. Gliszczynska-Swiglo A, Muzolf M (2007) pH-Dependent radical scavenging activity of folates. J Agric Food Chem 55: 8237–8242.
72. Bliek BJ, Steegers-Theunissen RP, Blok LJ, Santegoets LA, Lindemans J, et al. (2008) Genome-wide pathway analysis of folate-responsive genes to unravel the pathogenesis of orofacial clefting in man. Birth Defects Res A Clin Mol Teratol 82: 627–635.
73. Kondo S, Schutte BC, Richardson RJ, Bjork BC, Knight AS, et al. (2002) Mutations in IRF6 cause Van der Woude and popliteal pterygium syndromes. Nat Genet 32: 285–289.
74. Washbourne BJ, Cox TC (2006) Expression profiles of cIRF6, cLHX6 and cLHX7 in the facial primordia suggest specific roles during primary palatogenesis. BMC Dev Biol 6: 18.
75. Rocha CR, Lerner LK, Okamoto OK, Marchetto MC, Menck CF (2012) The role of DNA repair in the pluripotency and differentiation of human stem cells. Mutat Res.
76. Feng W, Leach SM, Tipney H, Phang T, Geraci M, et al. (2009) Spatial and temporal analysis of gene expression during growth and fusion of the mouse facial prominences. PLoS One 4: e8066.
77. Albino D, Brizzolara A, Moretti S, Falugi C, Mirisola V, et al. (2011) Gene expression profiling identifies eleven DNA repair genes down-regulated during mouse neural crest cell migration. Int J Dev Biol 55: 65–72.
78. de Mendonca Costa A, Bueno DF, Martins MT, Kerkis I, Kerkis A, et al. (2008) Reconstruction of large cranial defects in nonimmunosuppressed experimental design with human dental pulp stem cells. J Craniofac Surg 19: 204–210.
79. Irizarry RA, Hobbs B, Collin F, Beazer-Barclay YD, Antonellis KJ, et al. (2003) Exploration, normalization, and summaries of high density oligonucleotide array probe level data. Biostatistics 4: 249–264.
80. Tusher VG, Tibshirani R, Chu G (2001) Significance analysis of microarrays applied to the ionizing radiation response. Proc Natl Acad Sci U S A 98: 5116–5121.
81. Breitling R, Armengaud P, Amtmann A, Herzyk P (2004) Rank products: a simple, yet powerful, new method to detect differentially regulated genes in replicated microarray experiments. FEBS Lett 573: 83–92.
82. Raj A, Rifkin SA, Andersen E, van Oudenaarden A (2010) Variability in gene expression underlies incomplete penetrance. Nature 463: 913–918.
83. Benjamini Y, Hochberg Y (1995) Controlling the False Discovery Rate: A Practical and Powerful Approach to Multiple Testing. Journal of the Royal Statistical Society Series B (Methodological) 57: 289–300.
84. Severin J, Waterhouse AM, Kawaji H, Lassmann T, van Nimwegen E, et al. (2009) FANTOM4 EdgeExpressDB: an integrated database of promoters, genes, microRNAs, expression dynamics and regulatory interactions. Genome Biol 10: R39.
85. Vandesompele J, De Preter K, Pattyn F, Poppe B, Van Roy N, et al. (2002) Accurate normalization of real-time quantitative RT-PCR data by geometric averaging of multiple internal control genes. Genome Biol 3: RESEARCH0034.
86. Pfaffl MW (2001) A new mathematical model for relative quantification in real-time RT-PCR. Nucleic Acids Res 29: e45.
87. Huang X, Darzynkiewicz Z (2006) Cytometric assessment of histone H2AX phosphorylation: a reporter of DNA damage. Methods Mol Biol 314: 73–80.
88. Dastjerdi A, Robson L, Walker R, Hadley J, Zhang Z, et al. (2007) Tbx1 regulation of myogenic differentiation in the limb and cranial mesoderm. Dev Dyn 236: 353–363.

SUPPLEMENTARY FIGURES

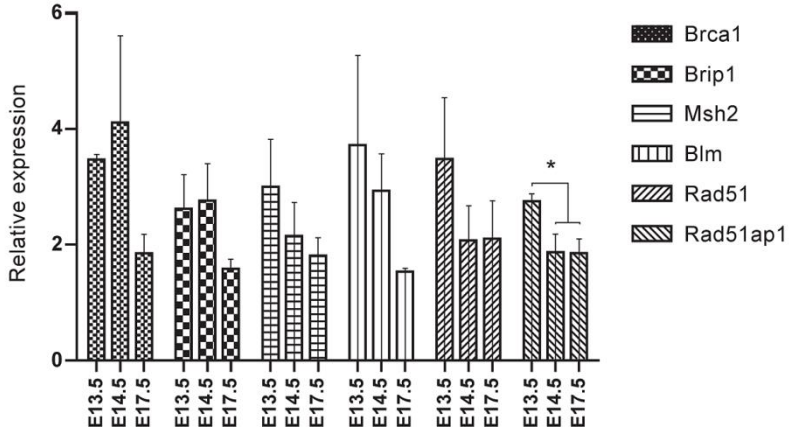

Figure S2: DNA repair genes are expressed in the developing palatal shelves. Gene expression of key DNA repair genes was assessed in murine palatal shelves at various stages of development, through RT-qPCR. (*) $p<0.05$.

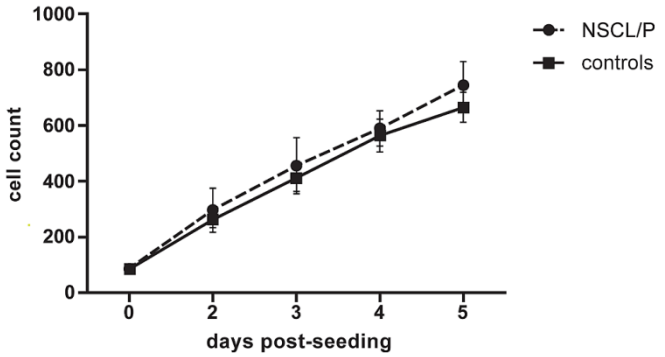

Figure S3: NSCL/P and control cells exhibit similar proliferation profiles. Proliferation assays were performed in 3 NSCL/P and 3 control cells, and revealed no significant differences (two-way ANOVA, $p>0.05$).

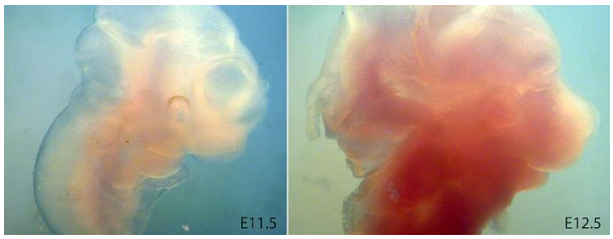

Figure S3: Negative control for the in situ hybridisation studies. Sagittal views of negative sense controls performed on E11.5 and E12.5 mouse embryos, showing no staining.

SUPPLEMENTARY TABLES

Table SI: List of DEGs obtained by comparing NSCL/P and control cells

AffyID	Symbol	Entrez Gene Name	Fold change	P-value
8112045 ° *	ESM1	endothelial cell-specific molecule 1	-5.330 ±2.83	0.000
7922976 ° *	PTGS2	prostaglandin-endoperoxide synthase 2 (prostaglandin G/H synthase and cyclooxygenase)	-3.709 ±2.11	0.000
8067233 ° *	PMEPA1	prostate transmembrane protein, androgen induced 1	-3.259 ±2.01	0.000
8142981 ° *	PODXL	podocalyxin-like	-2.920 ±1.89	0.000
8116780 ° *	DSP	desmoplakin	-2.736 ±1.8	0.000
8100798 ° *	SULT1B1	sulfotransferase family, cytosolic, 1B, member 1	-2.660 ±2.37	0.000
7915612 ° *	PTCH2	patched 2	-2.598 ±1.51	0.000
8124527 ° *	HIST1H1B	histone cluster 1, H1b	-2.587 ±1.51	0.000
7973067 ° *	PNP	purine nucleoside phosphorylase	-2.578 ±1.45	0.000
8151871 ° *	CCNE2	cyclin E2	-2.577 ±1.44	0.000
8091243 ° *	PCOLCE2 (includes EG:2657	procollagen C-endopeptidase enhancer 2	-2.568 ±1.58	0.000
7924461 ° *			-2.567 ±1.54	0.000
7939237 ° *	C11orf41	chromosome 11 open reading frame 41	-2.485 ±1.39	0.000
8059376 ° *	SERPINE2	serpin peptidase inhibitor, clade E (nexin, plasminogen activator inhibitor type 1), member 2	-2.463 ±1.56	0.000
8105267 ° *	ITGA2	integrin, alpha 2 (CD49B, alpha 2 subunit of VLA-2 receptor)	-2.440 ±1.69	0.000
8045688 ° *	TNFAIP6	tumor necrosis factor, alpha-induced protein 6	-2.436 ±1.45	0.000
7952785 ° *	OPCML	opioid binding protein/cell adhesion molecule-like	-2.431 ±1.67	0.000
7948902 ° *	SNHG1	small nucleolar RNA host gene 1 (non-protein coding)	-2.418 ±1.49	0.000
7939215 ° *	C11orf41	chromosome 11 open reading frame 41	-2.410 ±1.34	0.000
8180255 ° *			-2.404 ±1.33	0.000
8180321 ° *			-2.404 ±1.33	0.000
8145793 ° *	SNORD13	small nucleolar RNA, C/D box 13	-2.383 ±1.45	0.000
7936968 ° *	ADAM12	ADAM metallopeptidase domain 12	-2.339 ±1.67	0.000
7999754 ° *	XYLT1	xylosyltransferase I	-2.317 ±1.43	0.000
7981084 ° *	SERPINA9	serpin peptidase inhibitor, clade A (alpha-1 antiproteinase, antitrypsin), member 9	-2.307 ±1.28	0.000
7974689 ° *	DACT1	dapper, antagonist of beta-catenin, homolog 1 (Xenopus laevis)	-2.304 ±1.47	0.000
8086752 ° *			-2.279 ±1.5	0.001
8124388 ° *	HIST1H3A (includes others)	histone cluster 1, H3a	-2.273 ±1.29	0.001
7970793 ° *	SLC46A3	solute carrier family 46, member 3	-2.271 ±1.47	0.000
7909568 ° *	DTL	denticleless E3 ubiquitin protein ligase homolog (Drosophila)	-2.268 ±1.35	0.000
7897801 ° *	RNU5E-1	RNA, U5E small nuclear 1	-2.240 ±1.32	0.001
7996260 ° *			-2.233 ±1.63	0.000
8007071 ° *	CDC6 (includes EG:23834)	cell division cycle 6 homolog (S. cerevisiae)	-2.208 ±1.31	0.001
7976812 ° *	SNORD113-4	small nucleolar RNA, C/D box 113-4	-2.195 ±1.61	0.001
8154233 ° *	CD274	CD274 molecule	-2.184 ±1.49	0.001
8156043 ° *	PSAT1	phosphoserine aminotransferase 1	-2.151 ±1.28	0.001
7940147 ° *	FAM111B	family with sequence similarity 111, member B	-2.129 ±1.24	0.001
7953218 ° *	RAD51AP1	RAD51 associated protein 1	-2.120 ±1.26	0.001
8126798 °	GPR116	G protein-coupled receptor 116	-2.119 ±2.36	0.000
7919642 ° *	HIST2H2AB	histone cluster 2, H2ab	-2.102 ±1.2	0.002
8124391 ° *	HIST1H2AB/HIST1H2AE	histone cluster 1, H2ae	-2.098 ±1.24	0.002
8077499 ° *	LINC00312	long intergenic non-protein coding RNA 312	-2.086 ±1.51	0.001
7926259 ° *	MCM10 (includes EG:307126	minichromosome maintenance complex component 10	-2.078 ±1.2	0.002
8160431 ° *	MIR31HG	MIR31 host gene (non-protein coding)	-2.060 ±1.13	0.002
7950391 ° *	PGM2L1	phosphoglucomutase 2-like 1	-2.060 ±1.17	0.002
7943158 ° *	SCARNA9	small Cajal body-specific RNA 9	-2.060 ±1.27	0.002
7981978 ° *	SNORD116-15	small nucleolar RNA, C/D box 116-15	-2.054 ±1.23	0.002
8035838 ° *	ZNF724P	zinc finger protein 724, pseudogene	-2.037 ±1.15	0.002
8092640 ° *	RFC4	replication factor C (activator 1) 4, 37kDa	-2.022 ±1.08	0.002
8080847 ° *	C3orf14	chromosome 3 open reading frame 14	-2.018 ±1.11	0.002
8112376 ° *	CENPK	centromere protein K	-2.018 ±1.16	0.003
7981982 ° *	SNRPN	small nuclear ribonucleoprotein polypeptide N	-2.004 ±1.2	0.003
7981986 ° *	SNRPN	small nuclear ribonucleoprotein polypeptide N	-2.004 ±1.2	0.003
8083876 ° *	SKIL	SKI-like oncogene	-2.002 ±1.25	0.002
7927631 ° *	DKK1	dickkopf 1 homolog (Xenopus laevis)	-2.002 ±1.26	0.003
7922162 ° *	SLC19A2	solute carrier family 19 (thiamine transporter), member 2	-2.001 ±1.26	0.001
7998722 ° *	SNORD60	small nucleolar RNA, C/D box 60	-1.997 ±1.13	0.003
7906919 °	RGS4	regulator of G-protein signaling 4	-1.989 ±1.76	0.002
7929438 ° *	HELLS	helicase, lymphoid-specific	-1.976 ±1.18	0.004
7981976 ° *	SNORD116-14	small nucleolar RNA, C/D box 116-14	-1.967 ±1.25	0.004
8071212 ° *	CDC45	cell division cycle 45 homolog (S. cerevisiae)	-1.962 ±1.08	0.004
7910997 ° *	EXO1 (includes EG:26909)	exonuclease 1	-1.952 ±1.14	0.004
8061471 ° *	GINS1	GINS complex subunit 1 (Psf1 homolog)	-1.945 ±1.12	0.004
8138527 ° *	STEAP1B	STEAP family member 1B	-1.939 ±1.2	0.004
8030978 ° *	ZNF845	zinc finger protein 845	-1.938 ±1.23	0.004
7919269 ° *	GSTM2	glutathione S-transferase mu 2 (muscle)	-1.937 ±1.09	0.004
7919349 ° *	GSTM2	glutathione S-transferase mu 2 (muscle)	-1.937 ±1.09	0.004
8124385 ° *	HIST1H4A (includes others)	histone cluster 1, H4a	-1.937 ±1.11	0.004
7930980 °	PPAPDC1A	phosphatidic acid phosphatase type 2 domain containing 1A	-1.934 ±1.35	0.003
8140534 °	SEMA3C	sema domain, immunoglobulin domain (Ig), short basic domain, secreted, (semaphorin) 3C	-1.933 ±1.41	0.003
8004144 ° *	MIS12	MIS12, MIND kinetochore complex component, homolog (S. pombe)	-1.930 ±1.05	0.004
7952339 ° *	SNORD14C	small nucleolar RNA, C/D box 14C	-1.929 ±1.21	0.005
8081241 ° *	C3orf26	chromosome 3 open reading frame 26	-1.927 ±1.13	0.004
7995354 ° *	ORC6 (includes EG:23594)	origin recognition complex, subunit 6	-1.923 ±1.08	0.004
8127989 ° *	SNORD50B	small nucleolar RNA, C/D box 50B	-1.923 ±1.1	0.005
7948904 ° *	SNORD28	small nucleolar RNA, C/D box 28	-1.921 ±1.28	0.005
7986068 ° *	BLM	Bloom syndrome, RecQ helicase-like	-1.920 ±1.08	0.004
7973896 ° *	GSTM2	glutathione S-transferase mu 2 (muscle)	-1.918 ±1.05	0.005
7978568 ° *	GSTM2	glutathione S-transferase mu 2 (muscle)	-1.918 ±1.05	0.005
7915926 ° *	STIL	SCL/TAL1 interrupting locus	-1.915 ±1.15	0.004
7908072 °	LAMC2	laminin, gamma 2	-1.914 ±1.34	0.004
8141150 ° *	ASNS	asparagine synthetase (glutamine-hydrolyzing)	-1.913 ±1.11	0.004
7979710 ° *	PLEK2	pleckstrin 2	-1.913 ±1.12	0.004
7964271 ° *	PRIM1	primase, DNA, polypeptide 1 (49kDa)	-1.909 ±1.11	0.004
8015268 ° *	KRT34	keratin 34	-1.900 ±1.1	0.006
8095574 ° *	DCK	deoxycytidine kinase	-1.899 ±1.07	0.005
7964733 ° *	RPSAP52	ribosomal protein SA pseudogene 52	-1.899 ±1.22	0.005
8025402 ° *	ANGPTL4	angiopoietin-like 4	-1.898 ±1.06	0.004
8022674 ° *	CDH2	cadherin 2, type 1, N-cadherin (neuronal)	-1.895 ±1.26	0.003
7990345 °	SEMA7A	semaphorin 7A, GPI membrane anchor (John Milton Hagen blood group)	-1.883 ±1.37	0.002

8142975 °	mir-29	microRNA 29a	-1.883	±1.31	0.005
7981990 °			-1.881	±1.27	0.005
8102787 ° *			-1.878	±1.05	0.006
8041867 ° *	MSH2	mutS homolog 2, colon cancer, nonpolyposis type 1 (E. coli)	-1.872	±1.05	0.006
7965094 ° *	E2F7	E2F transcription factor 7	-1.868	±1.08	0.005
8052382 ° *	FANCL	Fanconi anemia, complementation group L	-1.860	±1.06	0.007
8079153 ° *	ABHD5	abhydrolase domain containing 5	-1.853	±1.02	0.007
7982792 ° *	RAD51	RAD51 homolog (S. cerevisiae)	-1.851	±1.03	0.007
7898375 ° *	GSTM2	glutathione S-transferase mu 2 (muscle)	-1.851	±1.03	0.007
7898411 ° *	GSTM2	glutathione S-transferase mu 2 (muscle)	-1.851	±1.03	0.007
7912800 ° *	GSTM2	glutathione S-transferase mu 2 (muscle)	-1.851	±1.03	0.007
7912850 ° *	GSTM2	glutathione S-transferase mu 2 (muscle)	-1.851	±1.03	0.007
7919576 ° *	GSTM2	glutathione S-transferase mu 2 (muscle)	-1.851	±1.03	0.007
7974882 ° *	SYT16	synaptotagmin XVI	-1.839	±1.13	0.005
8144036 ° *	XRCC2	X-ray repair complementing defective repair in Chinese hamster cells 2	-1.832	±1.04	0.007
7976621 ° *	VRK1	vaccinia related kinase 1	-1.831	±1	0.007
8139632 ° *	FIGNL1	fidgetin-like 1	-1.824	±1.06	0.008
8097449 °	PCDH10	protocadherin 10	-1.823	±1.64	0.005
8003298 ° *	SLC7A5	solute carrier family 7 (amino acid transporter light chain, L system), member 5	-1.819	±1.09	0.007
8006187 ° *	ATAD5	ATPase family, AAA domain containing 5	-1.816	±1.11	0.007
7974337 *			-1.814	±1.14	0.000
8086880 ° *	CDC25A	cell division cycle 25 homolog A (S. pombe)	-1.807	±0.99	0.009
8015769 ° *	BRCA1	breast cancer 1, early onset	-1.802	±1.08	0.009
7983306 ° *	WDR76	WD repeat domain 76	-1.801	±1.09	0.009
8127987 °	SNORD50A	small nucleolar RNA, C/D box 50A	-1.801	±1.15	0.009
8117368 °	HIST1H4A (includes others)	histone cluster 1, H4a	-1.800	±1.13	0.007
8109830 ° *	CCDC99	coiled-coil domain containing 99	-1.798	±1.11	0.009
8132843 ° *	HAUS6	HAUS augmin-like complex, subunit 6	-1.797	±1.08	0.007
8055672 ° *	MMADHC	methylmalonic aciduria (cobalamin deficiency) cblD type, with homocystinuria	-1.794	±1.05	0.010
7934979 °	ANKRD1	ankyrin repeat domain 1 (cardiac muscle)	-1.790	±2.18	0.000
8114287 ° *	SPOCK1	sparc/osteonectin, cwcv and kazal-like domains proteoglycan (testican) 1	-1.784	±1.08	0.007
8152703 °	FBXO32	F-box protein 32	-1.784	±1.26	0.006
7917771 *	DNTTIP2	deoxynucleotidyltransferase, terminal, interacting protein 2	-1.782	±1	0.000
8017262 °	BRIP1	BRCA1 interacting protein C-terminal helicase 1	-1.779	±1.11	0.008
7914878 °	CLSPN	claspin	-1.773	±1.12	0.010
8152582 *	DSCC1	defective in sister chromatid cohesion 1 homolog (S. cerevisiae)	-1.772	±0.97	0.000
8053797 *	ANKRD36C	ankyrin repeat domain 36C	-1.768	±1.06	0.000
7922846 ° *	FAM129A	family with sequence similarity 129, member A	-1.763	±1.06	0.009
8124537 *	HIST1H3A (includes others)	histone cluster 1, H3a	-1.756	±1.05	0.000
7917976 *	SASS6	spindle assembly 6 homolog (C. elegans)	-1.754	±0.99	0.000
8115490 °	ADAM19	ADAM metallopeptidase domain 19	-1.751	±1.32	0.004
7997381 *	CENPN	centromere protein N	-1.748	±0.99	0.000
8067029 °	KCNG1 (includes EG:241794	potassium voltage-gated channel, subfamily G, member 1	-1.746	±1.28	0.005
7981953 *			-1.746	±0.99	0.000
7981966 *			-1.746	±0.99	0.000
8034512 *	SNORD41	small nucleolar RNA, C/D box 41	-1.737	±1.03	0.000
8151684 °	MMP16	matrix metallopeptidase 16 (membrane-inserted)	-1.721	±1.68	0.003
8054217 *	TXNDC9	thioredoxin domain containing 9	-1.719	±0.94	0.000
8001197 °	NETO2	neuropilin (NRP) and tolloid (TLL)-like 2	-1.715	±1.12	0.009
8042830 *	MTHFD2	methylenetetrahydrofolate dehydrogenase (NADP+ dependent) 2, methenyltetrahydrofolate cyclohydr	-1.711	±0.96	0.000
7905088 *	HIST2H2AC	histone cluster 2, H2ac	-1.709	±0.96	0.000
7970763 °	FLT1	fms-related tyrosine kinase 1 (vascular endothelial growth factor/vascular permeability factor receptor)	-1.708	±1.31	0.008
8066074 *	DSN1 (includes EG:1000029	DSN1, MIND kinetochore complex component, homolog (S. cerevisiae)	-1.701	±0.98	0.000
8042588 *	MPHOSPH10	M-phase phosphoprotein 10 (U3 small nucleolar ribonucleoprotein)	-1.700	±0.96	0.000
7962579 °	AMIGO2	adhesion molecule with Ig-like domain 2	-1.699	±1.19	0.008
7971077 °	POSTN	periostin, osteoblast specific factor	-1.691	±1.67	0.005
7968351 °	C13orf33	chromosome 13 open reading frame 33	-1.688	±1.4	0.006
7989915 *	TIPIN	TIMELESS interacting protein	-1.688	±0.95	0.000
7950933 °	NOX4	NADPH oxidase 4	-1.688	±1.48	0.007
7936322 *	GPAM	glycerol-3-phosphate acyltransferase, mitochondrial	-1.664	±0.93	0.000
7917182 °	ELTD1	EGF, latrophilin and seven transmembrane domain containing 1	-1.642	±1.35	0.007
8039484 °	IL11	interleukin 11	-1.622	±1.35	0.008
8145361 °	NEFM	neurofilament, medium polypeptide	-1.388	±2.23	0.003
7951271 °	MMP1 (includes EG:300339)	matrix metallopeptidase 1 (interstitial collagenase)	-1.228	±2.5	0.004
7985786 °	ACAN	aggrecan	-1.204	±2.3	0.006
8112971 °	HAPLN1	hyaluronan and proteoglycan link protein 1	-0.939	±2.16	0.009
7976567 °	BDKRB1	bradykinin receptor B1	1.129	±2.02	0.009
8045533 °			1.354	±1.46	0.007
8015179 °			1.384	±1.4	0.002
8019588 °			1.384	±1.4	0.002
7903214 °	LPPR4	lipid phosphate phosphatase-related protein type 4	1.391	±2.01	0.001
8176719 °	EIF1AY	eukaryotic translation initiation factor 1A, Y-linked	1.412	±2.09	0.002
8176375 °	RPS4Y1	ribosomal protein S4, Y-linked 1	1.431	±2.26	0.001
7999909 °	GPRC5B	G protein-coupled receptor, family C, group 5, member B	1.434	±1.38	0.009
7938225 °	OLFML1	olfactomedin-like 1	1.441	±1.04	0.009
7969202 °			1.464	±1	0.009
8176655 °	NLGN4Y	neuroligin 4, Y-linked	1.466	±1.7	0.003
8037240 °	PSG1	pregnancy specific beta-1-glycoprotein 1	1.480	±1.28	0.009
8013521 °			1.482	±1.08	0.009
8097288 °	FAT4	FAT tumor suppressor homolog 4 (Drosophila)	1.487	±1.07	0.009
7934185 °	C10orf54	chromosome 10 open reading frame 54	1.487	±0.87	0.008
7950005 °	MRGPRF	MAS-related GPR, member F	1.494	±1.14	0.007
8068361 °	SLC5A3	solute carrier family 5 (sodium/myo-inositol cotransporter), member 3	1.512	±0.97	0.009
8104758 °	NPR3 (includes EG:18162)	natriuretic peptide receptor C/guanylate cyclase C (atrionatriuretic peptide receptor C)	1.518	±1.16	0.005
7903358 °	VCAM1	vascular cell adhesion molecule 1	1.528	±1.56	0.009
8058664 °			1.536	±1.05	0.006
8037657 °	DMPK	dystrophia myotonica-protein kinase	1.563	±0.9	0.004
7896748 °			1.570	±1.89	0.001
7911335 °			1.571	±1.59	0.002
8165694 °			1.571	±1.59	0.002
8176578 °	USP9Y	ubiquitin specific peptidase 9, Y-linked	1.578	±1.99	0.001
7975076 °	HSPA2	heat shock 70kDa protein 2	1.588	±1.23	0.005
8150962 °	TOX	thymocyte selection-associated high mobility group box	1.635	±1.39	0.002
7932254 °	ITGA8	integrin, alpha 8	1.637	±1.06	0.004

8045835 °	GALNT5	UDP-N-acetyl-alpha-D-galactosamine:polypeptide N-acetylgalactosaminyltransferase 5 (GalNAc-T5)	1.639	±1.38	0.002
8176624 °	DDX3Y	DEAD (Asp-Glu-Ala-Asp) box polypeptide 3, Y-linked	1.644	±2.36	0.000
7926875 °	BAMBI	BMP and activin membrane-bound inhibitor homolog (Xenopus laevis)	1.651	±1.02	0.003
8141140 °	DLX5	distal-less homeobox 5	1.660	±1.25	0.003
8013523 °			1.662	±1.43	0.002
7962058 °	TMTC1	transmembrane and tetratricopeptide repeat containing 1	1.665	±1.66	0.002
7896750 °			1.669	±1.55	0.002
7984364 °	SMAD3	SMAD family member 3	1.689	±0.93	0.002
8156358 °			1.691	±1.9	0.001
8171297 °	MID1 (includes EG:10033095	midline 1 (Opitz/BBB syndrome)	1.691	±1.2	0.003
8113120 °			1.701	±1.22	0.002
8165707 °			1.701	±1.22	0.002
8129666 °	SLC2A12	solute carrier family 2 (facilitated glucose transporter), member 12	1.703	±1.04	0.002
8112668 °	GCNT4	glucosaminyl (N-acetyl) transferase 4, core 2	1.708	±1	0.002
7950810 °	SYTL2	synaptotagmin-like 2	1.718	±0.99	0.002
8095110 °	KIT	v-kit Hardy-Zuckerman 4 feline sarcoma viral oncogene homolog	1.722	±1.22	0.002
7911343 °			1.727	±1.38	0.002
8165703 °			1.727	±1.38	0.002
7970565 °			1.731	±1.06	0.002
8008965 °			1.738	±1.13	0.002
7962559 °	SLC38A4	solute carrier family 38, member 4	1.738	±1.23	0.002
8052355 °	EFEMP1	EGF containing fibulin-like extracellular matrix protein 1	1.759	±2.09	0.001
8013987 °			1.824	±1.21	0.001
8160346 °	PTPLAD2	protein tyrosine phosphatase-like A domain containing 2	1.831	±1.2	0.002
7899615 °	SERINC2	serine incorporator 2	1.843	±1.13	0.001
8165663 °			1.863	±1.74	0.001
7911337 °			1.865	±1.92	0.000
7973871 °			1.865	±1.92	0.000
8165696 °			1.865	±1.92	0.000
8102831 °	MGARP	mitochondria-localized glutamic acid-rich protein	1.874	±1.21	0.001
8165709 °			1.914	±1.26	0.001
7911339 °			1.952	±2.12	0.000
8165698 °			1.952	±2.12	0.000
8045804 °			2.012	±1.98	0.000
8102532 °	PDE5A	phosphodiesterase 5A, cGMP-specific	2.024	±1.4	0.001
8104746 °	NPR3 (includes EG:18162)	natriuretic peptide receptor C/guanylate cyclase C (atrionatriuretic peptide receptor C)	2.032	±1.38	0.000
7985317 °	KIAA1199	KIAA1199	2.088	±1.9	0.000
8057677 °	SLC40A1	solute carrier family 40 (iron-regulated transporter), member 1	2.169	±1.51	0.000
8100310 °			2.221	±1.88	0.000
7933204 °	C10orf10	chromosome 10 open reading frame 10	2.301	±1.43	0.000
8051583 °	CYP1B1	cytochrome P450, family 1, subfamily B, polypeptide 1	2.318	±1.84	0.000
8083887 °	CLDN11	claudin 11	2.430	±1.6	0.000
7912537 °	DHRS3	dehydrogenase/reductase (SDR family) member 3	2.441	±1.43	0.000
8006433 °	CCL2	chemokine (C-C motif) ligand 2	2.913	±2.11	0.000

(*) Genes selected by SAM; (°) Genes selected by Rank Products

Table SII: Top enriched functions in the IPA interaction network

Function	Function Annotation	p-value	# Molec.
Cell Cycle			
recombination	DNA recombination	5.02E-09	7
recombination	recombination of cells	5.66E-05	3
homologous recombination	homologous recombination of DNA	4.42E-07	4
homologous recombination	homologous recombination of plasmid DNA	6.58E-05	2
homologous recombination	homologous recombination of cells	3.96E-02	1
checkpoint control	checkpoint control	4.96E-07	6
checkpoint control	checkpoint control of fibroblast cell lines	1.82E-04	2
DNA replication checkpoint	DNA replication checkpoint	1.99E-06	3
G2/M phase	G2/M phase	2.16E-05	6
G2/M phase	G2/M phase of tumor cell lines	6.16E-04	3
G2/M phase	G2/M phase of breast cancer cell lines	1.21E-03	2
G2/M phase	G2/M phase of cervical cancer cell lines	2.32E-02	1
G2/M phase	arrest in G2/M phase of breast cancer cell lines	3.32E-02	1
S phase checkpoint control	S phase checkpoint control of cervical cancer cell lines	1.08E-04	2
interphase	interphase	2.96E-04	9
interphase	arrest in interphase of fibroblast cell lines	1.79E-03	3
interphase	interphase of breast cancer cell lines	2.22E-03	3
interphase	arrest in interphase	1.19E-02	5
interphase	interphase of cervical cancer cell lines	1.29E-02	2
interphase	interphase of tumor cell lines	2.64E-02	4
interphase	arrest in interphase of tumor cell lines	4.69E-02	3
sister chromatid exchange	sister chromatid exchange	6.67E-04	2
sister chromatid exchange	sister chromatid exchange of DNA	3.70E-03	1
sister chromatid exchange	sister chromatid exchange of chromosomes	4.52E-03	1
sister chromatid exchange	sister chromatid exchange of cervical cancer cell lines	6.16E-03	1
G1/S phase transition	arrest in G1/S phase transition	9.41E-04	3
G1/S phase transition	arrest in G1/S phase transition of breast cancer cell lines	5.75E-03	1
meiosis	meiosis of germ cells	1.27E-03	3
meiosis	meiosis of primordial germ cells	2.47E-03	1
meiosis	meiosis of male germ cells	7.36E-03	2
morphology	morphology of spindle fibers	2.22E-03	2
S phase	S phase	2.33E-03	5
S phase	entry into S phase of tumor cell lines	8.63E-03	2
S phase	arrest in S phase of keratinocytes	9.43E-03	1
S phase	arrest in S phase	1.11E-02	2
S phase	entry into S phase	1.42E-02	3
S phase	S phase of fibroblast cell lines	1.55E-02	2
S phase	entry into S phase of cervical cancer cell lines	2.00E-02	1
S phase	re-entry into S phase of bone cancer cell lines	2.32E-02	1
S phase	entry into S phase of cancer cells	3.12E-02	1
S phase	arrest in S phase of fibroblast cell lines	3.72E-02	1
S phase	entry into S phase of breast cancer cell lines	4.71E-02	1
G1 phase	arrest in G1 phase of breast cancer cell lines	3.30E-03	2
G1 phase	arrest in G1 phase	1.13E-02	4
G1 phase	G1 phase of fibroblast cell lines	1.92E-02	2
G1 phase	arrest in G1 phase of carcinoma cell lines	4.79E-02	1
endomitosis	endomitosis of leukemia cell lines	3.70E-03	1
cell cycle progression	arrest in cell cycle progression of embryonic stem cell lines	4.11E-03	1
mitosis	delay in mitosis of breast cancer cell lines	4.11E-03	1
mitosis	entry into mitosis of embryonic cell lines	8.61E-03	1
mitosis	entry into mitosis of epithelial cell lines	8.61E-03	1
mitosis	entry into mitosis of kidney cell lines	1.15E-02	1
mitosis	entry into mitosis of colon cancer cell lines	1.51E-02	1
mitosis	mitosis of tumor cell lines	2.96E-02	2
mitosis	entry into mitosis of cervical cancer cell lines	3.00E-02	1

progression	progression of chromosomes	4.11E-03	1
DNA damage checkpoint	DNA damage checkpoint	5.26E-03	2
G2 phase	arrest in G2 phase of endometrial cancer cell lines	5.34E-03	1
G2 phase	arrest in G2 phase of embryonic stem cells	7.38E-03	1
G2 phase	arrest in G2 phase	1.26E-02	3
G2 phase	arrest in G2 phase of tumor cell lines	3.63E-02	2
G2 phase	arrest in G2 phase of lung cancer cell lines	4.19E-02	1
G2 phase	arrest in G2 phase of carcinoma cell lines	4.59E-02	1
organization	organization of chromosomes	6.19E-03	2
illegitimate recombination	illegitimate recombination of plasmid DNA	7.79E-03	1
senescence	senescence of fibroblasts	8.58E-03	2
aneuploidy	aneuploidy of fibroblasts	8.61E-03	1
aneuploidy	aneuploidy of cells	9.83E-03	2
abnormal morphology	abnormal morphology of meiotic spindles	9.43E-03	1
G2/M phase transition	arrest in G2/M phase transition	1.33E-02	2
reorganization	reorganization of chromatin	1.47E-02	1
homologous pairing	homologous pairing of DNA	1.76E-02	1
formation	formation of chromosomes	2.08E-02	1
segregation	segregation of chromosomes	2.34E-02	2
DNA Replication, Recombination, and Repair			
recombination	DNA recombination	5.02E-09	7
recombination	recombination of cells	5.66E-05	3
homologous recombination	homologous recombination of DNA	4.42E-07	4
homologous recombination	homologous recombination of plasmid DNA	6.58E-05	2
homologous recombination	homologous recombination of cells	3.96E-02	1
checkpoint control	checkpoint control	4.96E-07	6
checkpoint control	checkpoint control of fibroblast cell lines	1.82E-04	2
DNA replication checkpoint	DNA replication checkpoint	1.99E-06	3
repair	repair of DNA	7.53E-06	7
repair	repair of gene	1.31E-02	1
DNA damage response	DNA damage response of cells	8.46E-06	6
damage	damage of chromosomes	1.86E-05	4
metabolism	metabolism of DNA	4.47E-05	8
homologous recombination repair	homologous recombination repair of DNA	7.07E-05	3
formation	formation of chiasmata	8.55E-05	2
formation	formation of nuclear foci	8.94E-05	3
formation	formation of chromosome components	6.21E-04	3
formation	formation of sex bodies	4.11E-03	1
formation	formation of chromatin	5.34E-03	2
formation	formation of RAD51 nuclear focus	1.23E-02	1
formation	formation of chromosomes	2.08E-02	1
S phase checkpoint control	S phase checkpoint control of cervical cancer cell lines	1.08E-04	2
progression	progression of replication fork	1.14E-04	2
progression	progression of chromosomes	4.11E-03	1
replication	DNA replication	1.17E-04	6
replication	initiation of replication of DNA	2.51E-03	2
modification	modification of gene	2.22E-04	2
somatic hypermutation	somatic hypermutation	3.04E-04	2
breakage	breakage of chromosomes	3.91E-04	3
sister chromatid exchange	sister chromatid exchange	6.67E-04	2
sister chromatid exchange	sister chromatid exchange of DNA	3.70E-03	1
sister chromatid exchange	sister chromatid exchange of chromosomes	4.52E-03	1
sister chromatid exchange	sister chromatid exchange of cervical cancer cell lines	6.16E-03	1
breakdown	breakdown of chromosomes	6.97E-04	2
mutation	mutation of gene	6.97E-04	2
unwinding	unwinding of DNA	1.45E-03	2
unwinding	unwinding of DNA fragment	1.51E-02	1
mismatch repair	mismatch repair	1.71E-03	2
chromosomal instability	chromosomal instability	1.87E-03	2
double-stranded DNA break repair	double-stranded DNA break repair	2.36E-03	3

double-stranded DNA break repair	double-stranded DNA break repair of B-lymphocyte	3.70E-03	1
double-stranded DNA break repair	double-stranded DNA break repair of cells	7.41E-03	2
double-stranded DNA break repair	double-stranded DNA break repair of epithelial cells	9.02E-03	1
conversion	conversion of gene	2.88E-03	1
exchange	exchange of chromosomes	2.88E-03	1
exchange	exchange of sister chromatids	1.59E-02	1
joining	joining of DNA	4.09E-03	2
DNA damage checkpoint	DNA damage checkpoint	5.26E-03	2
organization	organization of chromosomes	6.19E-03	2
illegitimate recombination	illegitimate recombination of plasmid DNA	7.79E-03	1
quantity	quantity of nucleoprotein filaments	8.20E-03	1
abnormal morphology	abnormal morphology of meiotic spindles	9.43E-03	1
reorganization	reorganization of chromatin	1.47E-02	1
excision repair	excision repair	1.68E-02	2
homologous pairing	homologous pairing of DNA	1.76E-02	1
catabolism	catabolism of ATP	2.14E-02	2
segregation	segregation of chromosomes	2.34E-02	2
instability	instability of DNA	2.44E-02	1
ligation	ligation of DNA	3.24E-02	1
elongation	elongation of DNA	4.86E-02	1
Cellular Compromise			
damage	damage of chromosomes	1.86E-05	4
breakage	breakage of chromosomes	3.91E-04	3
breakdown	breakdown of chromosomes	6.97E-04	2
micronucleation	micronucleation of breast cancer cell lines	4.11E-03	1
atrophy	atrophy of motor neurons	8.20E-03	1
oxidative stress response	oxidative stress response of fibroblast cell lines	2.88E-02	1

Table SIII: Validation of the microarray assays

Gene	p-value
*CDC45L**	0.0058
PCOLCE2	0.0062
*BRCA1**	0.0083
*BRIP1**	0.0101
*DTL**	0.0113
*CDC25A**	0.0117
*RAD51AP1**	0.0118
E2F7	0.0124
*DKK1**	0.0166
CDH2	0.0169
LAMC2	0.0182
CCDC99	0.02
*BLM**	0.0209
*CDC6**	0.0238
DCK	0.0244
*RAD51**	0.0279
*HIST1H1B**	0.0496
PODXL	0.1062
MTHFD2	0.1113
ADAM12	0.1616
PCDH10	0.1679
HIST1H4B	0.2584
AMIGO2	0.3369
ITGA2	0.3459

(*) Genes pertaining to the BRCA1 similarity cluster

Table SIV: DEGs involved in the oxidative generation and repair of DSBs

Symbol	Function	Reference
GSTM2	ROS detoxification, glutathione metabolism	[26]
NOX4	Production of ROS	[27]
PTGS2	Peroxidase activity	[28]
SMAD3	oxidative stress response/TGFB-mediated growth inhibition	[29]
BRCA1	oxidative stress response/TGFB-mediated growth inhibition; Activation of base-excision repair/homologous recombination repair	[29], [31]
CLSPN	Stabilisation of the replication fork	[30]
TIPIN	Stabilisation of the replication fork	[30]
CDC45L	New DNA synthesis during DNA repair	[32]
MCM10	New DNA synthesis during DNA repair	[33]
GINS1	New DNA synthesis during DNA repair	[32]

Table SV: Cell cultures used in the study

Code	Gender	Clinical Status*	Microarray	qRT-PCR validation	Flow cytometry	H2O2 qRT-PCR
F3334	female	control	X	X	X	X
F3347	male	control	X	X	X	X
F3960	female	control	X	X		
F4217	male	control	X	X	X	X
F4319	female	control	X	X		X
F4386	female	control	X	X		
F4243	male	CLP/UR	X	X	X	X
F4244	male	CLP/UR	X	X	X	X
F4245	male	CLP/UR	X	X	X	X
F4293	female	CL/UL	X	X	X	X
F4294	female	CL/UL	X	X	X	X
F4311	male	CL/UL	X	X	X	X
F4388	male	CLP/UR	X	X	X	X
F3333	male	control				X
F5541	male	control				X
F5703	male	control				X
F6032	female	control			X	X
F6119	male	control			X	X
F6681	male	control				X
F4281	male	CLP/UL				X
F4282	male	CLP/UL				X
F5640	female	CL/UL				X
F5720	male	CLP/UR				X

(*) CL = Cleft Lip; CLP = Cleft Lip and Palate; UL = Unilateral Left; UR = Unilateral Right

Table SVI: Primer sequences used for qRT-PCR experiments

Gene	Primer Forward (5'-3')	Primer Reverse (5'-3')
ADAM12	TCTTGCTGCCGGATTTGTGGTT	AAGGGCGCACACACCTTAGTTT
AMIGO2	AGGTGCAAGAGTGACAGACACGG	CTCTTTCCTGGGTTAGTCGGTGC
BLM	AGCACATTGTGTCAGTCAGTGGG	CTGTGGCCGTAAGAGCCATCAC
BRCA1	AGGTGAAGCAGCATCTGGGTGTG	TGCATGGTATCCCTCTGCTGAGTGG
BRIP1	AGTTCAGCTTCGGTTTGCTCGGG	AGCACACAGCTCGTAGGGGTTCA
CCDC99	GCCCTAGAGAAAGCTCGTGTAGC	CCACCTCTGCAAACAAAGAGTTGC
CDC25A	TTCCCTACCTCAGAAGCTGTTGGG	AGTGCAGGCAGCCACGAGATAC
CDC45L	GTGTGTGACACCCATAGGCCAG	TCTAACCGTGTGCGCTTCTCAG
CDC6	TCAGGAAGAGGTATCCAGGCCAG	AATACCAACACAATCATGGGGCCC
CDH2	CGCAGTGTACAGAATCAGTGGCGG	AGTCGATTGGTTTGACCACGGTG
DCK	TCAAGCCACTCCAGAGACATGCTT	TGCAGGAGCCAGCTTTCATGTT
DKK1	ATTGACAACTACCAGCCGTACCCG	AGTAATTCCCGGGGCAGCACATAG
DTL	TATGGAAGGTCTCCACACCCTGG	GTGAAGTCAGATGGACACCAGCAC
E2F7	CCTGTGCCAGAAGTTTCTAGCTCG	GCGTCTCCTTTCCACACCAAGAC
HIST1H1B	TCTTGCCACCATGTCGGAAACCG	CGGCAGCCTTCTTAGTTGCCTTC
HIST1H4B	ACCGAAAAGTGCTGCGGGATAAC	ACCGGAAATTCGCTTAACCCCAC
ITGA2	TGTTAGCGCYCAGTCAAGGCATTT	TGCTGCACTGCATAGCCAAACTGT
LAMC2	AGGTTGATACCAGAGCCAAGAACGCT	TCATCTACACTGAGAGGCTGGTCCAT
MTHFD2	TCTCTAATGTCTGCTTTGGCTGCC	CAACAGCTTCATTTCGAACTGCCG
PCDH10	CCAACGAGACTAAACACCAGCGAG	CTATGTCGGCTTCCTGGAATGCAG
PCOLCE2	TGCTGAACCAAACGAAAGAGGGGA	ATGTGCCACACACAAGTGACTCCT
PODXL	TTCCAGGAAGTCAGACCGTGGTC	ACTGACCCCTGCCTCCTTTAGTTC
RAD51	GGCAATGCAGATGCAGCTTGAAGT	TTATGCCACACTGCTCTAACCGTG
RAD51AP1	GCAGTGCCTTGTACAAAGATGGCT	GTGGTGACTGTTGGAAGTTCCTTCA
E2F1	CCGCCATCCAGGAAAAGGTGTG	TTCAGGTCGACGACACCGTCAG
GAPDH	TGCACCACCAACTGCTTAGC	GGCATGGACTGTGGTCATGA
HPRT1	TGACACTGGCAAAACAATGC	GGTCCTTTTCACCAGCAAGCT
SDHA	TGGGAACAAGAGGGCATCTG	CCACCACTGCATCAAATTCA
HMBS	GGCAATGCGGCTGCAA	GGGTACCCACGCGAATCAC
Brca1	AGAAGAAAGGGCCTTCACAATGTCC	ACCATTTGTAAGCTGCATTCCCGTG
Brip1	GGGACGCGGACACACAAGCAG	ACTTCCCGTGCTTGCCATCCAG
Msh2	TGGCATTTAAGGCTTCTCCCGGC	ACCCATAACGCCAACGGAAGCTG
Blm	AGTGCTGCAACGACCCCTCG	AGCCATGATCCTCATCTGGCATCC
Rad51	AGATGGAGCAGCCATGTTCGCTG	TCTCAGGTACAGCCTGGTGGTTG
Rad51ap1	AAGTCACCATCTCAAGCCAAGGC	TTTCTGAACCTTCACCAGTGGCG
B2m	TCGCGGTCGCTTCAGTCGTC	TTCTCCGGTGGGTGGCGTGA
Tbp	CCACACCAGCTTCTGAGAGC	GACTGCAGCAAATCGCTTGGG
Tubb5	GACAGTGTGGCAACCAGATCG	CTGCAGGTCGCTGTCACCGT
Ywhaz	TGAGCAGAAGACGGAAGGTGC	GCGAAGCATTGGGGATCAAGA

CHAPTER III

In vitro phenotype screening in a neural crest cell model unveils disturbances in osteogenic differentiation in Richieri-Costa-Pereira syndrome

Gerson S. Kobayashi, Felipe A. A. Ishiy, Camila M. Musso, Luiz C. Caires, Ernesto Goulart, Andressa G. Morales, Karina Griesi-Oliveira, Patrícia Semedo-Kuriki, Naila Lourenço, Rodrigo Atique, and Maria Rita Passos-Bueno.

Abstract

Richieri-Costa-Pereira syndrome (RCPS) is a rare acrofacial dysostosis likely caused by disturbances in cranial neural crest development. RCPS is caused by expansion mutations in the 5'UTR of *EIF4A3*, but its pathogenetic mechanism is currently unknown. Here, we report the successful derivation of iPSC-derived neural crest cells (iNCCs) and iNCC mesenchymal derivatives from RCPS subjects, in order to investigate the aetiology of this syndrome. We show that RCPS cells possess increased osteogenic potential in comparison to controls, due to transcriptional dysregulation of osteogenesis-associated genes. Such dysregulation was also observed in RCPS knockdown cells, further supporting the relationship between reduced *EIF4A3* expression and alterations during osteogenic differentiation. This work appoints a possible pathogenetic mechanism for RCPS and provides grounds for the characterisation of craniofacial syndromes with the use of iNCC-based in vitro models.

CHAPTER III

In vitro phenotype screening in a neural crest cell model unveils disturbances in osteogenic differentiation in Richieri-Costa-Pereira syndrome

Gerson S. Kobayashi, Felipe A. A. Ishiy, Camila M. Musso, Luiz C. Caires, Ernesto Goulart, Andressa G. Morales, Karina Griesi-Oliveira, Patrícia Semedo-Kuriki, Naila Lourenço, Rodrigo Atique, and Maria Rita Passos-Bueno.

INTRODUCTION

Richieri-Costa-Pereira syndrome (RCPS; OMIM #268305) is a rare autosomal-recessive acrofacial dysostosis characterised by midline mandibular cleft, micrognathia, Robin sequence, laryngeal abnormalities, and radial and tibial defects, among other clinical findings (Favaro et al., 2011). Phenotype expressivity is variable, ranging from only mild defects in mandibular fusion to more severe clinical manifestations, such as craniofacial pansynostosis and agenesis of the mandible and epiglottis (Favaro et al., 2011; Raskin et al., 2013).

RCPS is caused by non-coding repeat expansions in the 5'UTR of the gene *EIF4A3*. The majority of affected individuals harbour 14-16 repeat alleles, whilst a missense mutation has been found in *trans* to a repeat expansion allele in one RCPS patient. These alterations are believed to bring about partial loss of function of *EIF4A3*, as *eif4a3* knockdown in a zebrafish model has generated embryos with alterations in craniofacial cartilage/bone and clefting of the lower jaw, and a 30-40% reduction of *EIF4A3* mRNA expression has been reported in RCPS patients' lymphocytes and adult mesenchymal cells (Favaro et al., 2014). *EIF4A3* encodes a DEAD box helicase (eIF4AIII) that acts as one of the core members of the exon-junction complex (EJC), a multi-protein complex involved in several cellular post-transcriptional events,

such as alternative splicing, nonsense-mediated mRNA decay, and translation initiation (Chan et al., 2004; Singh et al., 2013; Wang et al., 2014). Although a relationship between *EIF4A3* loss of function and RCPS has been established, the biological effects of such deficiency during human embryonic development are unknown, and the pathogenic mechanism responsible for the syndrome remains elusive.

The clinical signs of RCPS, notably its craniofacial phenotypes, are suggestive of disturbances in neural crest or neural crest-derived tissue development. Neural crest cells (NCCs) are a transient cell population originated from neuroectodermal cells located at the neural plate border during neurulation. The foremost segment of the neuraxis gives rise to cranial NCCs, which migrate and populate the mesenchyme of the developing pharyngeal arches. The cranial NCC-derived mesenchyme then undergoes proliferation and differentiation, resulting in a variety of structures, such as most of the cranioskeleton, ear components, larynx, among others (MacLean et al., 2009; Cordero et al., 2011; Gong, 2014). Disturbances in NCC development, such as increased apoptosis or alterations in migration and differentiation, are considered to be responsible for craniofacial phenotypes of a number of syndromes, including Treacher Collins syndrome, auriculo-condylar syndrome, and Nager syndrome (Passos-Bueno et al., 2009; Trainor & Andrews, 2013). Still, the impact of diminished *EIF4A3* expression on NCCs or NCC-derived mesenchymal cells is currently unknown.

Induced pluripotent stem cell (iPSC) technology offers an invaluable opportunity to unravel the pathogenesis of craniofacial syndromes. Patient-specific iPSCs can be used to generate NCCs harbouring pathogenic mutations, which in turn can be studied under controlled *in vitro* conditions. In addition, NCC cultures can be differentiated towards neural crest mesenchymal derivatives, such as osteoblasts, chondrocytes and adipocytes, thus expanding possibilities for investigating disease-related phenotypes (Menendez et al., 2013; Fukuta et al., 2014).

Here, we report the derivation of RCPS patient-derived iPSC lines to generate NCCs and NCC-derived mesenchymal cells, thus recapitulating craniofacial development *in vitro* to screen for altered cellular functions responsible for the syndrome. The phenotypic assessment of these cell types will contribute to elucidate the pathogenesis of RCPS, and, importantly, it provides further grounds for the characterisation of biological mechanisms responsible for human diseases with the use of NCC-based *in vitro* models.

RESULTS

Derivation of iPSC cultures

Dermal fibroblast cultures were derived from skin punch biopsies from 3 RCPS patients (F8417-1, F8417-2, and F6099-1; Table SI), previously genotyped elsewhere (Favaro et al., 2014). Patients F8417-1 and F8417-2 were homozygous for the 16-repeat allele, while F6099-1 had a 14-repeat allele in *trans* with the missense mutation p.Asp270Gly, as described by Favaro et al (2014).

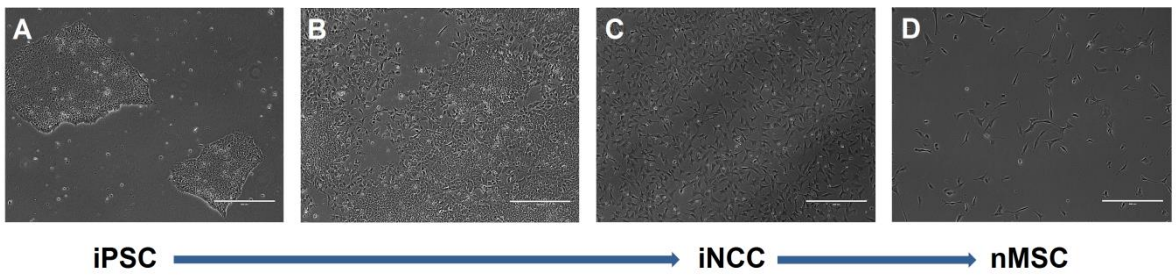

Figure 1: Cell morphology during differentiation. A) iPSC colonies before induction towards iNCCs; **B)** Cells at day 5 of differentiation to iNCCs; **C)** iNCCs after 15 days of differentiation; **D)** nMSCs after 6 days of differentiation from iNCCs. Pictures are representative of all differentiations carried out herein. Scale bar = 1000um

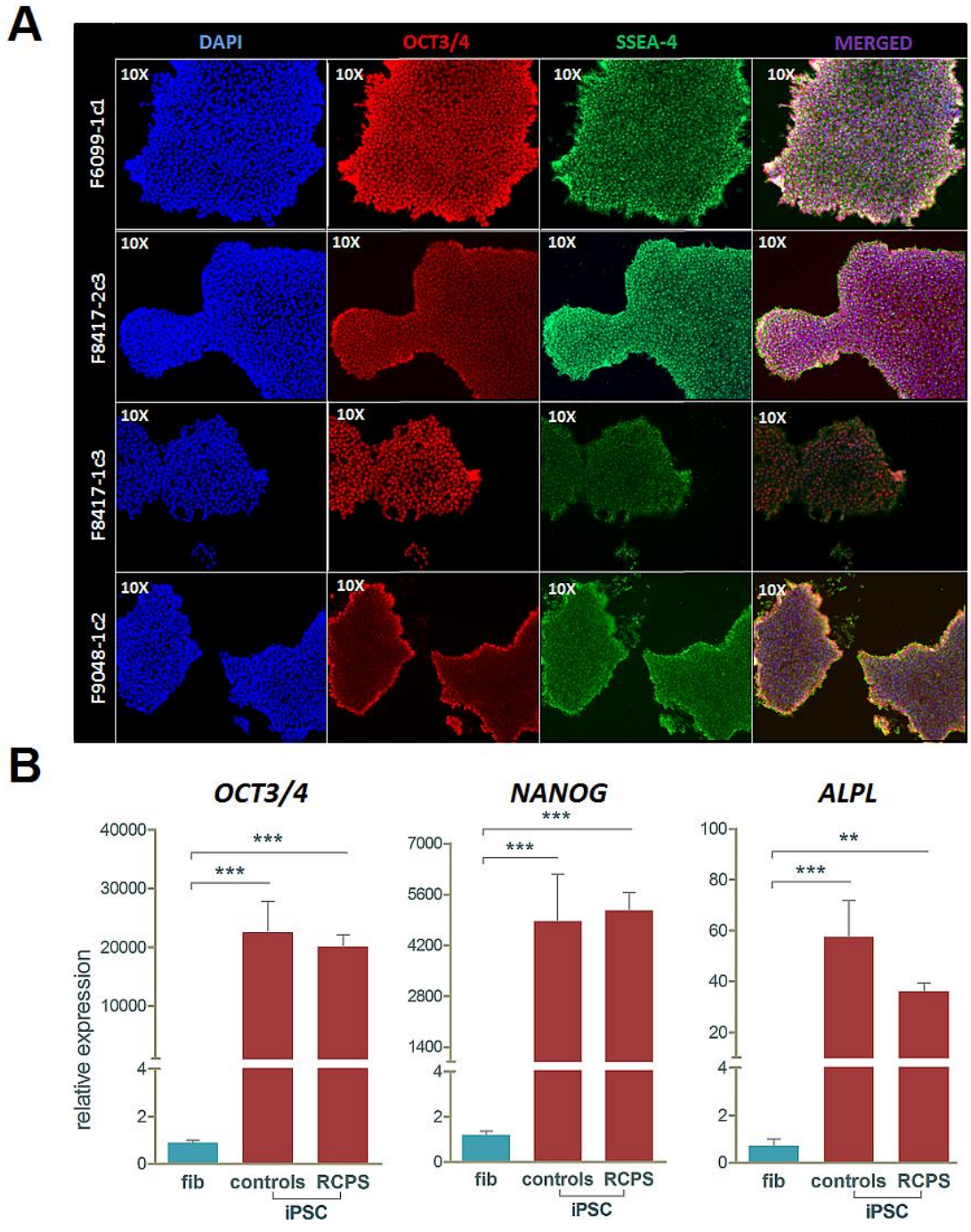

Figure 2: iPSC characterisation. A) Immunofluorescence micrographs depicting expression of pluripotency markers OCT3/4 and SSEA-4 in iPSCs; **B)** RT-qPCR showing transcriptional upregulation of pluripotency-associated genes *OCT3/4*, *NANOG*, and *ALPL* in controls and RCPS samples. Graphs were plotted relative to expression data of 2 adult fibroblasts (F9048-1 and F6099-1); (***) *p*-value < 0.001; (**) *p*-value < 0.01; Student's t-test.

After reprogramming, the iPSC lines (in addition to one unaffected control; F9048-1) displayed pluripotent stem cell-like morphology (Fig. 1A) and expressed pluripotency markers OCT3/4, SSEA-4, *NANOG*, and *ALPL* (Fig.2). These cells showed no detectable signs of chromosomal imbalances or genomic integration of the episomal vectors (Fig. S1); moreover, RCPS iPSCs showed lower abundance of *EIF4A3* transcripts as compared to controls (Fig. S2). The remaining control iPSCs used in this study had been generated with retroviral transduction and characterized elsewhere (Ishiy et al., 2014). Since no differences in expression of pluripotency markers or efficiency of differentiation were observed between these controls and the remaining iPSC lines, we opted to maintain them in the experiments described in this work. In total, 4 control and 3 RCPS iPSC cultures were used in this study.

iPSC-derived neural crest cells (iNCCs) express neural crest markers and show augmented expression of transcripts associated with craniofacial malformations

iPSC-derived neural crest cells (iNCCs) were induced from RCPS and control iPSCs under a methodology based on TGF-β/Activin pathway blockade and WNT pathway activation (Menendez et al., 2013; Fukuta et al., 2014). After differentiation, iNCC populations displayed typical neural crest cell morphology (Fig. 1C) and were positively stained for neural crest markers p75(NTR) and HNK1, with proportions of double-positive cells ranging between 81.1% and 97.6% (Fig. 3A). Moreover, RT-qPCR assays showed upregulation of neural crest markers *PAX3*, *TFAP2A*, *ZIC1* and *SOX10*, and downregulation of pluripotency markers *OCT3/4*, *NANOG*, and *ALPL*, when compared to the originating iPSCs (Fig. 3B). Finally, by comparing RCPS and control iNCCs, we confirmed lower *EIF4A3* transcript expression in RCPS subjects (Fig. S2A).

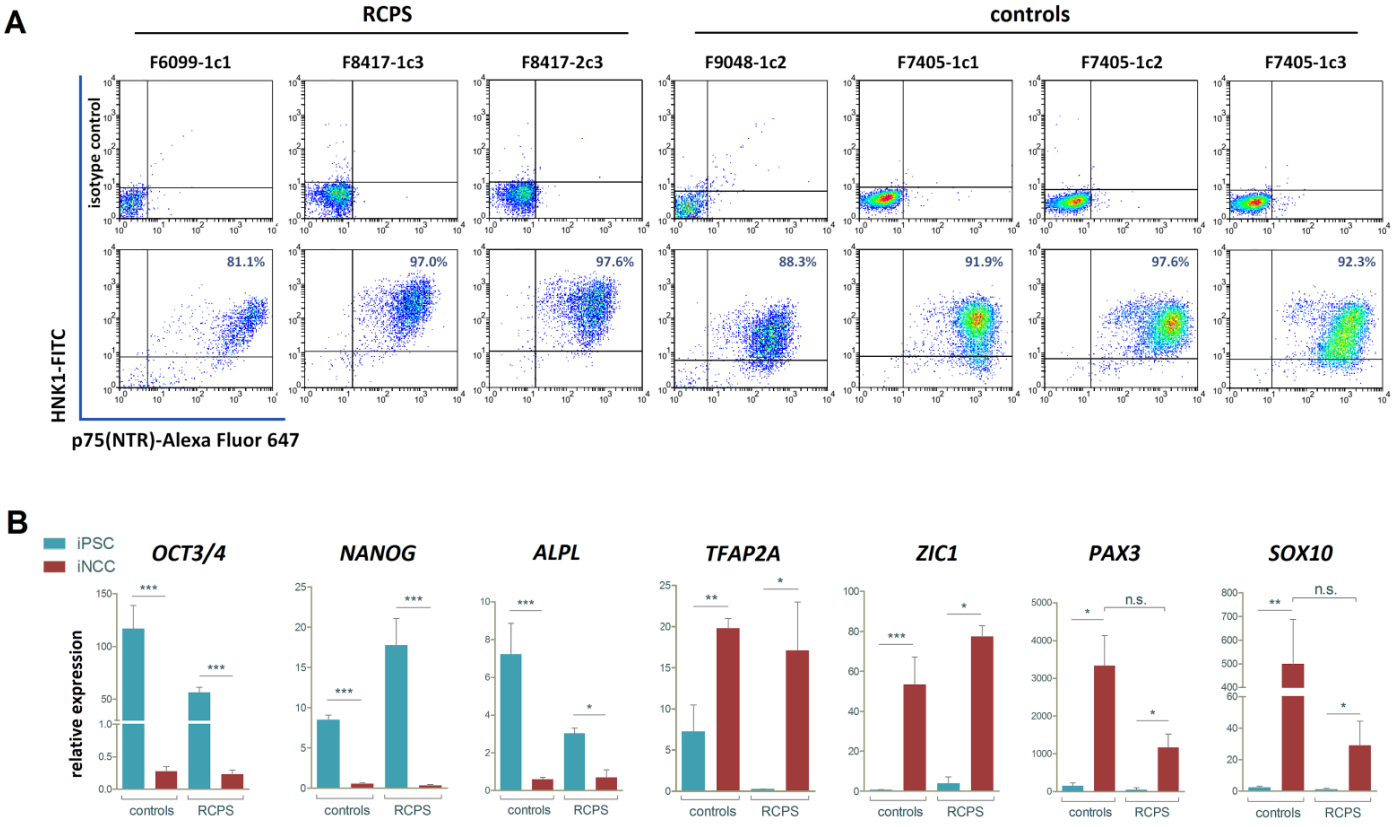

Figure 3: Characterisation of iNCCs. A) Biparametric flow cytometry dot plots for HNK1 and p75(NTR) expression in RCPS and control cells. Values represent p75(NTR)$^{+}$/HNK1^{+} events (upper right quadrant). **B)** RT-qPCR assessment of neural crest and pluripotency marker expression between iNCCs and the originating iPSCs. (*) $p < 0.05$; (**) $p < 0.01$; (***) $p < 0.001$; Student's t-test; n.s.=not significant.

Homogeneous neural crest-derived mesenchymal stem cell-like (nMSC) populations can be successfully derived from iNCCs

One of the hallmarks of the cranial neural crest is the ability to generate mesenchymal precursors that give rise to the craniofacial skeleton and other structures during embryonic development (Cordero et al., 2011; Bronner & LeDouarin, 2012). Therefore, to screen for cellular phenotypes possibly associated with the RCPS phenotype, we derived nMSCs from RCPS and control iNCCs. nMSCs showed spindle-shaped, fibroblast-like morphology (Fig. 1D), and transcriptional upregulation of mesenchymal marker *ENG* (CD105) and downregulation of neural crest marker *TFAP2A* in comparison to iNCCs (Fig. 4A). Moreover, nMSCs exhibited typical and homogeneous mesenchymal immunophenotype, with positive staining for mesenchymal markers CD73, CD166, CD90, and negative staining for endothelial marker CD31 (Fig. 4B). In agreement with their immunophenotype, nMSCs were able to be differentiated

towards mesenchymal derivatives *in vitro* (Fig. 4C). Finally, downregulation of *EIF4A3* was also confirmed in RCPS nMSCs, in comparison to controls (Fig. S2).

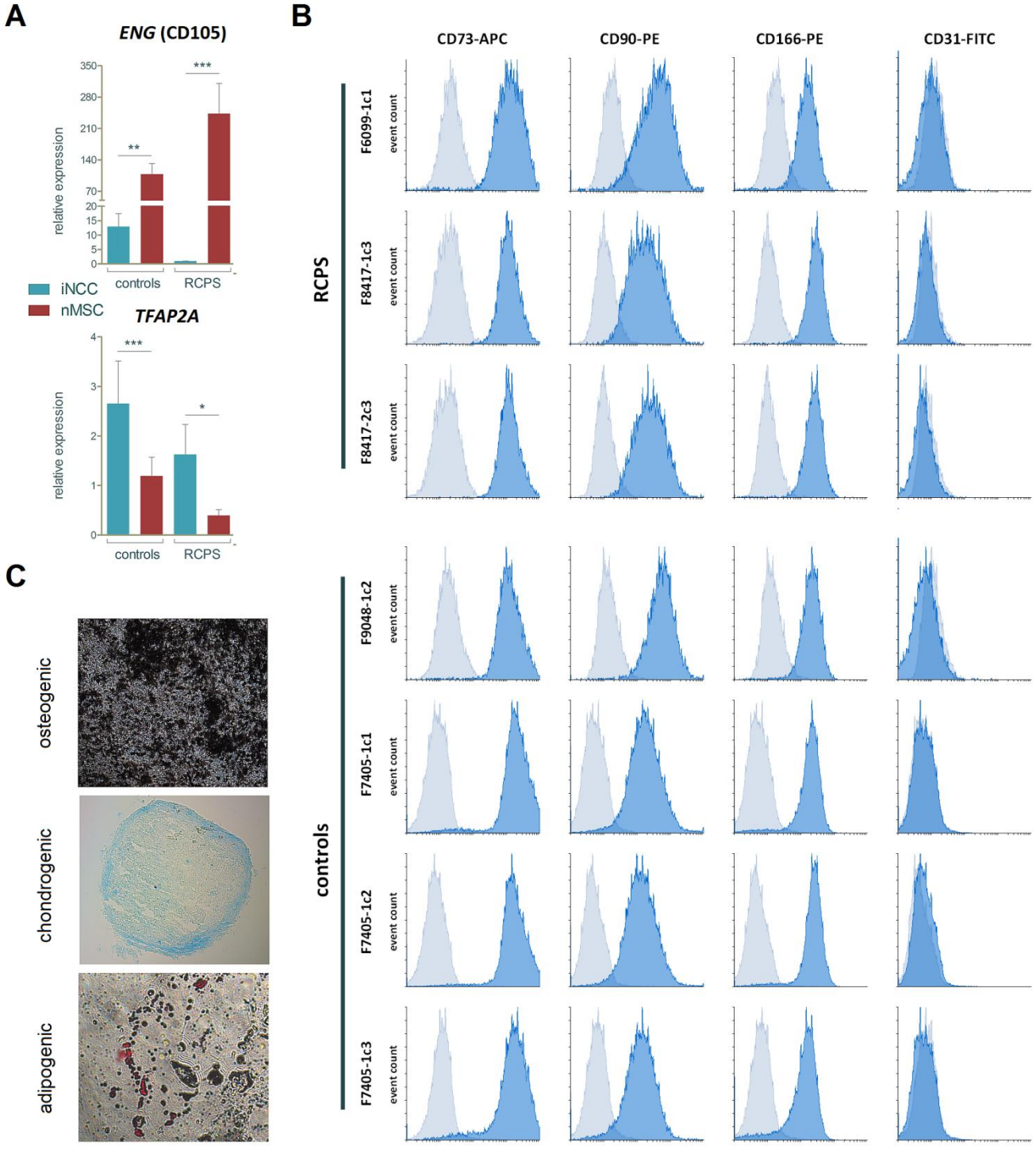

Figure 4: Characterisation of nMSCs. A) RT-qPCR assays showing upregulation of mesenchymal marker *ENG* (CD105) and downregulation of neural crest marker *TFAP2A* in nMSCs compared to iNCCs; (***) $p<0.001$; (**) $p<0.01$; (*) $p<0.05$; Student's t-test. **B)** Flow cytometry immunophenotype profiling of nMSCs showing positive staining for mesenchymal markers CD73, CD90 and CD166, and negative staining for endothelial marker CD31. Histograms represent event count (y-axis) vs. fluorescence (x-axis). Experimental data (blue) were plotted in overlay with data from isotype controls (light blue); **C)** Example of osteogenic, chondrogenic, and adipogenic differentiation of nMSCs, detected with Alizarin Red, Alcian Blue, and Oil Red staining, respectively. Pictures refer to results obtained for F7405-1c1.

Downregulation of *EIF4A3* transcripts is not associated with apoptotic activity in iNCCs and nMSCs from RCPS patients

Since apoptosis of neural crest cells or their cellular derivatives is considered to be a major contributor to the phenotype in a number of neural-crest-related diseases (Passos-Bueno et al., 2009, Cordero et al., 2011), we carried out Annexin V/7-AAD-based apoptosis assays in iNCCs and nMSCs under normal culture conditions. No significant differences in basal apoptosis between patients and controls in either cell type have been detected (Fig. S3A).

EIF4A3* deficiency is associated with alterations in osteogenic differentiation *in vitro

Because apoptosis did not appear to be a major cellular phenotype distinguishing RCPS from control cells, we hypothesised that the main craniofacial phenotypes seen in RCPS could instead be caused by disturbances in NCC mesenchymal differentiation leading to disturbances in cartilage formation and/or intramembranous ossification during craniofacial development.

Since differences in cell density may influence results on *in vitro* chondrogenic and osteogenic differentiation, all nMSCs were first subjected to proliferation assays. No significant differences in proliferative potential were detected between RCPS and control nMSCs (Fig. S3C).

nMSCs were induced towards chondrogenic differentiation, and monitored for expression of key chondrogenesis markers *SOX9*, *ACAN*, and *COL2A1*. In relation to controls, RCPS nMSCs showed augmented expression of early chondrogenesis marker *SOX9* and lower expression of late chondrogenesis marker *ACAN*, after 9 days of differentiation (Fig. S4A). However, after 21 days, we were unable to produce good-quality chondrocyte pellets from the RCPS samples and one control, so Alcian Blue staining analysis was not carried out.

During osteogenic differentiation, alkaline phosphatase (ALP) enzymatic activity was increased in RCPS cells after 9 days of osteoinduction, and Alizarin Red S staining revealed greater matrix mineralisation after 21 days, in comparison to controls (Fig. 5A, B). Next, we assessed expression of key genes involved in osteogenesis during the initial 6 days of differentiation. Compared to controls at day 6 of osteoinduction, RCPS cells exhibited upregulation of transcription factor *RUNX2*, as well as upregulation of early osteoblast marker *COL1A1*, and late-stage osteoblast marker *BGLAP*. Throughout the 6 days of differentiation, *ALPL* expression was higher in RCPS samples, but did not reach statistical significance (Fig. 5C). These findings suggest that the increased osteogenesis in RCPS nMSCs is prompted by transcriptional alterations of osteogenesis-associated genes during early differentiation.

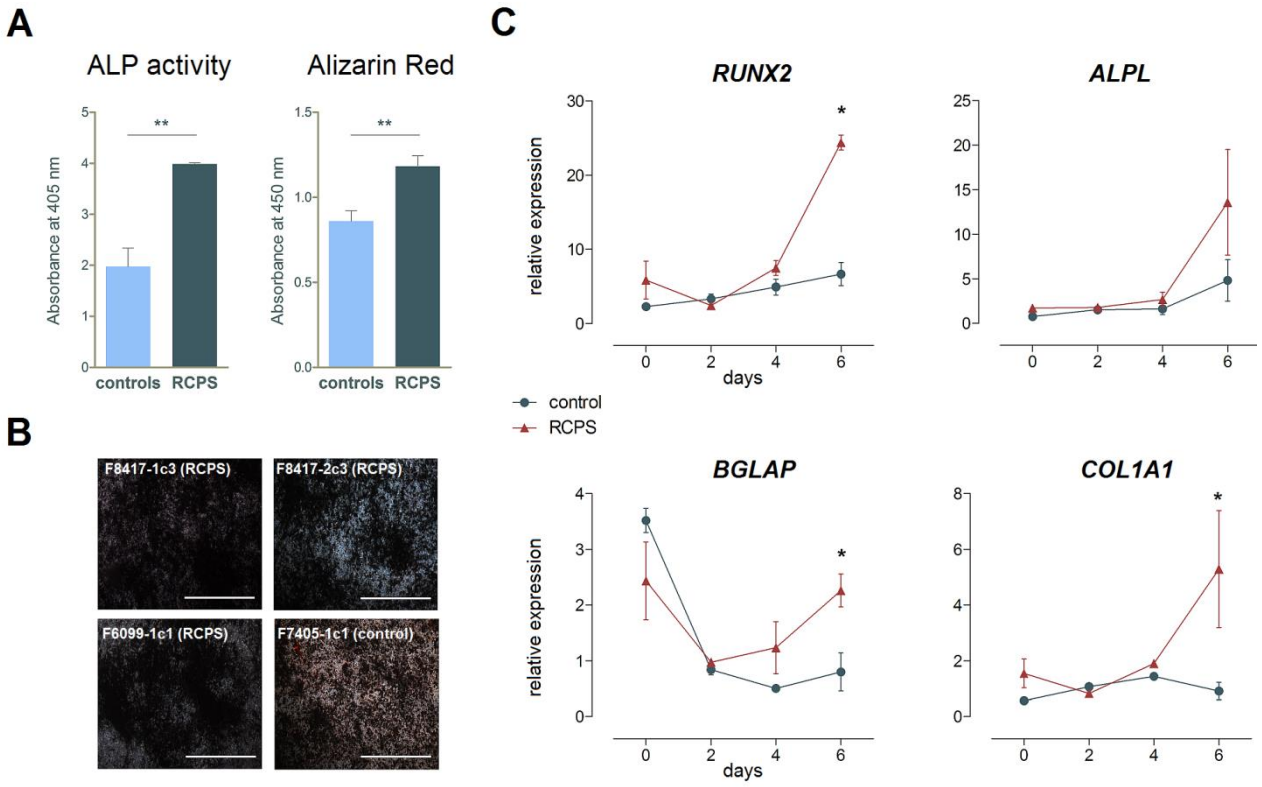

Figure 5: Alterations in osteogenic potential in RCPS nMSCs. A) Quantification of alkaline phosphatase (ALP) activity and Alizarin Red staining in nMSCs from RCPS and control subjects. (**) $p<0.01$, Student's t-test; **B)** Alizarin Red staining showing matrix mineralisation of RCPS samples x one representative control; Scale bars = 1000um, 10x magnification; **C)** Transcriptional profile of osteogenesis markers during the initial 6 days of osteoinduction. Values represent means ±SEM; (*) $p<0.05$, two-way ANOVA with Bonferroni post-tests.

EIF4A3 knockdown results in dysregulation of osteogenesis markers in nMSCs

To validate the findings obtained thus far, RNA interference assays were performed through stable shRNA-mediated knockdown of *EIF4A3* (shRNA-*EIF4A3*). Protein knockdown efficiency in *EIF4A3*-shRNA nMSCs was about 40% in two (F7405-1c1 and F7405-1c2) out of three independent nMSC replicates, as compared to the same nMSCs expressing a scrambled (scr) control shRNA (Fig. 6A). Although partial, this reduction in *EIF4A3* expression was similar to *EIF4A3* knockdown attempts reported in other works (40-60%; Singh et al., 2013; Wang et al., 2014). Knockdown was confirmed with the use of RT-qPCR in those 2 samples, which were submitted to subsequent analyses (Fig. S2B).

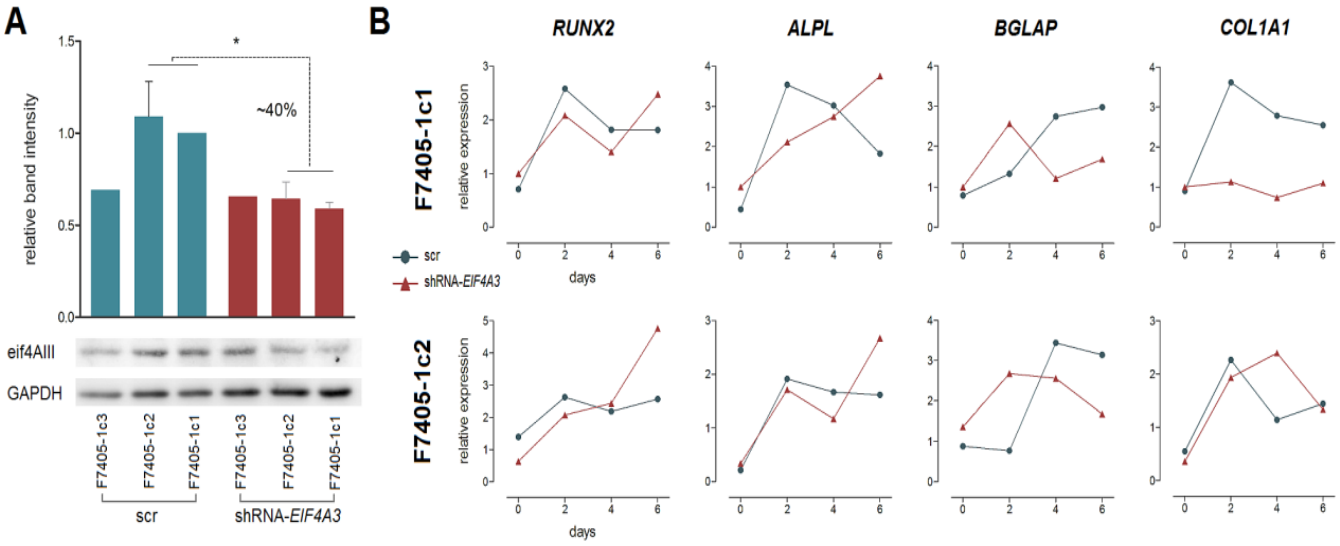

Figure 6: *EIF4A3* knockdown results in dysregulation of osteogenesis markers during early *in vitro* osteoinduction. A) Western blot assays for 3 nMSC knockdowns. Band intensities were normalised to an endogenous control (GAPDH) and calibrated to F7405-1c1 (scr). Error bars refer to two independent assays for F7405-1c1 and F7405-1c2; (*) $p<0.05$, Student's t-test; **B)** Transcriptional profile of osteogenesis markers during the initial 6 days of osteoinduction. Values represent means ±SEM.

The proliferation profile of both shRNA-*EIF4A3* nMSCs did not deviate from scr controls, confirming the findings for RCPS patients compared to controls (Fig. S3D). Also, for both nMSCs subjected to knockdown, we did not detect consistent changes in chondrogenesis marker expression between *EIF4A3*-shRNA nMSCs and scr nMSCs; therefore, we were unable to confirm if *EIF4A3* expression is associated with dysregulation of chondrogenesis-associated genes. Next, we sought to evaluate if early osteogenesis was also dysregulated in *EIF4A3* knockdown nMSCs. During the initial 6 days of osteoinduction, shRNA-*EIF4A3* nMSCs displayed dysregulated expression of osteogenesis markers, similarly to RCPS nMSCs: compared to scr controls, both knockdown nMSCs showed higher expression of *RUNX2* and *ALPL* at 6 days of differentiation; furthermore, the transcriptional pattern of *BGLAP* in shRNA-*EIF4A3* cells was clearly opposite to that of scr controls, with peak expression at day 2 of osteoinduction, and downregulation after 6 days. Finally, *COL1A1* exhibited discrepant expression patterns between the two *EIF4A3* knockdown nMSCs (Fig. S4B). Together, these results are compatible with the observed transcriptional dysregulation of early osteogenesis observed in RCPS nMSCs, confirming association between this behaviour and reduced *EIF4A3* mRNA expression.

DISCUSSION

Human craniofacial development is product of a coordinated series of spatio-temporally regulated morphogenetic events in which NCCs play a central role. Hence, development of neural crest-derived components is prone to errors due to genetic or environmental factors affecting NCC formation, migration, proliferation, or differentiation (Cordero et al., 2011; Bronner & LeDouarin, 2012; Zhang et al., 2014). Given its craniofacial

phenotype, RCPS is likely to arise from perturbations in NCC biology, as many of the structures affected in patients – the mandible, the larynx, and, in a severe case, the cranial sutures – possess a neural crest developmental component (Moody, 2015; Twigg & Wilkie, 2015; Maclean et al., 2009; Raskin et al., 2013; Favaro et al., 2014).

Here, to elucidate the pathogenetic mechanism responsible for RCPS, we generated patient-specific, iPSC-derived iNCCs and nMSCs. All iPSCs showed hallmarks of pluripotent stem cells, including high expression of pluripotency-associated genes and no signs of chromosomal imbalances, showing that reduced *EIF4A3* expression in RCPS patients' cells does not negatively impact iPSC generation. Moreover, iPSCs were efficiently differentiated into iNCCs exhibiting typical p75(NTR)/HNK1 double-positive staining and high expression of neural crest markers. The neural crest identity of all iNCCs was further confirmed through generation of homogeneous nMSC populations with mesenchymal immunophenotype and ability to give rise to mesenchymal derivatives *in vitro*, as previously reported (Menendez et al., 2011; Menendez et al., 2013; Fukuta et al., 2014). Taken together, these results show that our strategy successfully yielded disease-relevant cell types to study RCPS and other craniofacial syndromes *in vitro*.

Albeit some neural crest-related disorders have been attributed to increased cell death (Dixon et al., 2006; Brugmann et al., 2010), RCPS iNCCs and nMSCs did not show alterations in basal apoptosis by comparison to controls. However, this observation does not completely rule out the involvement of these processes in the pathogenesis of RCPS, as cells were tested under regular culture conditions, in the absence of challenges or additional induction signals. Thus, *EIF4A3* loss of function could nonetheless lead to cellular stress during high proliferative demands necessary for embryonic development *in vivo* (Twigg & Wilkie, 2015), as indicated by previous observations in an *eif4a3* zebrafish knockdown (Favaro et al., 2014).

The higher osteogenic potential along with abnormal expression of osteogenesis markers exhibited by *EIF4A3*-deficient nMSCs possibly reflects dysregulation of osteogenesis caused by reduced *EIF4A3* expression. The development of the cranioskeletal elements affected in RCPS is reliant on differentiation of neural crest-derived cells residing in the craniofacial mesenchyme, and dysregulation of differentiation pathways could be an underlying cause. For example, an essential promoter of cranioskeletal ossification is BMP signalling (Graf et al., 2015), which, when augmented, has been shown to result in a spectrum of craniofacial anomalies in mice, including cleft palate, agnathia or mandibular hypoplasia, and craniosynostosis (Stottman et al., 2001; Bonilla-Claudio et al., 2012; Li et al., 2013; Komatsu et al., 2013). In accordance, the most severe RCPS case reported to date also showed craniosynostosis and mandibular agenesis (Raskin et al., 2013). Moreover, RCPS exhibits clinical overlap with Nager syndrome (OMIM #154400), an acrofacial dysostosis caused by haploinsufficiency of *SF3B4*, a spliceosomal gene involved in inhibition of BMP-2-dependent osteogenesis and chondrogenesis (Nishanian et al., 2004; Watanabe et al., 2007); consequently, alterations in these differentiation mechanisms may also play a role in the pathogenesis of this syndrome (Lehalle et al., 2015; Trainor & Andrews, 2013) and other facial dysostoses, such as RCPS.

The abnormal behaviour in osteogenic differentiation seen in *EIF4A3*-deficient nMSCs may be related to the cellular function of eif4AIII, which is essential for EJC assembly and its recruitment to the spliceosome (Steckelberg et al., 2012). Recently, widespread changes in alternative splicing have been reported in HeLa cells depleted of eif4AIII and other EJC members (Wang et al., 2014), so aberrant expression of transcript variants may be accountable for such dysregulated differentiation in *EIF4A3*-deficient nMSCs. This idea is supported by the existence of disorders displaying phenotypic overlap with RCPS (e.g. mandibular hypoplasia, cleft palate, and limb anomalies), all caused by mutations in spliceosomal genes; these include *EFTUD2* (mandibulofacial dysostosis, Guion-Almeida type; OMIM #610536), *SNRPB*

(cerebrocostomandibular syndrome; OMIM #117650, and the previously mentioned *SF3B4* (Lehalle et al., 2015). Of note, the protein encoded by *EFTUD2* has been shown to interact with eif4AIII (Singh et al., 2012), further strengthening the importance of eif4AIII and the EJC for spliceosomal activity. Additional studies exploring disease-relevant cell types or animal models deficient for *EIF4A3* will be important to confirm whether splicing changes are responsible for the pathogenesis of RCPS and the aforementioned syndromes.

In summary, here we demonstrated that iPSC-derived iNCCs and nMSCs can be used to investigate RCPS and screen for disease-relevant cellular phenotypes *in vitro*. We show that decreased expression of *EIF4A3* is associated with dysregulated osteogenic potential in nMSCs, which possibly reflects disturbances of ossification in RCPS individuals during embryonic development. Importantly, this is the first work to use this approach to study a craniofacial syndrome, and thus it provides foundation for the characterisation of biological mechanisms responsible for craniofacial phenotypes with the use of iNCC-based models.

METHODS

Ethics statement

The experimental procedures involving samples from human subjects were approved by the Ethics Committee of Instituto de Biociências at Universidade de São Paulo, Brazil (accession number 39478314.8.0000.5464). Subjects donated biological samples only after providing signed informed consent.

Dermal fibroblast cultures

Skin biopsies were extracted from the lower posterior flank region with the use of 2-mm punch instruments and stored in DMEM/High Glucose (Life Technologies) supplemented with 100ug/mL Normocin (Invivogen), at 4°C. Within 24 hours, biopsies were rinsed with PBS and incubated in a dispase solution (1ug/mL; Sigma-Aldrich) in DMEM/High Glucose, overnight at 4°C. Specimens were then rinsed twice with PBS, their epidermis was removed, and the dermis was minced with a scalpel and seeded into 25cm^2 culture flasks containing fibroblast medium consisting of DMEM/High Glucose supplemented with 1% penicillin-streptomycin and 10% Foetal Bovine Serum (FBS; Life Technologies).

Generation of iPSCs

Fibroblasts were reprogrammed with the use of episomal vectors (pCXLE-hOCT3/4-shP53-F, addgene plasmid 27077; pCXLE-hSK, addgene plasmid 27078; pCXLE-hUL, addgene plasmid 27080), as described in Okita et al (2011), with the use of Amaxa Nucleofector II (program U-020) and NHDF nucleofection kit (Lonza), according to manufacturer's recommendations. Two days after nucleoporation, fibroblasts were co-cultivated with irradiated murine embryonic fibroblasts (Millipore) in embryonic stem cell medium (DMEM/F12 supplemented with 2mM GlutaMAX-I, 0.1mM non-essential aminoacids, 100uM 2-mercaptoethanol, 30ng/mL of bFGF and 20% of knockout serum replacement; all provided by Life Technologies). Typical iPSC colonies were transferred to Matrigel (BD-Biosciences)-coated plates and expanded in iPSC medium consisted of Essential 8™ Medium (Life Technologies) supplemented with 100ug/mL of Normocin (Invivogen). pCXLE-hOCT3/4-shP53-F, pCXLE-hSK, and pCXLE-hUL were a gift from Shinya Yamanaka.

End-point PCR and MLPA assays

Total DNA was extracted from iPSC cultures with the use of NucleoSpin Tissue (Macherey-Nagel), following supplier's instructions. For PCR reactions, primers targeting the OriP gene present in the backbone of the episomal vectors were used (oriP F 5'-TTC CAC GAG

GGT AGT GAA CC-3'; oriP R 5'-TCG GGG GTG TTA GAG ACA AC-3'), according to recommendations provided elsewhere (Epi5 Episomal iPSC Reprogramming Kit, Life Technologies). Multiplex Ligation-dependent Probe Amplification (MLPA) analysis was performed with subtelomeric kits (P036 and P070; MRC-Holland) to detect chromosomal imbalances, as previously described (Jehee et al., 2011).

Differentiation of iNCCs from iPSCs

Procedures for iNCC derivation were based on previously published methodology (Menendez et al., 2013; Fukuta et al., 2014). Before differentiation, iPSC colonies were adapted to single-cell passaging by rinsing cells with PBS followed by dissociation with Accutase (Life Technologies) for up to 5 minutes at room temperature, centrifugation at 200 g for 4 min and seeding onto Matrigel-coated dishes. After 2 subcultures, single cells were seeded onto 60-mm Matrigel-coated dishes at $5x10^4$ cells/cm^2. Two days post-seeding, medium was changed to iNCC differentiation medium, composed of Essential 6™ Medium (Life Technologies) supplemented with 8ng/mL bFGF (Life Technologies), 20uM SB431542 (Sigma-Aldrich), 1uM CHIR99021 (Sigma-Aldrich), and 100ug/mL Normocin; differentiation medium was changed daily. After ~2-4 days, neural crest-like cells were seen detaching from colony borders. Before reaching confluence, cultures were rinsed once with PBS and briefly incubated with Accutase at room temperature until differentiated cells detached and most undifferentiated colonies were left on the dish. Cell suspensions were centrifuged at 200 g for 4 minutes and re-seeded onto new Matrigel-coated dishes in fresh iNCC differentiation medium. With this method, passaging was performed whenever necessary, for 15 days, whereby morphologically homogeneous iNCC cultures were obtained. Differentiated iNCCs were cultivated for up to 8 passages in iNCC differentiation medium, replenished daily. In all procedures involving single-cell passaging, media were supplemented with 5uM Rock inhibitor (Sigma-Aldrich) upon seeding and maintained for 24 hours; after about 10 days of iNCC differentiation, Rock inhibitor was no longer needed to maintain cell viability.

Differentiation of nMSCs from iNCCs

nMSC populations were obtained through incubation of iNCCs with mesenchymal stem cell medium, as previously described (Menendez et al., 2011). In brief, iNCCs were seeded at $2x10^4$ cells/cm^2 onto non-coated 60-mm tissue culture dishes in nMSC medium (DMEM/F12 supplemented with 10% FBS, 2mM GlutaMAX-I, 0.1mM non-essential aminoacids, and 100ug/mL Normocin) containing 5uM Rock inhibitor. Cells were differentiated for 6 days and passaged with TrypLE™ Express (Life Technologies) when needed. nMSC cultures were expanded in nMSC medium for up to 6 passages, with medium changes every 3 days.

nMSC chondrogenic, osteogenic and adipogenic differentiation

For the osteogenic induction, cells were seeded in 12-well plates ($4x10^4$ cells per well), and after 3 days, medium was replaced with osteogenic induction medium (StemPro Osteogenesis Kit; Life Technologies). Differentiation medium was changed every 2-3 days. After 9 days, alkaline phosphatase activity was quantified through incubation with phosphatase substrate (Sigma-Aldrich), and the resulting p-nitrophenol was quantified colorimetrically using a Multiskan EX ELISA plate reader (Thermo Scientific) at 405 nm. After 21 days, extracellular matrix mineralisation was assessed through alizarin red staining. Briefly, cells were washed three times with PBS, fixed in 70% ethanol for 30 minutes at room temperature, washed 3x with distilled water, and finally stained with a 0.2% Alizarin Red S solution (Sigma-Aldrich) for 30 minutes at room temperature. After three washes with PBS, plates were air dried at room temperature. Staining was removed with a 20% methanol / 10% acetic acid solution and colorimetrically assessed using a Multiskan EX ELISA plate reader (Thermo Scientific) at 450nm.

For chondrogenesis, $1x10^5$ cells/well were plated into 6-well plates and after 3 days nMSC growth medium was replaced with chondrogenic medium (StemPro Chondrogenesis Kit; Life Technologies). To quantify chondrogenic markers, total RNA was extracted after 9 days of

differentiation. Chondrocyte pellets were produced by centrifuging 3x× 10^5 cells at 500g and incubating pellets in nMSC medium for 24 hours before switching to chondrogenic medium. After 21 days, pellets were fixed and frozen in Tissue-Tek O.C.T (Sakura), 5um cryosections were performed, sections were fixed with 4% paraformaldehyde and stained with Alcian Blue 0.1% in 0.1 N HCl.

Adipogenic differentiation was performed on 1x10^5 cells/well seeded into 6-well plates. After cells achieved 80% confluence, nMSC growth medium was replaced with adipogenesis medium (StemPro Adipogenesis Kit; Life Technologies). Cells were differentiated for 21 days, after which Oil red staining was performed. Cells were washed with PBS, fixed in 4% paraformaldehyde and stained with Oil Red 0.5% in isopropanol. Pictures were taken using an Axiovision microscope (Zeiss).

Apoptosis and proliferation assays

For the apoptosis assays, a total of 10^5 cells/well was seeded into 6-well culture plates. On the next day, apoptotic activity was measured with a kit based on Annexin V and 7-AAD staining (Guava Nexin Reagent), following manufacturer's instructions. Cells treated with 10uM H_2O_2 for 30 minutes were used as staining controls. Subpopulations were ascertained in a Guava flow cytometer (EMD Millipore) as follows: non-apoptotic cells: Annexin V(-) and 7-AAD(-); early apoptotic cells: Annexin V(+) and 7-AAD(-); late-stage apoptotic and dead cells: Annexin V(+) and 7-AAD(+).

Cell proliferation was assessed with the use of an XTT assay (Cell Proliferation Kit II; Roche), following supplier's instructions. Briefly, cells were seeded into 96-well culture plates at 2x10^3 cells/well, in quadruplicates. To quantify metabolically active cells, medium was changed to DMEM/F12 without phenol red (Life Technologies), a solution of XTT was added, and cells were incubated at 37°C for 3 hours. Immediately, plates were colorimetrically assessed in a microplate spectrophotometer (Epoch; BioTek) at 450nm.

Flow cytometry

To assess the immunophenotype of iNCCs, cells were detached with Accutase, and washed twice with 2 volumes of blocking solution (4% BSA in PBS without Ca^{2+} and Mg^{2+}). iNCCs were incubated with the conjugated antibodies in blocking solution in the dark for 1 hour at 4°C, washed twice with PBS, and fixed in 1% paraformaldehyde/PBS. The following antibodies were used: IgM k FITC Mouse Anti-Human CD57 (anti-HNK1; BD Pharmingen 561906), IgG1 k Alexa Fluor 647 Mouse Anti-Human CD271 (anti-p75NTR; BD Pharmingen 560877), FITC Mouse IgM k isotype control (BD Pharmingen 555583), and Alexa Fluor 647 Mouse IgG1 k isotype control (BD Pharmingen 557714). Antibody concentrations followed manufacturer's recommendations. A minimum of 5,000 events were acquired in a FACS Aria II flow cytometer (BD Biosciences) and analysed on WEASEL Flow Cytometry Software (v3.3).

nMSCs were dissociated with TrypLE Express and washed twice with 2 volumes of blocking solution (1% BSA in PBS without Ca^{2+} and Mg^{2+}). nMSCs were incubated in the aforementioned conditions with the following conjugated antibodies: FITC Mouse Anti-Human CD31 (BD Pharmingen 555445), APC Mouse Anti-Human CD73 (BD Pharmingen 560847), PE Mouse Anti-Human CD90 (BD Pharmingen 555596), PE Mouse Anti-Human CD166 (BD Pharmingen 559263), and FITC, PE and APC Mouse IgG1 κ Isotype Controls (BD Pharmingen 555748, 554681 and 555749, respectively). Antibody concentrations followed manufacturer's recommendations. At least 5,000 events were acquired in aFACS Aria II equipment and analysed on the Flowing software (v2.5).

shRNA-mediated knockdown

Retroviral plasmids containing shRNA sequences targeting human *EIF4A3* were acquired from Origene (TG313516), and chemically competent cells (One Shot TOP10 Competent Cells; Life Technologies) were transformed following manufacturer's guidelines, and amplified in LB broth (Life Technologies) supplemented with 25ug/mL kanamycin. Plasmids were extracted with the NucleoBond Xtra Midi kit (Macherey-Nagel). Viral particles

containing shRNA sequences were packaged in HEK293T cells and purified as described elsewhere (Griesi-Oliveira et al., 2014). F7405-1c1, F7405-1c2 and F7405-1c3 control iNCCs were seeded into Matrigel-coated 6-well plates (2x105 cells/well), and, on the next day, viral particles were added to the medium. After 24 hours, medium was changed and cells were grown for 7 days under puromycin (Life Technologies) selection (0.1ug/mL in iNCC medium). Subsequently, they were subjected to nMSC differentiation and maintained for at least one additional week in nMSC medium supplemented with 0.1ug/mL puromycin, before assessment of knockdown efficiency.

Real-time quantitative PCR (RT-qPCR)

Total RNA was obtained from cell populations with the use of Nucleospin RNA II extraction kit (Macherey-Nagel) following manufacturer's recommendations. Briefly, 1ug of total RNA was converted into cDNA using Superscript II (Life Technologies) and oligo-dT primers according to manufacturer's recommendations. Real-Time quantitative PCR reactions were performed with 2X Fast SYBR Green PCR Master Mix (Life Technologies) and 50nM–400nM of each primer. Fluorescence was detected using the 7500 Fast Real-Time PCR System (Life Technologies), under standard temperature protocol. Primer pairs were either designed with Primer-BLAST (http://www.ncbi.nlm.nih.gov/tools/primer-blast/) or retrieved from PrimerBank (http://pga.mgh.harvard.edu/primerbank/; primers are listed in Table SII), and their amplification efficiencies (E) were determined by serial cDNA dilutions $\log_{10}$-plotted against Ct values, in which $E=10^{-1/slope}$. Gene expression was assessed relative to a calibrator cDNA (ΔCt). Finally, NormFinder (Andersen et al., 20014) was used to determine the most stable endogenous control (among *ACTB*, *TBP*, *HMBS*, *GAPDH*, or *HPRT1*), and calculate normalization factors ($E^{-\Delta C}$)for each sample. The final relative expression values were determined based on a previous method (Pfaffl et al., 2001), by dividing $E^{-\Delta Ct}$ of target genes by $E^{-\Delta Ct}$ the endogenous control. All relative expression values were log-transformed for analysis and graphed in linear scale, unless stated otherwise. Primers were supplied by Exxtend.

Western blot

nMSCs were grown in 75cm^2 culture flasks until 80% confluence in nMSC growth medium. Total protein lysates were obtained using PhosphoSafe (EMD Millipore) containing a protease inhibitor cocktail (Sigma-Aldrich). Protein concentration was determined using a bicinchoninic acid assay kit according to manufacturer's instructions (Thermo Fisher Scientific). Total cell lysates (20 ug) were separated by SDS-PAGE and dry-transferred to nitrocellulose membranes with the iBlot system (Life Technologies) according to manufacturer's recommendations. Membranes were blocked in buffer TBS-T (1M Tris–HCl pH 7.5, 5M NaCl, 0.1% Tween-20) with 5% BSA under constant stirring for 1 hour at room temperature, washed 4x with TBS-T, and incubated with anti-eif4AIII (1:2,000 dilution in TBS-T/BSA; ab32485; Abcam) primary antibody overnight at 4°C under constant stirring. Detection was performed using anti-rabbit IgG, HRP-linked Antibody (1:2,500 dilution in TBS-T/BSA; #7074; Cell Signaling) under constant stirring for 1 h at room temperature, followed by incubation with ECL Prime substrate (GE Healthcare) and capture in the Image Quant LAS 4000 Mini (GE Healthcare). GAPDH was used as a loading control (1:10,000 dilution in TBS-T/BSA; NB300-324; Novus Biologicals). Densitometric analyses were performed on the Image Quant TL 8.1 software (GE Healthcare). eif4AIII protein levels were quantified and normalized to the corresponding GAPDH levels.

Immunofluorescence

Cells were fixed in 4% paraformaldehyde for 20 minutes at room temperature, followed by permeabilisation with PBS 0.2% Triton X-100 for 30 minutes at 4°C. Blocking was carried out with PBS 5% BSA for 1 hour at room temperature, followed by incubation with with primary antibodies in blocking solution overnight at 4°C. After washing 3x with PBS, cells were incubated with secondary antibodies in blocking solution at 4°C for 1 hour, in the dark, followed by two PBS washes and counterstaining with DAPI solution (Life Technologies) for 2

minutes at room temperature. After a final PBS wash, cells were analysed with a fluorescent microscope (Axiovision; Zeiss). Antibodies used were: primary Anti-OCT4 antibody (ab19857; Abcam) at 3ug/mL + secondary Goat anti-Rabbit IgG (H+L) Secondary Antibody, Alexa Fluor 546 conjugate (A-11010; Life Technologies) at 1:1,000 dilution; primary Anti-SSEA4 antibody [MC813] (ab16287; Abcam) at 15ug/mL + secondary Goat anti-Mouse IgG (H+L) Secondary Antibody, Alexa Fluor 488 conjugate (A-11001; Life Technologies) at 1:1,000 dilution.

Statistical analysis:

All experiments were performed in triplicates, unless stated otherwise herein. Statistical comparisons were performed on the Graphpad Prism software. Values were represented as means ± standard error. The level of statistical significance was set at $p<0.05$.

Web Resources

OMIM – Online Mendelian Inheritance in Men - http://www.omim.org/

Primer-BLAST - http://www.ncbi.nlm.nih.gov/tools/primer-blast/

Primer Bank - https://pga.mgh.harvard.edu/primerbank/

SUPPLEMENTARY FIGURES

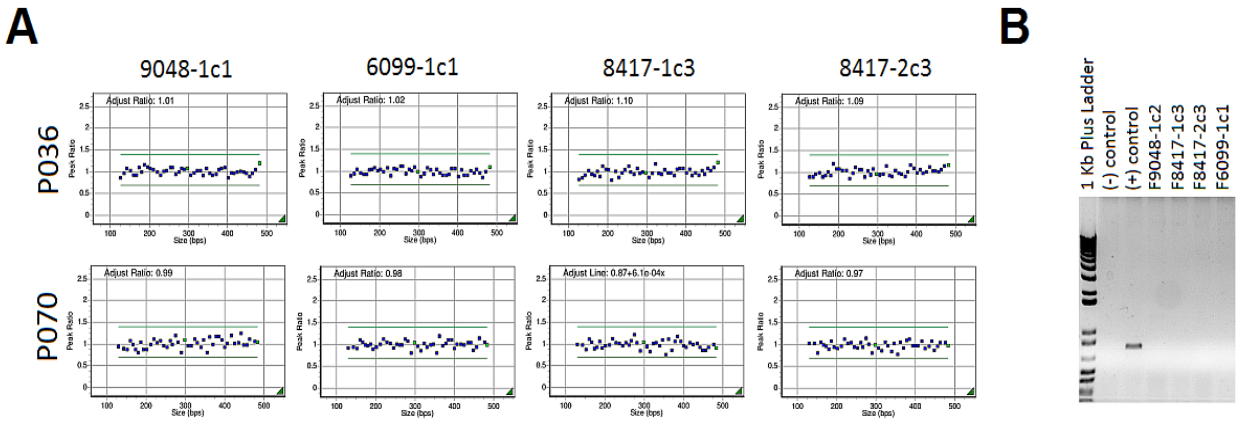

Figure S1: Characterisation of iPSCs. A) MLPA analysis with peak ratios for subtelomeric probes (blue dots) and control probes (green dots) with the use of 2 kits, showing no chromosomal imbalances; **B)** End-point PCR for vector backbone gene *OriP*, showing no genomic integration of episomal plasmids in iPSC cultures. DNA from one iPSC line in which genomic integration had been detected was used as the positive (+) control.

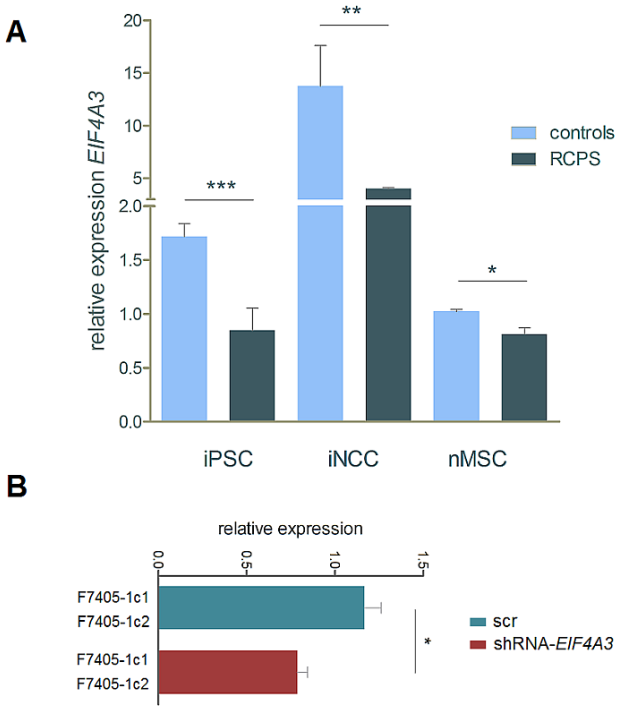

Figure S2: A) RT-qPCR assessment of *EIF4A3* mRNA expression in iPSCs, iNCCs, and nMSCs. **B)** RT-qPCR for *EIF4A3* mRNA expression in knockdown (shRNA-*EIF4A3*) and control (scr) nMSCs. Values represent means ±SEM; (***) $p<0.001$; (**) $p<0.01$; (*) $p<0.05$, Student's t-test.

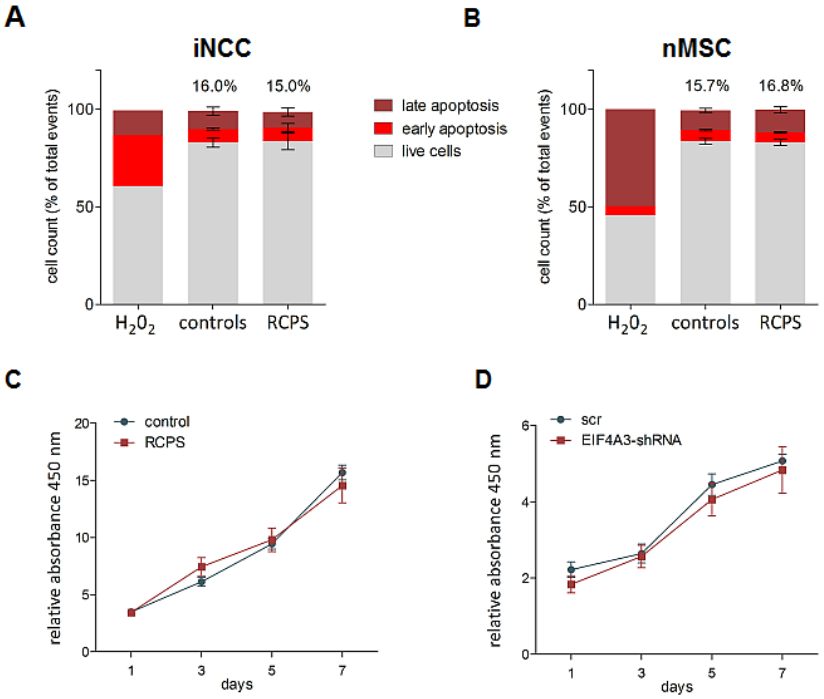

Figure S3: Apoptosis and proliferation A, B) 7-AAD/Annexin V flow cytometry results depicting the fraction of live cells, and cells undergoing early and late apoptosis in nMSCs **(A)** and iNCCs **(B)**. Percentages represent the sums of early and late apoptotic events. H_2O_2-treated cells were used as positive staining controls. **B)** XTT assay depicting the proliferation profile of control and TCS nMSCs. XTT assay showing proliferation of scr and *EIF4A3* shRNA nMSCs.

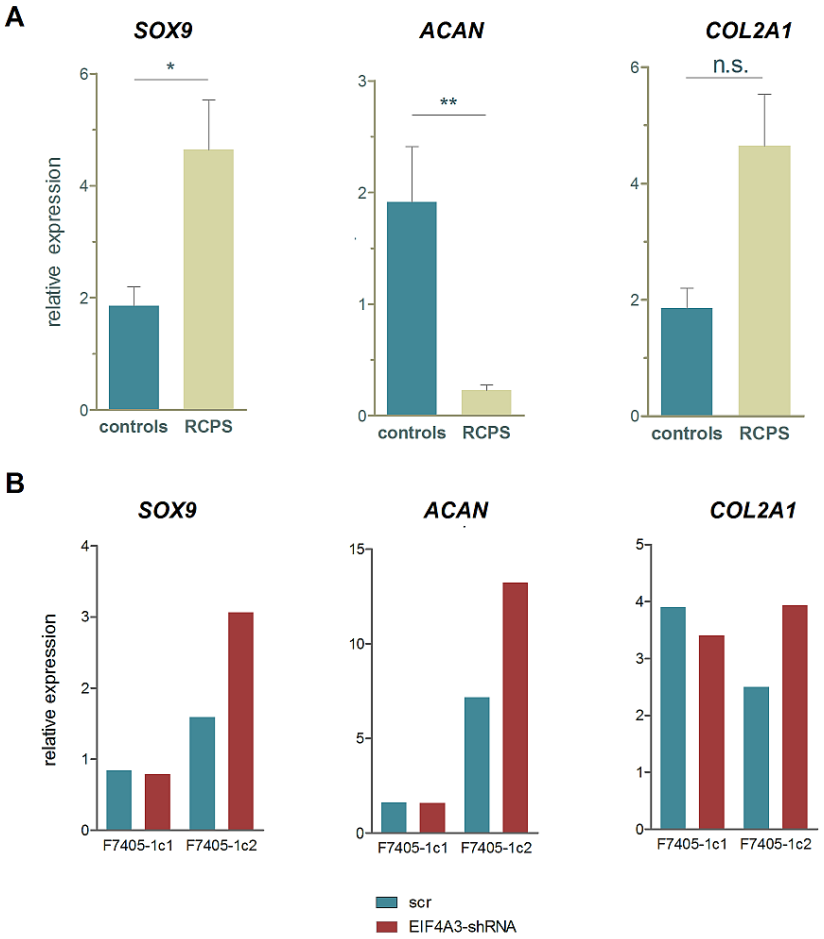

Figure S4: Chondrogenesis in *EIF4A3*-deficient nMSCs. RT-PCR assays showing the transcriptional profile of chondrogenesis-associated transcripts after 9 days of chondrogenic differentiation in (**A)** RCPS and control nMSCs and **(B)** *EIF4A3* knockdown and scr control nMSCs. (***) p<0.001; (**) p<0.01; (*) p<0.05; Student's t-test; n.s. = not significant.

SUPPLEMENTARY TABLES

Table SI: Cell samples used in the study.

Cell/clone	Subject	Age*	Gender	Phenotype	Genotype *EIF4A3***	Reprogramming method
F7405-1c1 F7405-1c2 F7405-1c3	F7405-1	27	male	control	-	retroviral
F9048-1c3	F9048-1	20	male	control	-	episomal
F8417-1c3	F8417-1	11	female	RCPS	16 repeats|16 repeats	episomal
F8417-2c3	F8417-2	9	male	RCPS	16 repeats|16repeats	episomal
F6099-1c1	F6099-1	10	male	RCPS	14 repeats|c.809A>G	episomal
F7405-1c1 F7405-1c2	F7405-1	-	-	scr control shRNA	-	-
F7405-1c1 F7405-1c2	F7405-1	-	-	*EIF4A3* shRNA	-	-

*age upon skin biopsy
**please refer to Favaro et al (2014) for additional information

Table SII: Primer sequences used in RT-qPCR.

Target	Forward primer (5'-3')	Reverse Primer (5'-3')
ACTB	TGAAGTGTGACGTGGACATC	GGAGGAGCAATGATCTTGAT
GAPDH	ATCACCATCTTCCAGGAGCG	GGGCAGAGATGATGACCCTTT
HPRT1	CCTGGCGTCGTGATTAGTGAT	AGACGTTCAGTCCTGTCCATAA
HMBS	AGCTTGCTCGCATACAGACG	AGCTCCTTGGTAAACAGGCTT
TBP	GTGACCCAGCATCACTGTTTC	GCAAACCAGAAACCCTTGCG
OCT3/4	GTGGTCAGCCAACTCGTCA	CCAAAAACCCTGGCACAAACT
NANOG	TGGACACTGGCTGAATCCTTC	CGTTGATTAGGCTCCAACCAT
EIF4A3	GGAGATCAGGTCGATACGGC	GATCAGCAACGTTCATCGGC
PAX3	AAGCCCAAGCAGGTGACAAC	CTCGGATTTCCCAGCTGAAC
ZIC1	AAGGTCCACGAATCCTCCTC	TTGTGGTCGGGTTGTCTG
TFAP2A	CTCCGCCATCCCTATTAACAAG	GACCCGGAACTGAACAGAAGA
SOX10	CCTCACAGATCGCCTACACC	CATATAGGAGAAGGCCGAGTAGA
ENG	TGCACTTGGCCTACAATTCCA	AGCTGCCCACTCAAGGATCT
SOX9	AGCGAACGCACATCAAGAC	CTGTAGGCGATCTGTTGGGG
ACAN	TTTCAAGAAGGCGAGGCGTCCG	TGGCTGAAGGCAAGCCTGGT
COL2A1	GGCAATAGCAGGTTCACGTACA	CGATAACAGTCTTGCCCCACTT
RUNX2	AGTGGACGAGGCAAGAGTTTC	GTTCCCGAGGTCCATCTACTG
ALPL	GATACAAGCACTCCCACTTCATCTG	CTGTTCAGCTCGTACTGCATGTC
COL1A1	GGGCCAAGACGAAGACAT	CAACACCCTTGCCGTTGTCG
BGLAP	GGCGCTACCTGTATCAATGG	GTGGTCAGCCAACTCGTCA

REFERENCES

Bonilla-Claudio, M., J. Wang, et al. Bmp signaling regulates a dose-dependent transcriptional program to control facial skeletal development. Development, v.139, n.4, Feb, p.709-19. 2012.

Bronner, M. E. e N. M. Ledouarin. Development and evolution of the neural crest: an overview. Dev Biol, v.366, n.1, Jun 1, p.2-9. 2012.

Brugmann, S. A., N. C. Allen, et al. A primary cilia-dependent etiology for midline facial disorders. Hum Mol Genet, v.19, n.8, Apr 15, p.1577-92. 2010.

Chan, C. C., J. Dostie, et al. eIF4A3 is a novel component of the exon junction complex. RNA, v.10, n.2, Feb, p.200-9. 2004.

Cordero, D. R., S. Brugmann, et al. Cranial neural crest cells on the move: their roles in craniofacial development. Am J Med Genet A, v.155A, n.2, Feb, p.270-9. 2011.

Dixon, J., N. C. Jones, et al. Tcof1/Treacle is required for neural crest cell formation and proliferation deficiencies that cause craniofacial abnormalities. Proc Natl Acad Sci U S A, v.103, n.36, Sep 5, p.13403-8. 2006.

Favaro, F. P., L. Alvizi, et al. A noncoding expansion in EIF4A3 causes Richieri-Costa-Pereira syndrome, a craniofacial disorder associated with limb defects. Am J Hum Genet, v.94, n.1, Jan 2, p.120-8. 2014.

Favaro, F. P., R. M. Zechi-Ceide, et al. Richieri-Costa-Pereira syndrome: a unique acrofacial dysostosis type. An overview of the Brazilian cases. Am J Med Genet A, v.155A, n.2, Feb, p.322-31. 2011.

Fukuta, M., Y. Nakai, et al. Derivation of mesenchymal stromal cells from pluripotent stem cells through a neural crest lineage using small molecule compounds with defined media. PLoS One, v.9, n.12, p.e112291. 2014.

Gong, S. G. Cranial neural crest: migratory cell behavior and regulatory networks. Exp Cell Res, v.325, n.2, Jul 15, p.90-5. 2014.

Graf, D., Z. Malik, et al. Common mechanisms in development and disease: BMP signaling in craniofacial development. Cytokine Growth Factor Rev, Nov 24. 2015.

Griesi-Oliveira, K., A. Acab, et al. Modeling non-syndromic autism and the impact of TRPC6 disruption in human neurons. Mol Psychiatry, Nov 11. 2014.

Jehee, F. S., J. T. Takamori, et al. Using a combination of MLPA kits to detect chromosomal imbalances in patients with multiple congenital anomalies and mental retardation is a valuable choice for developing countries. Eur J Med Genet, v.54, n.4, Jul-Aug, p.e425-32. 2011.

Komatsu, Y., P. B. Yu, et al. Augmentation of Smad-dependent BMP signaling in neural crest cells causes craniosynostosis in mice. J Bone Miner Res, v.28, n.6, Jun, p.1422-33. 2013.

Lehalle, D., D. Wieczorek, et al. A review of craniofacial disorders caused by spliceosomal defects. Clin Genet, v.88, n.5, Nov, p.405-15. 2015.

Li, L., Y. Wang, et al. Augmented BMPRIA-mediated BMP signaling in cranial neural crest lineage leads to cleft palate formation and delayed tooth differentiation. PLoS One, v.8, n.6, p.e66107. 2013.

Maclean, G., P. Dolle, et al. Genetic disruption of CYP26B1 severely affects development of neural crest derived head structures, but does not compromise hindbrain patterning. Dev Dyn, v.238, n.3, Mar, p.732-45. 2009.

Menendez, L., M. J. Kulik, et al. Directed differentiation of human pluripotent cells to neural crest stem cells. Nat Protoc, v.8, n.1, Jan, p.203-12. 2013.

Menendez, L., T. A. Yatskievych, et al. Wnt signaling and a Smad pathway blockade direct the differentiation of human pluripotent stem cells to multipotent neural crest cells. Proc Natl Acad Sci U S A, v.108, n.48, Nov 29, p.19240-5. 2011.

Moody, S. Principles of Developmental Genetics: Publisher: Academic Press, v.1. 2015. 784 p.

Nishanian, T. G. e T. Waldman. Interaction of the BMPR-IA tumor suppressor with a developmentally relevant splicing factor. Biochem Biophys Res Commun, v.323, n.1, Oct 8, p.91-7. 2004.

Okita, K., T. Yamakawa, et al. An efficient nonviral method to generate integration-free human-induced pluripotent stem cells from cord blood and peripheral blood cells. Stem Cells, v.31, n.3, Mar, p.458-66. 2012.

Passos-Bueno, M. R., C. C. Ornelas, et al. Syndromes of the first and second pharyngeal arches: A review. Am J Med Genet A, v.149A, n.8, Aug, p.1853-9. 2009.

Pfaffl, M. W. A new mathematical model for relative quantification in real-time RT-PCR. Nucleic Acids Res, v.29, n.9, May 1, p.e45. 2001.

Raskin, S., M. Souza, et al. Richieri-costa and Pereira syndrome: severe phenotype. Am J Med Genet A, v.161A, n.8, Aug, p.1999-2003. 2013.

Singh, K. K., L. Wachsmuth, et al. Two mammalian MAGOH genes contribute to exon junction complex composition and nonsense-mediated decay. RNA Biol, v.10, n.8, Aug, p.1291-8. 2013.

Steckelberg, A. L., J. Altmueller, et al. CWC22-dependent pre-mRNA splicing and eIF4A3 binding enables global deposition of exon junction complexes. Nucleic Acids Res, v.43, n.9, May 19, p.4687-700. 2015.

Stottmann, R. W., R. M. Anderson, et al. The BMP antagonists Chordin and Noggin have essential but redundant roles in mouse mandibular outgrowth. Dev Biol, v.240, n.2, Dec 15, p.457-73. 2001.

Trainor, P. A. e B. T. Andrews. Facial dysostoses: Etiology, pathogenesis and management. Am J Med Genet C Semin Med Genet, v.163C, n.4, Nov, p.283-94. 2013.

Twigg, S. R. e A. O. Wilkie. New insights into craniofacial malformations. Hum Mol Genet, Jun 17. 2015.

Wang, Z., V. Murigneux, et al. Transcriptome-wide modulation of splicing by the exon junction complex. Genome Biol, v.15, n.12, p.551. 2014.

Watanabe, H., M. Shionyu, et al. Splicing factor 3b subunit 4 binds BMPR-IA and inhibits osteochondral cell differentiation. J Biol Chem, v.282, n.28, Jul 13, p.20728-38. 2007.

Zhang, D., S. Ighaniyan, et al. The neural crest: a versatile organ system. Birth Defects Res C Embryo Today, v.102, n.3, Sep, p.275-98. 2014.

Chapter IV

Alterations in neural crest-derived mesenchymal cells in the aetiology of Treacher Collins syndrome

Gerson S. Kobayashi, Felipe A. A. Ishiy, Camila M. Musso, Luiz C. Caires, Ernesto Goulart, Roberto D. Fanganiello, Patrícia Semedo-Kuriki, Naila Lourenço, Karina Griesi-Oliveira, Ângela M. Suzuki, Maria Rita Passos-Bueno.

Abstract

Apoptosis of pre-migratory cranial neural crest cells is considered to be the major phenotypic driver of Treacher Collins syndrome (TCS), a mandibulofacial dysostosis caused by loss-of-function mutations in *TCOF1*. However, the effect of these mutations on post-migratory, neural crest-derived mesenchymal cells and their skeletogenic fate remains elusive. To address this question, we report the establishment and phenotype assessment of neural crest-derived mesenchymal cells (nMSCs) from TCS iPSCs. We show that TCS nMSCs display both increased apoptosis and aberrant osteo-chondrogenic profiles *in vitro*. In comparison to controls, TCS cells showed changes in osteogenic potential and dysregulated expression of chondrogenesis markers during osteogenic and chondrogenic differentiation. These results suggest that cellular properties of neural crest-derived mesenchymal cells are impacted by *TCOF1* loss of function, providing additional clues to unravel the pathogenesis of TCS.

CHAPTER IV

Alterations in neural crest-derived mesenchymal cells in the aetiology of Treacher Collins syndrome

Gerson S. Kobayashi, Felipe A. A. Ishiy, Camila M. Musso, Luiz C. Caires, Ernesto Goulart, Roberto D. Fanganiello, Patrícia Semedo-Kuriki, Naila Lourenço, Karina Griesi-Oliveira, Ângela M. Suzuki, Maria Rita Passos-Bueno.

INTRODUCTION

Treacher Collins Syndrome (TCS1, OMIM #154500; TCS2, OMIM#613717; TCS3, OMIM #248390) is a rare mandibulofacial dysostosis present in 1:50,000 live births. Despite showing overlap with other craniofacial syndromes, the clinical presentation of TCS is very typical and includes hypoplasia of facial bones, particularly the zygomatic bones and the mandible, external ear anomalies and conductive hearing loss (Trainor et al., 2009). Genetic alterations in the genes *TCOF1*, *POLR1C* and *POLR1D* are the currently established underlying causes of TCS. Loss-of-function mutations in *TCOF1*, responsible for the vast majority of cases (Splendore et al., 2000), result in haploinsufficiency of its encoded protein, Treacle, which is involved in ribosome biogenesis (Gonzales et al., 2005); concurrently, *POLR1C* and *POLR1D* mutations are also linked to deficiency in ribosome biogenesis due to impairment of RNA polymerase I/III (Dauwerse et al., 2011; Trainor and Merrill, 2014).

Human craniofacial development is a multi-stage process in which neural crest cells (NCCs) play a major role. Initially, cranial NCCs emerge from the neuroepithelium at the foremost region of the neuraxis and migrate to constitute the mesenchyme of the pharyngeal

arches. Subsequently, the neural crest-derived mesenchymal cells undergo proliferation and differentiation to generate a range of craniofacial components, including facial bones, cartilage, and connective tissue (Bhatt et al., 2013; Gong et al., 2014; Twigg & Wilkie, 2015). During this process, *TCOF1* loss of function is considered to impair ribosome biogenesis leading to increased apoptosis and proliferation deficit of NCCs, ultimately resulting in hypoplasia of facial bone and cartilage, as reported in animal models (Dixon et al., 1997; Jones et al., 1999; Dixon et al., 2006; Jones et al., 2008; Weiner et al., 2012). Still, the direct impact exerted by *TCOF1* pathogenic mutations in human post-migratory craniofacial mesenchymal cells is not well characterised, nor is its effects on their differentiation properties.

Induced pluripotent stem cells (iPSCs) stand as an invaluable tool to model human disease, as patient-specific iPSCs can be generated and differentiated towards affected cell types. This possibility has recently embraced craniofacial diseases, as directed generation of neural crest cells (iNCCs) from iPSCs is now attainable. iNCC cultures can, in turn, be induced towards iNCC mesenchymal derivatives, such as osteoblasts, chondrocytes and adipocytes, expanding possibilities for investigating disease-related phenotypes (Menendez et al., 2013; Fukuta et al., 2014, Matsumoto et al., 2015). Although multipotent post-migratory neural crest-derived mesenchymal cells have been successfully isolated from mouse embryos and studied *in vitro* (Zhao et al., 2006), mouse neural crest development possess intrinsic features not observed in other species (Barriga et al., 2015) and may not faithfully represent human craniofacial development in every aspect. Furthermore, studies exploring the properties of NCC-derived mesenchymal cells are scarce, especially regarding the effect of mutations associated with craniofacial syndromes.

Here, we investigated cellular phenotypes of neural crest-derived mesenchymal cells from TCS patients. These cells were obtained by inducing TCS iPSCs towards a neural crest stage, in an attempt to recapitulate human craniofacial development *in vitro*. Our results show

the effectiveness of this approach in investigating craniofacial phenotypes, and they provide insight into the impact of *TCOF1* loss of function in human neural crest-derived craniofacial mesenchymal cells.

RESULTS

Generation of TCS and control iPSCs

All iPSC cultures displayed embryonic stem cell-like morphology and expressed pluripotency markers *NANOG, OCT3/4, ALPL*, and SSEA-4 (Fig. S1A), and subtelomeric MLPA assays showed no chromosomal imbalances in either control or TCS iPSCs (Fig. S1B). Both TCS subjects had been molecularly characterised in another work (Masotti et al., 2009) and harboured the following genotypes: subject F2441-1 - c.4344dupA (p.Arg1448fs); subject F2625-1 - c.431delC (p.Thr144fs). We generated 5 independent iPSC clones from the TCS iPSCs (F2441-1c1-c2; F2625-1c1-c3). Control samples comprised 3 individuals and a total of 6 clones (F7405-1-c1-c3, F7007-1c1-c2, and F9048-1c1; Table SI); albeit F9048-1 was reprogrammed with episomal vectors, it showed no differences in expression of pluripotency markers in comparison to the other iPSCs, and it was therefore included in the experiments described herein. Reduced expression of *TCOF1* mRNA was confirmed in TCS iPSCs, as compared to controls (Fig. 1).

iPSC-derived neural crest cells express neural crest markers

iPSC-derived neural crest cells (iNCCs) were induced from TCS and control iPSCs with a methodology based on TGF-β/Activin pathway blockade and WNT pathway activation (Menendez et al., 2013; Fukuta et al., 2014). After differentiation, TCS and control iNCC populations displayed typical neural crest cell morphology and expressed neural crest markers p75(NTR) and HNK1. Of note, the TCS iNCCs displayed decreased HNK1 expression, and the proportion of $HNK1^{+}$ cells varied between 43.7% and 66.9%% (Fig. 2A). RT-qPCR assays revealed upregulation of neural crest markers *PAX3*, *TFAP2A*, *ZIC1* and *SOX10*, and downregulation of pluripotency markers *OCT3/4*, *NANOG*, and *ALPL*, when compared with the originating iPSCs (Fig 2B). Finally, reduction of *TCOF1* transcript expression (~25% reduction) was confirmed in TCS iNCCs, when compared to controls (Fig 1).

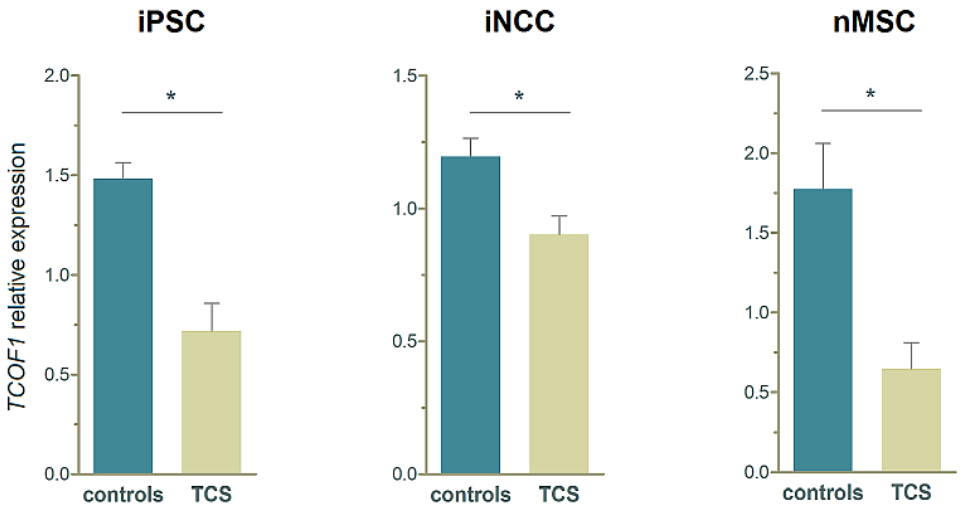

Figure 1: Characterisation of *TCOF1* expression in TCS cells. RT-qPCR assessment of *TCOF1* transcript abundance in iPSCs, iNCCs and nMSCs from controls and TCS subjects. (*) $p < 0.05$; Student's t-test.

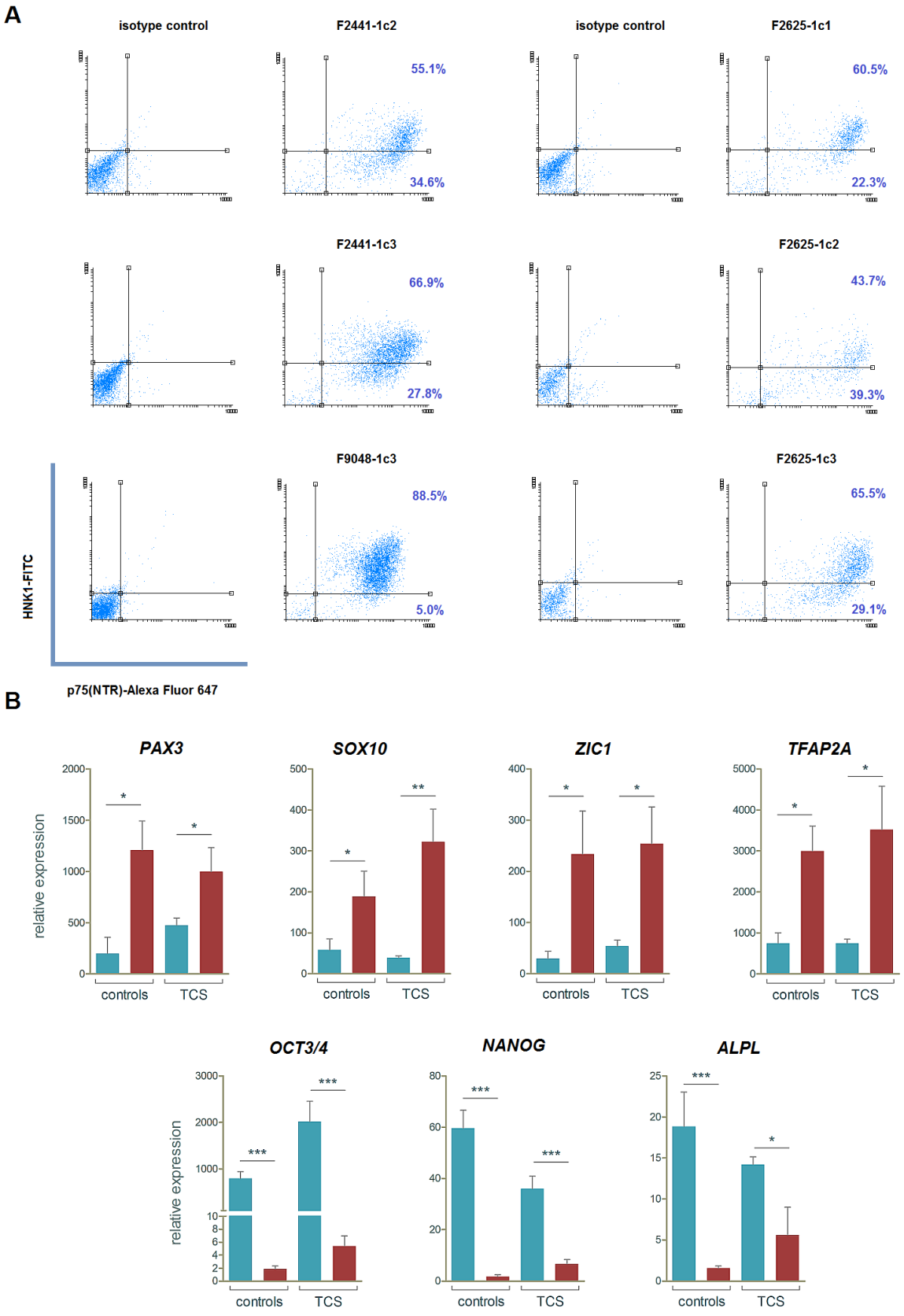

Figure 2: Characterisation of iNCCs. A) Biparametric flow cytometry dot plots for HNK1 and p75(NTR) expression in TCS and a representative control. Values in represent p75(NTR)$^{+}$ cell fractions either positively (upper right) or negatively (lower right) stained for HNK1. **B)** RT-qPCR assessment of neural crest (upper panel) and pluripotency marker (lower panel) expression between iNCCs and the originating iPSCs. (*) $p < 0.05$; (**) $p < 0.01$; (***) $p < 0.001$; Student's t-test.

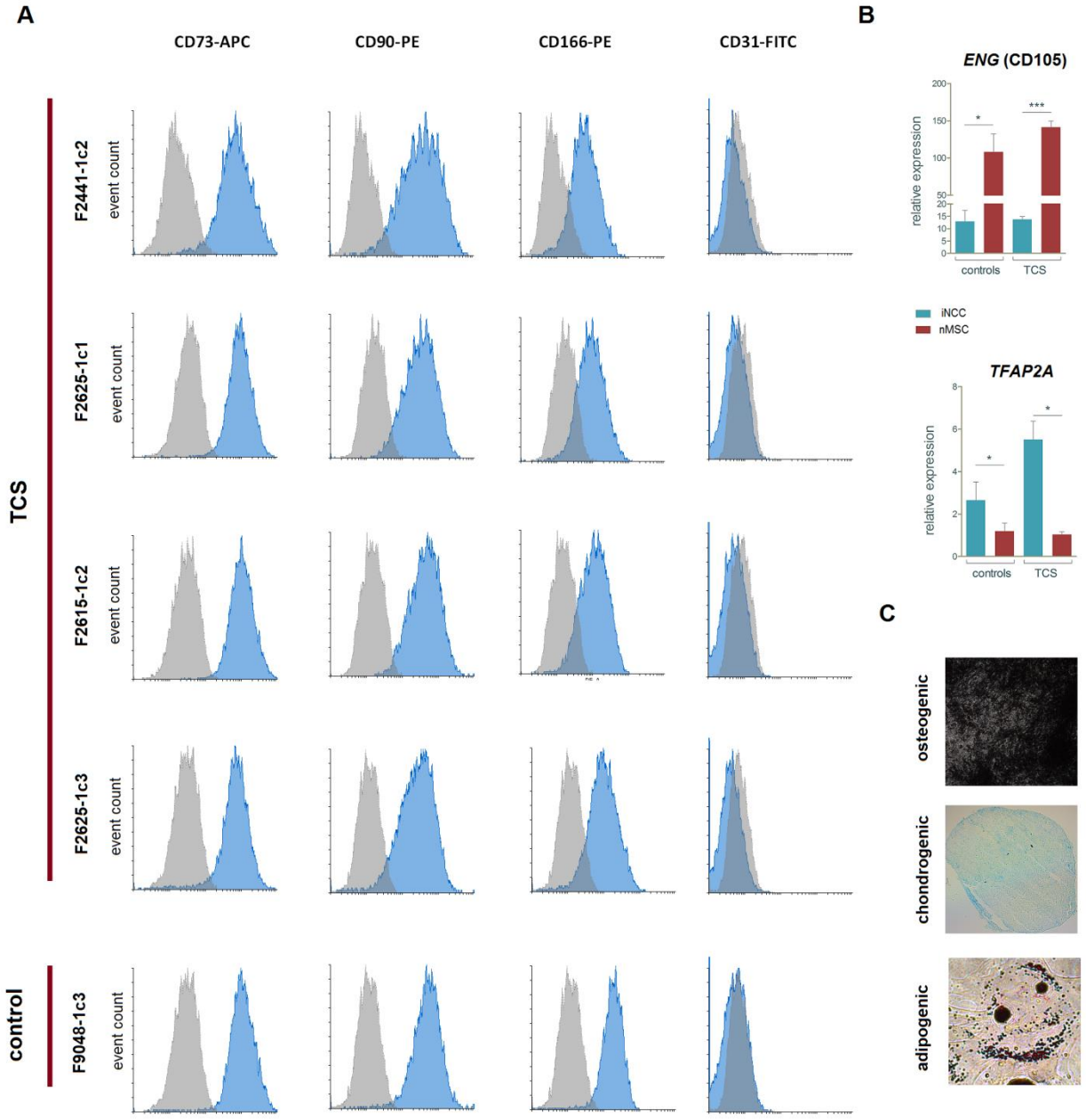

Figure 3: Characterisation of nMSCs. A) Flow cytometry immunophenotype profiling of nMSCs showing positive staining for mesenchymal markers CD73, CD90 and CD166, and negative staining for endothelial marker CD31. Histograms represent event count (y-axis) vs. fluorescence (x-axis). Experimental data (blue) were plotted in overlay with data from isotype controls (light blue). **B)** RT-qPCR assays showing upregulation of mesenchymal marker *ENG* (CD105) and downregulation of neural crest marker *TFAP2A* in nMSCs compared to iNCCs; (***) $p<0.001$; (*) $p<0.05$; Student's t-test. **C)** Example of osteogenic, chondrogenic, and adipogenic differentiation of nMSCs, detected with Alizarin Red, Alcian Blue, and Oil Red staining, respectively.

Multipotent neural crest-derived mesenchymal stem-like cells (nMSCs) can be efficiently generated from TCS iNCCs

In spite of the lower HNK1 expression in TCS iNCCs, they were submitted to differentiation towards the mesenchymal lineage. Both TCS and control nMSC populations

showed spindle-shaped fibroblast-like morphology (data not shown), and notably, surface antigen profiling revealed a homogeneous mesenchymal immunophenotype, with positively stained cells for mesenchymal markers CD73, CD166 and CD90, and negative staining for endothelial marker CD31 (Fig. 3A). In agreement, nMSCs showed downregulation of *OCT3/4*, *NANOG* and *ALPL* and upregulation of mesenchymal marker *ENG* (CD105), when compared with the original iPSCs (Fig. 3B). These cells also displayed tri-lineage potential, being able to undergo osteogenic, chondrogenic and adipogenic *in vitro* differentiation (Fig. 3C). Strikingly, *TCOF1* mRNA expression was greatly reduced in TCS nMSCs (~64% reduction) as compared to controls (Fig. 1).

TCS nMSCs exhibit alterations in osteogenic and chondrogenic potential

During the first 6 days of osteoinduction, all nMSCs showed the expected transcriptional behaviour, with upregulation of early osteogenesis markers *RUNX2*, *ALPL* and *COL1A1,* and downregulation of late osteoblast marker *BGLAP* (Fig. S2). Further examination of *in vitro* osteogenic differentiation revealed increased osteopotential in TCS nMSC populations: in comparison to controls, these cells displayed higher alkaline phosphatase (ALP) activity after 9 days of osteoinduction and more deposition of mineralised matrix after 21 days (Fig. 4A; Fig. S2).

During chondrogenic differentiation, we observed altered expression of key transcripts involved in chondrogenesis in TCS nMSCs, which exhibited upregulation of *ACAN* and *COL2A1* in comparison to controls at day 9 (Fig. 4B). Alcian blue staining of extracellular glycosaminoglycans after 21 days of *in vitro* chondrogenic differentiation did not reveal pronounced differences between TCS and control nMSCs (data not shown).

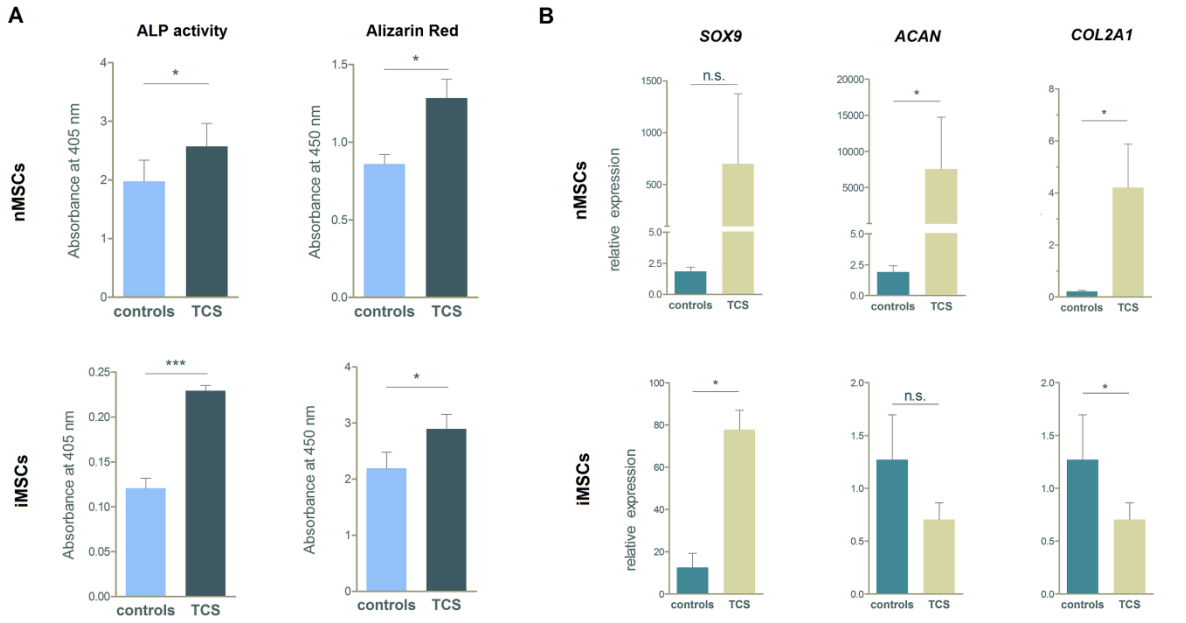

Figure 4: TCS nMSCs and iMSCs show alterations in osteogenic and chondrogenic potential, in comparison to controls. **A)** Colorimetric quantification of alkaline phosphatase (ALP) activity after 9 days and matrix mineralisation after 21 days of osteogenic differentiation. **B)** RT-PCR assays showing the transcriptional profile of chondrogenesis-associated transcripts after 9 days of chondrogenic differentiation. (***) $p<0.001$; (**) $p<0.01$; (*) $p<0.05$; Student's t-test; n.s. = not significant.

Basal apoptosis is increased in TCS nMSCs

Since increased apoptosis of NCCs is regarded as a major driver of the craniofacial phenotypes seen in TCS (Dixon et al., 2006), we sought for differences in apoptotic events between TCS and control iNCCs and nMSCs, as proof-of-principle evidence to support our cellular model. While apoptosis in TCS iNCCs did not deviate from control iNCCs, augmented early and late apoptosis was observed in TCS nMSCs. Unexpectedly, this observation was not associated with detectable changes in proliferative potential of these cells, in relation to controls (Fig. 5).

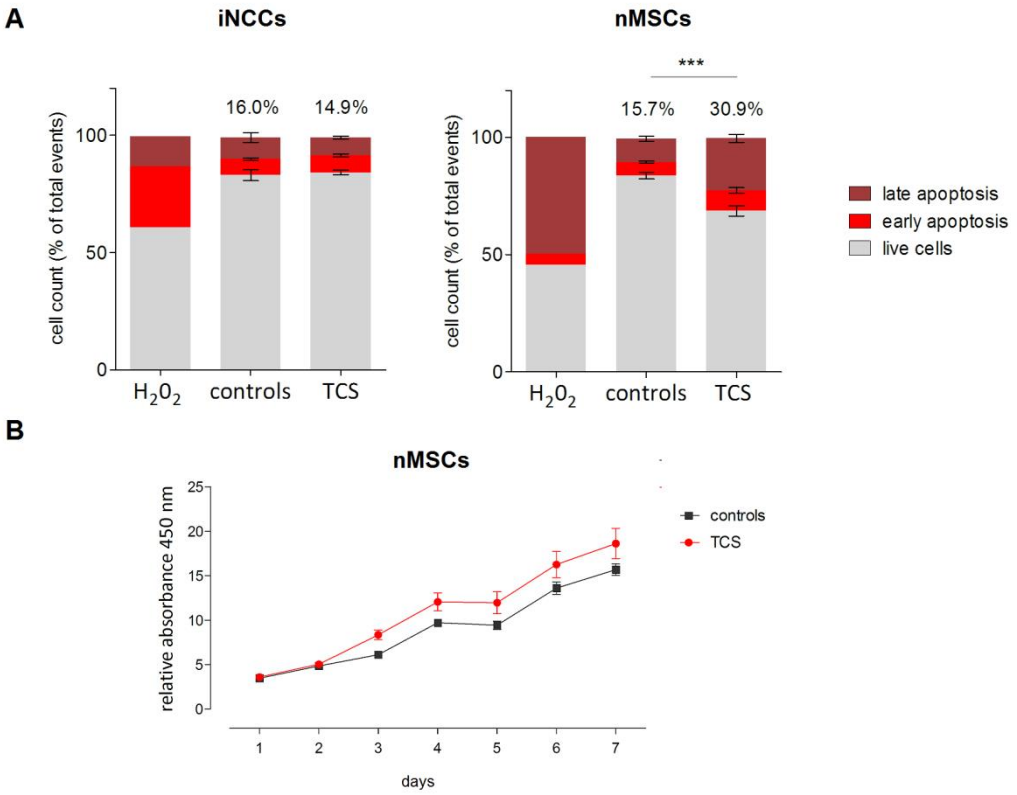

Figure 5: Increased apoptosis in TCS nMSCs. A) 7-AAD/Annexin V flow cytometry results depicting the fraction of live cells, and cells undergoing early and late apoptosis in nMSCs and iNCCs. Percentages represent the sums of early and late apoptotic events. H_2O_2-treated cells were used as positive staining controls. (***) $p<0.001$; Student's t-test. **B)** XTT assay depicting the proliferation profile of control and TCS nMSCs. No statistically significant differences were observed; two-way ANOVA with Bonferroni post-tests.

TCS non-neural crest mesenchymal cells partially reproduce the TCS nMSC phenotype

To evaluate if subjecting patients' cells through a neural crest stage is necessary to generate mesenchymal cells displaying disease-relevant phenotypes, we sought to replicate the results obtained thus far in mesenchymal stem-like cells directly induced from iPSCs (iMSCs). Akin to nMSCs, iMSCs possessed a characteristic and homogeneous mesenchymal immunophenotype (positive for CD105, CD73 and CD90; negative for CD31, CD34 and CD45; Fig. S3A); also, iMSCs showed transcriptional upregulation of *ENG* (CD105) and downregulation of pluripotency markers *OCT3/4*, *NANOG* and *ALPL*, upon differentiation from iPSCs (Fig. S3B).

TCS iMSCs showed a 34% reduction in *TCOF1* expression, when compared with controls (Fig. S3C).

Osteogenic differentiation assays performed on iMSCs showed comparable results in relation to nMSCs. ALP enzymatic activity and mineralised matrix deposition were significantly higher in TCS iMSCs at days 9 and 21 of osteoinduction, respectively (Fig. 4A). Furthermore, the transcriptional profile of genes involved in chondrogenesis at day 9 of differentiation also deviated from controls, with diminished *COL2A1* expression and increased *SOX9* expression in TCS iMSCs (Fig. 4B).

Finally, no differences in either basal apoptosis or proliferation were detected between TCS and control iMSCs (Fig. S3D, E).

DISCUSSION

The development of iPSC technology has opened new possibilities to study human craniofacial diseases, as neural crest-derived, patient-specific cell types harbouring pathogenic mutations can be generated and studied *in vitro* under controlled conditions. Several studies in animal models have consistently appointed insufficient NCC migration due to apoptosis as the main determinant of the TCS phenotype (Dixon et al., 1997; Jones et al., 1999; Dixon et al., 2006; Jones et al., 2008; Weiner et al., 2012). Here, we used iPSCs to generate an *in vitro* equivalent of human neural crest-derived mesenchymal cells in order to evaluate the phenotypical outcomes of *TCOF1* haploinsufficiency on this cell type. We successfully generated iPSCs from TCS patients which, akin to control iPSCs, had no signs of chromosomal imbalances and displayed high expression of pluripotency-associated genes; further, they demonstrated the ability to give rise to iNCCs and nMSCs, and to be directly differentiated into iMSCs. Hence, diminished *TCOF1* expression had no apparent effect on iPSC generation.

The properties of the iNCCs and nMSCs reported here are congruent with the expected neural crest and mesenchymal phenotypes, as shown in other works (Menendez et al., 2011; Menendez et al., 2013; Fukuta et al., 2014; Kreitzer et al., 2014). All iNCCs displayed transcriptional upregulation of neural crest markers in comparison to the iPSCs. Of note, iNCC cultures from TCS patients comprised a p75(NTR)$^{+}$/HNK1^{-} cell fraction, in contrast to the double-positive control iNCCs here and to a TCS iNCC line reported elsewhere (Menendez et al., 2013); still, other works have reported generation of iPSC-derived neural crest cells solely based on p75(NTR) readout (Fukuta et al., 2014; Kreitzer et al., 2014), indicating that HNK1 expression is not entirely crucial to characterise this cell type. Nevertheless, we showed that the mixed TCS iNCC populations here can be successfully converted to nMSCs: all nMSCs displayed *bona fide* mesenchymal stem cell characteristics, possessed homogeneous immunophenotype with high expression of mesenchymal markers, and showed plasticity to generate osteoblasts, chondrocytes and adipocytes *in vitro*. These results show that the nMSCs reported here are suitable for assessment of mesenchymal differentiation and other cellular parameters, and they suggest that lower HNK1 expression in iNCCs is not a limiting factor to generate neural crest-derived mesenchymal cells *in vitro*.

According to previous observations in animal models (Dixon et al., 1997; Jones et al., 1999; Dixon et al., 2006; Jones et al., 2008; Weiner et al., 2012), one expected finding for *TCOF1*-deficient NCCs would be augmented apoptosis, but no deviations in this parameter were detected when comparing TCS iNCCs to control iNCCs. This observation could be related to the lower HNK1 expression detected in TCS iNCCs. HNK1 is an *in vitro* neural crest marker solely found expressed in migratory NCCs in animal models (Bronner-Fraser, 1987; Sadaghiani & Vielkind, 1990; Del Barrio & Nieto, 2004; Giovannone et al., 2015), arguably implying that the mixture of HNK1^{+}/HNK1^{-} iNCCs from TCS patients comprises migratory and non-migratory iNCCs, which may show different apoptosis rates in face of *TCOF1* haploinsufficiency. In agreement, in *Tcof1*$^{+/-}$ mice, migratory NCCs are viable, while increased apoptosis is confined

to the neuroepithelial, pre-migratory NCCs (Dixon et al., 2006). Alternatively, since apoptosis was assessed in iNCCs grown under normal culture conditions, differences in apoptosis between TCS and control iNCCs may only be detectable after subjecting cells to additional challenges or inductive signals.

The greater amount of apoptotic cells detected in TCS nMSCs here associates *TCOF1* haploinsufficiency with cell death in neural crest-derived mesenchymal cells. The pathogenic mechanism proposed for TCS predicts that insufficiency of *TCOF1* transcripts upon high demand for ribosome synthesis leads to cellular stress and apoptosis (Dixon et al., 2006). As neural crest-derived mesenchymal cells must undergo rapid proliferation before differentiation (Achileos & Trainor, 2012; Twigg & Wilkie, 2015), these results suggest that mesenchymal apoptosis may occur prior to differentiation within the embryonic craniofacial complex. However, such inference must be assimilated with caution, as increased apoptosis did not result in observable proliferation deficits in TCS nMSCs, and whether the apoptosis rates observed are sufficiently high to project measurable differences in proliferation remains to be determined. Accordingly, akin to iNCCs, apoptosis was assessed in nMSCs under regular culture conditions, which may not produce enough apoptotic cells to result in proliferation changes in TCS samples. Nonetheless, it will be interesting to see if viability of *TCOF1*-deficient neural crest-derived mesenchymal cells is compromised under high proliferative demand *in vitro* or in TCS animal models.

The mesenchymal differentiation assays showed dissimilarities in the osteogenic and chondrogenic potential between control and TCS samples, both in nMSCs and iMSCs. Although no peak expression of osteogenesis markers was observed in TCS cells within the first 6 days of osteoinduction, ALP activity and matrix mineralisation were unmistakably increased in TCS nMSCs and iMSCs, indicating enhanced osteopotential with peak expression of these markers likely occurring beyond the assessed time window. Transcriptional dysregulation of key genes

involved in chondrogenesis was observed in TCS nMCs and iMSCs as compared to controls, albeit with an apparent lack of difference in alcian blue-stained chondrocyte pellets. This finding might be related to the limited sensitivity of the technique (Solchaga et al., 2011), and more studies are necessary to confirm if the transcriptional alterations of chondrogenesis-associated genes results in differences between TCS and control samples. Still, although NCC apoptosis has been considered to be the major contributor to the craniofacial manifestations of TCS, our results indicate association between mesenchymal differentiation and *TCOF1*/Treacle function in humans. There is an unequivocal cross-talk between ribosome biogenesis and osteo-chondrogenesis due to interactions amongst members of both pathways (Trainor & Merril, 2014). For example, *Runx2*, a key transcription factor involved in osteo-chondral differentiation, has been shown to interact with UBF-1 to downregulate rRNA synthesis and cell proliferation during differentiation (Trainor & Merril, 2014; Pratap et al., 2003; Galindo et al., 2005; Ali et al., 2008); notably, Treacle co-localises with UBF-1 and RNA polymerase I in nucleolar regions (Valdez et al., 2004), further suggesting that functional impairment of Treacle may influence osteo-chondral differentiation. Hence, better understanding the relationship between *TCOF1* haploinsufficiency and mesenchymal differentiation not only provides insight into craniofacial development, but may also be invaluable for the surgical rehabilitation of TCS patients, which often lacks long-term stable results after mandibular distraction osteogenesis (Stelnicki et al., 2002; Gursoy et al., 2008).

Our results suggest that recapitulating craniofacial development by transitioning iPSCs through a neural crest stage may be advantageous to study TCS and other Mendelian craniofacial dysmorphologies. Increased apoptosis was only observed in nMSCs derived from iNCCs, whilst the number of apoptotic cells in TCS iMSC cultures directly differentiated from iPSCs was similar to that in controls; therefore, *TCOF1* mutations may specifically affect neural crest-derived mesenchymal cells *in vitro*. This is supported by the broader difference in *TCOF1* mRNA expression detected between TCS patients and control subjects for nMSCs (~64%) in

comparison to iMSCs here (~34%) and adult mesenchymal cells described in a previous work (~31%) (Masotti et al., 2009). The reasons for such dramatic reduction of *TCOF1* transcripts in TCS nMSCs as compared to other types of mesenchymal cells are unclear, but they may include compensatory expression from the non-mutated allele, as previously proposed for TCS adult cells (Isaac et al., 2000), or cell type-specific differential expression of the mutated allele due to epigenetic, environmental, or stochastic factors (Kaern et al., 2005; Gimelbrant et al., 2007). Either way, the greater reduction in the amount of *TCOF1* transcripts in TCS nMSCs suggest that disruption of neural crest-derived mesenchymal cell development might play a role in the aetiology of TCS in humans, attesting the importance of considering this cell type when investigating craniofacial phenotypes.

In summary, here we describe an *in vitro* model for studying neural crest-derived mesenchymal cells from TCS syndrome patients. Our findings suggest apoptosis as a phenotypical outcome of *TCOF1* haploinsufficiency in neural crest-derived mesenchymal cells and they suggest that mesenchymal differentiation towards osteoblast and chondrocyte lineages may be altered in TCS. Future studies should focus on further dissecting how reduced amounts of Treacle affect proliferation and differentiation of neural crest-derived mesenchymal cells undergoing osteo-chondrogenic specification *in vitro* and *in vivo*.

METHODS

Biological samples and ethics statement

Facial periosteum fragments were obtained from TCS subjects submitted to reconstructive plastic surgery at Hospital das Clínicas, University of São Paulo, Brazil. Punch biopsy skin fragments were obtained from 2 healthy control subjects from the lower back

region, under local anaesthesia. The study was approved by the ethical committee of Instituto de Biociências, University of São Paulo, Brazil (accession number 39478314.8.0000.5464), and informed consent was obtained from both patients and control subjects or from their legal guardians. Periosteal fibroblasts were extracted according to a previously published protocol (Fanganiello et al., 2007). Dermal fibroblasts were isolated according to the methods described in Aasen & Belmonte (2010).

Generation of human induced pluripotent stem cells (iPSCs)

Fibroblasts from two TCS patients were reprogrammed via *SOX2*, *c-MYC*, *OCT4* and *KLF4* retroviral transduction, as originally reported in Takahashi et al, 2007. Two control fibroblasts had also been reprogrammed with this method, as described elsewhere (Ishiy et al., 2014). One additional control fibroblast sample was reprogrammed with the use of episomal vectors (pCXLE-hOCT3/4-shP53-F, addgene plasmid 27077; pCXLE-hSK, addgene plasmid 27078; pCXLE-hUL, addgene plasmid 27080), as described in Okita et al (2011), with the use of Amaxa Nucleofector II (program U-020) and NHDF nucleofection kit (Lonza), according to manufacturer's recommendations. Two days after transduction/nucleoporation, fibroblasts were co-cultivated with irradiated murine embryonic fibroblasts (Millipore) in embryonic stem cell medium (DMEM/F12 supplemented with 2mM GlutaMAX-I, 0.1mM non-essential aminoacids, 100uM 2-mercaptoethanol, 30ng/ml of bFGF and 20% of knockout serum replacement; all provided by Life Technologies). Typical iPSC colonies formed on feeder cells were transferred to matrigel (BD-Biosciences)-coated plates and expanded in Essential 8™ Medium (Life Technologies) supplemented with 100ug/mL of Normocin (Invivogen). pCXLE-hOCT3/4-shP53-F, pCXLE-hSK, and pCXLE-hUL were a gift from Shinya Yamanaka.

MLPA assays

Total DNA was extracted from iPSC cultures with the use of NucleoSpin Tissue (Macherey-Nagel), following supplier's instructions. Multiplex Ligation-dependent Probe Amplification (MLPA) analysis was performed with subtelomeric kits (P036 and P070; MRC-Holland) to detect chromosomal imbalances, as previously described (Jehee et al., 2011).

Differentiation of iNCCs from iPSCs

Procedures for iNCC derivation were based on previously published methodology (Menendez et al., 2013; Fukuta et al., 2014). Before differentiation, iPSC colonies were adapted to single-cell passaging by rinsing cells with PBS followed by dissociation with Accutase (Life Technologies) for up to 5 minutes at room temperature, centrifugation at 200 g for 4 min and seeding onto Matrigel-coated dishes. After 2 subcultures, single cells were seeded onto 60-mm Matrigel-coated dishes at $5x10^4$ cells/cm^2. Two days post-seeding, medium was changed to iNCC differentiation medium, composed of Essential 6™ Medium (Life Technologies) supplemented with 8ng/mL bFGF (Life Technologies), 20uM SB431542 (Sigma-Aldrich), 1uM CHIR99021 (Sigma-Aldrich), and 100ug/mL Normocin; differentiation medium was changed daily. After ~2-4 days, neural crest-like cells were seen detaching from colony borders. Before reaching confluence, cultures were rinsed once with PBS and briefly incubated with Accutase at room temperature until differentiated cells detached and most undifferentiated colonies were left on the dish. Cell suspensions were centrifuged at 200 g for 4 minutes and re-seeded onto new Matrigel-coated dishes in fresh iNCC differentiation medium. With this method, passaging was performed whenever necessary, for 15 days, whereby morphologically homogeneous iNCC cultures were obtained. Differentiated iNCCs were cultivated for up to 8 passages in iNCC differentiation medium, replenished daily. In all procedures involving single-cell passaging, media were supplemented with 5uM Rock inhibitor

(Sigma-Aldrich) upon seeding and maintained for 24 hours; after about 10 days of iNCC differentiation, Rock inhibitor was no longer needed to maintain cell viability.

Differentiation of nMSCs from iNCCs

nMSC populations were obtained through incubation of iNCCs with mesenchymal stem cell medium, as previously described (Menendez et al., 2011). In brief, iNCCs were seeded at $2x10^4$ cells/cm^2 onto non-coated 60-mm tissue culture dishes in nMSC medium (DMEM/F12 supplemented with 10% FBS, 2mM GlutaMAX-I, 0.1mM non-essential aminoacids, and 100ug/mL Normocin) containing 5uM Rock inhibitor. Cells were differentiated for 6 days and passaged with TrypLE™ Express (Life Technologies) when needed. nMSC cultures were expanded in nMSC medium for up to 6 passages, with medium changes every 3 days.

Direct derivation of iMSCs from iPSCs

iMSCs were generated following published methods (Ishiy et al., 2015). Briefly, iPSC colonies were treated with Accutase and cells were plated onto Matrigel-coated tissue culture dishes at $1×10^4$ cells/cm^2 in iMSC differentiation medium (DMEM/High Glucose with 10% FBS, 1% penicillin/streptomycin, 1% nonessential amino acids, and 5ng/mL of bFGF) for 14 days, with media changes every 3 days. For subsequent passages, single-cell suspensions were prepared using TrypLE Express and cells were passaged with a 1:3 split ratio in standard culture flasks (Corning) without Matrigel coating.

Chondrogenic, osteogenic and adipogenic differentiation

For the osteogenic induction, cells were seeded in 12-well plates ($4x10^4$ cells per well), and after 3 days, medium was replaced with osteogenic induction medium (StemPro Osteogenesis Kit; Life Technologies). Differentiation medium was changed every 2-3 days. After 9 days, alkaline phosphatase activity was quantified through incubation with

phosphatase substrate (Sigma-Aldrich), and the resulting p-nitrophenol was quantified colorimetrically using a Multiskan EX ELISA plate reader (Thermo Scientific) at 405 nm. After 21 days, extracellular matrix mineralisation was assessed through alizarin red staining. Briefly, cells were washed three times with PBS, fixed in 70% ethanol for 30 minutes at room temperature, washed 3x with distilled water, and finally stained with a 0.2% Alizarin Red S solution (Sigma-Aldrich) for 30 minutes at room temperature. After three washes with PBS, plates were air dried at room temperature. Staining was removed with a 20% methanol / 10% acetic acid solution and colorimetrically assessed using a Multiskan EX ELISA plate reader (Thermo Scientific) at 450nm.

For chondrogenesis, $1x10^5$ cells/well were plated into 6-well plates and after 3 days growth medium was replaced with chondrogenic medium (StemPro Chondrogenesis Kit; Life Technologies). To quantify chondrogenic markers, total RNA was extracted after 9 days of differentiation. Chondrocyte pellets were produced by centrifuging $3x\times 10^5$ cells at 500g and incubating pellets in nMSC medium for 24 hours before switching to chondrogenic medium. After 21 days, pellets were fixed and frozen in Tissue-Tek O.C.T (Sakura), 5um cryosections were performed, sections were fixed with 4% paraformaldehyde and stained with Alcian Blue 0.1% in 0.1 N HCl.

Adipogenic differentiation was performed on $1x10^5$ cells/well seeded into 6-well plates. After cells achieved 80% confluence, growth medium was replaced with adipogenesis medium (StemPro Adipogenesis Kit; Life Technologies). Cells were differentiated for 21 days, after which Oil red staining was performed. Cells were washed with PBS, fixed in 4% paraformaldehyde and stained with Oil Red 0.5% in isopropanol. Pictures were taken using an Axiovision microscope (Zeiss).

Apoptosis and proliferation Assays

For the apoptosis assays, a total of $1x10^5$ cells/well was seeded into 6-well culture plates. On the next day, apoptotic activity was measured with a kit based on Annexin V and 7-AAD staining (Guava Nexin Reagent), following manufacturer's instructions. Cells treated with 10uM H_2O_2 for 30 minutes were used as staining controls. Subpopulations were ascertained in a Guava flow cytometer (EMD Millipore) as follows: non-apoptotic cells: Annexin V(-) and 7-AAD(-); early apoptotic cells: Annexin V(+) and 7-AAD(-); late-stage apoptotic and dead cells: Annexin V(+) and 7-AAD(+).

Cell proliferation was assessed with the use of an XTT assay (Cell Proliferation Kit II; Roche), following supplier's instructions. Briefly, cells were seeded into 96-well culture plates at $2x10^3$ cells/well, in quadruplicates. To quantify metabolically active cells, medium was changed to DMEM/F12 without phenol red (Life Technologies), a solution of XTT was added, and cells were incubated at 37°C for 3 hours. Immediately, plates were colorimetrically assessed in a microplate spectrophotometer (Epoch; BioTek) at 450nm.

Flow cytometry

To assess the immunophenotype of iNCCs, cells were detached with Accutase, and washed twice with 2 volumes of blocking solution (4% BSA in PBS without Ca^{2+} and Mg^{2+}). iNCCs were incubated with the conjugated antibodies in blocking solution in the dark for 1 hour at 4°C, washed twice with PBS, and fixed in 1% paraformaldehyde/PBS. The following antibodies were used: IgM k FITC Mouse Anti-Human CD57 (anti-HNK1; BD Pharmingen 561906), IgG1 k Alexa Fluor 647 Mouse Anti-Human CD271 (anti-p75NTR; BD Pharmingen 560877), FITC Mouse IgM k isotype control (BD Pharmingen 555583), and Alexa Fluor 647 Mouse IgG1 k isotype control (BD Pharmingen 557714). Antibody concentrations followed manufacturer's recommendations. A minimum of 5,000 events were acquired in a FACS Aria II flow cytometer (BD Biosciences) and analysed on Flowing software (v2.5).

nMSCs and iMSCs were dissociated with TrypLE Express and washed twice with 2 volumes of blocking solution (1% BSA in PBS without Ca^{2+} and Mg^{2+}). Cells were incubated in the aforementioned conditions with the following conjugated antibodies: FITC Mouse Anti-Human CD31 (BD Pharmingen 555445), APC Mouse Anti-Human CD73 (BD Pharmingen 560847), PE Mouse Anti-Human CD90 (BD Pharmingen 555596), FITC Mouse Anti-Human CD105 (BD Pharmingen 551443), PE Mouse Anti-Human CD166 (BD Pharmingen 559263), and FITC, PE and APC Mouse IgG1 κ Isotype Controls (BD Pharmingen 555748, 554681 and 555749, respectively). Antibody concentrations followed manufacturer's recommendations. At least 5,000 events were acquired in a FACS Aria II equipment and analysed on the Flowing software (v2.5) and Guava Express PRO (Millipore).

RNA extraction and Real-time quantitative PCR (RT-qPCR)

Total RNA was obtained from cell populations with the use of Nucleospin RNA II extraction kit (Macherey-Nagel) following manufacturer's recommendations. Briefly, 1ug of total RNA was converted into cDNA using Superscript II (Life Technologies) and oligo-dT primers according to manufacturer's recommendations. Real-Time quantitative PCR reactions were performed with 2X Fast SYBR Green PCR Master Mix (Life Technologies) and 50nM–400nM of each primer. Fluorescence was detected using the 7500 Fast Real-Time PCR System (Life Technologies), under standard temperature protocol. Primer pairs were either designed with Primer-BLAST (http://www.ncbi.nlm.nih.gov/tools/primer-blast/) or retrieved from PrimerBank (http://pga.mgh.harvard.edu/primerbank/; primers are listed in Table SII), and their amplification efficiencies (E) were determined by serial cDNA dilutions $\log_{10}$-plotted against Ct values, in which $E=10^{-1/slope}$. Gene expression was assessed relative to a calibrator cDNA (ΔCt). Finally, NormFinder (Andersen et al., 20014) was used to determine the most stable endogenous control (among *ACTB*, *TBP*, *HMBS*, *GAPDH*, or *HPRT1*), and calculate normalization factors ($E^{-\Delta Ct}$) for each sample. The final relative expression values were

determined based on a previous method (Pfaffl et al., 2001), by dividing $E^{-\Delta Ct}$ of target genes by $E^{-\Delta Ct}$ of the endogenous control. All relative expression values were log-transformed for analysis and graphed in linear scale, unless stated otherwise. Primers were supplied by Exxtend.

Statistical analysis:

All experiments were performed in triplicates, unless stated otherwise herein. Statistical comparisons were performed on the Graphpad Prism software. Values were represented as means ± standard error. The level of statistical significance was set at $p<0.05$.

Web Resources

OMIM – Online Mendelian Inheritance in Men - http://www.omim.org/

Primer-BLAST - http://www.ncbi.nlm.nih.gov/tools/primer-blast/

Primer Bank - https://pga.mgh.harvard.edu/primerbank/

SUPPLEMENTARY FIGURES

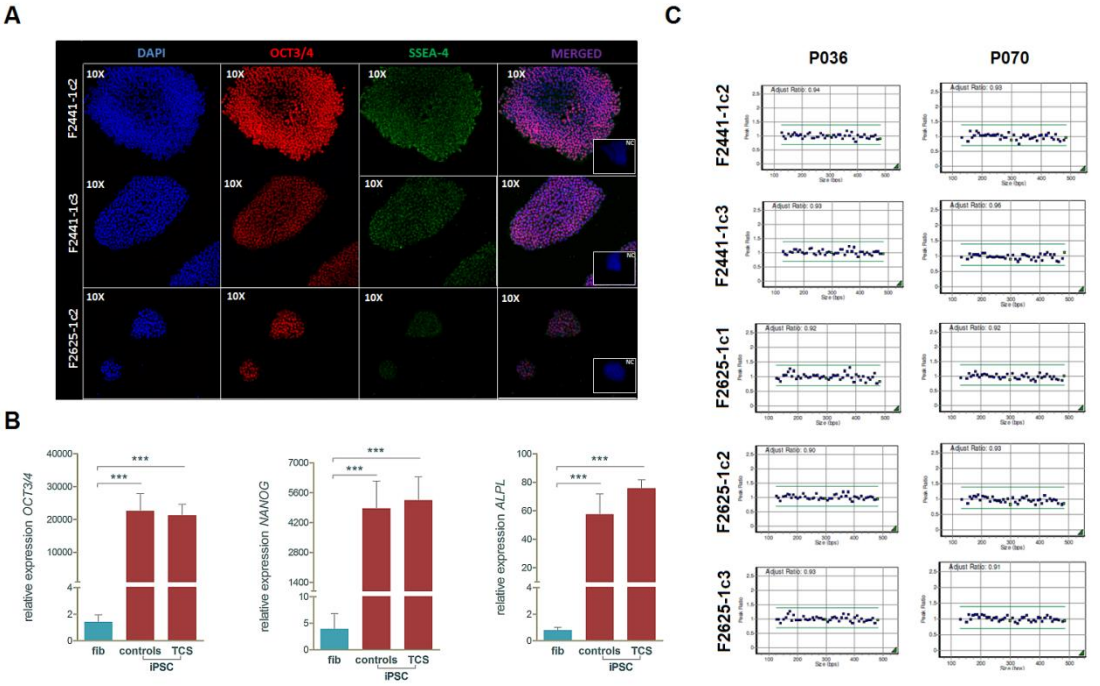

Figure S1: iPSC characterisation. A) Immunofluorescence micrographs showing expression of pluripotency markers OCT3/4 and SSEA-4 in TCS iPSCs. NC=negative control **B)** RT-qPCR showing transcriptional upregulation of pluripotency-associated genes *OCT3/4*, *NANOG*, and *ALPL* in controls and TCS samples. Graphs were plotted relative to expression data of 2 adult fibroblasts (F2625-1 and F2441-1); (***) *p*-value < 0.001; Student's t-test. **C)** MLPA analysis with peak ratios for subtelomeric probes (blue dots) and control probes (green dots) with the use of 2 kits, showing no chromosomal imbalances. Control iPSCs had been previously characterised in Chapter III and Ishiy et al (2015).

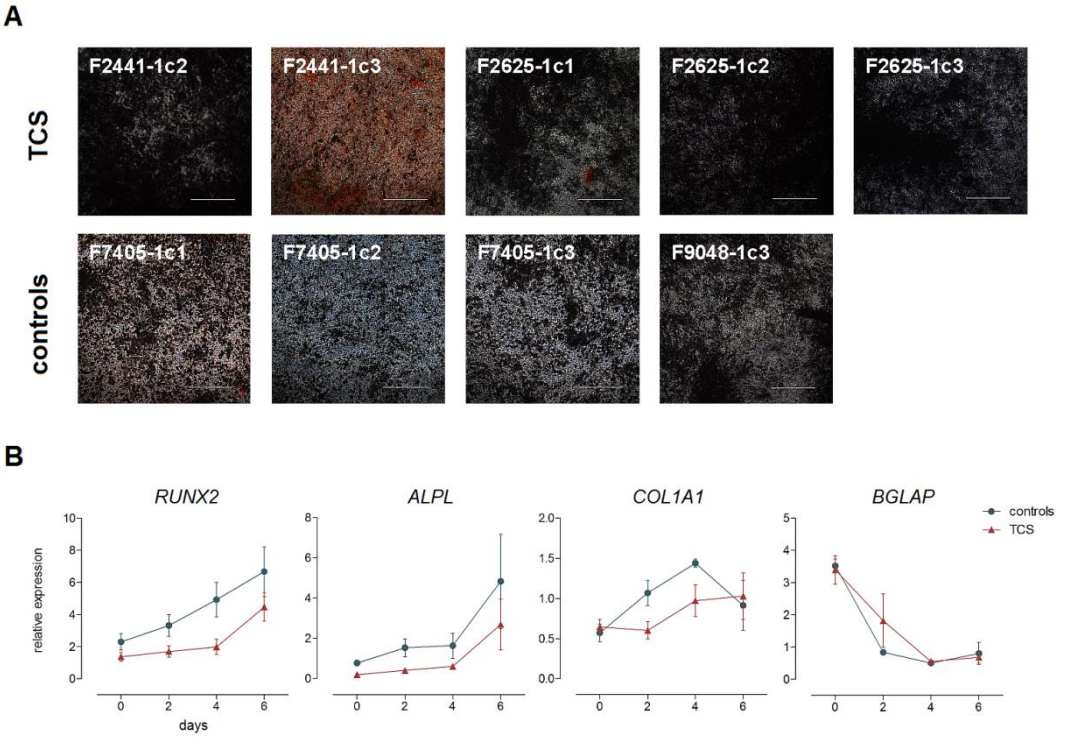

Figure S2: Osteogenic differentiation of control and TCS nMSCs. A) Alizarin Red staining showed increased matrix mineralisation in TCS samples as compared to controls. Scale bars=500um **B)** Transcriptional profile of osteogenesis-associated genes during the initial 6 days of osteoinduction. No statistically significant differences were observed; two-way ANOVA with Bonferroni post-tests.

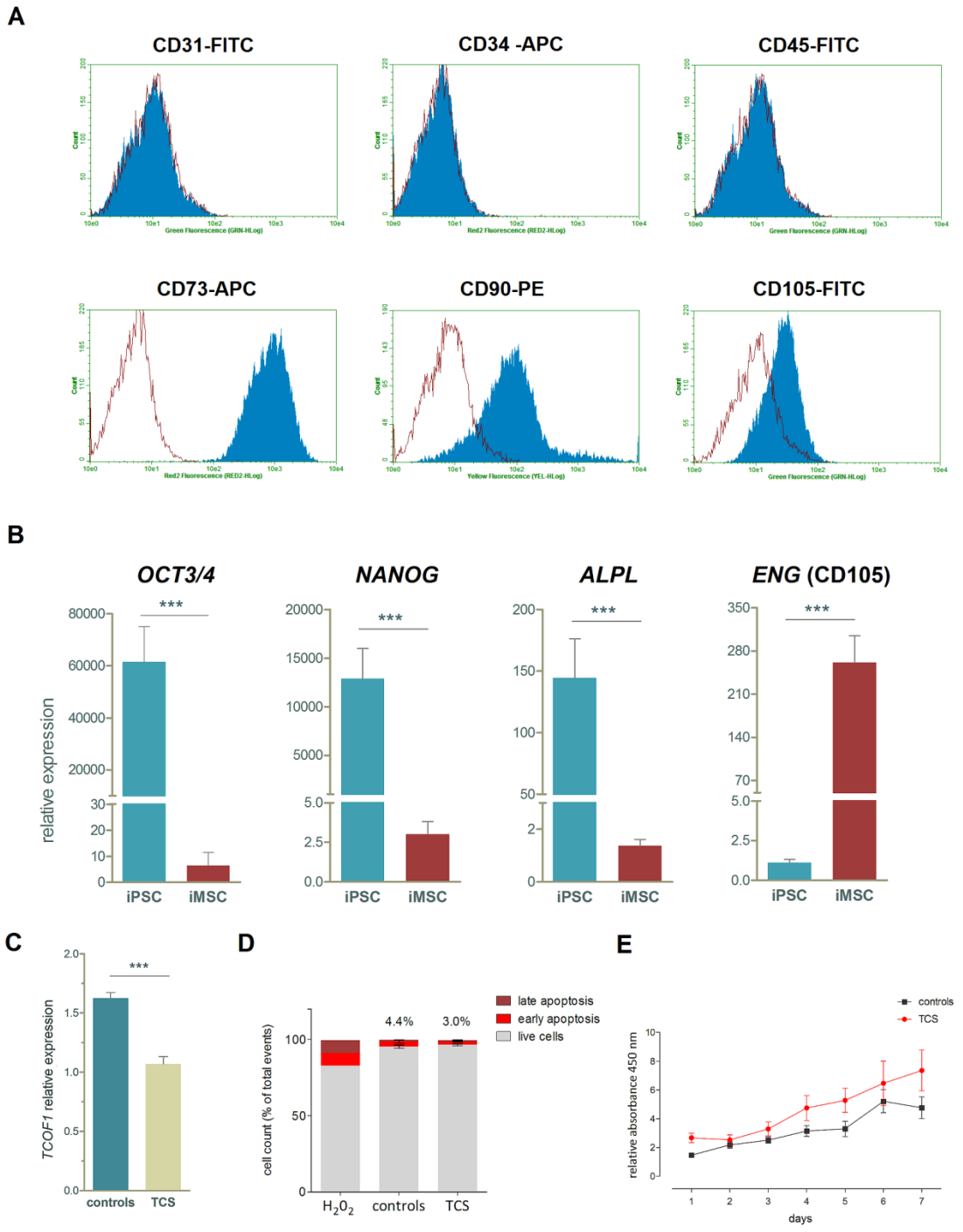

Figure S3: Characterisation and phenotype assessment of TCS iMSCs. A) Representative flow cytometry histograms showing staining for mesenchymal cell markers CD73, CD90 and CD105, and non-mesenchymal markers CD31, CD34 and CD45. **B)** RT-qPCR assessment of pluripotency markers *OCT3/4,* NANOG, and *ALPL,* and mesenchymal marker *ENG* in iMSCs compared to the originating iPSCs. **C)** *TCOF1* transcript expression between control and TCS iMSCs. **D)** 7-AAD/Annexin V flow cytometry results depicting the fraction of live cells, and cells undergoing early and late apoptosis in iMSCs. Percentages represent the sums of early and late apoptotic events. H_2O_2-treated cells were used as positive staining controls. **E)** XTT assay depicting the proliferation profile of control and TCS iMSCs.

SUPPLEMENTARY TABLES

Table SI: Sample information.

Subject	Clinical status	Age*	Gender	Parental somatic cell	Reprogramming method	Clone	iPSC- derived cell type
F7405-1	control	27	male	dermal fibroblasts	retroviral	F7405-1c1	iNCC/nMSC/iMSC
						F7405-1c2	iNCC/nMSC/iMSC
						F7405-1c3	iNCC/nMSC/iMSC
F7007-1	control	23	male	dermal fibroblasts	retroviral	F7007-1c2	iMSC
						F7007-1c4	iMSC
F9048-1	control	20	male	dermal fibroblasts	episomal	F9048-1c3	iNCC/nMSC
F2441-1	TCS	9	female	periosteal fibroblasts	retroviral	F2441-1c2	iNCC/nMSC/iMSC
						F2441-1c3	iNCC/nMSC/iMSC
F2625-1	TCS	30	female	periosteal fibroblasts	retroviral	F2625-1c1	iNCC/nMSC/iMSC
						F2625-1c2	iNCC/nMSC/iMSC
						F2625-1c3	iNCC/nMSC/iMSC

* age upon collection of tissue sample

Table SII: Primer sequences used in RT-qPCR.

Target	Forward primer (5'-3')	Reverse Primer (5'-3')
ACTB	TGAAGTGTGACGTGGACATC	GGAGGAGCAATGATCTTGAT
GAPDH	ATCACCATCTTCCAGGAGCG	GGGCAGAGATGATGACCCTTT
HPRT1	CCTGGCGTCGTGATTAGTGAT	AGACGTTCAGTCCTGTCCATAA
HMBS	AGCTTGCTCGCATACAGACG	AGCTCCTTGGTAAACAGGCTT
TBP	GTGACCCAGCATCACTGTTTC	GCAAACCAGAAACCCTTGCG
OCT3/4	GTGGTCAGCCAACTCGTCA	CCAAAAACCCTGGCACAAACT
NANOG	TGGACACTGGCTGAATCCTTC	CGTTGATTAGGCTCCAACCAT
TCOF1	GCCCCTGGAAAAGTTGTCACT	GGTTTCTCACTGGTGGCTTCAC
PAX3	AAGCCCAAGCAGGTGACAAC	CTCGGATTTCCCAGCTGAAC
ZIC1	AAGGTCCACGAATCCTCCTC	TTGTGGTCGGGTTGTCTG
TFAP2A	CTCCGCCATCCCTATTAACAAG	GACCCGGAACTGAACAGAAGA
SOX10	CCTCACAGATCGCCTACACC	CATATAGGAGAAGGCCGAGTAGA
ENG	TGCACTTGGCCTACAATTCCA	AGCTGCCCACTCAAGGATCT
SOX9	AGCGAACGCACATCAAGAC	CTGTAGGCGATCTGTTGGGG
ACAN	TTTCAAGAAGGCGAGGCGTCCG	TGGCTGAAGGCAAGCCTGGT
COL2A1	GGCAATAGCAGGTTCACGTACA	CGATAACAGTCTTGCCCCACTT
RUNX2	AGTGGACGAGGCAAGAGTTTC	GTTCCCGAGGTCCATCTACTG
ALPL	GATACAAGCACTCCCACTTCATCTG	CTGTTCAGCTCGTACTGCATGTC
COL1A1	GGGCCAAGACGAAGACAT	CAACACCCTTGCCGTTGTCG
BGLAP	GGCGCTACCTGTATCAATGG	GTGGTCAGCCAACTCGTCA

REFERENCES

Aasen, T. e J. C. Izpisua Belmonte. Isolation and cultivation of human keratinocytes from skin or plucked hair for the generation of induced pluripotent stem cells. Nat Protoc, v.5, n.2, Feb, p.371-82. 2010.

Achilleos, A. e P. A. Trainor. Neural crest stem cells: discovery, properties and potential for therapy. Cell Res, v.22, n.2, Feb, p.288-304. 2012.

Ali, S. A., S. K. Zaidi, et al. Phenotypic transcription factors epigenetically mediate cell growth control. Proc Natl Acad Sci U S A, v.105, n.18, May 6, p.6632-7. 2008.

Barriga, E. H., P. A. Trainor, et al. Animal models for studying neural crest development: is the mouse different? Development, v.142, n.9, May 1, p.1555-60. 2015.

Bhatt, S., R. Diaz, et al. Signals and switches in Mammalian neural crest cell differentiation. Cold Spring Harb Perspect Biol, v.5, n.2, Feb. 2013.

Bronner-Fraser, M. Perturbation of cranial neural crest migration by the HNK-1 antibody. Dev Biol, v.123, n.2, Oct, p.321-31. 1987.

Dauwerse, J. G., J. Dixon, et al. Mutations in genes encoding subunits of RNA polymerases I and III cause Treacher Collins syndrome. Nat Genet, v.43, n.1, Jan, p.20-2. 2011.

Del Barrio, M. G. e M. A. Nieto. Relative expression of Slug, RhoB, and HNK-1 in the cranial neural crest of the early chicken embryo. Dev Dyn, v.229, n.1, Jan, p.136-9. 2004.

Dixon, J., K. Hovanes, et al. Sequence analysis, identification of evolutionary conserved motifs and expression analysis of murine tcof1 provide further evidence for a potential function for the gene and its human homologue, TCOF1. Hum Mol Genet, v.6, n.5, May, p.727-37. 1997.

Dixon, J., N. C. Jones, et al. Tcof1/Treacle is required for neural crest cell formation and proliferation deficiencies that cause craniofacial abnormalities. Proc Natl Acad Sci U S A, v.103, n.36, Sep 5, p.13403-8. 2006.

Fanganiello, R. D., A. L. Sertie, et al. Apert p.Ser252Trp mutation in FGFR2 alters osteogenic potential and gene expression of cranial periosteal cells. Mol Med, v.13, n.7-8, Jul-Aug, p.422-42. 2007.

Fukuta, M., Y. Nakai, et al. Derivation of mesenchymal stromal cells from pluripotent stem cells through a neural crest lineage using small molecule compounds with defined media. PLoS One, v.9, n.12, p.e112291. 2014.

Galindo, M., J. Pratap, et al. The bone-specific expression of Runx2 oscillates during the cell cycle to support a G1-related antiproliferative function in osteoblasts. J Biol Chem, v.280, n.21, May 27, p.20274-85. 2005.

Gimelbrant, A., J. N. Hutchinson, et al. Widespread monoallelic expression on human autosomes. Science, v.318, n.5853, Nov 16, p.1136-40. 2007.

Giovannone, D., B. Ortega, et al. Chicken trunk neural crest migration visualized with HNK1. Acta Histochem, v.117, n.3, Apr, p.255-66. 2015.

Gong, S. G. Cranial neural crest: migratory cell behavior and regulatory networks. Exp Cell Res, v.325, n.2, Jul 15, p.90-5. 2014.

Gonzales, B., D. Henning, et al. The Treacher Collins syndrome (TCOF1) gene product is involved in pre-rRNA methylation. Hum Mol Genet, v.14, n.14, Jul 15, p.2035-43. 2005.

Gursoy, S., J. Hukki, et al. Five year follow-up of mandibular distraction osteogenesis on the dentofacial structures of syndromic children. Orthod Craniofac Res, v.11, n.1, Feb, p.57-64. 2008.

Isaac, C., K. L. Marsh, et al. Characterization of the nucleolar gene product, treacle, in Treacher Collins syndrome. Mol Biol Cell, v.11, n.9, Sep, p.3061-71. 2000.

Ishiy, F. A., R. D. Fanganiello, et al. Improvement of In Vitro Osteogenic Potential through Differentiation of Induced Pluripotent Stem Cells from Human Exfoliated Dental Tissue towards Mesenchymal-Like Stem Cells. Stem Cells Int, v.2015, p.249098. 2015.

Jehee, F. S., J. T. Takamori, et al. Using a combination of MLPA kits to detect chromosomal imbalances in patients with multiple congenital anomalies and mental retardation is a valuable choice for developing countries. Eur J Med Genet, v.54, n.4, Jul-Aug, p.e425-32. 2011.

Jones, N. C., P. G. Farlie, et al. Detection of an appropriate kinase activity in branchial arches I and II that coincides with peak expression of the Treacher Collins syndrome gene product, treacle. Hum Mol Genet, v.8, n.12, Nov, p.2239-45. 1999.

Jones, N. C., M. L. Lynn, et al. Prevention of the neurocristopathy Treacher Collins syndrome through inhibition of p53 function. Nat Med, v.14, n.2, Feb, p.125-33. 2008.

Kaern, M., T. C. Elston, et al. Stochasticity in gene expression: from theories to phenotypes. Nat Rev Genet, v.6, n.6, Jun, p.451-64. 2005.

Kreitzer, F. R., N. Salomonis, et al. A robust method to derive functional neural crest cells from human pluripotent stem cells. Am J Stem Cells, v.2, n.2, p.119-31. 2013.

Masotti, C., C. C. Ornelas, et al. Reduced transcription of TCOF1 in adult cells of Treacher Collins syndrome patients. BMC Med Genet, v.10, p.136. 2009.

Matsumoto, Y., M. Ikeya, et al. New Protocol to Optimize iPS Cells for Genome Analysis of Fibrodysplasia Ossificans Progressiva. Stem Cells, v.33, n.6, Jun, p.1730-42. 2015.

Menendez, L., M. J. Kulik, et al. Directed differentiation of human pluripotent cells to neural crest stem cells. Nat Protoc, v.8, n.1, Jan, p.203-12. 2013.

Menendez, L., T. A. Yatskievych, et al. Wnt signaling and a Smad pathway blockade direct the differentiation of human pluripotent stem cells to multipotent neural crest cells. Proc Natl Acad Sci U S A, v.108, n.48, Nov 29, p.19240-5. 2011.

Okita, K., T. Yamakawa, et al. An efficient nonviral method to generate integration-free human-induced pluripotent stem cells from cord blood and peripheral blood cells. Stem Cells, v.31, n.3, Mar, p.458-66. 2012.

Pfaffl, M. W. A new mathematical model for relative quantification in real-time RT-PCR. Nucleic Acids Res, v.29, n.9, May 1, p.e45. 2001.

Pratap, J., M. Galindo, et al. Cell growth regulatory role of Runx2 during proliferative expansion of preosteoblasts. Cancer Res, v.63, n.17, Sep 1, p.5357-62. 2003.

Sadaghiani, B. e J. R. Vielkind. Distribution and migration pathways of HNK-1-immunoreactive neural crest cells in teleost fish embryos. Development, v.110, n.1, Sep, p.197-209. 1990.

Solchaga, L. A., K. J. Penick, et al. Chondrogenic differentiation of bone marrow-derived mesenchymal stem cells: tips and tricks. Methods Mol Biol, v.698, p.253-78. 2011.

Splendore, A., E. O. Silva, et al. High mutation detection rate in TCOF1 among Treacher Collins syndrome patients reveals clustering of mutations and 16 novel pathogenic changes. Hum Mutat, v.16, n.4, Oct, p.315-22. 2000.

Stelnicki, E. J., W. Y. Lin, et al. Long-term outcome study of bilateral mandibular distraction: a comparison of Treacher Collins and Nager syndromes to other types of micrognathia. Plast Reconstr Surg, v.109, n.6, May, p.1819-25; discussion 1826-7. 2002.

Takahashi, K., K. Tanabe, et al. Induction of pluripotent stem cells from adult human fibroblasts by defined factors. Cell, v.131, n.5, Nov 30, p.861-72. 2007.

Trainor, P. A., J. Dixon, et al. Treacher Collins syndrome: etiology, pathogenesis and prevention. Eur J Hum Genet, v.17, n.3, Mar, p.275-83. 2009.

Trainor, P. A. e A. E. Merrill. Ribosome biogenesis in skeletal development and the pathogenesis of skeletal disorders. Biochim Biophys Acta, v.1842, n.6, Jun, p.769-78. 2014.

Twigg, S. R. e A. O. Wilkie. New insights into craniofacial malformations. Hum Mol Genet, Jun 17. 2015.

Valdez, B. C., D. Henning, et al. The Treacher Collins syndrome (TCOF1) gene product is involved in ribosomal DNA gene transcription by interacting with upstream binding factor. Proc Natl Acad Sci U S A, v.101, n.29, Jul 20, p.10709-14. 2004.

Weiner, A. M., N. L. Scampoli, et al. Fishing the molecular bases of Treacher Collins syndrome. PLoS One, v.7, n.1, p.e29574. 2012.

Zhao, H., P. Bringas, Jr., et al. An in vitro model for characterizing the post-migratory cranial neural crest cells of the first branchial arch. Dev Dyn, v.235, n.5, May, p.1433-40. 2006.

Chapter V

DISCUSSION AND CONCLUSIONS

This work consisted in the functional evaluation of neural crest (NC)-derived cell models in order to shed light on the pathogenesis of three congenital craniofacial malformations (CFMs): non-syndromic cleft lip/palate (NSCL/P), Richieri-Costa-Pereira syndrome (RCPS), and Treacher Collins syndrome (TCS). First and foremost, our results demonstrate the applicability of patient-derived cell cultures in investigating the pathogenesis of craniofacial phenotypes. Moreover, they show the importance of examining disease-relevant cell types, in this case, post-natal stem cells from exfoliated deciduous teeth (SHED), which are derived from the cranial NC, and iPSC-derived NC cells (iNCCs) and their mesenchymal derivatives.

In Chapter II, we confirmed that NSCL/P SHED have an expression signature and that gene networks governing cellular defences against DNA damage may play a role in the aetiology of NSCL/P. SHED cultures from NSCL/P subjects exhibited transcriptional dysregulation of gene networks responsible for DNA double-strand-break (DSB) repair and cell cycle control, a phenomenon that, if biologically relevant, should be coupled with observable cellular phenotypes (Kobayashi, 2011). Indeed, we showed that, upon exposure to H_2O_2, NSCL/P SHED accumulate DSBs and display increased cell death, in comparison to controls; furthermore, we detected co-expression of key genes involved in DSB repair (*Brca1*, *Rad51* and *E2f1)* in similar domains within the facial prominences of murine embryos, in critical stages of lip and palate morphogenesis. These findings thus confirm a functional effect for the observed NSCL/P-specific transcriptional profile, and importantly, they suggest that, during craniofacial development, the action of environmental insults allied to genetic or epigenetic factors upstream of the observed transcriptional dysregulation could be involved in the aetiology of NSCL/P. Finally, our results are in accordance with the proposed aetiological overlap between NSCL/P and cancer, as a number of dysregulated genes detected here have also been implicated in tumourigenesis (e.g. *CDC6*, *BLM*, *BRCA1*, *RAD51*, *MSH2*; Borlado & Mendes, 2008; Calin et al., 1998; Gao et al., 2011; Seifert & Reichrath, 2006; Rosen et al., 2006).

Bearing in mind the morphogenetic events necessary for proper craniofacial development, the relationship between a CFM such as NSCL/P and disrupted cellular DNA repair mechanisms/cancer is not unexpected. As intense NC-derived mesenchymal cell proliferation is required for growth and differentiation of the facial prominences (Twigg & Wilkie, 2015), and therefore increased DNA damage and cell death are likely to negatively affect this process. Such assumption is supported by the existence of craniofacial alterations associated with a number of disorders specifically caused by mutations in DNA repair genes, such as Nijmegen breakage syndrome, *ERCC1*-associated cerebro-oculo-facio-skeletal syndrome, and Cornelia de Lange syndrome-4 and TCS (Berardinelli et al., 2007; Jaspers et al., 2007; Deardoff et al., 2012; Ciccia et al., 2014). Moreover, recent studies have reported association between genetic variants within DNA repair genes and NSCL/P, namely *BLM*, *E2F1*, *BRIP1*, and *RAD51* (Mostowska et al., 2014; Machado et al., 2015), further supporting our findings and strengthening the relationship between NSCL/P and impairment of cellular defences against DNA damage.

Chapters III and IV comprehend the employment of iNCCs derived from iPSCs to investigate the pathogenesis of RCPS and TCS, two facial dysostoses in which disturbances in cranial NC cell development are thought to have an aetiological role. The successful derivation of iPSC lines and iNCCs from RCPS and TCS patients displaying reduced amounts of *EIF4A3* and *TCOF1* transcripts, respectively, shows that somatic cell reprogramming to a pluripotent state and neural crest induction are not constrained by expression of these genes, at least in the context of patient's cells or under the method reported herein. Importantly, the adaptation of a methodology to easily produce iPSC-derived iNCCs (Menendez et al., 2013; Fukuta et al., 2014) to our cell culture conditions enables the study of other neural crest-related diseases for which biological material is available in our centre.

In Chapter III, the assessment of iNCC-derived mesenchymal stem-like cells (nMSCs) revealed augmented osteogenic potential of RCPS cells in comparison to controls. This behaviour was clearly accompanied by transcriptional alteration of genes important for osteogenesis, such as *RUNX2*, *ALPL* and *BGLAP*, during initial stages of nMSC differentiation, a dysregulation that was also observed in *EIF4A3* knockdown nMSCs. Although additional confirmatory differentiation assays with *EIF4A3* knockdowns are needed, the results reported here suggest that aberrant expression of the aforementioned genes in early differentiation account for the increment in the osteopotential of RCPS nMSCs. Since craniofacial

development is sensitive to perturbations, alterations in osteopotential of cranial NC-derived mesenchymal cells could be accountable for the clinical manifestations of patients. These cells are responsible for the development and ossification of the craniofacial skeleton, which is promoted by the BMP pathway (Graf et al., 2015). Mouse models showing augmented *Bmp* signalling (bearing constitutive expression of *Bmp4, Bmpr1a* or loss of *Bmp* antagonists Chordin and Noggin) manifest a range of craniofacial defects, including craniosynostosis, cleft palate, and mandibular hypoplasia or agnathia, thus reproducing craniofacial characteristics of RCPS (Stottman et al., 2001; Bonilla-Claudio et al., 2012; Li et al., 2013; Komatsu et al., 2013; Favaro et al., 2011; Raskin et al., 2013). Consequently, an otherwise expected increment in bone formation can ultimately lead to developmental bone deficits. If ossification disturbances are responsible for the cranioskeletal findings in RCPS patients, our results can arguably be transposed to their limbs, which frequently show radial/tibial defects, hand anomalies and club feet; therefore, low amounts of *EIF4A3* transcripts could affect ossification of those structures, although a neural crest component in appendicular skeleton development has yet to be confirmed (Isern et al., 2014; Favaro et al., 2011). Alternatively, given the role of endochondral ossification in limb skeletal development, it will be important to further assess the chondrogenic potential of RCPS nMSCs, as discussed next.

Since the craniofacial phenotype of RCPS revolves around mandible development, alterations in chondropotential would also be expected in nMSCs from affected patients. Lower jaw formation relies upon proper ontogenesis of the Meckel's cartilage (Moody, 2014), so fluctuations in chondrogenesis could ultimately result in mandibular ossification defects. The fact that we were unable to produce chondrocyte pellets from any RCPS patients raises the attractive possibility that chondrogenesis can be disrupted by decreased *EIF4A3* expression, as previously observed in a zebrafish model (Favaro et al., 2014). However, this could not be confirmed in the two independent nMSC replicates under *EIF4A3* knockdown, which showed inconsistent patterns of expression for chondrogenesis markers *SOX9*, *ACAN*, and *COL2A1*. Further attempts to quantify chondrogenic potential of RCPS and *EIF4A3* knockdown nMSCs are therefore worthwhile, and should be carried out in the near future.

The cellular functions attributed to the protein encoded by *EIF4A3* highly indicate that RCPS cells could indeed display dysregulated patterns of mRNA expression. The protein eIF4AIII belongs to the exon junction complex (EJC), playing important roles in RNA post-transcriptional control, including mRNA splicing through EJC-spliceosome interactions (Michelle et al., 2012; Wang et al., 2014; Steckelberg et al., 2015). Recently, depletion of

eIF4AIII in HeLa cells has been reported to produce a generalised shift in mRNA splicing patterns (Wang et al., 2014), thus suggesting that reduced *EIF4A3* expression could lead to aberrant splicing of specific mRNA species, as observed in *Xenopus* embryos (Haremaki & Weinstein, 2012); accordingly, aberrant transcript expression along the osteogenesis molecular hierarchy could be responsible for the cellular phenotypes detected in RCPS nMSCs. Mutations in spliceosomal genes are responsible for a number of clinically overlapping CFM syndromes: RCPS, mandibulofacial dysostosis Guion-Almeida type, Nager syndrome, Burn-Mckeown syndrome, and cerebrocostomandibular syndrome (Lehalle et al., 2015). This staggering observation implies that splicing defects are likely to result in impairment of similar developmental processes during craniofacial morphogenesis, and therefore the results generated in this work should prime other researchers to concentrate efforts in examining NC-derived mesenchymal cell differentiation properties in tissues or animal models relevant for the aforementioned syndromes. Finally, the dissection of the splicing profile of RCPS should benefit from RNA sequencing (RNAseq) technology, with which accurate quantification of alternative or novel mRNA variants is achievable. In this regard, iNCCs from RCPS and control subjects have already been subjected to RNAseq, and a comparative transcriptome analysis is currently underway. These results will contribute to further clarifying the pathogenesis of RCPS and possibly of other spliceosome-related syndromes.

Results reported in Chapter IV suggest that NC-derived mesenchymal cell characteristics are impacted by *TCOF1*/Treacle haploinsufficiency. TCS nMSCs showed augmented apoptosis, and their osteogenic and chondrogenic differentiation properties were altered in comparison to controls. Although the pathogenetic mechanism so far ascribed to TCS involves apoptosis of pre-migratory cranial NC cells (Dixon et al., 2006), our findings indicate that disturbances in NC-derived mesenchymal cells after migration could also be involved in the aetiology of the syndrome. Consequently, the cranial bone and cartilage deficits observed in TCS patients could arise from a combination of dysregulated osteo-chondrogenic differentiation and apoptosis of post-migratory NCs, in addition to the already established pre-migratory NC cell apoptosis; importantly, these results have potential implications for the surgical rehabilitation of TCS patients, in which mandibular distraction osteogenesis frequently lacks long-lasting results (Stelnicki et al., 2002; Gursoy et al., 2008), a limitation that could be related to anomalous differentiation and/or survival of mesenchymal cells residing in the mandible. Finally, further assays to quantify osteo-chondrogenic potential with the use of *TCOF1*-deficient isogenic cells (such knockdown cells) will aid in the corroboration of the aforementioned findings.

If the changes in differentiation potential observed in TCS nMSCs are caused by reduced Treacle expression, the molecular pathways controlling osteogenic/chondrogenic differentiation and ribosome biogenesis must be functionally coupled. Indeed, chondrogenesis-associated regulators *Runx2* and *Runx3* are known to associate with rDNA to regulate transcription through interaction with UBF1, an important factor involved in ribosome synthesis. In addition, *Runx2*, a master regulator of osteogenesis, inhibits UBF1 to attenuate rRNA production and control cell division during osteodifferentiation (Trainor & Merril, 2014). These observations establish a connection between Treacle function, ribosome biogenesis, and osteo-chondrogenic differentiation, as Treacle has been shown to co-localise with UBF1 and RNA Polymerase I, being essential for rDNA transcription (Valdez et al., 2004). However, with the present data we cannot demonstrate how the increased osteopotential of TCS nMSCs reflects the craniofacial alterations of the syndrome, to which reduced bone and cartilage formation has been attributed in TCS animal models (Dixon et al., 2006; Weiner et al., 2012). Therefore, we hypothesise that the deviant osteo-chondrogenic behaviour of TCS nMSCs rather represents a dysregulation of these processes, which, during embryonic development, could lead to corruption of cartilage and bone production. Additional studies focusing on the phenotype and differentiation properties of cranial NC-derived mesenchymal cells with the use of TCS *in vivo* models will be essential to clarify this issue.

It is currently unknown whether iNCCs derived from iPSCs comprise a mixed population of cranial and non-cranial NCs or a non-specified population capable of acquiring multiple NC fates (Fukuta et al., 2014; Kreitzer et al., 2014). Such uncertainty regarding the nature of *in vitro*-produced NC cells is exemplified by the $HNK1^{+}$ and HNK^{-} iNCCs generated from TCS iPSCs, which could represent migratory and non-migratory NC cells. Nonetheless, the presence of cranial NC cells (or progenitors capable of giving rise to cranial NC cells) in the iNCC populations reported here is unquestionable given their ability to originate mesenchymal derivatives (e.g. osteoblasts and chondrocytes), and it will be interesting to assess expression profiles specifically ascribed to cranial NC cells (such as expression patterns of *HOX* transcripts) to better characterise the iNCCs generated in this work. Moreover, irrespective of their nature, these iNCCs are invaluable tools for a preliminary screening for possible pathogenic mechanisms involved in CFMs, which was the objective of this thesis. We acknowledge that complementary *in vivo* experimentation will be paramount to corroborate our findings; in this sense, our group is currently undertaking RCPS modelling with the use of Crispr/Cas9 technology to generate zebrafish lines harbouring the *eif4a3* 5' UTR expansion mutations

present in affected patients, which will enable a thorough *in vivo* phenotypical confirmation and characterisation of the alterations observed in RCPS nMSCs.

In conclusion, we demonstrated the applicability of NC-derived cell types to provide clues regarding the pathogenetic mechanisms leading to CFMs. Since CFMs are consequence of disturbances in NC-derived tissue development, the cell types explored in this study constitute adequate *in* vitro models to investigate craniofacial phenotypes. We identified a possible aetiological determinant of susceptibility to cleft lip/palate, and we provided evidence establishing a relationship between altered mesenchymal differentiation and the craniofacial phenotypes of RCPS and TCS. These novel findings will aid in dissecting the aetiology of CFMs by providing grounds to direct future efforts in craniofacial research.

REFERENCES

Berardinelli, F., A. Di Masi, et al. A case report of a patient with microcephaly, facial dysmorphism, chromosomal radiosensitivity and telomere length alterations closely resembling "Nijmegen breakage syndrome" phenotype. Eur J Med Genet, v.50, n.3, May-Jun, p.176-87. 2007.

Bonilla-Claudio, M., J. Wang, et al. Bmp signaling regulates a dose-dependent transcriptional program to control facial skeletal development. Development, v.139, n.4, Feb, p.709-19. 2012.

Borlado, L. R. e J. Mendez. CDC6: from DNA replication to cell cycle checkpoints and oncogenesis. Carcinogenesis, v.29, n.2, Feb, p.237-43. 2008.

Calin, G., V. Herlea, et al. The coding region of the Bloom syndrome BLM gene and of the CBL proto-oncogene is mutated in genetically unstable sporadic gastrointestinal tumors. Cancer Res, v.58, n.17, Sep 1, p.3777-81. 1998.

Ciccia, A., J. W. Huang, et al. Treacher Collins syndrome TCOF1 protein cooperates with NBS1 in the DNA damage response. Proc Natl Acad Sci U S A, v.111, n.52, Dec 30, p.18631-6. 2014.

Deardorff, M. A., J. J. Wilde, et al. RAD21 mutations cause a human cohesinopathy. Am J Hum Genet, v.90, n.6, Jun 8, p.1014-27. 2012.

Dixon, J., N. C. Jones, et al. Tcof1/Treacle is required for neural crest cell formation and proliferation deficiencies that cause craniofacial abnormalities. Proc Natl Acad Sci U S A, v.103, n.36, Sep 5, p.13403-8. 2006.

Favaro, F. P., L. Alvizi, et al. A noncoding expansion in EIF4A3 causes Richieri-Costa-Pereira syndrome, a craniofacial disorder associated with limb defects. Am J Hum Genet, v.94, n.1, Jan 2, p.120-8. 2014.

Favaro, F. P., R. M. Zechi-Ceide, et al. Richieri-Costa-Pereira syndrome: a unique acrofacial dysostosis type. An overview of the Brazilian cases. Am J Med Genet A, v.155A, n.2, Feb, p.322-31. 2011.

Fukuta, M., Y. Nakai, et al. Derivation of mesenchymal stromal cells from pluripotent stem cells through a neural crest lineage using small molecule compounds with defined media. PLoS One, v.9, n.12, p.e112291. 2014.

Gao, L. B., X. M. Pan, et al. RAD51 135G/C polymorphism and breast cancer risk: a meta-analysis from 21 studies. Breast Cancer Res Treat, v.125, n.3, Feb, p.827-35. 2010.

Graf, D., Z. Malik, et al. Common mechanisms in development and disease: BMP signaling in craniofacial development. Cytokine Growth Factor Rev, Nov 24. 2015.

Gursoy, S., J. Hukki, et al. Five year follow-up of mandibular distraction osteogenesis on the dentofacial structures of syndromic children. Orthod Craniofac Res, v.11, n.1, Feb, p.57-64. 2008.

Haremaki, T. e D. C. Weinstein. Eif4a3 is required for accurate splicing of the Xenopus laevis ryanodine receptor pre-mRNA. Dev Biol, v.372, n.1, Dec 1, p.103-10. 2012.

Isern, J., A. Garcia-Garcia, et al. The neural crest is a source of mesenchymal stem cells with specialized hematopoietic stem cell niche function. Elife, v.3, p.e03696. 2014.

Jaspers, N. G., A. Raams, et al. First reported patient with human ERCC1 deficiency has cerebro-oculo-facio-skeletal syndrome with a mild defect in nucleotide excision repair and severe developmental failure. Am J Hum Genet, v.80, n.3, Mar, p.457-66. 2007.

Kobayashi, G. S. Transcriptome analysis of mesenchymal stem cells to investigate the aetiology of non-syndromic cleft lip and palate. (Dissertation). Instituto de Biociências, Universidade de São Paulo, São Paulo, 2011. 93 p.

Komatsu, Y., P. B. Yu, et al. Augmentation of Smad-dependent BMP signaling in neural crest cells causes craniosynostosis in mice. J Bone Miner Res, v.28, n.6, Jun, p.1422-33. 2013.

Kreitzer, F. R., N. Salomonis, et al. A robust method to derive functional neural crest cells from human pluripotent stem cells. Am J Stem Cells, v.2, n.2, p.119-31. 2013.

Lehalle, D., D. Wieczorek, et al. A review of craniofacial disorders caused by spliceosomal defects. Clin Genet, v.88, n.5, Nov, p.405-15. 2015.

Li, L., Y. Wang, et al. Augmented BMPRIA-mediated BMP signaling in cranial neural crest lineage leads to cleft palate formation and delayed tooth differentiation. PLoS One, v.8, n.6, p.e66107. 2013.

Machado, R. A., H. S. Moreira, et al. Interactions between RAD51 rs1801321 and maternal cigarette smoking as risk factor for nonsyndromic cleft lip with or without cleft palate. Am J Med Genet A, Oct 27. 2015.

Menendez, L., M. J. Kulik, et al. Directed differentiation of human pluripotent cells to neural crest stem cells. Nat Protoc, v.8, n.1, Jan, p.203-12. 2013.

Michelle, L., A. Cloutier, et al. Proteins associated with the exon junction complex also control the alternative splicing of apoptotic regulators. Mol Cell Biol, v.32, n.5, Mar, p.954-67. 2012.

Moody, S. Principles of Developmental Genetics: Publisher: Academic Press, v.1. 2015. 784 p.

Mostowska, A., K. K. Hozyasz, et al. Genetic variants in BRIP1 (BACH1) contribute to risk of nonsyndromic cleft lip with or without cleft palate. Birth Defects Res A Clin Mol Teratol, v.100, n.9, Sep, p.670-8. 2014.

Raskin, S., M. Souza, et al. Richieri-costa and Pereira syndrome: severe phenotype. Am J Med Genet A, v.161A, n.8, Aug, p.1999-2003. 2013.

Rosen, E. M., S. Fan, et al. BRCA1 regulation of transcription. Cancer Lett, v.236, n.2, May 18, p.175-85. 2006.

Seifert, M. e J. Reichrath. The role of the human DNA mismatch repair gene hMSH2 in DNA repair, cell cycle control and apoptosis: implications for pathogenesis, progression and therapy of cancer. J Mol Histol, v.37, n.5-7, Sep, p.301-7. 2006.

Steckelberg, A. L., J. Altmueller, et al. CWC22-dependent pre-mRNA splicing and eIF4A3 binding enables global deposition of exon junction complexes. Nucleic Acids Res, v.43, n.9, May 19, p.4687-700. 2015.

Stelnicki, E. J., W. Y. Lin, et al. Long-term outcome study of bilateral mandibular distraction: a comparison of Treacher Collins and Nager syndromes to other types of micrognathia. Plast Reconstr Surg, v.109, n.6, May, p.1819-25; discussion 1826-7. 2002.

Stottmann, R. W., R. M. Anderson, et al. The BMP antagonists Chordin and Noggin have essential but redundant roles in mouse mandibular outgrowth. Dev Biol, v.240, n.2, Dec 15, p.457-73. 2001.

Trainor, P. A. e A. E. Merrill. Ribosome biogenesis in skeletal development and the pathogenesis of skeletal disorders. Biochim Biophys Acta, v.1842, n.6, Jun, p.769-78. 2014.

Twigg, S. R. e A. O. Wilkie. New insights into craniofacial malformations. Hum Mol Genet, Jun 17. 2015.

Valdez, B. C., D. Henning, et al. The Treacher Collins syndrome (TCOF1) gene product is involved in ribosomal DNA gene transcription by interacting with upstream binding factor. Proc Natl Acad Sci U S A, v.101, n.29, Jul 20, p.10709-14. 2004.

Wang, Z., V. Murigneux, et al. Transcriptome-wide modulation of splicing by the exon junction complex. Genome Biol, v.15, n.12, p.551. 2014.

Weiner, A. M., N. L. Scampoli, et al. Fishing the molecular bases of Treacher Collins syndrome. PLoS One, v.7, n.1, p.e29574. 2012.

ABSTRACT

Craniofacial malformations (CFMs) comprise a large and heterogeneous group of disorders in which tissues of the skull and face are affected. Affected subjects suffer from significant functional impairment and morbidity, and understanding the aetiology of these disorders is of great importance, as it may lead to the development or improvement of preventive and therapeutic strategies in the future. CFMs are largely considered to arise from developmental disturbances in the cranial neural crest and its cranioskeletal and cartilaginous mesenchymal derivatives. Neural crest-derived cell models have the potential to provide invaluable insight into the pathogenesis of CFMs, as functional studies can be to assess phenotypes in disease-relevant cell lineages. In this work, we applied this strategy to investigate three craniofacial disorders: non-syndromic cleft lip/palate (NSCL/P), Richieri-Costa-Pereira syndrome (RCPS), and Treacher Collins syndrome (TCS). NSCL/P was investigated through transcriptomic and functional assays on stem cells from human exfoliated deciduous teeth, which are neural crest-derived, adult mesenchymal cells. We identified a NSCL/P-specific dysregulated transcriptional signature involving a gene network responsible for DNA double-strand break repair that results in accumulation of DNA damage in patients' cells. These findings revealed a novel pathogenetic mechanism for NSCL/P and support previous observations pointing towards an aetiological overlap between this disease and cancer. RCPS and TCS were investigated with the use of a novel approach to generate neural crest cells from patient-specific induced pluripotent stem cells (iPSCs) as a means to recapitulate craniofacial development. We demonstrated that RCPS and TCS somatic cells can be successfully used to generate iPSCs and iPSC-derived neural crest cells and their mesenchymal derivatives. Phenotype screening showed that RCPS neural crest-derived mesenchymal cells display dysregulation of osteogenic differentiation, which was supported by confirmatory knockdown assays. Further, we report elevated apoptosis in TCS neural crest-derived mesenchymal cells, which was allied to alterations in chondrogenic and osteogenic differentiation. These results will aid in clarifying the pathogenic mechanism determining RCPS and TCS, revealing that neural crest mesenchymal cells are altered in these syndromes. In conclusion, we attested the applicability of NC-derived cell types to provide clues regarding the pathogenetic mechanisms leading to CFMs, and these novel findings will aid in dissecting the aetiology of CFMs by providing grounds to direct future efforts in craniofacial research.

RESUMO

As malformações craniofaciais (MCFs) compreendem uma vasta e heterogênea gama de doenças que envolvem o acometimento de tecidos do crânio e da face, sendo que indivíduos afetados enfrentam morbidade e deficiências funcionais relevantes. O entendimento da etiologia das MCFs é de extrema importância, pois poderá levar ao desenvolvimento ou melhoria de estratégias preventivas e terapêuticas. As MCFs são oriundas principalmente de distúrbios no desenvolvimento da crista neural cranial e seus derivados mesenquimais. Neste contexto, modelos baseados em células derivadas de crista neural são de grande potencial para o entendimento das MCFs, já que estudos funcionais podem ser realizados nestas células para averiguar fenótipos diretamente relacionados às doenças. Neste trabalho, nós empregamos esta estratégia na investigação de três tipos de MCFs: fissuras labiopalatinas não sindrômicas (FLP NS), síndrome de Richieri-Costa-Pereira (SRCP) e síndrome de Treacher Collins (STC). As FLP NS foram investigadas por meio de ensaios transcriptômicos e funcionais em células-tronco de polpa de dente decíduo, que são células mesenquimais adultas derivadas de crista neural cranial. Identificamos uma assinatura de expressão gênica específica às FLP NS, com desregulação de uma rede gênica responsável pelo reparo de quebras duplas no DNA, resultando no acúmulo deste tipo de lesão em células de indivíduos afetados pela doença. Estes achados revelam um novo mecanismo patogênico para as FLP NS e corroboram observações prévias que sugeriam sobreposição de etiologias entre esta doença e o câncer. A SRCP e a STC foram investigadas com o uso de uma nova metodologia para a geração de células de crista neural a partir de células-tronco pluripotentes induzidas (*induced pluripotent stem cells;* iPSCs) para recapitular o desenvolvimento craniofacial. Realizamos triagem de fenótipos celulares e identificamos desregulação de diferenciação osteogênica em células mesenquimais derivadas de crista neural de pacientes com SRCP, o que foi corroborado por ensaios de RNA de interferência. Além disso, mostramos que células mesenquimais de crista neural de pacientes com STC apresentam apoptose elevada aliada a alterações durante diferenciação osteogênica e condrogênica. Estes resultados revelam que células mesenquimais de crista neural estão alteradas na SRCP e STC, colaborando para o esclarecimento dos mecanismos patogênicos responsáveis por estas síndromes. Assim sendo, nós evidenciamos a aplicabilidade da modelagem de MCFs por meio de células oriundas da crista neural, e esses achados inéditos contribuirão para um melhor entendimento da etiologia das MCFs, e servem de base para futuras estratégias de pesquisa na área de doenças craniofaciais.

Appendix

Hindawi Publishing Corporation
Plastic Surgery International
Volume 2012, Article ID 782821, 11 pages
doi:10.1155/2012/782821

Review Article

Genetics and Management of the Patient with Orofacial Cleft

Luciano Abreu Brito, Joanna Goes Castro Meira, Gerson Shigeru Kobayashi, and Maria Rita Passos-Bueno

Human Genome Research Center, Institute of Biosciences, University of São Paulo, 05508-090 São Paulo, SP, Brazil

Correspondence should be addressed to Maria Rita Passos-Bueno, passos@ib.usp.br

Received 4 August 2012; Accepted 1 October 2012

Academic Editor: Renato Da Silva Freitas

Cleft lip or palate (CL/P) is a common facial defect present in 1 : 700 live births and results in substantial burden to patients. There are more than 500 CL/P syndromes described, the causes of which may be single-gene mutations, chromosomopathies, and exposure to teratogens. Part of the most prevalent syndromic CL/P has known etiology. Nonsyndromic CL/P, on the other hand, is a complex disorder, whose etiology is still poorly understood. Recent genome-wide association studies have contributed to the elucidation of the genetic causes, by raising reproducible susceptibility genetic variants; their etiopathogenic roles, however, are difficult to predict, as in the case of the chromosomal region 8q24, the most corroborated locus predisposing to nonsyndromic CL/P. Knowing the genetic causes of CL/P will directly impact the genetic counseling, by estimating precise recurrence risks, and the patient management, since the patient, followup may be partially influenced by their genetic background. This paper focuses on the genetic causes of important syndromic CL/P forms (van der Woude syndrome, 22q11 deletion syndrome, and Robin sequence-associated syndromes) and depicts the recent findings in nonsyndromic CL/P research, addressing issues in the conduct of the geneticist.

1. Introduction

Cleft lip or palate (CL/P) is a common human congenital defect promptly recognized at birth. Despite the variability driven by socioeconomic status and ethnic background,the worldwide prevalence of CL/P is often cited as 1 : 700 live births; nevertheless, the different methods of ascertainment may lead to fluctuations in the prevalence rates [1]. Essentially, CL/P results from failure of fusion of the maxillary processes or palatal shelves, which occur between the 4th and 12th weeks of embryogenesis (as reviewed by Mossey et al. [2]). Cellular processes of proliferation, differentiation, and apoptosis, which are essential for appropriate lip and palate morphogenesis, are regulated by complex molecular signaling pathways; therefore, genetic and environmental factors that dysregulate those pathways are subject of intensive research as it is expected that their understanding will accelerate the development of preventive measures. Maternal alcohol intake or exposure to tobacco and several chemicals, such as retinoic acid and folate antagonists (e.g., valproic acid), among others, has been shown to be teratogenic, thus representing risk factors to embryos during the first trimester of pregnancy (reviewed by Bender [3] and by Dixon et al. [4]). Despite their etiological importance as environmental predisposition factors to CL/P,we will focus in this paper on the genetic causes of CL/P.

Within CL/P, cleft lip with or without cleft palate (CL ± P) is considered a distinct entity from cleft palate only (CP), based on the different embryonic origin when palate development occurs, that is, the closure of the palatal shelves occurs between 8th and 12th weeks of the human gestation [5] while lip formation is concluded at the 7th week [6]. Accordingly, this subdivision is clearly supported by epidemiological findings [4]; however, in some syndromic forms of CL/P, both entities may segregate in the same family [7–10]. CL/P can occur as the only malformation (nonsyndromic (NS), representing 70% of CL ± P cases and 50% of CP cases) or associated with other clinical features (syndromic, 30% of CL ± P and 50% of CP cases; [11]), a classification that we will consider in the next topics.

The majority of children affected by CL/P require a lasting and costly multidisciplinary treatment for complete rehabilitation. The precise clinical diagnosis of CL/P patients, which is not always simple, is crucial for an accurate genetic counseling, patient management, and definition of surgical strategies, as reviewed below.

2. Genetic Factors

2.1. Syndromic CL/P. Mutations in single genes and chromosomal abnormalities are the most common mechanisms underlying syndromic CL/P. The Online Mendelian Inheritance in Man database (OMIM) describes more than 500 syndromes with CL/P as part of the phenotype. Furthermore, several cases of trisomy of chromosomes 13, 18, and 21 associated with CL/P were described, as well as partial deletions and duplications of other chromosomes [12]. These findings suggest that there may be several genomic regions containing loci which, in excess or in insufficiency, may lead to CL/P.

In this paper, we highlight van der Woude syndrome (VWS) and Velocardiofacial syndrome (VCFS), due to their high frequency among CL/P cases, together with Robin sequence (RS), a clinical feature that may be associated with other syndromes, including VCFS.

2.1.1. Van der Woude Syndrome (VWS). Van der Woude syndrome (VWS; OMIM 119300), the most frequent form of syndromic CL/P, accounts for 2% of all CL/P cases [13]. VWS is a single gene disorder with an autosomal dominant pattern of inheritance. Its penetrance is high (89–99%; [14]) and it is clinically characterized mainly by CL ± P or CP, fistulae on the lower lip, and hypodontia [15]. There is a wide spectrum of clinical variability, in which patients lacking fistulae are indistinguishable from individuals affected by nonsyndromic forms. Kondo et al. [16] showed that missense and nonsense mutations in interferon regulatory factor 6 (IRF6) were responsible for the majority of VWS cases. Although the pathogenic mutations may occur in any region of the gene, about 80% of them have been found in exons 3, 4, 7, and 9 (reviewed by Durda et al. [17]). It is predicted that the pathogenic mutations leading to SVW cause loss of function of the protein encoded by the gene [16].

Although we can estimate that the recurrence risk for future children of affected patients is 50%, it is still not possible to predict the severity of the disease in a fetus with a pathogenic mutation in *IRF6*, as there is no clear genotype-phenotype correlation. The pathogenic mutations in *IRF6* seem to play its major harmful effect during embryonic development, indicating that *IRF6* plays a critical functional role in craniofacial development. However, *IRF6* also seems to act after birth, as children with VWS have an increased frequency of wound complications after surgical cleft repair than children with NS CL ± P [18].

The spectrum of clinical variability of VWS has recently been expanded by the demonstration that mutations in *IRF6* are also causative of the Popliteal Pterygium Syndrome (PPS; OMIM 119500), an allelic, autosomal dominant disorder that presents, besides the facial anomalies typical of VWS, bilateral popliteal webs, syndactyly, and genital anomalies [17]. Most of the pathogenic mutations causative of PPS are located in exon 4 of the *IRF6* gene [16]. There are a strong genotype-phenotype correlation associated with VWS and PPS, but how the different mutations lead to PPS or VWS is still uncertain [19].

Since most of the VWS and PPS cases can be diagnosed by clinical evaluation, the necessity of genetic testing should be evaluated in each case.

2.1.2. Velocardiofacial Syndrome or 22q11.2 Deletion Syndrome. Velocardiofacial syndrome (VCFS; OMIM 192430) is an autosomal dominant disorder mainly characterized by the presence of cardiac anomalies (conotruncal defects, predominantly tetralogy of Fallot and conoventricular septal defects), CP or submucosal CP, velopharyngeal incompetence, facial dysmorphia, thymic hypoplasia, and learning disabilities [20]. The major known mutational mechanism causative of VCFS is a submicroscopic deletion at 22q11.2, usually spanning 1.5 Mb to 3 Mb. The spectrum of clinical variability is very wide, with the mildest cases presenting only two clinical signs of the syndrome in contrast to the full blown phenotype of the syndrome. Patients with DiGeorge syndrome (DGS; OMIM 188400), a condition with a great clinical overlap with VCFS, is also caused by deletions at 22q11.2, and thus represents a single entity; the term "22q11.2 deletion syndrome" is now commonly used to refer to all these cases. The clinical diagnosis for this group of patients is usually difficult, and genetic tests are often recommended in the presence of at least two clinical features of the syndrome, such as velopharingeal insufficiency and cardiac defects [21]. Moreover, patients may develop late onset psychosis or behavior disturbances, such as schizophrenia or bipolar disorders [22]. The severity of the syndrome is not dependent on the size of the deletion [23, 24] and several studies have pointed loss of one copy of *TBX1* as the major etiological agent within 22q11.2 leading to the phenotypic alterations [25, 26]. However, other environmental or genomic factors may also influence phenotype manifestation. Therefore, identification of 22q11.2 deletion patients is important for genetic counseling purposes as well as for discussing prognosis and surgical intervention, as the choice of surgical procedure depends upon the presence of abnormal and misplaced internal carotid arteries, which is relatively common in these patients (reviewed by Saman and Tatum [27]) The recurrence risk is high (50%) for carriers of the 22q11 deletion and it is still not possible to predict the severity of the disorder in fetuses with this alteration.

2.1.3. Robin Sequence and Associated Syndromes. Robin sequence (RS), also referred as Pierre Robin sequence, is characterized by the presence of micro or retrognathia, respiratory distress, and glossoptosis, with or without CP [28, 29]. It is also associated with high morbidity secondary to a compromised airway, feeding difficulties, and speech problems. It can occur isolatedly (called NS RS), but most of the time it is associated with a genetic syndrome [30].

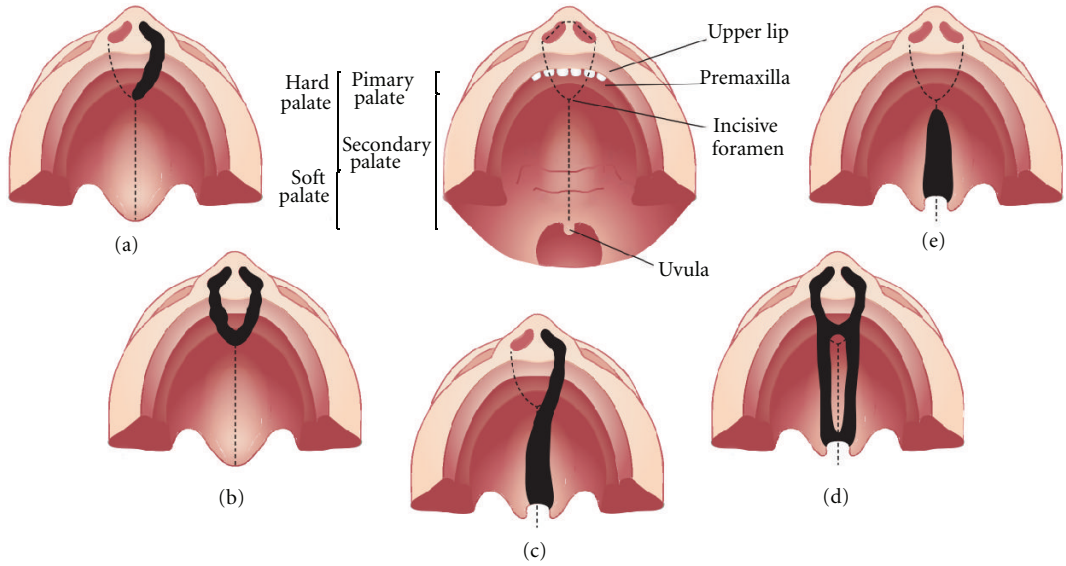

Figure 1: Representation of the most common types of cleft affecting the palate. (a) Unilateral cleft lip with alveolar involvement; (b) bilateral cleft lip with alveolar involvement; (c) unilateral cleft lip associated with cleft palate; (d) bilateral cleft lip and palate; (e) cleft palate only.

Therefore, RS must not be regarded as a definitive diagnosis, and defining the presence of an associated syndrome has implications for future case management and determination of recurrence risks [30]. The most common syndromes associated with RS are Stickler syndrome and VCFS, both with an autosomal dominant pattern of inheritance and with several additional clinical complications that are not present in NS RS.

The pathogenesis of NS RS is heterogeneous and not well defined. NS RS has been considered the result of intrauterine fetal constraint where extrinsic physical forces (e.g., oligohydramnios, breech position, or abnormal uterine anatomy) inhibit normal mandibular growth. Micrognathia in early fetal development may in turn cause the tongue to remain between the palatal shelves, thus interfering with palate closure [29, 31]. However, this mechanism has been challenged by the identification of several genetic alterations associated with RS, including chromosomal deletions such as 2q24.1-33.3, 4q32-qter, 11q21-23.1, and 17q21-24.3 [32] and microchromosomal deletions involving regulatory elements surrounding *SOX9* [33]. NS RS usually occurs as the unique case in the family and the recurrence risk for future pregnancies of the couple with one affected child is low [34].

2.2. Nonsyndromic CL ± P (NS CL ± P). NS CL ± P includes a wide spectrum of clinical variability, from a simple unilateral lip scar to bilateral cleft lip and cleft of the palate, as partly represented in Figure 1. Different epidemiological evidence, as familial recurrence, observed in 20–30% of the cases [35, 36] and twin concordance rates (40–60% for monozygotic and 3–5% for dizygotic; [37]), suggest an important genetic component in NS CL ± P etiology. High heritability rates have been estimated in several studies (reaching 84% in Europe [38],78% in China [39] and 74% in South America [40]; in Brazil, our group found estimates ranging from 45% to as high as 85%, depending on the population ascertained [36]). The most accepted genetic model for NS CL ± P is the multifactorial, in which genetic and environmental factors play a role in phenotype determination.

Researchers have conducted different approaches to seek for genetic NS CL ± P susceptibility *loci*. Linkage analysis and association studiesof candidate genes were, initially, the most popular approaches, and the first gene suggested to be associated with NS CL ± P was transforming growth factor alpha (TGFα), by Ardinger et al. [41]. Thereafter, linkage analyses raised some other genomic regions as possible susceptibility factors, as 6p24-23 [42] (recently studied by Scapoli et al. [43]), 4q21 [44], 19q13 [45], and 13q33 [46]. Additional studies, however, faced a lack of reproducibility of the emerged genomic *loci*, as reviewed in detail by others [4, 47], suggesting the existence of a strong genetic heterogeneity underlying the predisposition to the disease (i.e., different causal *loci* might be acting in the different studied families).

Candidate genes analyzed through association studies emerged not only from initial findings by linkage analysis, but also from: (1) the gene role in lip or palate embryogenesis, as suggested by animal model studies (e.g., *TGFα*, in the pioneer study by Ardinger et al. [41] and *MSX1* [48]); (2) gene role in the metabolism of putative environmental risk factors (e.g, *MTHFR*, involved in folate metabolism and firstly tested by Tolarova et al. [49], and *RARα*, which encodes a nuclear retinoic acid receptor, tested initially by Chenevix-Trench et al. [50]); (3) from the identification of chromosomal anomalies in patients (as *SUMO1* [51]), and (4) from their role in syndromic CL/P, such as van der Woude (*IRF6*, its causal gene, was firstly associated with NS CL ± P by Zucchero et al. [52]), Cleft Lip/Palate Ectodermal Dysplasia Syndrome (caused by mutations in *PVRL1* [53], firstly associated with NS CL ± P by Sözen et al. [54]) and EEC and AEC (both caused by mutations in *TP63* [55], associated with NS CL ± P by Leoyklang et al. [56]), among others.

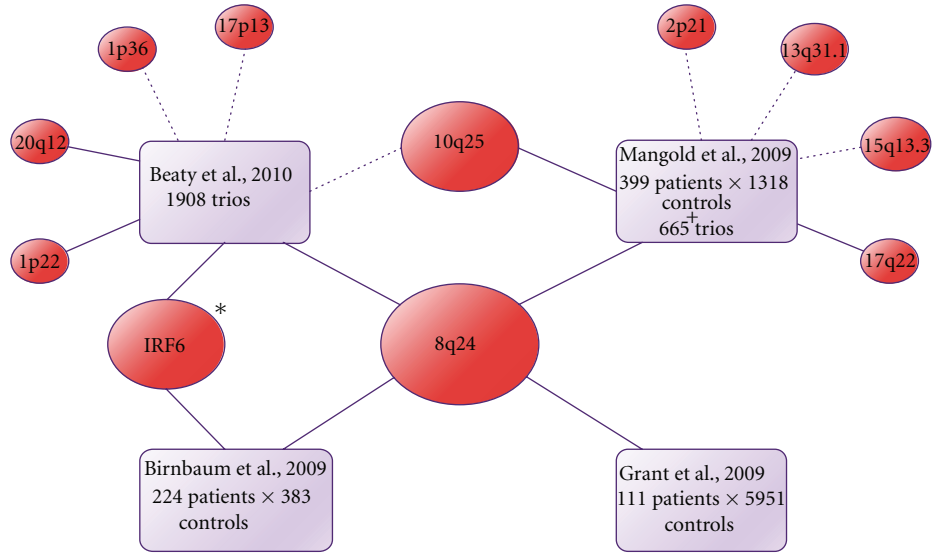

Figure 2: Diagram depicting the main lociassociated with NS CL ± P in the GWAS performed by Birnbaum et al. [72], Grant et al. [73], Mangold et al. [65], and Beaty et al. [64], which mixed case-control and trios (probands and their parents) approaches. Dotted lines represent borderline associations, whereas solid lines represent significant associations at the commonly accepted GWAS threshold ($P < 10E - 7$). (*) Mangold et al. [65] found evidence of interaction between IRF6 and GREM1, a gene located in 15q13.3 region, in NS CL ± P susceptibility.

Among all *loci* that arose through linkage and candidate gene association studies, the *IRF6* gene was the only *locus* to be consistently associated with NS CL ± P, as first shown by Zucchero et al. [52]. Rahimov et al. [57] identified a common nucleotide variant (namely rs642961) in an *IRF6* regulatory sequence conferring risk to NS CL ± P that could potentially dysregulate *IRF6* transcription levels and consequently dysregulate other signaling pathways. The variant rs642961 has been repeatedly associated in other studies in Europe [58, 59], Latin America [60, 61], and Asia, [62, 63]. Nevertheless, the role of rs641961 in embryonic development and how it predisposes to NS CL±P remains to be elucidated.

With the advent of high-throughput genotyping technologies, which allowed for a deeper investigation at the genomic level without prior hypothesis of candidate regions to be tested, the landscape changed substantially. Genome-wide association studies (GWASs) came up from these advances, providing remarkable contribution to the understanding of NS CL ± P etiology. Four large GWASs were performed on NS CL ± P so far, and their main findings are summarized in Figure 2. Markers within a gene desert in the chromosomal region 8q24 were unequivocally implicated in NS CL ± P susceptibility, since they shared similar results. A second promising locus that emerged from these studies is the region 10q25. Other minor association studies have replicated association for both 8q24 and 10q25 [59, 60, 66–69]. Therefore, the *IRF6* gene and the chromosomal regions 8q24 and 10q25 are, to date, the most corroborated *loci* implicated in NS CL ± P. However, contrary to *IRF6* association, for which a punctual susceptibility variant has been identified, finding the functional causative mutations and the molecular pathogenesis beneath the associations observed for 8q24 and 10q25 regions remains a challenge; Table 1 summarizes the main candidate genes proposed by these studies. Recently, a GWAS performed in 34 consanguineous families from a Colombian isolated population suggested that the *loci* 11p12, 11q25 and 8p23.2 may harbor recessive genes underlying NS CL ± P etiology [70]; these results, however, will need further replication. A recent linkage analysis applying high-throughput genotyping also suggested a role for the region of FOXE1 (9q22-q33) in NS CL ± P susceptibility [71]; nevertheless, this locus lacks reproducibility in other studies.

The difficulty of replication of the investigated *loci* may be a consequence of the genetic heterogeneity in NS CL ± P, that is, susceptibility variants differing from patient to patient; also, susceptibility variants may be different across unrelated populations. Beaty et al. [64] highlighted a stronger evidence for 8q24 in Europeans compared to Asians. Ethnic heterogeneity was also observed by Blanton et al. [67]; we have observed differences even across the Brazilian country populations [69], and a study with a Kenyan population failed in finding this association [74]. On the other hand, the Asians in the study reported by Beaty et al. [64] presented the most solid association for 20q12 and 1p22, compared to the European sample. It is possible that such differences may be a consequence of low statistical power in the subsample of a given ethnicity, as observed by Murray et al. [75]. Anyhow, these findings stress the value of testing non-European populations in order to identify the risk factors of NS clefting for each population, and to better understand the genetic architecture of the disease.

Regardless of the success of GWAS in identifying new susceptibility *loci*, those consistently implicated in NS CL ± P fail in explaining the complete genetic contribution proposed. This "failure" has been a common observation in many other traits, such as type 2 diabetes, height, and early onset myocardial infarction [76], and there is a current debate on where the remaining genetic causes

Table 1: Main GWAS hits and genes possibly involved according to the authors.

Region	Possible gene involved	Function*
8q24	No know gene	
10q25	VAX1 [64]	Transcription factor, apparently involved in the development of the anterior ventral forebrain.
1p22	ABCA4 [64]	Transmembrane protein expressed in retinal photoreceptors. Mutations are involved with retinopathies.
17q22	NOG [65]	Secreted protein; binds and inactivates TGFβ[1] proteins. Mutations are involved with bony fusion malformations, mainly in head and hands.
20q12	MAFB [64]	Transcription factor, acts in the differentiation and regulation of hematopoietic cell lineages. Mutations cause multicentric carpotarsal osteolysis syndrome.
1p36	PAX7 [64]	Transcription factor. Plays a role during neural crest development. Defects cause a form of rhabdomyosarcoma.
2p21	THADA [65]	Unclear function. Defects are related with thyroid tumors.
13q31.1	SPRY2 [65]	Citoplasm protein, colocalized with cytoskeleton proteins. Possibly acts as antagonist of FGF[2].
15q13.1	FMN1 [65]	Peripheral membrane protein plays a role in cell-cell adhesion.
	GREM1 [65]	Secreted protein; BMP[3] antagonist, expressed in fetal brain, small intestine, and colon.
17p13	NTN1 [64]	Extracellular matrix protein, mediates axon outgrowth and guidance. It may regulate diverse cancer tumorigenesis.

*According to OMIM database.
[1]Transforming growth factor beta.
[2]Fibroblast growth factor.
[3]Bone morphogenetic protein.

could be hidden. One hypothesis is that gene-gene and gene-environment interactions may represent a substantial additional risk; however, their evaluation is still difficult with the current research tools. It is also possible that a combination of rare mutations per individual can be responsible for a large proportion of cases. New technologies to perform exome and genome sequencing are promising approaches to bridge this gap, and have potential to bring out new susceptibility variants. The use of other approaches, such as expression analysis, can also bring new insights into the causative pathways behind this malformation. In this respect, we have recently shown that dental pulp stem cells from NS CL ± P patients exhibit dysregulation of a set of genes involved in extracellular matrix remodeling, an important biological process for lip and palate morphogenesis [77].

2.3. Nonsyndromic CPO (NS CPO). Cleft palate only is also a common malformation with a wide variability spectrum, comprising mildest phenotypes involving only uvula bifida to more severe cases, the majority of which include cleft of the soft and hard palates (Figure 1). The higher recurrence risk observed for close relatives compared to the general population [78, 79], and the higher concordance in monozygotic compared to dizygotic twins [80, 81] evidence the presence of genetic components in the etiology of NS CPO. Akin to NS CL ± P, NS CPO is believed to result from a combination of genetic and environmental factors [78]. However, in contrast to NS CL ± P, only a few studies on the genetic basis of NS CPO have been conducted, probably because of its lower prevalence and difficulty of ascertainment.

A first linkage genome scan to find NS CPO susceptibility loci was performed in 24 Finnish families by Koillinen et al. [82], which suggested 1p32, 2p24-25, and 12q21 as candidate regions; all of them, however, reached only borderline significance. Recently, Ghassibe-Sabbagh et al. [83] demonstrated the involvement of the Fas-associated factor-1 gene (*FAF1*) with NS CPO and provided insights into the gene's function in facial chondrogenic development, using a combination of an association study in a large multiethnic sample, gene expression analysis and animal model. Beaty et al., [84] performed a GWAS in 550 trios (proband and parents) of mixed ancestries and, although they did not find significant results by testing the associations of genetic markers with phenotype, they obtained interesting results when they performed the association tests conditioning on environmental variables (maternal smoking, alcohol consumption, and vitamin supplementation): association of TBK1, ZNF236, MLLT3, SMC2, and BAALC was suggested. None of the *loci* raised in these studies were in common with those emerged for NS CL ± P. Similarly, in search of a possible common etiology between NS CL ± P and NS CPO, many researchers tested the involvement of NS CL ± P candidate loci with NS CPO, but negative or conflicting results were reported for TGFα, TGFβ3, MSX1, SUMO1, BCL3, IRF6 and 8q24 [57, 72, 85–90].

A number of studies in mice has shown that defects in several genes lead to cleft palate, often accompanied by a set of other defects, as reviewed by Cobourne [91].

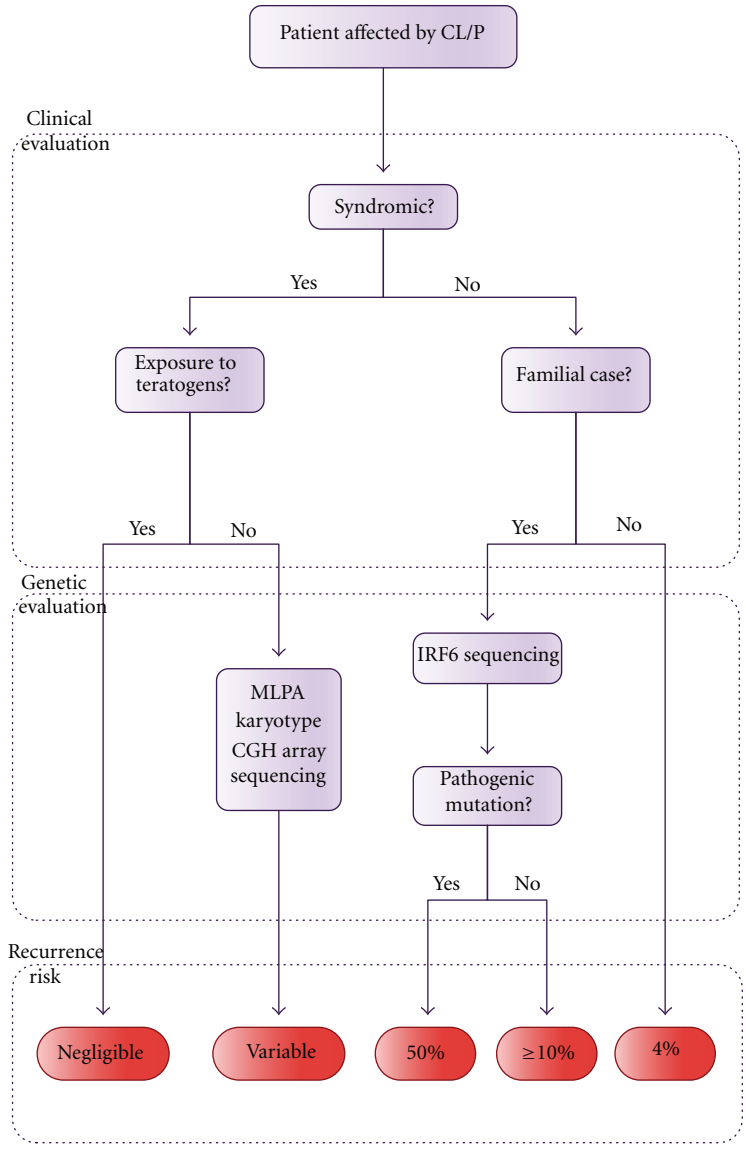

Figure 3: Flowchart depicting the genetic evaluation of a CL/P patient.

Among those genes, the *MSX1* was the most penetrant, that is, alterations in *MSX1* led to CPO more frequently than alterations in other genes. Some authors have also reported chromosomal duplications, deletions and rearrangements in NS CPO patients [92–94]. Nonetheless, the genes located within those chromosomal regions lack confirmation with regards to their pathogenic role.

3. Genetic Management of the Family with CL/P-Affected Children

The clinical evaluation of a CL/P patient, outlined in Figure 3, starts with his/her classification in syndromic and nonsyndromic cases, based on the presence or absence of other dysmorphisms or malformations, together with an investigation of the occurrence of relatives with similar features.

Among the syndromic cases, it is first necessary to investigate the possibility of non-genetic causes, for example, exposure to teratogens during the first trimester of gestation. In cases of CL/P arising from the action of teratogenic agents during embryogenesis, the recurrence risk is negligible since exposure to teratogens in a next pregnancy does not recur. Once the possibility of a teratogenic origin for CL/P is ruled out, the geneticist should raise the diagnostic hypothesis of genetic syndromes and recommend the most adequate test (however, these tests might also be useful in the cases of teratogenic exposure, in order to refute chromosomal abnormalities). The most commonly performed tests are the karyotype, Multiplex Ligation-dependent Probe Amplification (MLPA), Comparative Genomic Hybridization array (CGH-array), gene target sequencing, and exome sequencing. Whilst the karyotype is a cytogenetic technique which allows for detection of large structural and numeric chromosomal

anomalies in a low resolution, MLPA and CGH-array are quantitative molecular tests that enable the investigation of gain or loss of genetic material at the submicroscopic level. MLPA is applied to investigate specific targets in the genome while CGH-array can be used to screen the whole genome with a very high resolution. MLPA or CGH-array are the recommended tests to be used for a first screening, depending on the available resources [95, 96].

Gene target sequencing is recommended when one or more genes are known to be causative of the disorder. There is a trend towards the use of next generation sequencing particularly in diseases associated with genetic heterogeneity, as this approach permits the simultaneous testing of several genes, thus resulting in a more cost-effective test in the long run. Recurrence risk estimates for future children of the parents of one affected patient is dependent on the definition of the etiological mechanisms of the disease, evidencing the importance of selecting the appropriate test, combined with the clinical evaluation, for the establishment of the diagnosis.

In nonsyndromic cases, due to our full lack of understanding with regards to their etiological mechanisms, the recurrence risks have been empirically determined by epidemiological studies. As expected for a multifactorial model of inheritance, these risks can be influenced by several factors, such as gender of the affected propositus, severity of the orofacial cleft, and number of affected relatives [97]. The recurrence risk among families with one first-degree affected relative has been estimated as 4% for NS CL ± P and 2% for NS CPO [98]. These estimates may vary depending on the population. In Brazil, the recurrence risk has been estimated at only 2% among families with one first-degree NS CL ± P affected relative [36].

In NS cases, the identification of other individuals with CL/P in the family should be always interpreted with caution. Due to genetic heterogeneity associated with NS CL/P, a family with several affected individuals can actually represent the segregation of a single-gene disorder, which would not be promptly recognized based solely on clinical evaluation. For example, among 102 families with at least two individuals affected by NS CL/P, we identified 4 families with pathogenic mutations in *IRF6*, which actually represented VWS cases. Due to the high prevalence of VWS, we thus recommend *IRF6* genetic testing in familial cases of NS CL/P [99].

CL/P is a complex group of disorders and the adequate genetic management of the family requires evaluation by a trained group of geneticists in order to best define the diagnosis of the affected propositus, evaluation of prognosis, surgery indications, and, finally, recurrence risk estimates for the individuals at risk. With the advance of genomic technology, we expect that new advances and understanding of the genetic mechanisms leading to CL/P will be achieved in the upcoming years.

Glossary

Association Analysis: correlates the occurrence, in two groups of individuals (e.g., affected and unaffected), of one genetic variant with the phenotype. If the frequency difference of one genotyped variant is statistically significant between the two groups, the genomic region harboring the variant will be associated with the trait. This approach is better suited to identify common and low impact genetic variants of shared origin.

Exome Sequencing: sequencing focused on the 2% of the genome which constitutes the protein-coding genes (exome). Despite the low proportion of the genome, 85% of the high-impact mutations already identified rely on the exome [100], which makes this approach highly promising.

Genetic Marker: any polymorphism loci of known location which is suitable for gene mapping. Single nucleotide polymorphisms (SNPs), which involve one nucleotide substitution, are the most used for this purpose (e.g., in GWAS). A large number of SNPs can be analyzed simultaneously through the use of semi-automated equipments and microchips.

GWAS: association analysis at the genomic level. Requires the genotyping of thousands or millions of genetic markers, and has been made possible after advances in the characterization of the human genome (e.g., the Human Genome Project and the HapMap Project (http://www.hapmap.org/)) and automation of genotypic analysis. This strategy is suitable for identifying common low-effect variants without prior hypothesis. Finding association of the trait with a genetic marker does not necessarily mean that the marker is directly involved with the disease; most likely, the chromosomal region harboring this marker also comprises one or more susceptibility factors. Finding the real cause behind the association signal is currently a challenge.

Heritability: fraction of phenotypic variance in a population attributable to genetic factors.

Linkage Analysis: approach that searches for genomic regions which cosegregate among affected individuals within a family, by genotyping known genetic markers spread throughout the genome. Powerful to detect genes of high impact, but loci of small or moderate effect are usually missed. Large families with many affected individuals are required.

Polymorphism: genomic locus that admits two or more variants in the population and its rarest variant has a populational frequency greater than 1%.

Whole-Genome Sequencing: sequencing analysis of the whole genome, including coding and noncoding regions.

Acknowledgments

The authors are grateful to Regina de Siqueira Bueno for the assistance with the images, and all the colleagues and patients involved with cleft research. The authors are funded by CEPID/FAPESP and CNPq/CAPES.

References

[1] P. Mossey and E. Castilla, "Global registry and database on craniofacial anomalies," in *Proceedings of the World Health Organization Registry Meeting on Craniofacial Anomalies*, Bauru, Brazil, 2001.

[2] P. A. Mossey, J. Little, R. G. Munger, M. J. Dixon, and W. C. Shaw, "Cleft lip and palate," *The Lancet*, vol. 374, no. 9703, pp. 1773–1785, 2009.
[3] P. L. Bender, "Genetics of cleft lip and palate," *Journal of Pediatric Nursing*, vol. 15, no. 4, pp. 242–249, 2000.
[4] M. J. Dixon, M. L. Marazita, T. H. Beaty, and J. C. Murray, "Cleft lip and palate: understanding genetic and environmental influences," *Nature Reviews Genetics*, vol. 12, no. 3, pp. 167–178, 2011.
[5] J. J. Kerrigan, J. P. Mansell, A. Sengupta, N. Brown, and J. R. Sandy, "Palatogenesis and potential mechanisms for clefting," *Journal of the Royal College of Surgeons of Edinburgh*, vol. 45, no. 6, pp. 351–358, 2000.
[6] R. Jiang, J. O. Bush, and A. C. Lidral, "Development of the upper lip: morphogenetic and molecular mechanisms," *Developmental Dynamics*, vol. 235, no. 5, pp. 1152–1166, 2006.
[7] F. C. Fraser, "Updating the genetics of cleft lip and palate," *Birth Defects*, vol. 10, no. 8, pp. 107–111, 1974.
[8] D. E. Neilson, J. W. Brunger, S. Heeger, M. Bamshad, and N. H. Robin E, "Mixed clefting type in Rapp-Hodgkin syndrome," *American Journal of Medical Genetics*, vol. 108, no. 4, pp. 281–284, 2002.
[9] M. Kot and J. Kruk-Jeromini, "Analysis of family incidence of cleft lip and/or palate," *Medical Science Monitor*, vol. 13, no. 5, pp. CR231–CR234, 2007.
[10] K. D. Rutledge, C. Barger, J. H. Grant, and N. H. Robin, "IRF6 mutations in mixed isolated familial clefting," *American Journal of Medical Genetics A*, vol. 152, no. 12, pp. 3107–3109, 2010.
[11] P. Stanier and G. E. Moore, "Genetics of cleft lip and palate: syndromic genes contribute to the incidence of non-syndromic clefts," *Human Molecular Genetics*, vol. 13, no. 1, pp. R73–R81, 2004.
[12] S. Gabrielli, M. Piva, T. Ghi et al., "Bilateral cleft lip and palate without premaxillary protrusion is associated with lethal aneuploidies," *Ultrasound in Obstetrics and Gynecology*, vol. 34, no. 4, pp. 416–418, 2009.
[13] B. C. Schutte, A. Sander, M. Malik, and J. C. Murray, "Refinement of the Van der Woude gene location and construction of a 3.5- Mb YAC contig and STS map spanning the critical region in 1q32-q41," *Genomics*, vol. 36, no. 3, pp. 507–514, 1996.
[14] A. B. Burdick, D. Bixler, and Puckett Cl., "Genetic analysis in families with Van Der Woude syndrome," *Journal of Craniofacial Genetics and Developmental Biology*, vol. 5, no. 2, pp. 181–208, 1985.
[15] A. van der Woude, "Fistula labii inferioris congenita and its association with cleft lip and palate," *The American Journal of Human Genetics*, vol. 6, no. 2, pp. 244–256, 1954.
[16] S. Kondo, B. C. Schutte, R. J. Richardson et al., "Mutations in IRF6 cause Van der Woude and popliteal pterygium syndromes," *Nature Genetics*, vol. 32, no. 2, pp. 285–289, 2002.
[17] K. M. Durda, B. C. Schutte, and J. C. Murray, "IRF6-Related Disorders," 1993.
[18] J. L. P. Jones, J. W. Canady, J. T. Brookes et al., "Wound complications after cleft repair in children with Van der Woude syndrome," *Journal of Craniofacial Surgery*, vol. 21, no. 5, pp. 1350–1353, 2010.
[19] H. J. Little, N. K. Rorick, L. I. Su et al., "Missense mutations that cause Van der Woude syndrome and popliteal pterygium syndrome affect the DNA-binding and transcriptional activation functions of IRF6," *Human Molecular Genetics*, vol. 18, no. 3, pp. 535–545, 2009.
[20] R. J. Shprintzen, R. B. Goldberg, M. L. Lewin et al., "A new syndrome involving cleft palate, cardiac anomalies, typical facies, and learning disabilities: velo-cardio-facial syndrome," *Cleft Palate Journal*, vol. 15, no. 1, pp. 56–62, 1978.
[21] B. C. Sommerlad, F. V. Mehendale, M. J. Birch, D. Sell, C. Hattee, and K. Harland, "Palate re-repair revisited," *Cleft Palate-Craniofacial Journal*, vol. 39, no. 3, pp. 295–307, 2002.
[22] R. J. Shprintzen, R. Goldberg, K. J. Golding-Kushner, and R. W. Marion, "Late-onset psychosis in the velo-cardio-facial syndrome," *American Journal of Medical Genetics*, vol. 42, no. 1, pp. 141–142, 1992.
[23] C. Carlson, H. Sirotkin, R. Pandita et al., "Molecular definition of 22q11 deletions in 151 velo-cardio-facial syndrome patients," *American Journal of Human Genetics*, vol. 61, no. 3, pp. 620–629, 1997.
[24] P. Sandrin-Garcia, D. V. M. Abramides, L. R. Martelli, E. S. Ramos, A. Richieri-Costa, and G. A. S. Passos, "Typical phenotypic spectrum of velocardiofacial syndrome occurs independently of deletion size in chromosome 22q11.2," *Molecular and Cellular Biochemistry*, vol. 303, no. 1-2, pp. 9–17, 2007.
[25] C. Chieffo, N. Garvey, W. Gong et al., "Isolation and characterization of a gene from the DiGeorge chromosomal region homologous to the mouse Tbx1 gene," *Genomics*, vol. 43, no. 3, pp. 267–277, 1997.
[26] S. Merscher, B. Funke, J. A. Epstein et al., "TBX1 is responsible for cardiovascular defects in velo-cardio-facial/DiGeorge syndrome," *Cell*, vol. 104, no. 4, pp. 619–629, 2001.
[27] M. Saman and S. A. Tatum III, "Recent advances in surgical pharyngeal modification procedures for the treatment of velopharyngeal insufficiency in patients with cleft palate," *Archives of Facial Plastic Surgery*, vol. 14, no. 2, pp. 85–88, 2012.
[28] J. C. Carey, R. M. Fineman, and F. M. Ziter, "The Robin sequence as a consequence of malformation, dysplasia, and neuromuscular syndromes," *Journal of Pediatrics*, vol. 101, no. 5, pp. 858–864, 1982.
[29] K. N. Evans, K. C. Sie, R. A. Hopper, R. P. Glass, A. V. Hing, and M. L. Cunningham, "Robin sequence: from diagnosis to development of an effective management plan," *Pediatrics*, vol. 127, no. 5, pp. 936–948, 2011.
[30] R. J. Shprintzen, "The implications of the diagnosis of Robin sequence," *The Cleft Palate-Craniofacial Journal*, vol. 29, no. 3, pp. 205–209, 1992.
[31] J. Schubert, H. Jahn, and M. Berginski, "Experimental aspects of the pathogenesis of Robin sequence," *Cleft Palate-Craniofacial Journal*, vol. 42, no. 4, pp. 372–376, 2005.
[32] L. P. Jakobsen, M. A. Knudsen, J. Lespinasse et al., "The genetic basis of the Pierre Robin Sequence," *Cleft Palate-Craniofacial Journal*, vol. 43, no. 2, pp. 155–159, 2006.
[33] S. Benko, J. A. Fantes, J. Amiel et al., "Highly conserved non-coding elements on either side of SOX9 associated with Pierre Robin sequence," *Nature Genetics*, vol. 41, no. 3, pp. 359–364, 2009.
[34] L. J. Sheffield, J. A. Reiss, K. Strohm, and M. Gilding, "A genetic follow-up study of 64 patients with the Pierre Robin complex," *American Journal of Medical Genetics*, vol. 28, no. 1, pp. 25–36, 1987.
[35] R. T. Lie, A. J. Wilcox, and R. Skjaerven, "A population-based study of the risk of recurrence of birth defects," *New England Journal of Medicine*, vol. 331, no. 1, pp. 1–4, 1994.
[36] L. A. Brito, L. A. Cruz, K. M. Rocha et al., "Genetic contribution for non-syndromic cleft lip with or without cleft palate (NS CL/P) in different regions of Brazil and

implications for association studies," *American Journal of Medical Genetics A*, vol. 155, no. 7, pp. 1581–1587, 2011.

[37] K. Christensen and P. Fogh-Andersen, "Cleft lip (± cleft palate) in Danish twins, 1970–1990," *American Journal of Medical Genetics*, vol. 47, no. 6, pp. 910–916, 1993.

[38] E. Calzolari, M. Milan, G. B. Cavazzuti et al., "Epidemiological and genetic study of 200 cases of oral cleft in the Emilia Romagna region of northern Italy," *Teratology*, vol. 38, no. 6, pp. 559–564, 1988.

[39] D. N. Hu, J. H. Li, and H. Y. Chen, "Genetics of cleft lip and cleft palate in China," *American Journal of Human Genetics*, vol. 34, no. 6, pp. 999–1002, 1982.

[40] B. G. Menegotto and F. M. Salzano, "Clustering of malformations in the families of South American oral cleft neonates," *Journal of Medical Genetics*, vol. 28, no. 2, pp. 110–113, 1991.

[41] H. H. Ardinger, K. H. Buetow, G. I. Bell, J. Bardach, D. R. VanDemark, and J. C. Murray, "Association of genetic variation of the transforming growth factor-alpha gene with cleft lip and palate," *American Journal of Human Genetics*, vol. 45, no. 3, pp. 348–353, 1989.

[42] H. Eiberg, D. Bixler, and L. S. Nielsen, "Suggestion of linkage of a major locus for nonsyndromic orofacial cleft with F13A and tentative assignment to chromosome 6," *Clinical Genetics*, vol. 32, no. 2, pp. 129–132, 1987.

[43] L. Scapoli, M. Martinelli, F. Pezzetti et al., "Expression and association data strongly support JARID2 involvement in nonsyndromic cleft lip with or without cleft palate," *Human Mutation*, vol. 31, no. 7, pp. 794–800, 2010.

[44] S. Beiraghi, T. Foroud, S. Diouhy et al., "Possible localization of a major gene for cleft lip and palate to 4q," *Clinical Genetics*, vol. 46, no. 3, pp. 255–256, 1994.

[45] J. Stein, J. B. Mulliken, S. Stal et al., "Nonsyndromic cleft lip with or without cleft palate: evidence of linkage to BCL3 in 17 multigenerational families," *American Journal of Human Genetics*, vol. 57, no. 2, pp. 257–272, 1995.

[46] U. Radhakrishna, U. Ratnamala, M. Gaines et al., "Genomewide scan for nonsyndromic cleft lip and palate in multigenerational Indian families reveals significant evidence of linkage at 13q33.1-34," *American Journal of Human Genetics*, vol. 79, no. 3, pp. 580–585, 2006.

[47] F. Carinci, L. Scapoli, A. Palmieri, I. Zollino, and F. Pezzetti, "Human genetic factors in nonsyndromic cleft lip and palate: an update," *International Journal of Pediatric Otorhinolaryngology*, vol. 71, no. 10, pp. 1509–1519, 2007.

[48] I. Satokata and R. Maas, "Msx1 deficient mice exhibit cleft palate and abnormalities of craniofacial and tooth development," *Nature Genetics*, vol. 6, no. 4, pp. 348–356, 1994.

[49] M. Tolarova, I. van Rooij, and M. Pastor, "A common mutation in the MTHFR gene is a risk factor for nonsyndromic cleft lip and palate anomalies," *The American Journal of Human Genetics*, vol. 63, p. 27, 1998.

[50] G. Chenevix-Trench, K. Jones, A. C. Green, D. L. Duffy, and N. G. Martin, "Cleft lip with or without cleft palate: associations with transforming growth factor alpha and retinoic acid receptor loci," *American Journal of Human Genetics*, vol. 51, no. 6, pp. 1377–1385, 1992.

[51] F. S. Alkuraya, I. Saadi, J. J. Lund, A. Turbe-Doan, C. C. Morton, and R. L. Maas, "SUM01 haploinsufficiency leads to cleft lip and palate," *Science*, vol. 313, no. 5794, p. 1751, 2006.

[52] T. M. Zucchero, M. E. Cooper, B. S. Maher et al., "Interferon regulatory factor 6 (IRF6) gene variants and the risk of isolated cleft lip or palate," *New England Journal of Medicine*, vol. 351, no. 8, pp. 769–780, 2004.

[53] K. Suzuki, D. Hu, T. Bustos et al., "Mutations of PVRL1, encoding a cell-cell adhesion molecule/herpesvirus receptor, in cleft lip/palate-ectodermal dysplasia," *Nature Genetics*, vol. 25, no. 4, pp. 427–430, 2000.

[54] M. A. Sözen, K. Suzuki, M. M. Tolarova, T. Bustos, J. E. Fernández Iglesias, and R. A. Spritz, "Mutation of PVRL1 is associated with sporadic, non-syndromic cleft lip/palate in northern Venezuela," *Nature Genetics*, vol. 29, no. 2, pp. 141–142, 2001.

[55] T. Rinne, H. G. Brunner, and H. van Bokhoven, "p63-associated disorders," *Cell Cycle*, vol. 6, no. 3, pp. 262–268, 2007.

[56] P. Leoyklang, P. Siriwan, and V. Shotelersuk, "A mutation of the p63 gene in non-syndromic cleft lip," *Journal of Medical Genetics*, vol. 43, no. 6, p. e28, 2006.

[57] F. Rahimov, M. L. Marazita, A. Visel et al., "Disruption of an AP-2α binding site in an IRF6 enhancer is associated with cleft lip," *Nature Genetics*, vol. 40, no. 11, pp. 1341–1347, 2008.

[58] S. Birnbaum, K. U. Ludwig, H. Reutter et al., "IRF6 gene variants in Central European patients with non-syndromic cleft lip with or without cleft palate," *European Journal of Oral Sciences*, vol. 117, no. 6, pp. 766–769, 2009.

[59] A. Mostowska, K. K. Hozyasz, P. Wojcicki, B. Biedziak, P. Paradowska, and P. P. Jagodzinski, "Association between genetic variants of reported candidate genes or regions and risk of cleft lip with or without cleft palate in the polish population," *Birth Defects Research A* , vol. 88, no. 7, pp. 538–545, 2010.

[60] A. Rojas-Martinez, H. Reutter, O. Chacon-Camacho et al., "Genetic risk factors for nonsyndromic cleft lip with or without cleft palate in a mesoamerican population: evidence for IRF6 and variants at 8q24 and 10q25," *Birth Defects Research A*, vol. 88, no. 7, pp. 535–537, 2010.

[61] L. A. Brito, C. Bassi, C. Masotti et al., "IRF6 is a risk factor for nonsyndromic cleft lip in the Brazilian population," *American Journal of Medical Genetics A*, vol. 158, no. 9, pp. 2170–2175, 2012.

[62] Y. Pan, J. Ma, W. Zhang et al., "IRF6 polymorphisms are associated with nonsyndromic orofacial clefts in a Chinese Han population," *American Journal of Medical Genetics A*, vol. 152, no. 10, pp. 2505–2511, 2010.

[63] J. Shi, T. Song, X. Jiao, C. Qin, and J. Zhou, "Single-nucleotide polymorphisms (SNPs) of the IRF6 and TFAP2A in non-syndromic cleft lip with or without cleft palate (NSCLP) in a northern Chinese population," *Biochemical and Biophysical Research Communications*, vol. 410, no. 4, pp. 732–736, 2011.

[64] T. H. Beaty, J. C. Murray, M. L. Marazita et al., "A genome-wide association study of cleft lip with and without cleft palate identifies risk variants near MAFB and ABCA4," *Nature Genetics*, vol. 42, no. 6, pp. 525–529, 2010.

[65] E. Mangold, K. U. Ludwig, S. Birnbaum et al., "Genome-wide association study identifies two susceptibility loci for nonsyndromic cleft lip with or without cleft palate," *Nature Genetics*, vol. 42, no. 1, pp. 24–26, 2010.

[66] T. Nikopensius, L. Ambrozaityte, K. U. Ludwig et al., "Replication of novel susceptibility locus for nonsyndromic cleft lip with or without cleft palate on chromosome 8q24 in Estonian and Lithuanian patients," *American Journal of Medical Genetics A*, vol. 149, no. 11, pp. 2551–2553, 2009.

[67] S. H. Blanton, A. Burt, S. Stal, J. B. Mulliken, E. Garcia, and J. T. Hecht, "Family-based study shows heterogeneity of a susceptibility locus on chromosome 8q24 for nonsyndromic

cleft lip and palate," *Birth Defects Research A*, vol. 88, no. 4, pp. 256–259, 2010.

[68] T. Nikopensius, S. Birnbaum, K. U. Ludwig et al., "Susceptibility locus for non-syndromic cleft lip with or without cleft palate on chromosome 10q25 confers risk in Estonian patients," *European Journal of Oral Sciences*, vol. 118, no. 3, pp. 317–319, 2010.

[69] L. A. Brito, L. M. Paranaiba, C. F. Bassi et al., "Region 8q24 is a susceptibility locus for nonsyndromic oral clefting in Brazil," *Birth Defects Research A*, vol. 94, no. 6, pp. 464–468, 2012.

[70] M. Camargo, D. Rivera, L. Moreno et al., "GWAS reveals new recessive loci associated with non-syndromic facial clefting," *European Journal of Medical Genetics*, vol. 55, no. 10, pp. 510–514, 2012.

[71] L. M. Moreno, M. A. Mansilla, S. A. Bullard et al., "FOXE1 association with both isolated cleft lip with or without cleft palate, and isolated cleft palate," *Human Molecular Genetics*, vol. 18, no. 24, pp. 4879–4896, 2009.

[72] S. Birnbaum, K. U. Ludwig, H. Reutter et al., "Key susceptibility locus for nonsyndromic cleft lip with or without cleft palate on chromosome 8q24," *Nature Genetics*, vol. 41, no. 4, pp. 473–477, 2009.

[73] S. F. Grant, K. Wang, H. Zhang et al., "A genome-wide association study identifies a locus for nonsyndromic cleft lip with or without cleft palate on 8q24," *The Journal of pediatrics*, vol. 155, no. 6, pp. 909–913, 2009.

[74] R. C. Weatherley-White, S. Ben, Y. Jin, S. Riccardi, T. D. Arnold, and R. A. Spritz, "Analysis of genomewide association signals for nonsyndromic cleft lip/palate in a Kenya African Cohort," *American Journal of Medical Genetics A*, vol. 155, no. 10, pp. 2422–2425, 2011.

[75] T. Murray, M. A. Taub, I. Ruczinski et al., "Examining markers in 8q24 to explain differences in evidence for association with cleft lip with/without cleft palate between Asians and Europeans," *Genetic Epidemiology*, vol. 36, no. 4, pp. 392–399, 2012.

[76] T. A. Manolio, F. S. Collins, N. J. Cox et al., "Finding the missing heritability of complex diseases," *Nature*, vol. 461, no. 7265, pp. 747–753, 2009.

[77] D. F. Bueno, D. Y. Sunaga, G. S. Kobayashi et al., "Human stem cell cultures from cleft lip/palate patients show enrichment of transcripts involved in extracellular matrix modeling by comparison to controls," *Stem Cell Reviews and Reports*, vol. 7, no. 2, pp. 446–457, 2011.

[78] K. Christensen and L. E. Mitchell, "Familial recurrence-pattern analysis of nonsyndromic isolated cleft palate—a Danish registry study," *American Journal of Human Genetics*, vol. 58, no. 1, pp. 182–190, 1996.

[79] A. Sivertsen, A. J. Wilcox, R. Skjærven et al., "Familial risk of oral clefts by morphological type and severity: population based cohort study of first degree relatives," *BMJ*, vol. 336, no. 7641, pp. 432–434, 2008.

[80] R. E. A. Nordström, T. Laatikainen, T. O. Juvonen, and R. E. Ranta, "Cleft-twin sets in Finland 1948–1987," *Cleft Palate-Craniofacial Journal*, vol. 33, no. 4, pp. 340–347, 1996.

[81] D. Grosen, C. Bille, I. Petersen et al., "Risk of oral clefts in twins," *Epidemiology*, vol. 22, no. 3, pp. 313–319, 2011.

[82] H. Koillinen, P. Lahermo, J. Rautio, J. Hukki, M. Peyrard-Janvid, and J. Kere, "A genome-wide scan of non-syndromic cleft palate only (CPO) in Finnish multiplex families," *Journal of Medical Genetics*, vol. 42, no. 2, pp. 177–184, 2005.

[83] M. Ghassibe-Sabbagh, L. Desmyter, T. Langenberg et al., "FAF1, a gene that is disrupted in cleft palate and has conserved function in Zebrafish," *American Journal of Human Genetics*, vol. 88, no. 2, pp. 150–161, 2011.

[84] T. H. Beaty, I. Ruczinski, J. C. Murray et al., "Evidence for gene-environment interaction in a genome wide study of nonsyndromic cleft palate," *Genetic Epidemiology*, vol. 35, no. 6, pp. 469–478, 2011.

[85] S. J. Hwang, T. H. Beaty, S. R. Panny et al., "Association study of transforming growth factor alpha (TGFα) TaqI polymorphism and oral clefts: Indication of gene-environment interaction in a population-based sample of infants with birth defects," *American Journal of Epidemiology*, vol. 141, no. 7, pp. 629–636, 1995.

[86] G. M. Shaw, C. R. Wasserman, E. J. Lammer et al., "Orofacial clefts, parental cigarette smoking, and transforming growth factor-alpha gene variants," *American Journal of Human Genetics*, vol. 58, no. 3, pp. 551–561, 1996.

[87] R. Shiang, A. C. Lidral, H. H. Ardinger et al., "Association of transforming growth-factor alpha gene polymorphisms with nonsyndromic cleft palate only (CPO)," *American Journal of Human Genetics*, vol. 53, no. 4, pp. 836–843, 1993.

[88] A. C. Lidral, P. A. Romitti, A. M. Basart et al., "Association of MSX1 and TGFB3 with nonsyndromic clefting in humans," *American Journal of Human Genetics*, vol. 63, no. 2, pp. 557–568, 1998.

[89] L. E. Mitchell, J. C. Murray, S. O'Brien, and K. Christensen, "Evaluation of two putative susceptibility loci for oral clefts in the Danish population," *American Journal of Epidemiology*, vol. 153, no. 10, pp. 1007–1015, 2001.

[90] J. T. Hecht, J. B. Mulliken, and S. H. Blanton, "Evidence for a cleft palate only locus on chromosome 4 near MSX1," *American Journal of Medical Genetics*, vol. 110, no. 4, pp. 406–407, 2002.

[91] M. T. Cobourne, "The complex genetics of cleft lip and palate," *European Journal of Orthodontics*, vol. 26, no. 1, pp. 7–16, 2004.

[92] C. Brewer, S. Holloway, P. Zawalnyski, A. Schinzel, and D. FitzPatrick, "A chromosomal duplication map of malformations: regions of suspected haplo- and triplolethality—and tolerance of segmental aneuploidy—in humans," *American Journal of Human Genetics*, vol. 64, no. 6, pp. 1702–1708, 1999.

[93] C. M. Brewer, J. P. Leek, A. J. Green et al., "A locus for isolated cleft palate, located human chromosome 2q32," *American Journal of Human Genetics*, vol. 65, no. 2, pp. 387–396, 1999.

[94] C. Brewer, S. Holloway, P. Zawalnyski, A. Schinzel, and D. Fitzpatrick, "A chromosomal deletion map of human malformations," *American Journal of Human Genetics*, vol. 63, no. 4, pp. 1153–1159, 1998.

[95] S. DeVries, J. W. Gray, D. Pinkel, F. M. Waldman, and D. Sudar, "Comparative genomic hybridization," in *Current Protocols in Human Genetics*, chapter 4, unit 4.6, 2001.

[96] F. S. Jehee, J. T. Takamori, P. F. Vasconcelos Medeiros et al., "Using a combination of MLPA kits to detect chromosomal imbalances in patients with multiple congenital anomalies and mental retardation is a valuable choice for developing countries," *European Journal of Medical Genetics*, vol. 54, no. 4, pp. e425–e432, 2011.

[97] D. Grosen, C. Chevrier, A. Skytthe et al., "A cohort study of recurrence patterns among more than 54000 relatives of oral cleft cases in Denmark: support for the multifactorial threshold model of inheritance," *Journal of Medical Genetics*, vol. 47, no. 3, pp. 162–168, 2010.

[98] R. J. Gorlin, M. M. Cohen Jr., and R. C. M. Hennekam, *Syndromes of the Head and Neck*, Oxford University Press, New York, NY, USA, 4th edition, 2001.

[99] F. S. Jehee, B. A. Burin, K. M. Rocha et al., "Novel mutations in IRF6 in nonsyndromic cleft lip with or without cleft palate: When should IRF6 mutational screening be done?" *American Journal of Medical Genetics A*, vol. 149, no. 6, pp. 1319–1322, 2009.

[100] J. Majewski, J. Schwartzentruber, E. Lalonde, A. Montpetit, and N. Jabado, "What can exome sequencing do for you?" *Journal of Medical Genetics*, vol. 48, no. 9, pp. 580–589, 2011.

BRIEF REPORT

Human Mutation

OFFICIAL JOURNAL HGVS HUMAN GENOME VARIATION SOCIETY www.hgvs.org

Rare Variants in the Epithelial Cadherin Gene Underlying the Genetic Etiology of Nonsyndromic Cleft Lip with or without Cleft Palate

Luciano Abreu Brito,[1] Guilherme Lopes Yamamoto,[1] Soraia Melo,[2,3] Carolina Malcher,[1] Simone Gomes Ferreira,[1] Joana Figueiredo,[2,3] Lucas Alvizi,[1] Gerson Shigeru Kobayashi,[1] Michel Satya Naslavsky,[1] Nivaldo Alonso,[4] Temis Maria Felix,[5] Mayana Zatz,[1] Raquel Seruca,[2,3,6] and Maria Rita Passos-Bueno[1]*

[1] *Centro de Pesquisa sobre o Genoma Humano e Células-Tronco, Departamento de Genética e Biologia Evolutiva, Instituto de Biociências, Universidade de São Paulo, São Paulo, Brasil;* [2] *IPATIMUP, Institute of Molecular Pathology and Immunology, University of Porto, Porto, Portugal;* [3] *Instituto de Investigação e Inovação em Saúde, Universidade do Porto, Porto, Portugal;* [4] *Hospital das Clínicas, Faculdade de Medicina, Universidade de São Paulo, São Paulo, Brasil;* [5] *Laboratório de Medicina Genômica, Centro de Pesquisa Experimental, Hospital de Clínicas de Porto Alegre, Porto Alegre, Brasil;* [6] *Faculty of Medicine, University of Porto, Porto, Portugal*

Communicated by Iain McIntosh

Received 2 February 2015; accepted revised manuscript 17 June 2015.
Published online 29 June 2015 in Wiley Online Library (www.wiley.com/humanmutation). DOI: 10.1002/humu.22827

ABSTRACT: **Nonsyndromic orofacial cleft (NSOFC) is a complex disease of still unclear genetic etiology. To investigate the contribution of rare epithelial cadherin (*CDH1*) gene variants to NSOFC, we target sequenced 221 probands. Candidate variants were evaluated via in vitro, in silico, or segregation analyses. Three probably pathogenic variants (c.760G>A [p.Asp254Asn], c.1023T>G [p.Tyr341*], and c.2351G>A [p.Arg784His]) segregated according to autosomal dominant inheritance in four nonsyndromic cleft lip with or without cleft palate (NSCL/P) families (Lod score: 5.8 at θ = 0; 47% penetrance). A fourth possibly pathogenic variant (c.387+5G>A) was also found, but further functional analyses are needed (overall prevalence of *CDH1* candidate variants: 2%; 15.4% among familial cases). *CDH1* mutational burden was higher among probands from familial cases when compared to that of controls ($P = 0.002$). We concluded that *CDH1* contributes to NSCL/P with mainly rare, moderately penetrant variants, and *CDH1* haploinsufficiency is the likely etiological mechanism.**
Hum Mutat 36:1029–1033, 2015. © 2015 Wiley Periodicals, Inc.

KEY WORDS: ***CDH1*; oral clefts; gastric cancer; two-hit model; rare variant**

Nonsyndromic cleft lip with or without cleft palate (NSCL/P) and nonsyndromic cleft palate only (NSCPO) are two complex disorders within the nonsyndromic orofacial cleft (NSOFC) spectrum [Gorlin et al., 2001]. While the genetic etiology of NSCPO is largely unclear, genetic *loci* have been systematically implicated in NSCL/P, such as common low-risk 8q24, 10q25, and *IRF6* variants [Rahimov et al., 2008; Birnbaum et al., 2009; Mangold et al., 2010, Brito et al., 2012aa, 2012b]. However, given the high heritability attributed to NSCL/P [Hu et al., 1982; Calzolari et al., 1988; Brito et al., 2011], searching for alternative genetic variants or mechanisms is necessary to bridge the missing heritability gap of these malformations.

Rare germline variants in the gene encoding the adhesion molecule epithelial cadherin, *CDH1* (MIM# 192090), have long been associated with diffuse gastric cancer and lobular breast cancer [van Roy and Berx, 2008]. Most recently, C*DH1* mutations have been reported in OFC patients in association with gastric cancer [Frebourg et al., 2006; Kluijt, et al. 2012; Benusiglio et al., 2013] or not [Vogelaar et al., 2013; Bureau et al., 2014]. These findings raise the questions as to what the proportion of NSOFC cases underlain by *CDH1* variants and their attributed penetrance is, and which types of mutations or mechanisms lead to OFC, cancer, or both phenotypes.

Here, we performed a variant screening for *CDH1* (NM_004360.3) coding region in 221 NSOFC probands (affected by NSCL/P [$n = 189$] or NSCPO [$n = 32$], either from nonfamilial [$n = 138$] or familial cases [$n = 83$]; Supp. Table S1). Sequencing was performed by using next-generation sequencing (NGS, exome or targeted gene sequencing) and Sanger sequencing (SS), and applied for 65 and 156 probands, respectively. Additional NGS or SS was performed for extra members of familial cases, when available. When exome sequencing was performed in affected members of the same family, we filtered out variants with minor allele frequency greater than 1% in public databases (1000 Genomes Project, and NHLBI ESP exomes) and in our in-house database of 609 Brazilian control exomes (Supp. Methods). Among the 221 probands, we identified a total of 47 variants, of which 12 were absent in our controls (two missense, one nonsense, and nine noncoding or synonymous variants; Supp. Table S2). Variants were submitted to the LOVD database (at http://www.lovd.nl/CDH1).

The novel missense variant c.760G>A (p.Asp254Asn, exon 6) was the most likely causative variant among the main candidates detected by exome analysis (mean coverage of 60×; average of 25,140 variants called for each individual; Supp. Table S3) in families F3788

Additional Supporting Information may be found in the online version of this article.

*Correspondence to: Maria Rita dos Santos e Passos-Bueno, Rua do Matão 277, sala 200, Cidade Universitária, São Paulo, SP, 05508-090, Brasil. Tel.: 5511 3091-7740, E-mail: passos@ib.usp.br

Contract grant sponsor(s): Fundação de Amparo à Pesquisa do Estado de São Paulo (FAPESP; CEPID Project 2013/08028-1); Conselho Nacional de Desenvolvimento Científico e Tecnológico (CNPq; 401952/2010-0); Fundos FEDER através do Programa Operacional Factores de Competitividade (COMPETE); Portuguese Foundation for Science and Technology (FCT; PTDC/SAU-ONC/110294/2009, PTDC/BIM-ONC/0171/2012, PEst-OE/EEI/LA0009/2013, and JF post-doctoral grant SFRH/BPD/87705/2012).

and F617 (four affected individuals sequenced in each family; Supp. Fig. S1a and b). Both families segregate NSCL/P, and haplotype analysis of the exome data did not support a close relationship between these families (data not shown). SS of additional two affected and eight unaffected members from these two families supported segregation in accordance with an autosomal dominant model with incomplete penetrance estimated at 53%. Assuming this penetrance, a Lod score of 4.8 was obtained at recombination fraction (θ) 0, under an allele frequency of 0.0001. The other novel missense variant, c.2351G>A (p.Arg784His, exon 15), was found in the proband of family F1387 through SS. Segregation with NSCL/P was evidenced by its presence in three affected relatives (Supp. Fig. S1c), and penetrance was estimated at 62%. Further, the loss-of-function variant c.1023T>G (exon 8), predicted to create a stop codon at position 341 of *CDH1* (p.Tyr341*), was found in the proband of family F7618 (Supp. Fig. S1d) through SS. Segregation with NSCL/P was suggested by its presence in an affected first cousin once removed. Although this represents the first association between this variant and NSCL/P, an association with hereditary diffuse gastric cancer (HDGC) has been previously observed [Guilford et al., 2010]. Penetrance was estimated at 31% in this family. Considering the four pedigrees, an overall 47% penetrance of NSCL/P was estimated, with a maximum Lod score of 5.86 at $\theta = 0$ (individual Lod scores: F3788: 2.3; F617: 2.5; F1387: 0.9; F7618: 0.2).

Among the remaining nine noncoding or synonymous novel variants, only two variants were significantly scored by in silico tools for pathogenicity prediction (Supp. Table S4). Variant c.387+5G>A, which possibly decreases exon 3 splice donor site recognition, was found in a NSCL/P proband from a nonfamilial case (parental DNA unavailable for testing whether it is a de novo variant). We considered this variant as possibly pathogenic, although further functional studies are necessary. Variant c.2514C>T (exon 16), present in two unrelated probands (one isolated and one familial case), was discarded as pathogenic as it did not segregate with NSCL/P in the familial case.

E-cadherin consists of three major domains: a short cytoplasmic, a single transmembrane, and a large extracellular domain, with five repetitive subdomains [Paredes et al., 2012]. The p.Asp254Asn substitution is located at a calcium-binding site comprised by the amino acid sequence Asp–Gln–Asn–Asp, at position 254–257 of CDH1 [Tepass et al., 2000]. This site, in turn, is located in the outmost extracellular subdomain, which plays a major role in the molecular adhesive properties between cadherin trans-dimers [Shapiro et al., 1995]. Calcium binding in the extracellular subdomains is necessary for the cis-dimerization of E-cadherin, and for conferring rigidity to the extracellular domain [Nagar et al., 1996; Pertz et al., 1999]. Importantly, an amino acid substitution in a nearby calcium-binding site has been reported to completely suppress the cellular adhesive properties of E-cadherin in vitro [Ozawa et al., 1990]. The p.Arg784His substitution is located in the cytoplasmic domain, which is important for the assembly of catenins and for promoting cellular signaling [Nelson and Nusse, 2004]. Analyses with in silico tools indicated that these two missense variants are located in highly conserved regions of E-cadherin and probably impair protein function (Supp. Table S4). To determine their pathogenic potential in vitro, we transiently transfected Chinese Hamster Ovary (ATCC number: CCL-61) cells, which are negative for E-cadherin expression, with vectors encoding the wild-type (WT) E-cadherin and variants p.Asp254Asn and p.Arg784His (Supp. Methods). As revealed by Western blot and immunocytochemistry analysis, Asp254Asn cells showed decreased total E-cadherin protein expression ($P = 0.00053$; Fig. 1A), as well as reduced amount of E-cadherin located in the plasma membrane (Fig. 1B), when compared with cells expressing the WT protein. Furthermore, mutant cells were unable to form cellular aggregates and exhibited a scattered phenotype, contrary to the WT cells, thus clearly indicating impaired adhesive function (Fig. 1C). Even though no structural impact was predicted in the mutated CDH1 protein (performed with FoldX, http://foldx.crg.es/: $\Delta\Delta G = -0.81$ kcal/mol), our in vitro assays suggest that p.Asp254Asn may lead to premature degradation, as shown for other cancer-related *CDH1* pathogenic variants [Simoes-Correia et al., 2008, 2012; Figueiredo et al., 2013]. The functional effect of this variant could also be related to disturbances in calcium ion binding, given its location. Arg784His cells, in turn, showed no observable difference from WT cells in total E-cadherin amount, its location in the plasma membrane, and its adhesive behavior (Fig. 1A–C). However, this result should not be sufficient to rule out the pathogenicity of this variant, since this in vitro assay may not be able to detect other types of functional effects, such as changes in interactions with other proteins, altering subsequent signaling pathways.

Families F3788 (p.Asp254Asn) and F1387 (p.Arg784His), the only two we were able to reascertain for cancer family history, include mutation carriers aged up to 70 years without cancer. This observation suggests that, under certain circumstances, *CDH1* variants might cause NSCL/P alone. The invasive potential of Asp254Asn and Arg784His cells, investigated by an in vitro Matrigel matrix invasion assay, was similar to that of WT cells (Fig. 1D). Thus, it is possible that some E-cadherin mutations increase the risk of NSCL/P alone, while others increase risk of gastric cancer (mutations associated with higher invasiveness). However, it is of note that the current landscape of *CDH1* mutations associated with gastric cancer and CL/P does not suggest any preferential distribution of mutations along the E-cadherin molecule (Fig. 2).

The overall prevalence of rare, possibly pathogenic *CDH1* variants here reported was 2% (5 out of 221 NSOFC probands). To date, the *CDH1* mutational repertoire in the literature associated with OFC includes 10 different mutations. Six of these mutations have been reported in families also segregating gastric cancer (four affecting mRNA splicing, one nonsense, and one frameshift deletion) [Frebourg et al., 2006; Kluijt et al., 2012; Benusiglio et al., 2013] and four were found in individuals with uncertain history of gastric cancer (one nonsense [Bureau et al., 2014] and three missense in a European cohort [Vogelaar et al., 2013]). Revisiting the list of variants described in the European cohort, we observed that the missense variant c.88C>A, which was reported in two patients from that study, was also found in two of our Brazilian controls; after removing this variant, the prevalence of possibly pathogenic *CDH1* mutations in the European cohort becomes 2%, instead of the previously reported 5% and now similar to our estimate. Furthermore, considering that two of the possibly pathogenic mutations here reported (p.Asp254Asn and p.Tyr341*) and most of the 10 above-mentioned mutations are predicted to cause *CDH1* loss-of-function, haploinsufficiency in critical stages of embryonic development seems to be the most likely mechanism by which rare variants in *CDH1* lead to OFC.

To investigate whether the group of 221 NSOFC probands presents a higher burden of *CDH1* rare variants compared to that of 609 Brazilian controls, we performed a gene-based sequence kernel association test (SKAT) [Wu et al., 2011]. A complementary two-tailed Fisher's exact test was performed to compare the proportion of individuals carrying at least one rare *CDH1* variant between probands and controls. Only variants with minor allele frequency <1% and with nonneutral prediction in at least one in silico tool were selected for these tests. To avoid methodological bias in the tests, we only included variants from regions that were

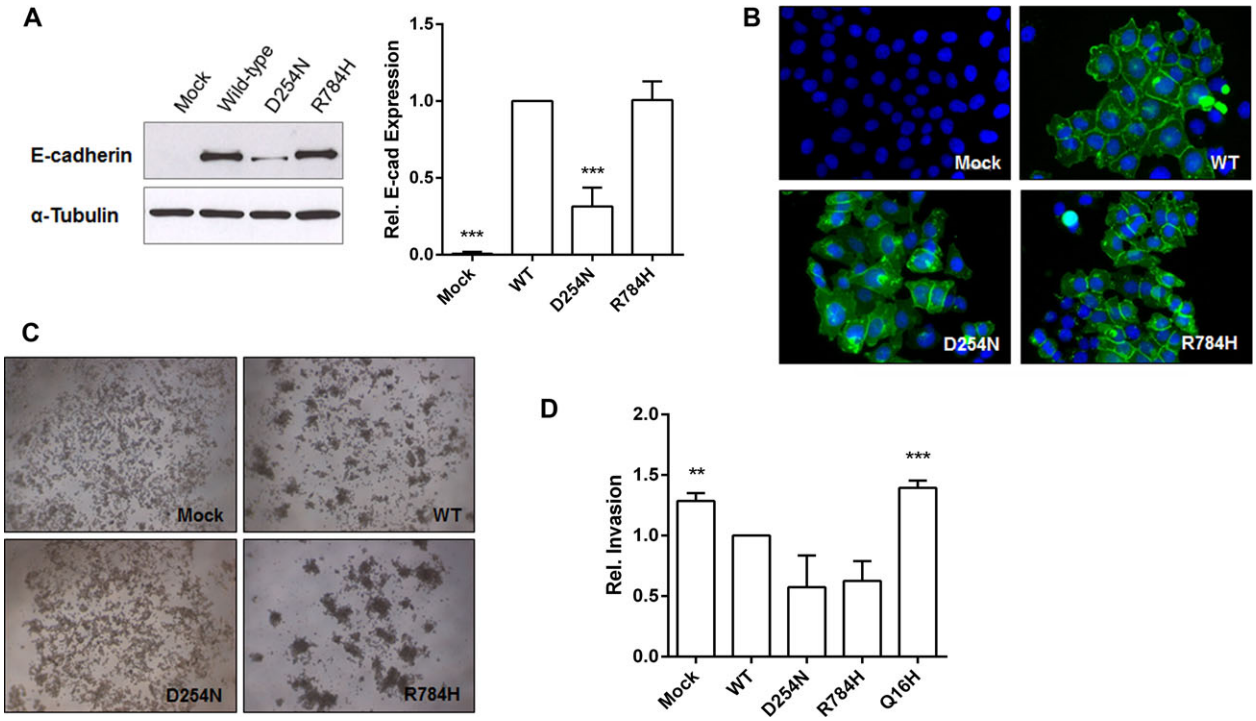

Figure 1. In vitro functional characterization of *CDH1* missense variants p.Asp254Asn (D254N) and p.Arg784His (R784H). **A:** Protein expression levels of Chinese Hamster Ovary cells transfected with the WT E-cadherin, the variants D254N and R784H, and the empty vector (Mock). α-Tubulin was used as a loading control. Band intensity was quantified and normalized against WT E-cadherin-expressing cells. The graph shows the average $\pm$ SE of E-cadherin protein level in five independent experiments. **B:** Immunocytochemistry showing E-cadherin subcellular localization (green staining). Nuclei counterstained with DAPI (blue). Scale bar represents 100 μm. **C:** Cell–cell adhesive properties assessed by slow aggregation assays. **D:** Invasive ability of cells expressing WT or the D254N and R784H variants. The graph shows the number of invasive cells $\pm$ SE of five independent experiments. Cells expressing a known invasive mutation associated with gastric cancer (Q16H), used as a positive control, showed higher invasive potential than the studied mutations.

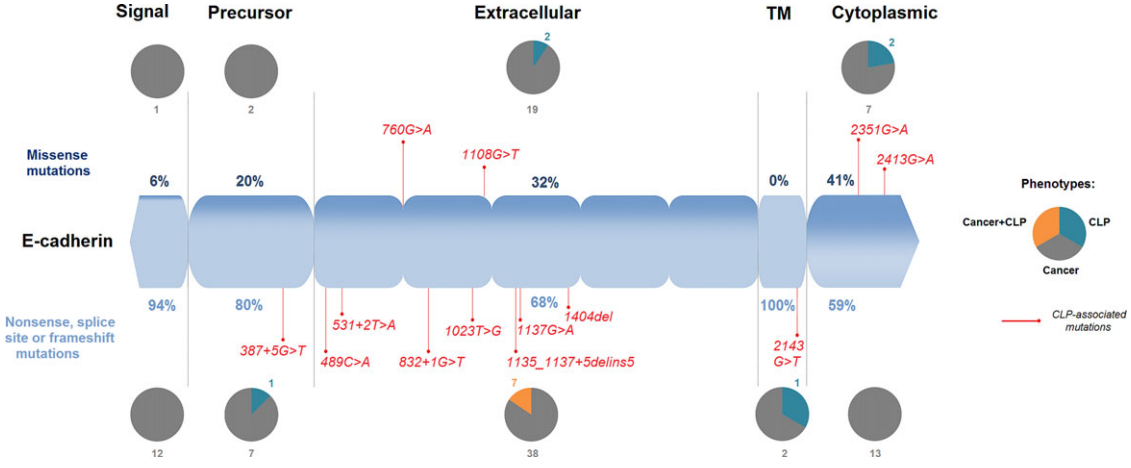

Figure 2. Scheme of CDH1 protein showing the distribution of *CDH1* germline mutations (missense $\times$ nonsense/splice site/frameshift) associated with gastric cancer [Corso et al., 2012], cleft lip/palate, and both phenotypes. Circles depict the proportion of mutations associated with each phenotype along the protein domains (signal, precursor, extracellular, transmembrane [TM], and cytoplasmic).

covered by both SS and NGS (with minimum coverage of 25×; Supp. Table S5). No significant differences in variant enrichment were detected by SKAT when comparing the 221 NSOFC probands with our 609 control exomes (P = 0.25). Similarly, no significant difference was detected in the number of individuals carrying these variants (two-tailed Fisher's exact test P = 0.85; patients: 9/221 [4%]; controls: 28/609 [5%]). Most of the probably pathogenic variants here reported (p.Asp254Asn, p.Tyr341*, and p.Arg784His) were found in familial cases with at least two affected members aside from the probands (4 out of 26 families matching the same condition, or 15.4%). Considering only probands from families with at least two additional affected individuals, significant differences were detected by SKAT (P = 0.002) and by two-tailed Fisher's exact test (P = 0.002; patients: 6/26 [23%]; controls: 28/609 [5%]). These findings

suggest that the most noteworthy *CDH1* etiological contribution to NSOFC arises from the fraction of NSCL/P cases involving moderate penetrance, which is best represented by familial cases. Since the previously suggested association between common variants and NSCL/P [Letra et al., 2009; Hozyasz et al., 2014] has not been supported by a large meta-analysis with GWAS data [Ludwig et al., 2012], rare variants seem to be the major contribution of *CDH1* to NSCL/P etiology.

Given the lack of correlation between type/location of *CDH1* rare pathogenic variants and NSCL/P or HDGC (Fig. 2), we speculate that a common underlying molecular mechanism could explain both phenotypes. Penetrance of *CDH1* germline mutations implicated in HDGC depends on a second hit, which frequently occurs via promoter hypermethylation of the nonmutated allele, possibly triggered by environmental factors [Oliveira et al., 2009; Zeng et al., 2015]. In this regard, a lifetime exposure to such factors would be in agreement with the higher penetrance in HDGC (80%) [Pharoah et al., 2001], as compared to NSCL/P (47%). Germline, pathogenic variants in *CDH1* could determine the resultant phenotype (NSCL/P or gastric cancer) under the influence of the following factors: time (early development or later in life), tissue (craniofacial or gastric structures), and exposure to environmental factors. In addition, given the prevalence of *CDH1* pathogenic variants found in this study, we believe that the NSCL/P-associated *CDH1* mutations are currently underrepresented, and future research should focus on their identification.

In summary, our results indicate a consistent role of rare, loss-of-function, moderately penetrant *CDH1* variants in NSCL/P etiology. To better comprehend the mechanisms linking *CDH1* to NSCL/P, as well as the risk of gastric cancer among NSCL/P individuals with mutations in *CDH1*, further studies are needed. Finally, *CDH1* testing in NSCL/P familial cases should be discussed for genetic counseling purposes.

Acknowledgments

We thank the Operation Smile Brazil team and Dr. Daniela Bueno (Hospital Menino Jesus) for the productive collaboration, and Suzana Ezquina, Vitor Aguiar, Vanessa Simões, Dr. Paulo A. Otto, and Dr. Rui M. Ferreira for helpful discussions.

Disclosure statement

The authors declare no conflict of interest.

References

Benusiglio PR, Caron O, Consolino E, Duvillard P, Coulet F, Blayau M, Malka D. 2013. Cleft lip, cleft palate, hereditary diffuse gastric cancer and germline mutations in CDH1. Int J Cancer 132:2470.

Birnbaum S, Ludwig KU, Reutter H, Herms S, Steffens M, Rubini M, Baluardo C, Ferrian M, Almeida de Assis N, Alblas MA, Barth S, Freudenberg J, et al. 2009. Key susceptibility locus for nonsyndromic cleft lip with or without cleft palate on chromosome 8q24. Nat Genet 41:473–477.

Brito LA, Bassi CF, Masotti C, Malcher C, Rocha KM, Schlesinger D, Bueno DF, Cruz LA, Barbara LK, Bertola DR, Meyer D, Franco D, et al. 2012a. IRF6 is a risk factor for nonsyndromic cleft lip in the Brazilian population. Am J Med Genet A 158:2170–2175.

Brito LA, Cruz LA, Rocha KM, Barbara LK, Silva CB, Bueno DF, Aguena M, Bertola DR, Franco D, Costa AM, Alonso N, Otto PA, et al. 2011. Genetic contribution for non-syndromic cleft lip with or without cleft palate (NS CL/P) in different regions of Brazil and implications for association studies. Am J Med Genet A 155A:1581–1587.

Brito LA, Paranaiba LM, Bassi CF, Masotti C, Malcher C, Schlesinger D, Rocha KM, Cruz LA, Bárbara LK, Alonso N, Franco D, Bagordakis E, et al. 2012b. Region 8q24 is a susceptibility locus for nonsyndromic oral clefting in Brazil. Birth Defects Res A Clin Mol Teratol 94:464–468.

Bureau A, Parker MM, Ruczinski I, Taub MA, Marazita ML, Murray JC, Mangold E, Noethen MM, Ludwig KU, Hetmanski JB, Bailey-Wilson JE, Cropp CD, et al. 2014. Whole exome sequencing of distant relatives in multiplex families implicates rare variants in candidate genes for oral clefts. Genetics 197: 1039–1044.

Calzolari E, Milan M, Cavazzuti GB, Cocchi G, Gandini E, Magnani C, Moretti M, Garani GP, Salvioli GP, Volpato S. 1988. Epidemiological and genetic study of 200 cases of oral cleft in the Emilia Romagna region of northern Italy. Teratology 38:559–564.

Corso G, Marrelli D, Pascale V, Vindigni C, Roviello F. 2012. Frequency of CDH1 germline mutations in gastric carcinoma coming from high- and low-risk areas: metanalysis and systematic review of the literature. BMC Cancer 12:8.

Figueiredo J, Soderberg O, Simoes-Correia J, Grannas K, Suriano G, Seruca R. 2013. The importance of E-cadherin binding partners to evaluate the pathogenicity of E-cadherin missense mutations associated to HDGC. Eur J Hum Genet 21:301–309.

Fitzgerald RC, Hardwick R, Huntsman D, Carneiro F, Guilford P, Blair V, Chung DC, Norton J, Ragunath K, VanKrieken JH, Dwerryhouse S, Caldas C. 2010. Hereditary diffuse gastric cancer: updated consensus guidelines for clinical management and directions for future research. J Med Genet 47:436–444.

Frebourg T, Oliveira C, Hochain P, Karam R, Manouvrier S, Graziadio C, Vekemans M, Hartmann A, Baert-Desurmont S, Alexandre C, Lejeune Dumoulin S, Marroni C, et al. 2006. Cleft lip/palate and CDH1/E-cadherin mutations in families with hereditary diffuse gastric cancer. J Med Genet 43:138–142.

Gorlin RJ, Cohen MMJ, Hennekam RCM. 2001. Syndromes of the head and neck. New York: Oxford University Press. p 1344.

Guilford P, Humar B, Blair V. 2010. Hereditary diffuse gastric cancer: translation of *CDH1* germline mutations into clinical practice. Gastric Cancer 13: 1–10.

Hozyasz KK, Mostowska A, Wojcicki P, Lasota A, Offert B, Balcerek A, Dunin-Wilczynska I, Jagodzinski PP. 2014. Nucleotide variants of the cancer predisposing gene CDH1 and the risk of non-syndromic cleft lip with or without cleft palate. Fam Cancer 13:415–421.

Hu DN, Li JH, Chen HY, Chang HS, Wu BX, Lu ZK, Wang DZ, Liu XG. 1982. Genetics of cleft lip and cleft palate in China. Am J Hum Genet 34:999–1002.

Kluijt I, Siemerink EJ, Ausems MG, van Os TA, de Jong D, Simoes-Correia J, van Krieken JH, Ligtenberg MJ, Figueiredo J, van Riel E, Sijmons RH, Plukker JT, et al. 2012. CDH1-related hereditary diffuse gastric cancer syndrome: clinical variations and implications for counseling. Int J Cancer 131:367–376.

Letra A, Menezes R, Granjeiro JM, Vieira AR. 2009. AXIN2 and CDH1 polymorphisms, tooth agenesis, and oral clefts. Birth Defects Res A Clin Mol Teratol 85: 169–173.

Ludwig KU, Mangold E, Herms S, Nowak S, Reutter H, Paul A, Becker J, Herberz R, AlChawa T, Nasser E, Böhmer AC, Mattheisen M, et al. 2012. Genome-wide meta-analyses of nonsyndromic cleft lip with or without cleft palate identify six new risk loci. Nat Genet 44:968–971.

Mangold E, Ludwig KU, Birnbaum S, Baluardo C, Ferrian M, Herms S, Reutter H, de Assis NA, Chawa TA, Mattheisen M, Steffens M, Barth S, et al. 2010. Genome-wide association study identifies two susceptibility loci for nonsyndromic cleft lip with or without cleft palate. Nat Genet 42:24–26.

Nagar B, Overduin M, Ikura M, Rini JM. 1996. Structural basis of calcium-induced E-cadherin rigidification and dimerization. Nature 380:360–364.

Nelson WJ, Nusse R. 2004. Convergence of Wnt, beta-catenin, and cadherin pathways. Science 303:1483–1487.

Oliveira C, Sousa S, Pinheiro H, Karam R, Bordeira-Carriço R, Senz J, Kaurah P, Carvalho J, Pereira R, Gusmão L, Wen X, Cipriano MA et al. 2009. Quantification of epigenetic and genetic 2nd hits in CDH1 during hereditary diffuse gastric cancer syndrome progreesion. Gastroenterology 136:2137–2148.

Ozawa M, Engel J, Kemler R. 1990. Single amino acid substitutions in one $Ca2^+$ binding site of uvomorulin abolish the adhesive function. Cell 63:1033–1038.

Paredes J, Figueiredo J, Albergaria A, Oliveira P, Carvalho J, Ribeiro AS, Caldeira J, Costa AM, Simoes-Correia J, Oliveira MJ, Pinheiro H, Pinho SS, et al. 2012. Epithelial E- and P-cadherins: role and clinical significance in cancer. Biochim Biophys Acta 1826:297–311.

Pertz O, Bozic D, Koch AW, Fauser C, Brancaccio A, Engel J. 1999. A new crystal structure, $Ca2^+$ dependence and mutational analysis reveal molecular details of E-cadherin homoassociation. EMBO J 18:1738–1747.

Pharoah PD, Guilford P, Caldas C. 2001. Incidence of gastric cancer in CDH1 (E-cadherin) mutation carriers from hereditary diffuse gastric cancer families. Gastroenterology 121:1348–1353.

Rahimov F, Marazita ML, Visel A, Cooper ME, Hitchler MJ, Rubini M, Domann FE, Govil M, Christensen K, Bille C, Melbye M, Jugessur A, et al. 2008. Disruption of an AP-2alpha binding site in an IRF6 enhancer is associated with cleft lip. Nat Genet 40:1341–1347.

Shapiro L, Fannon AM, Kwong PD, Thompson A, Lehmann MS, Grubel G, Legrand JF, Als-Nielsen J, Colman DR, Hendrickson WA. 1995. Structural basis of cell-cell adhesion by cadherins. Nature 374:327–337.

Simoes-Correia J, Figueiredo J, Lopes R, Stricher F, Oliveira C, Serrano L, Seruca R. 2012. E-cadherin destabilization accounts for the pathogenicity of missense mutations in hereditary diffuse gastric cancer. PLoS One 7:e33783.

Simoes-Correia J, Figueiredo J, Oliveira C, van Hengel J, Seruca R, van Roy F, Suriano G. 2008. Endoplasmic reticulum quality control: a new mechanism of E-cadherin regulation and its implication in cancer. Hum Mol Genet 17:3566–3576.

Tepass U, Truong K, Godt D, Ikura M, Peifer M. 2000. Cadherins in embryonic and neural morphogenesis. Nat Rev Mol Cell Biol 1:91–100.

van Roy F, Berx G. 2008. The cell-cell adhesion molecule E-cadherin. Cell Mol Life Sci 65:3756–3788.

Vogelaar IP, Figueiredo J, van Rooij IA, Simoes-Correia J, van der Post RS, Melo S, Seruca R, Carels CE, Ligtenberg MJ, Hoogerbrugge N. 2013. Identification of germline mutations in the cancer predisposing gene CDH1 in patients with orofacial clefts. Hum Mol Genet 22:919–926.

Wu MC, Lee S, Cai T, Li Y, Boehnke M, Lin X. 2011. Rare-variant association testing for sequencing data with the sequence kernel association test. Am J Hum Genet 89:82–93.

Yamaoka Y, Kato M, Asaka M. 2008. Geographic differences in gastric cancer incidence can be explained by differences between Helicobacter pylori strains. Intern Med 47:1077–1083.

Zeng W, Zhu J, Shan L, Han Z, Aerxiding P, Quhai A, Zeng F, Wang Z, Li H. 2015. The clinicopathological significance of CDH1 in gastric cancer: a meta-analysis and systematic review. Drug Des Devel Ther 13:2149–2157.

RESEARCH ARTICLE

AMERICAN JOURNAL OF medical genetics PART A

Craniosynostosis In 10q26 Deletion Patients: A Consequence of Brain Underdevelopment or Altered Suture Biology?

**Ágatha Cristhina Faria,[1,2] Eliete Rabbi-Bortolini,[3] Maria R. G. O. Rebouças,[4] Andréia L. A. de S. Thiago Pereira,[5] Milena G. Tonini Frasson,[5] Rodrigo Atique,[6] Naila Cristina V. Lourenço,[6] Carla Rosenberg,[6] Gerson S. Kobayashi,[6] Maria Rita Passos-Bueno,[6] and Flávia Imbroisi Valle Errera[1,2]*

[1]Programa de Graduação em Biotecnologia, Centro de Ciências da Saúde, Universidade Federal do Espírito Santo (UFES), Vitória, Espírito Santo, Brasil

[2]Laboratório de Genética Humana e Molecular, Centro de Pesquisa ICALP, Escola Superior de Ciências da Santa Casa de Misericórdia (EMESCAM), Vitória, Espírito Santo, Brasil

[3]Laboratório de Genética e Biologia Molecular, Associação Educacional de Vitória, Vitória, Espírito Santo, Brasil

[4]Divisão de Genética Clínica, Hospital Estadual Infantil Nossa Senhora da Glória (HEINSG), Vitória, Espírito Santo, Brasil

[5]Unidade de Neonatologia, Hospital Santa Casa de Misericórdia, Vitória, Espírito Santo, Brasil

[6]Centro de Pesquisas Sobre o Genoma Humano e Células Tronco, Departamento de Genética e Biologia Evolutiva, Instituto De Biociências, Universidade de São Paulo (USP), São Paulo, São Paulo, Brasil

Manuscript Received: 24 November 2014; Manuscript Accepted: 16 October 2015

Approximately a hundred patients with terminal 10q deletions have been described. They present with a wide range of clinical features always accompanied by delayed development, intellectual disability and craniofacial dysmorphisms. Here, we report a girl and a boy with craniosynostosis, developmental delay and other congenital anomalies. Karyotyping and molecular analysis including Multiplex Ligation dependent probe amplification (MLPA) and Array Comparative Genomic Hybridization (aCGH) were performed in both patients. We detected a 13.1 Mb pure deletion at 10q26.12-q26.3 in the girl and a 10.9 Mb pure deletion at 10q26.13-q26.3 in the boy, both encompassing about 100 genes. The clinical and molecular findings in these patients reinforce the importance of the *DOCK1* smallest region of overlap I (SRO I), previously suggested to explain the clinical signs, and together with a review of the literature suggest a second 3.5 Mb region important for the phenotype (SRO II). Genotype-phenotype correlations and literature data suggest that the craniosynostosis is not directly related to dysregulated signaling in suture development, but may be secondary to alterations in brain development instead. Further, genes at 10q26 may be involved in the molecular crosstalk between brain and cranial vault.

Key words: craniofacial dysmorphisms; synostosis; brain development; array CGH; *HMX2*; *HMX3*; *EBF3*; 10q26

How to Cite this Article:
Faria ÁC, Rabbi-Bortolini E, Rebouças MRGO, Pereira ALAdST, Frasson MGT, Atique R, Lourenço NCV, Rosenberg C, Kobayashi GS, Passos-Bueno MR, Errera FIV. 2015. Craniosynostosis in 10q26 deletion patients: A consequence of brain underdevelopment or altered suture biology?.
Am J Med Genet Part A 9999A:1–7.

INTRODUCTION

To date, nearly 100 patients with terminal 10q deletions have been described. They present with a wide range of clinical

Grant sponsor: Casadinho/PROCAD CNPq 06/2011; Grant number: 552672/2011-4; Grant sponsor: Research Program for the Unified Health System (DECIT/CNPq/FAPES); Grant number: PPSUS/50809717/2010; Grant sponsor: Espirito Santo Research Foundation (FAPES); Grant sponsor: São Paulo Research Foundation (FAPESP/CEPID).
*Correspondence to:
Flávia Imbroisi Valle Errera, Ph.D., Laboratório de Genética Humana e Molecular, Centro de Pesquisa ICALP, Escola Superior de Ciências da Santa Casa de Misericórdia (EMESCAM), Avenida Nossa Senhora da Penha, 2190, Santa Luiza, Vitória, Espírito Santo, Brasil.
E-mail: Flavia.errera@gmail.com
Article first published online in Wiley Online Library (wileyonlinelibrary.com): 00 Month 2015
DOI 10.1002/ajmg.a.37448

features, but invariably accompanied by delayed development, intellectual disability and craniofacial dysmorphisms [Courtens et al., 2006]. Besides the common clinical findings, a considerable phenotypic heterogeneity has been observed even in patients belonging to the same family and sharing the same deletion. In view of the consistent clinical findings usually observed in these patients, it has been proposed that the 10q26 microdeletion syndrome is a recognizable entity (OMIM #609625) [Wulfsberg et al., 1989; Schrander-Stumpel et al., 1991]. However, it is still unclear if there is a correlation between deletion size and clinical features. These difficulties can be in part due to heterogeneity and complexity of the chromosomal alterations, as some patients may harbor duplication or loss of other chromosomal segments (copy number variations or CNVs) in addition to the 10q deletion. With the availability of high resolution molecular techniques it is now possible to clinically compare patients in which the 10q deletion is the only structural alteration, and who are herein referred as "patients with pure 10q deletions."

Recently, based on high resolution genomic technology in patients with pure 10q deletions, some authors have suggested haploinsufficiency of a smallest region of overlap (SRO) encompassing *DOCK1* to be critical for phenotype development [Yatsenko et al., 2009]. Few studies testing this hypothesis have been published and whether this is the only important region for the phenotype remains unclear. Accordingly, some authors have reported patients with altered suture closure or head shape and neurodevelopmental alterations with deletions not encompassing the *DOCK*1 region [Miller et al., 2009; Plaisancié et al., 2014; Choucair et al., 2015; Vera-Carbonell et al., 2015]. Thus, reports of additional patients with pure 10q26 deletions is important to clarify the correlation between the genes within this region and the craniofacial phenotype.

Here we describe the clinical and molecular findings in two patients with pure deletions of 10q26 who had craniosynostosis, other congenital anomalies, and developmental delay. We also review the literature in an attempt to establish a genotype-phenotype correlation.

CLINICAL REPORT

Patient 1

The female patient was born at 39.2 weeks of gestation to a 39-year-old mother and 41-year-old father. There was no family history of intellectual disability, developmental delay or congenital malformations, although her mother reported that she had a cardiac arrhythmia. Pregnancy and delivery were uneventful. The patient had Apgar scores of 8 at 5 and 10 min after birth. Birth weight was 3.405 g (<2nd centile), length 48 cm (<3rd centile) and occipitofrontal circumference (OFC) was 36.5 cm (>97th centile). Clinical examination at birth identified scaphocephaly, bitemporal narrowing, ocular proptosis, facial asymmetry, microtia, anteriorized anus, and diastasis of *rectus abdominis*. A 3D computed tomography (CT) scan showed fusion of the sagittal suture, which explained the scaphocephaly (Fig. 1A).

At 1 month of age, hypotonia, strabismus, thin upper lip, small nose, retrognathia, short neck, clinodactyly of the 4th and 5th fingers, single palmar crease and hypoplastic nails were noted. Her weight, length and OFC were 3.350 g (3rd centile), 48 cm (<3rd centile), and 36 cm (32nd centile), respectively. Surgery was performed to correct the scaphocephaly at 5 months of age. She sat without support at 19 months of age. She was reevaluated at the age of 2 years and 3 months (Fig. 1B); at the time her weight was 8 kg (<3rd centile), length was 74 cm (<3rd centile) and OFC was 43.7 cm (<3rd centile). She had a significant language delay, being only able to communicate by sounds. She had spastic movements and still did not walk independently.

Audiometry revealed bilateral hearing loss. Patent ductus arteriosus (PDA) and ventricular septal defect (VSD) were noted on echocardiography. Cranial magnetic resonance imaging (MRI) did not show any evidence of major structural abnormalities of the brain. Complementary laboratorial investigations (temporal bone

FIG. 1. (A) Cranial 3D CT scan of the patient 1 performed at the age of 7 days: note the closure of the sagittal suture. (B) Patient 1 at the age of 2 years and 3 months. Note low-set, malformed ears (microtia), retrognathia, strabismus, long philtrum and thin upper lip. (C) Cranial 3D CT scan of patient 2, note closure of the left lambdoid suture. [Color figure can be seen in the online version of this article, available at http://wileyonlinelibrary.com/journal/ajmga]

CT, abdominal and renal ultrasounds, transfontanelar ultrasound, ophthalmologic examination and X-ray of the dorsal-lumbar spine) were normal. There were no seizures. She was sociable and friendly.

Patient 2

The male patient was born at 39 weeks of gestation to a 29-year-old mother and 39-year-old father, who were both healthy and non-consanguineous. There is no family history of intellectual disability, developmental delay or congenital malformations. Delivery via Cesarean section delivery was uneventful. The patient had Apgar scores of 8 and 9 at 5 and 10 min, respectively. Birth weight was 2.790 g (<2nd centile), length 45 cm (<3rd centile), and OFC was 32 cm (<3rd centile). Clinical examination at birth identified facial asymmetry and apparently low-set ears. He had hypoglycemia at birth which was corrected with parenteral nutrition for 4 days. Breastfeeding was unsuccessful and he received milk by orogastric feeding until the 4th day of life. Craniosynostosis was diagnosed soon after birth, and a 3D CT scan showed fusion of the left lambdoid suture. He was diagnosed with left posterior plagiocephaly.

Surgery was performed to correct the plagiocephaly at 6 months of age. He sat without support at 2 years of age. At the age of 2 years and 3 months, strabismus, prominent nose with broad nasal bridge, long philtrum, thin upper lip, and prominent and low-set ears, were observed. Central hypotonia was also noted. Ophthalmologic examination identified myopia. PDA was noted on the echocardiography. He was still unable to walk and speak at that age.

METHODS

Karyotyping

Chromosomal analysis of peripheral blood lymphocytes was performed according to routine procedures using GTG-banding at approximately 400–550 band resolution per haploid set [Modified from Moorhead et al., 1960].

Molecular Analysis

DNA from plasma was isolated with the Gentra Puregene kit (Qiagen-Sciences, MD). DNA concentration and purity were evaluated with a NanoDrop 2000 UV-vis spectrophotometer (Thermo Scientific, Waltham, MA). Multiplex ligation-dependent probe amplification (MLPA) was performed using subtelomeric kits for all chromosomes (P036-E1, P070-B2, and P064-B2—MRC-Holland®, Amsterdam, Netherlands), according to manufacturer's instructions.

Array Genomic Comparative Hybridization (aCGH) of patient 1 was carried out with CytoSure ISCA array 4 × 180k (Oxford Gene Technology, OGT, UK) according to manufacturer's recommendations. The aCGH of patient 2 was performed with qChip Post 60k (Quantitative Genomic Medicine Laboratories, SL—qGenomics, Barcelona, Spain). Data were processed with Feature Extraction software and subsequently analyzed with the Genomic Workbench software (both from Agilent Technologies, Santa Clara, CA).

RESULTS

Patient 1

Conventional GTG cytogenetic analysis revealed a normal female karyotype (46,XX). MLPA showed a subtelomeric deletion at 10q26.2-q26.3. Cytogenetic analysis and MLPA of the parents were normal (data not shown), suggesting a de novo deletion in the proband.

Next, we performed aCGH analysis to better characterize the chromosomal alteration. We identified a deletion of approximately 13.1 Mb at 10q26.12-q26.3 (chr10:122,095,511-135,203,489, GRCh37/hg19), encompassing 115 RefSeq genes (NCBI Reference Sequence; http://www.ncbi.nlm.nih.gov/ Annotation release 105) (Fig. 2A; Supplementary Table SI). The proximal breakpoint occurred in an intergenic region upstream of *SEC23IP* and the distal breakpoint in the 6th intron of *PAOX* (UCSC genome browser; arr 10q26.12-q26.3 (122,095,511–135,203,489) x1 according to ISCN [2013] nomenclature). No other pathogenic CNV was detected, allowing us to classify this 10q deletion as pure.

Patient 2

Conventional GTG cytogenetic analysis of the patient revealed a normal male karyotype (46,XY). MLPA showed a subtelomeric deletion at 10q26.2-q26.3 (data not shown). Cytogenetic analysis and MLPA of the parents were normal (data not shown), suggesting a de novo deletion in the proband.

Subsequent aCGH analysis showed a deletion of approximately 10.9 Mb at 10q26.13-q26.3 (chr10:124,475,398–135,403,809, GRCh37/hg19), encompassing 106 RefSeq genes (NCBI Reference Sequence; http://www.ncbi.nlm.nih.gov/ Annotation release 105) (Fig. 2B; Supplementary Table SII). The proximal and distal breakpoints occurred in an intergenic region upstream of *C10ORF120* and *SPRNP1*, respectively (UCSC genome browser; arr 10q26.13-q26.3 (124,475,398–135,403,809) ×1 according to ISCN [2013] nomenclature). No other pathogenic CNV was detected, allowing us to classify this 10q deletion as pure.

DISCUSSION

Most of the clinical signs of our patients are very similar to those of the 16 other patients with pure 10q26 deletions previously characterized through high resolution molecular techniques (Table I) [Piccione et al., 2008; Miller et al., 2009; Yatsenko et al., 2009 patients 4 and 5; Iourov et al., 2014; Plaisancié et al., 2014; Vera-Carbonell et al., 2015; Choucair et al., 2015]. The striking finding in our patients and in patient 4 of Miller et al. [2009] is craniosynostosis. The main suture involved in patient 1 is the sagittal suture, with complete fusion of the anterior, central, and posterior sections (FFF pattern) [Heuzé et al., 2010], whereas the main suture involved in patient 2 is the left lambdoid suture. Miller's patient displayed synostosis of the metopic and sagittal sutures. Therefore, the penetrance of craniosynostosis among individuals with pure 10q26 deletions can be estimated at around 18.7% (3/16), and the suture involved varies.

The large deletion in both of our patients overlaps with most of the other pure 10q26 deletions previously characterized (Fig. 3).

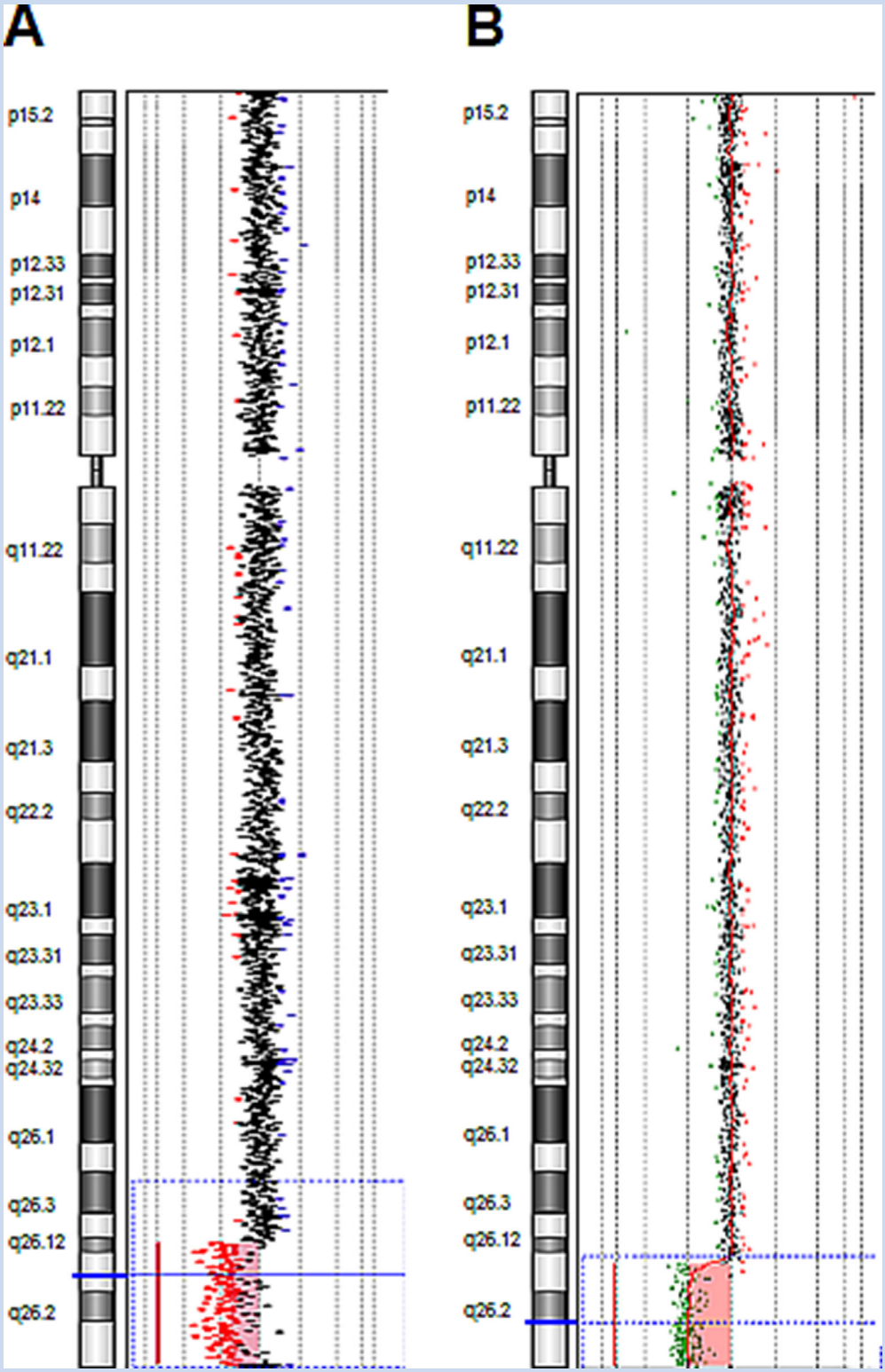

FIG. 2. (A) aCGH profile of the chromosome 10 of the patient 1. The red dots show the deleted region. (B) aCGH profile of the chromosome 10 of the patient 2. The green dots show the deleted region. [Color figure can be seen in the online version of this article, available at http://wileyonlinelibrary.com/journal/ajmga]

TABLE I. Comparison of Clinical Features of Patients With 10q26 Pure Deletions

Study	Yatsenko et al., 2009[&]		Iourov et al., 2014	Piccione et al., 2008[&]	Plaisancié et al. 2014				Miller et al., 2008				Vera-Carbonell et al., 2015			Choucair et al.,2015	Present report[&]	
Patients	Patient 4	Patient 5	1	1	Patient 1	Patient 2	Patient 3	Patient 4	Patient 1	Patient 2	Patient 3[&]	Patient 4[&]	Patient 1[&]	Patient 2	Patient 3	1[&]	Patient 1	Patient 2
Breakpoint/Deletions	10q26.12-q26.2	10q26.12-q26.2	10q26.2-q26.3	10q26.13-qter	10q26.2-q26.3	10q26.2-q26.3	10q26.2-q26.3	10q26.2-q26.3	10q26.2-qter	10q26.2-qter	10q26.12-qter	10q25.3-q26.13	q26.12-qter	q26.13-qter	q26.13-qter	q26.11-q26.13	10q26.12-q26.3	10q26.13-q26.3
Size deletion, Mb	5.8	5.8	5,8	11,4	4	7,1	7,1	7,1	6.1	6.1	12.4	7.0	13.4	9.3	9.1	4,5	13,1	10,9
Deletion interval, GRCh37/hg 19	122,888,789 - 128,830,242	122,888,789 - 128,830,242	128,190,760 - 133,998,503	123,638,405 - 135,404,523	130,426,530 - 135,399,508	128,130,622 - 135,215,584	128,130,622 - 135,215,584	128,130,622 - 135,215,584	129,437,673 - 135,434,303	129,380,861 - 135,434,303	122,970,216 - 135,434,303	118,506,755 - 125,492,105	122,014,670 - 135,404,523	126,105,636 - 135,404,523	126,193,727 - 135,352,420	119,512,117 - 124,082,152	122,095,511 - 135,203,489	124,475,398 - 135,403,809
SRO I	P	P	P	P	A	P	P	P	A	P	P	A	P	P	P	A	P	P
SRO II	A	A	P	P	P	P	P	P	P	P	P	A	P	P	P	A	P	P
Gender	F	M	M	M	F	F	F	F	F	F	M	M	F	F	F	M	F	M
Age at first examination	2 y	25 y	28 m	newborn	3 y	6 y	29 y	16 y	3 y	14 m	8 m	newborn	17 y	9 y	5 y	6 y	newborn	2,3 y
Inheritance	familial	NR	NR	de novo	de novo	familial	familial	familial	de novo	NA	NA	de novo	de novo	de novo	de novo	de novo	de novo	de novo
Clinical Features																		
Short stature (<3rd centile)	P	NR	A	A	A	P	NR	P	A	P	P	P	P	P	P	A	P	P
Long philtrum	A	A	A	P	P	P	P	P	NR	A	A	P	A	P	P	NR	P	P
Thin upper lip	P	P	A	P	P	P	P	P	NR	NR	NR	P	A	P	P	P	P	P
Craniofacial dysmorphisms	P	P	P	P	P	P	P	P	P	A	P	P	P	P	P	P	P	P
Hypertelorism	P	P	A	A	A	P	P	P	NR	A	P	A	NR	NR	NR	A	A	A
Strabismus	A	A	A	P	A	A	A	A	P	P	P	P	P	NR	A	P	P	P
Large, malformed, low-set ears	P	P	P	P	P	P	P	P	NR	NR	P	P	P	P	P	P	P	P
Genital anomalies	A	A	A	P	A	A	A	A	A	A	P	P	P	A	P	P	P	A
Urinary tract anomaly	A	A	A	A	A	A	A	A	NR	NR	P	A	P	P	A	A	A	A
Congenital heart disease	P	A	A	P	A	A	A	A	NR	NR	P	A	A	A	A	A	P	P
Limb abnormalities	P	P	P	A	P	P	P	P	P	P	P	P	P	A	P	A	P	A
Craniosynostosis	A	A	A	A	A	A	A	A	NR	NR	A	P, Sagittal and Metopic	NR	NR	NR	A	P, Sagittal	P, Lambdoid
Dysmorphic head size or shape	P	P	P	P	P	P	P	P	P	A	P	P	P	A	P	P	P	P
CNS malformations	NR	NR	NR	NR	P	A	A	A	A	NR	A	NR	NR	NR	P	A	A	
Microcephaly	P	P	NR	P	A	P	P	P	A	A	A	P	P	A	P	P	P	P
Intelectual disability	P	P	P	P	P	P	P	P	P	NA	P	P	P	P	P	P	P	P

F, female; M, male; y, years; m, months; P, feature present; A, feature absent; NR, not reported; NA, not applicable.
[&]Patients with the 1 Mb common region deleted.

The *DOCK*1 region, suggested as the SRO to explain the craniofacial, cardiac and neuropsychiatric phenotypes [Yatsenko et al., 2009] is included in the region encompassed by the deletions in the present report (Fig. 3), reinforcing the relevance of this SRO for the phenotype of 10q26 deletion patients. However, this SRO was not included in the 10q26 deletion described in four other patients with craniofacial alterations [Miller et al., 2009; Plaisancié et al., 2014; Choucair et al., 2015] (Fig. 3; Table I). These observations suggest that changes in cranial morphology and growth may also depend on haploinsufficiency of genes mapped outside of this SRO.

A reanalysis of pure 10q26 deletion patients including our probands identified a novel 3.5 Mb region shared by most individuals (chr10:130,426,530-133,998,503; GRCh37/hg19) (Fig. 3). Except for two affected patients [patient 2 in Miller et al., 2009; patient 2 in Vera-Carbonell et al., 2015], all exhibited altered cranial shape or size (Table I). For reference, we will call this second region 'SRO II' and the SRO defined by Yatsenko et al., [2009] will be termed here after 'SRO I'. SRO II contains seven RefSeq genes (*MGMT*; *EBF3*; *GLRX3*; *TCERG1L*; *PPP2R2D*; *BNIP3* and *JAKMIP3*) and two microRNAs (miRNAs) (miR4297; miR378C). Four of these genes (*MGMT*, *EBF3*, *PPP2R2D* and *BNIP3*) are involved with brain function and their haploinsufficiency might contribute to intellectual disability among 10q26 deletion patients [Chiara et al., 2012; Iourov et al., 2014; Toffolatti et al., 2014]. Two of these genes, *PPP2R2D*, which modulates TGF-β pathway; and *EBF3*, a transcription factor, are also involved with osteogenic differentiation [Chiara et al., 2012]. Little is known about the two miRNA genes within this region, but each of them has approximately 200 predicted targets [http://mirdb.org/miRDB/], including *BMP6* and PTPRE. BMP6 is involved in early osteogenesis during embryonic development [Chen et al., 2012] and *PTPRE*, which maps to at 10q26.2 but out of the SRO II region, is a phosphatase involved in the formation and differentiation of osteoblasts [Chiusaroli et al., 2004]. Therefore, 4 out of the 7 genes within SRO II are relevant for brain function and two are also involved with bone development.

Genes at SRO I and SRO II are mainly associated with brain function and cancer. It is possible that haploinsufficiency of SRO I or SRO II is important for the craniofacial and neuropsychiatric phenotype, but none of the genes located in those regions are obvious candidates for the craniosynostosis observed in our patients. Further analysis of our patients and patient 4 of Miller et al., [2009] (who also has craniosynostosis) revealed a new shared region of about 1 Mb (chr10:124,475,398–125,492,105; GRCh37/hg19) outside SRO I and SRO II, containing 16 RefSeq genes (Supplementary Table SIII). Of these, the homeobox genes *HMX2* and *HMX3* are involved in the morphogenesis of vestibular components of the inner ear [Wang et al., 2001] and in the development of the central nervous system in *Drosophila* and neural tube and hypothalamus in mice [Wang et al., 2000; Wang and Lufkin, 2005]. The function of most of the remaining genes in this 1 Mb shared interval is poorly known and are not known to be related to bone differentiation or primary craniosynostosis (Supplementary Table SIII).

Primary craniosynostosis can be the result of mutations in genes important for the maintenance of suture patency, such as dominant gain-of-function mutations in *FGFR1*, *FGFR2*, *or FGFR3*, among others [Passos-Bueno et al., 2008; Wilkie et al., 2010]. The suture fusion in these cases almost invariably involves the coronal

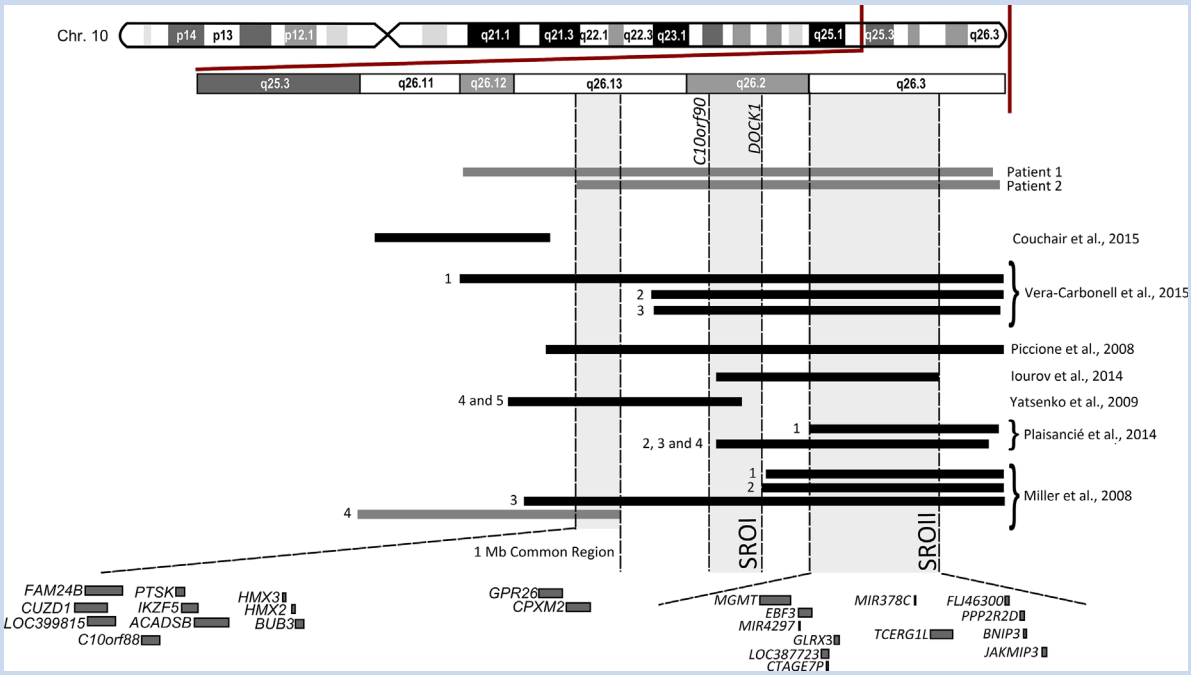

FIG. 3. Schematic physical map of the 10q terminal region (10q25.1-q26.3). The regions, genes of interest and the patients discussed in this study are represented. The grey horizontal bars represent the deleted segment in each patient with craniosynostosis. The black horizontal bars represent the deleted segment in each patient without craniosynostosis. The smallest region overlap I (SRO I), the smallest region overlap II (SRO II) and the 1 Mb common region shared by the patients with craniosynostosis are identified by gray shadows with dotted lines. [Color figure can be seen in the online version of this article, available at http://wileyonlinelibrary.com/journal/ajmga]

suture, and although altered head shape is often observed, microcephaly is not usually reported in these patients. In some circumstances, craniosynostosis can be secondary to reduced brain growth or occur post-ventricular shunting for hydrocephalus [Andersson, 1966; Kloss, 1968; Cohen, 1980]. Our two patients had severe neurodevelopmental delay. Even though brain malformation had been reported in some patients with deletion 10q26 [Chitkara et al., 2011; Piard et al., 2014; Vera-Carbonell et al., 2015], MRI of patient 1 did not reveal any brain anomalies. Nevertheless, it is possible that haploinsufficiency of genes important for neuronal function are responsible for the intellectual disability in these patients, and their craniosynostosis might be correlated with altered brain function via a common disturbance in signaling pathways. In some instances it may be difficult to classify the craniosynostosis as primary, or secondary to microcephaly. In both of our patients, craniosynostosis was present at birth. However, patient 1 had macrocephaly at birth, but subsequently demonstrated slowed growth of the brain and resultant microcephaly. In patient 2, both microcephaly and craniosynostosis were present at birth. Reports have shown that cranial growth is not necessarily correlated with the growth of the brain [Richtsmeier and Flaherty, 2013], and therefore, the synostosis in 10q26 patients might not be only a consequence of microcephaly or small brain size. Thus, we speculate that some genes in the 10q26 region could be involved both in skull and brain development, which in turn would suggest that changes in molecular signaling events induced by haploinsufficiency of 10q26 genes involved in brain development could also play a role in the induction of craniosynostosis.

In summary, the analysis in the present report together with data from the literature suggests SRO II as a second region important for the phenotype of 10q26 microdeletion syndrome. In addition, genes within the deleted region that are involved in central nervous system development may also be responsible for the craniosynostosis observed in some cases. Brain and skull functions are thought to be regulated by many signaling networks in common, which entail a cooperative and complementary morphogenetic pathway between these tissues through a still unknown mechanism [reviewed in Richtsmeier and Flaherty, 2013]. The characterization of additional patients harboring microscopic chromosomal alterations and who have craniosynostosis and altered brain function, such as those with 10q26 deletions, will contribute to a better understanding of these phenotypes, as well as of the relationship between brain and skull development.

Web Resources

Online Mendelian Inheritance in Man (OMIM): http://www.ncbi.nlm.nih.gov/omim.
UCSC Genome Browser: https://genome.ucsc.edu/.
DECIPHER: https://decipher.sanger.ac.uk/.
NCBI Reference Sequence: http://www.ncbi.nlm.nih.gov/.
MiRDB: http://mirdb.org/miRDB/.

ACKNOWLEDGMENTS

We thank the patient's family for the cooperation. We are grateful to the research team and undergraduate students of the Congenital Anomalies Project. This research was supported by the National Council for the Development of Science and Technology (CNPq) through Casadinho/PROCAD 06/2011 (No. 552672/2011-4), Ministry of Health Department of Science and Technology (DECIT), CNPq, and Espírito Santo Research Foundation (FAPES) in—Research Program for the Unified Health System (PPSUS/50809717/2010), and São Paulo Research Foundation (FAPESP/CEPID).

REFERENCES

Andersson H. 1966. Craniosynostosis as a complication after operation for hydrocephalus. Acta Paediatr Scand 55:192–196.

Chen G, Deng C, Li YP. 2012. TGF-β and BMP signaling in osteoblast differentiation and bone formation. Int J Biol Sci 8:272–288.

Chiara F, Badaloni A, Croci L, Yeh ML, Cariboni A, Hoerder-Suabedissen A, Consalez GG, Eickholt B, Shimogori T, Parnavelas JG, Rakić S. 2012. Early B-cell factors 2 and 3 (EBF2/3) regulate early migration of Cajal-Retzius cells from the cortical hem. Dev Biol 1 365:277–289.

Chiusaroli R, Knobler H, Luxenburg C, Sanjay A, Granot-Attas S, Tiran Z, Miyazaki T, Harmelin A, Baron R, Elson A. 2004. Tyrosine phosphatase epsilon is a positive regulator of osteoclast function in vitro and in vivo. Mol Biol Cell 15:234–244.

Chitkara R, Rajani A, Bernstein J, Shah S, Hahn JS, Barnes P, Hintz SR. 2011. Newborn with prenatally diagnosed choroidal fissure cyst and panhypopituitarism and review of the literature. AJP Rep 1:111–114.

Choucair N, Abou Ghoch J, Fawaz A, Mégarbané A, Chouery E. 2015. 10q26. 1 Microdeletion: Redefining the critical regions for microcephaly and genital anomalies. Am J Med Genet A 9999:1–7.

Courtens W, Wuyts W, Rooms L, Pera SB, Wauters J. 2006. A subterminal deletion of the long arm of chromosome 10: A clinical report and review. Am J Med Genet A 140:402–409.

Cohen MM. 1980. Perspectives on craniosynostosis. West J Med 132: 507–513.

Heuzé Y, Boyadjiev SA, Marsh JL, Kane AA, Cherkez E, Boggan JE, Richtsmeier JT. 2010. New insights into the relationship between suture closure and craniofacial dysmorphology in sagittal nonsyndromic craniosynostosis. J Anat 217:85–96.

Iourov IY, Vorsanova SG, Kurinnaia OS, Yurov YB. 2014. An interstitial deletion at 10q26.2q26.3. Case Rep Genet 2014:505832.

Kloss JL. 1968. Craniosynostosis secondary to ventriculoatrial shunt. Am J Dis Child 116:315–317.

Miller N D, Nance M A, Wohler E S, Hoover-Fong J E, Lisi E, Thomas G H, Pevsner J. 2009. Molecular (SNP) analyses of overlapping hemizygous deletions of 10q25.3 to 10qter in four patients: Evidence for HMX2 and HMX3 as candidate genes in hearing and vestibular function. Am J Med Gen A 149:669–680.

Moorhead PS, Nowell PC, Mellman WJ, Battips DM, Hungerford DA. 1960. Chromosome preparations of leukocytes cultured from human peripheral blood. Exp Cell Res 20:613–616.

Passos-Bueno MR, Sertié AL, Jehee FS, Fanganiello R, Yeh E. 2008. Genetics of craniosynostosis: Genes, syndromes, mutations and genotype-phenotype correlations. In: Rice DP, Craniofacial Sutures, editors. Development, diseases and treatment. Front oral biol. Basel: Ed. Karger. pp 107–143.

Piard J, Mignot B, Arbez-Gindre F, Aubert D, Morel Y, Roze V, McElreavy K, Jonveaux P, Valduga M, Van Maldergem L. 2014. Severe sex differentiation disorder in a boy with a 3.8 Mb 10q25.3-q26.12 microdeletion encompassing E MX2. Am J Med Genet Part A 164A: 2618–2622.

Piccione M, Antona V, Piro E, Cavani S, Malacarne M, Pierluigi M, Corsello G. 2008. *10q*ter deletion: A new case. Am J Med Genet A 146A: 2435–2438.

Plaisancié J, Bouneau L, Cances C, Garnier C, Benesteau J, Leonard S, Bourrouillou G, Calvas P, Vigouroux A, Julia S, Bieth E. 2014. Distal *10q* monosomy: New evidence for a neurobehavioral condition? Eur J Med Genet 57:47–53.

Richtsmeier JT, Flaherty K. 2013. Hand in glove: Brain and skull in development and dysmorphogenesis. Acta Neuropathol 125:469–489.

Schrander-Stumpel C, Fryns JP, Hamers G. 1991. The partial monosomy *10q* syndrome: Report on two patients and review of the developmental data. J Ment Defic Res 35:259–267.

Toffolatti L, Scquizzato E, Cavallin S, Canal F, Scarpa M, Stefani PM, Gherlinzoni F, Dei Tos AP. 2014. MGMT promoter methylation and correlation with protein expression in primary central nervous system lymphoma. Virchows Arch 465:579–586.

Vera-Carbonell A, Lopez-Gonzalez V, Bafalliu JA, Ballesta-Martınez MJ, Fernandez A, Guillen-Navarro E, Lopez-Exposito I. 2015. Clinicalcomparison of 10q26 overlapping deletions: Delineating the critical region for urogenital anomalies. Am J Med Genet Part A 167A:786–790.

Wang W, Lo P, Frasch M, Lufkin T. 2000. Hmx: An evolutionary conserved homeobox gene family expressed in the developing nervous system in mice and Drosophila. Mech Dev 99:123–137.

Wang W, Chan EK, Baron S, Van de Water T, Lufkin T. 2001. Hmx2 homeobox gene control of murine vestibular morphogenesis. Development 128:5017–5029.

Wang W, Lufkin T. 2005. Hmx homeobox gene function in inner ear and nervous system cell-type specification and development. Exp Cell Res 306:373–379.

Wilkie AO, Byren JC, Hurst JA, Jayamohan J, Johnson D, Knight SJ, Lester T, Richards PG, Twigg SR, Wall SA. 2010. Prevalence and complications of single-gene and chromosomal disorders in craniosynostosis. Pediatrics 126:391–400.

Wulfsberg EA, Weaver RP, Cunniff CM, Jones MC, Jones KL. 1989. Chromosome *10q*ter deletion syndrome: A review and report of three new cases. Am J Med Genet 32:364–367.

Yatsenko SA, Kruer MC, Bader PI, Corzo D, Schuette J, Keegan CE, Nowakowska B, Peacock S, Cai WW, Peiffer DA, Gunderson KL, Ou Z, Chinault AC, Cheung SW. 2009. Identification of critical regions for clinical features of distal 10q deletion syndrome. Clin Genet 76:54–62.

SUPPORTING INFORMATION

Additional supporting information may be found in the online version of this article at the publisher's web-site.

Hindawi Publishing Corporation
Stem Cells International
Volume 2015, Article ID 249098, 9 pages
http://dx.doi.org/10.1155/2015/249098

Research Article

Improvement of *In Vitro* Osteogenic Potential through Differentiation of Induced Pluripotent Stem Cells from Human Exfoliated Dental Tissue towards Mesenchymal-Like Stem Cells

Felipe Augusto Andre Ishiy,[1] Roberto Dalto Fanganiello,[1] Karina Griesi-Oliveira,[1] Angela May Suzuki,[1] Gerson Shigeru Kobayashi,[1] Andressa Gois Morales,[1] Luciane Portas Capelo,[2] and Maria Rita Passos-Bueno[1]

[1]*Department of Genetics and Evolution, Institute of Bioscience, University of Sao Paulo, 05508-090 Sao Paulo, SP, Brazil*
[2]*Science and Technology Institute, Federal University of Sao Paulo, 12247-014 Sao Jose dos Campos, SP, Brazil*

Correspondence should be addressed to Maria Rita Passos-Bueno; passos@ib.usp.br

Received 30 September 2014; Revised 19 December 2014; Accepted 29 December 2014

Academic Editor: Jack Parent

Constraints for the application of MSCs for bone reconstruction include restricted self-renewal and limited cell amounts. iPSC technology presents advantages over MSCs, providing homogeneous cellular populations with prolonged self-renewal and higher plasticity. However, it is unknown if the osteogenic potential of iPSCs differs from that of MSCs and if it depends on the iPSCs originating cellular source. Here, we compared the *in vitro* osteogenesis between stem cells from human deciduous teeth (SHED) and MSC-like cells from iPSCs from SHED (iPS-SHED) and from human dermal fibroblasts (iPS-FIB). MSC-like cells from iPS-SHED and iPS-FIB displayed fibroblast-like morphology, downregulation of pluripotency markers and upregulation of mesenchymal markers. Comparative *in vitro* osteogenesis analysis showed higher osteogenic potential in MSC-like cells from iPS-SHED followed by MSC-like cells from iPS-FIB and SHED. CD105 expression, reported to be inversely correlated with osteogenic potential in MSCs, did not display this pattern, considering that SHED presented lower CD105 expression. Higher osteogenic potential of MSC-like cells from iPS-SHED may be due to cellular homogeneity and/or to donor tissue epigenetic memory. Our findings strengthen the rationale for the use of iPSCs in bone bioengineering. Unveiling the molecular basis behind these differences is important for a thorough use of iPSCs in clinical scenarios.

1. Introduction

Clinical demand for bone tissue is evident to supplant bony structures lost due to trauma, disease, or congenital malformation. Cell replacement therapies represent a promising strategy for bone engineering, and human mesenchymal stem cells (MSCs) isolated from various adult tissues have been extensively investigated as a potential cell source for bone regenerative treatments [1, 2]. However, large-scale applications are constrained since MSCs are found in limited amounts, are highly heterogeneous, and their long-term in vitro expansion can lead to senescence and spontaneous differentiation [3, 4]. Additionally, the differentiation potential of MSCs may vary depending on the tissue of origin [5].

Generation of human induced pluripotent stem cells (hiPSCs) was first achieved using dermal fibroblasts [6, 7]. Thereafter, hiPSCs have been derived from an ample variety of starting cells, including MSCs. Reprogramming MSCs to hiPSC is an attractive approach to circumvent issues associated with the direct use of MSCs since it allows the production of cells with robust *in vitro* self-renewal capacity and with differentiation multipotential. Controlling differentiation cues *in vivo* is a significant challenge and direct transplantation of pluripotent stem cells may result in tumor formation [8]. Therefore, derivation of MSC-like cells from

pluripotent stem cells has been pursued by a number of researchers [9–11].

Most types of MSCs are not easily obtained using minimally invasive procedures. Stem cells from human exfoliated deciduous teeth (SHED) can be easily isolated from a readily accessible tissue source, expanded under simple culture conditions, and banked. Even though SHED have been reported to be especially useful to restore bone [12, 13], as mentioned above, their inherent population heterogeneity and limited expansion capacity restrict their use for therapeutic purposes. While hiPSCs have been generated from SHED (iPS-SHED) [14], there is no report exploring the *in vitro* osteogenic potential of MSC-like cells derived from iPS-SHED populations. Therefore, the goal of this study is threefold: (1) to verify if MSC-like cells from iPS-SHED and SHED isolated from the same donors exhibit similar *in vitro* osteogenic potential; (2) to compare the osteogenic potential of MSC-like cells from iPS-SHED with MSC-like cells from hiPSCs derived from mature dermal fibroblasts (iPS-FIB), considered the most accessible cell source for iPSC generation; (3) to compare the expression of CD105 between these cellular populations, which has been inversely correlated with an increased osteogenic potential [15].

2. Materials and Methods

2.1. Isolation of Stem Cells from Human Exfoliated Dental Tissue (SHED), Human Dermal Fibroblasts, and Generation of Human Induced Pluripotent Stem Cells (hiPSCs). SHED were obtained from teeth of 6 independent subjects by enzymatic digestion of pulp from deciduous teeth as described in Miura et al., 2003 [12]. Human adult dermal fibroblasts, the most accessible and feasible cell source for iPSC generation [14], were obtained according to the protocol detailed in Aasen and Belmonte 2010, adapted for fibroblast isolation [16]. hiPSCs were obtained from SHED from 2 independent subjects (3 clones derived from each) and fibroblast cell populations from 3 independent subjects (2 clones each). *SOX2*, *c-MYC*, *OCT4,* and *KLF4* ectopic expression were induced through retroviral transduction, as originally reported in Takahashi et al., 2007 [6]. Two days after transduction, SHED and fibroblasts were cocultivated with irradiated murine embryonic fibroblasts (Millipore) in embryonic stem cell medium Dulbecco's modified Eagle/F12 medium (DMEM/F12) supplemented with 2 mM GlutaMAX-I, 0.1 mM nonessential amino acids, 55 uM 2-mercaptoethanol, 30 ng/mL of bFGF, and 20% of knockout serum replacement all provided by Life Technologies. Typical hiPSC colonies formed on feeder cells were transferred to matrigel (BD-Biosciences) coated plates and expanded in Essential 8 Medium (Life Technologies) supplemented with 100 ug/mL of normocin (Invivogen). hiPSCs displayed embryonic stem cell-like morphology, expressed pluripotency markers (*NANOG, OCT3, OCT4*), and displayed trilineage differentiation potential after embryoid body differentiation and *in vivo* teratoma formation (see Supplementary Figure 1 in Supplementary Material available online at http://dx.doi.org/10.1155/2015/249098). This project was approved by the local ethical committee (Protocol number 121/2001-FR. 435054).

2.2. Derivation of MSC-Like Cells from iPS-SHED and iPS-FIB. iPS-SHED and iPS-FIB colonies from confluent plates were detached with accutase (Life Technologies). hiPSC colonies were partially dissociated via manual pipetting and the cells were plated onto matrigel-coated tissue culture dishes at 1×10^4 cells/cm^2 in MSC differentiation culture medium (Dulbecco's modified Eagle medium High Glucose—DMEM with 10% fetal bovine serum, 1% penicillin/streptomycin, 1% nonessential amino acids, and 5 ng/mL of bFGF) for 14 days with media changes every 3 days. For subsequent passages, single-cell suspensions were prepared using TrypLE reagent (Life Technologies) and cells were passaged with a 1 : 3 split ratio in standard culture flasks (Corning) without matrigel coating.

2.3. Characterization of MSC-Like Cells from iPS-SHED and from iPS-FIB. SHED and MSC-like cells from iPS-SHED and from iPS-FIB were harvested and resuspended to 10^5 cells in 100 uL of PBS containing 1% BSA. Cells were separately labeled with FITC, PE, PE-Cy5, PERCP-Cy5.5, or APC-H7 conjugated rat anti-human antibodies CD29, CD31 (Biolegend), CD34, CD45, CD73, CD90 CD105, and CD166 (Becton Dickinson) on ice and protected from light for 40 min. An isotype-matched mAb was used as a control (Becton Dickinson). Data were acquired and analyzed with the FACSAria II cytometer and CellQuest software (Becton Dickinson). Multipotential differentiations of MSC-like cells from iPS-SHED and from iPS-FIB were performed as previously described by de Mendonça Costa et al., 2008 [13], and representative pictures of adipogenesis, osteogenesis, and chondrogenesis were included as supplementary Figure 2.

2.4. Real-Time Quantitative PCR. Total RNA was obtained from cell populations with the use of Nucleospin RNA II extraction kit (Macherey-Nagel) following manufacturer's recommendations. Briefly, one microgram of total RNA was converted into cDNA using Superscript II (Life Technologies), according to the manufacturer's recommendations. Real-time quantitative PCR reactions were performed with 2x SYBR Green PCR Master Mix (Life Technologies) and 25 nM–200 nM of each primer. Fluorescence was detected using ABI Prism 7500 Sequence Detection System, under standard temperature protocol. Primer pairs were designed with Primer-BLAST (http://www.ncbi.nlm.nih.gov/tools/primer-blast/; primer sequences are listed in Table 1, and their amplification efficiencies (E) were determined by serial cDNA dilutions $\log_{10}$-plotted against Ct values, in which $E = 10^{-1/\text{slope}}$. Expression of target genes was assessed relative to a calibrator cDNA (ΔCt). Finally, GeNorm v3.4 [17] was used to determine the most stable endogenous controls (among *ACTB, TBP, and HMBS*) and calculate normalization factors for each sample. The final expression values were determined based on a previous method [18], dividing $E^{-\Delta Ct}$ by the corresponding normalization factor.

2.5. In Vitro Osteogenic Induction. For osteogenic induction, MSC-like cells from iPS-SHED and from iPS-FIB were plated in 12-well plates (4×10^4 cells per well) and after

Table 1: Primers used for real-time quantitative PCR experiments.

Target	NM	Forward primer	Reverse primer
OCT3 (pluripotency)	NM_001173531.1	gtggtcagccaactcgtca	ccaaaaaccctggcacaaact
OCT4 (pluripotency)	NM_002701.3	cctcacttcactgcactgta	caggttttctttccctagct
NANOG (pluripotency)	NM_024865	tggacactggctgaatccttc	cgttgattaggctccaaccat
RUNX2	NM_001024630.3	agtggacgaggcaagagtttc	gttcccgaggtccatctactg
ALP	NM_000478.4	gatacaagcactcccacttcatctg	ctgttcagctcgtactgcatgtc
BGLAP	NM_199173	ggcgctacctgtatcaatgg	gtggtcagccaactcgtca
COL1A1	NM_000088.3	gggccaagacgaagacat	caacacccttgccgttgtcg
DLX5	NM_005221	accagccagaagaagtgac	ccttctctgtaatgcggcca
CD105 (*ENG*)	NM_001144950	tgcacttggcctacaattcca	agctgcccactcaaggatct
ACTB (endogenous control)	NM_001101	tgaagtgtgacgtggacatc	ggaggagcaatgatcttgat
TBP (endogenous control)	NM_001172085	gtgacccagcatcactgtttc	gcaaaccagaaaccccttgcg
HMBS (endogenous control)	NM_001024382	agcttgctcgcatacagacg	agctccttggtaaacaggctt

3 days, medium was replaced with osteogenic induction medium (Stem Pro Osteogenesis Kit-Life Technologies). Culture medium was changed every 2-3 days and cultures were maintained for 21 days. After 9 days of osteogenic induction, alkaline phosphatase activity was quantified through a biochemical assay: cells were treated with phosphatase substrate (Sigma-Aldrich), and the resulting p-nitrophenol was quantified colorimetrically using a Multiskan EX ELISA plate reader (Thermo Scientific) at 405 nm. After 21 days mineralization of extracellular matrix was assessed through alizarin red staining. Briefly, cells were washed three times with PBS, fixed with a 70% ethanol solution for 30 minutes at room temperature, followed by three distilled water washes, and finally stained with a 0.2% alizarin red S solution (Sigma-Aldrich) for 30 minutes at room temperature. After three washes with PBS, plates were air-dried at room temperature; pictures were taken. Staining was removed with 20% methanol/10% acetic acid solution and measured colorimetrically using a Multiskan EX ELISA plate reader (Thermo Scientific) at 450 nm. von Kossa staining was also performed after 14 and 21 days of osteogenic induction: cell cultures were washed once with PBS, a 1% silver nitrate solution was added, and the plate was exposed to UV light for 40 minutes. After UV light exposure the plate was rinsed with distilled water. Sodium thiosulfate (3%) was added for 5 minutes, the plates were then rinsed in water, and Van Gieson solution was added for 5 minutes. Plates were washed with 100% ethanol and air-dried for image analysis.

2.6. Statistical Analysis. All experiments were performed in triplicate. Unpaired Student's t-test was used for single comparisons. Error bars in bar graphs represent standard deviation. The level of statistical significance was set at $P < 0.05$.

3. Results

After 12 days of induction of iPS-SHED and iPS-FIB with MSC medium under feeder-free conditions, MSC-like cells derived from iPS-SHED and from iPS-FIB achieved 80% confluence in 25 cm^2 flasks and showed a spindle-shaped fibroblast-like morphology (Figure 1(a)). *OCT3*, *OCT4*, *NANOG*, and *ALP* mRNAs were significantly downregulated in MSC-like cells from iPS-SHED and from iPS-FIB when compared with the original hiPSC populations ($P < 0.05$, Figures 1(b′) and 1(b″)). Moreover MSC-like cells from iPS-SHED and from iPS-FIB expressed high levels of mesenchymal markers (CDs 29, 73, 90, and 105 and CD 166) and low levels of endothelial (CD 31) and hematopoietic (CDs 34 and 45) markers (Figure 2).

Next, we assessed the *in vitro* osteogenic potential of MSC-like cells from iPS-SHED, MSC-like cells from iPS-FIB and SHED during early *in vitro* osteogenesis by quantifying gene expression of key osteogenesis markers (*DLX5* and *RUNX2*, two early transcription factors associated with osteogenesis, *ALP* and *COL1A1*, two early osteoblast markers, and *BGLAP*, a late osteoblast marker). *ALP* gene expression was upregulated in all cellular populations from day 2 to day 6 but showed higher expression in days 4 and 6 in MSC-like cells from iPS-SHED and from iPS-FIB in comparison with SHED ($P < 0.001$). *DLX5* peaked at day 2 in MSC-like cells from iPS-SHED and from iPS-FIB and was upregulated in SHED at all time points ($P < 0.001$). *RUNX2* was also upregulated in SHED until day 6 of osteogenic induction, in comparison with MSC-like cells from iPS-SHED and from iPS-FIB ($P < 0.001$). *COL1A1* was upregulated in MSC-like cells from iPS-SHED and in SHED from day 2 to day 6 ($P < 0.001$) but showed no significant upregulation in MSC-like cells from iPS-FIB during this period. *BGLAP* was not upregulated during this early stage of osteoinduction in any cellular population, as expected for a late osteoblast marker (Figure 3(a)).

ALP enzymatic activity was higher in MSC-like cells from iPS-SHED when compared with MSC-like cells from iPS-FIB (2.3-fold increase, $P < 0.01$) and with SHED (2.54-fold increase, $P < 0.001$) after 9 days of *in vitro* osteoinduction (Figure 3(b)). Alizarin red S staining revealed more matrix mineralization in MSC-like cells from iPS-SHED when compared with SHED (4.36- fold increase, $P < 0.001$) and with MSC-like cells from iPS-FIB (1.45-fold increase, $P < 0.01$) after 21 days of osteoinduction

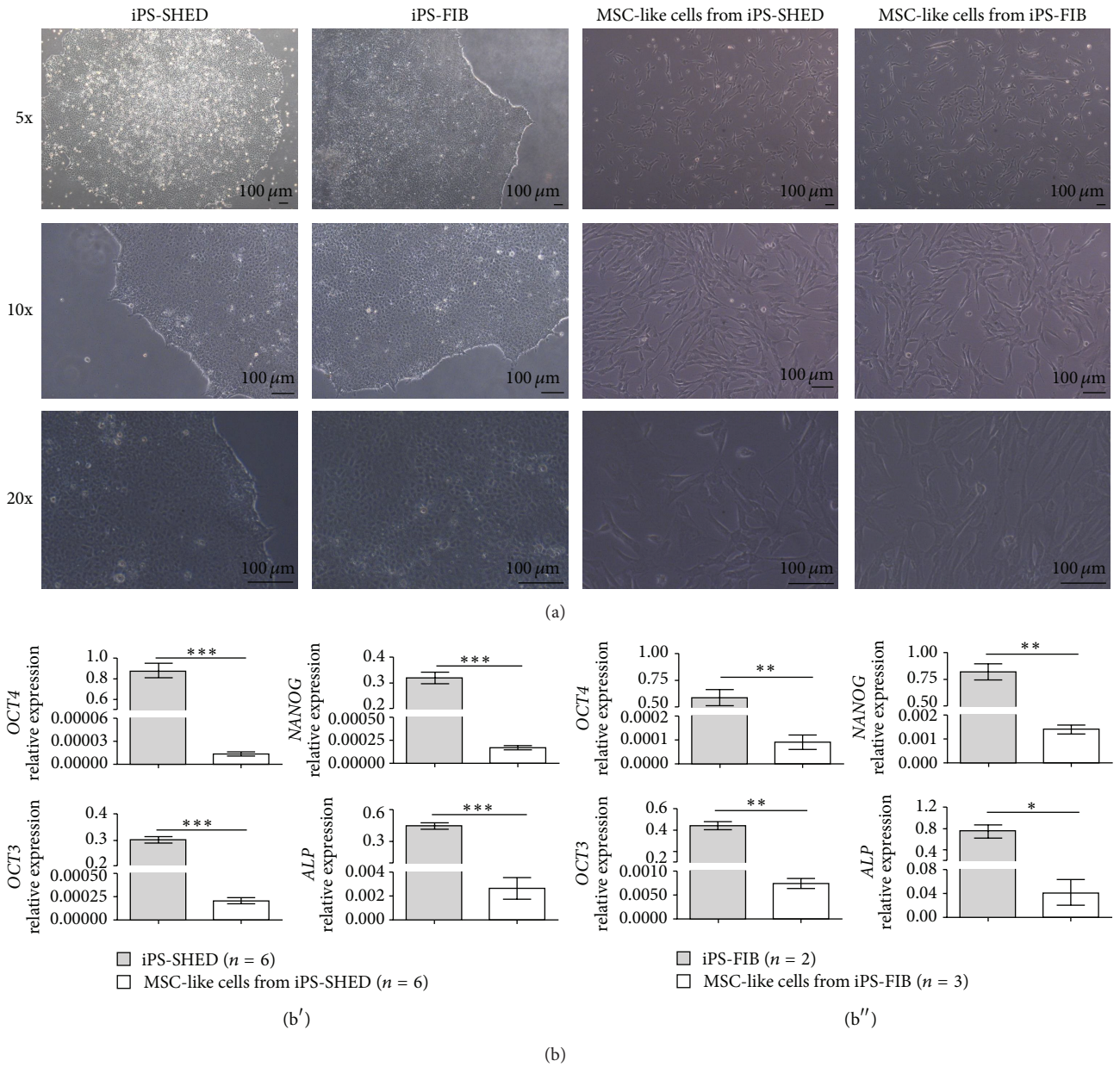

Figure 1: (a) Morphology of undifferentiated hiPSC colonies cultured on matrigel and MSC-like cells from iPS-SHED and iPS-FIB after 12 days of *in vitro* mesenchymal induction. Scale bar = 100 um. (b) Real-time quantitative PCR analysis of pluripotency markers in undifferentiated hiPSCs ((b′) SHED and (b″) fibroblasts) and in MSC-like cells from iPS-SHED and from iPS-FIB. *ACTB*, *TBP*, and *HMBS* were used as endogenous controls. Values represent means +/− SD, $P < 0.05$ (*), $P < 0.01$ (**), and $P < 0.001$ (***).

(Figure 3(c)). In this time point, MSC-like cells from iPS-FIB showed a 2.99-fold increase ($P < 0.001$) in mineralized matrix production when compared with SHED. These data were validated by von Kossa staining after 14 and 21 days of *in vitro* osteogenesis (Figure 3(e)).

Finally, we compared the expression of *CD105* mRNAs between SHED, MSC-like cells from iPS-SHED and from iPS-FIB and found a lower expression of this gene in SHED when compared with the latter cellular populations ($P < 0.001$, Figure 3(d)).

4. Discussion

iPSC technology has gained attention to engender cellular populations to be used in tissue engineering, displaying self-renewal, pluripotency, and differentiation plasticity similar to embryonic stem cells. Furthermore, the use of hiPSCs is not hindered by the ethical issues associated with the use of human embryos and permits the generation of therapeutically relevant cell types genetically compatible to patients, evading rejection drawbacks that may follow transplantation of nonautologous cells [19].

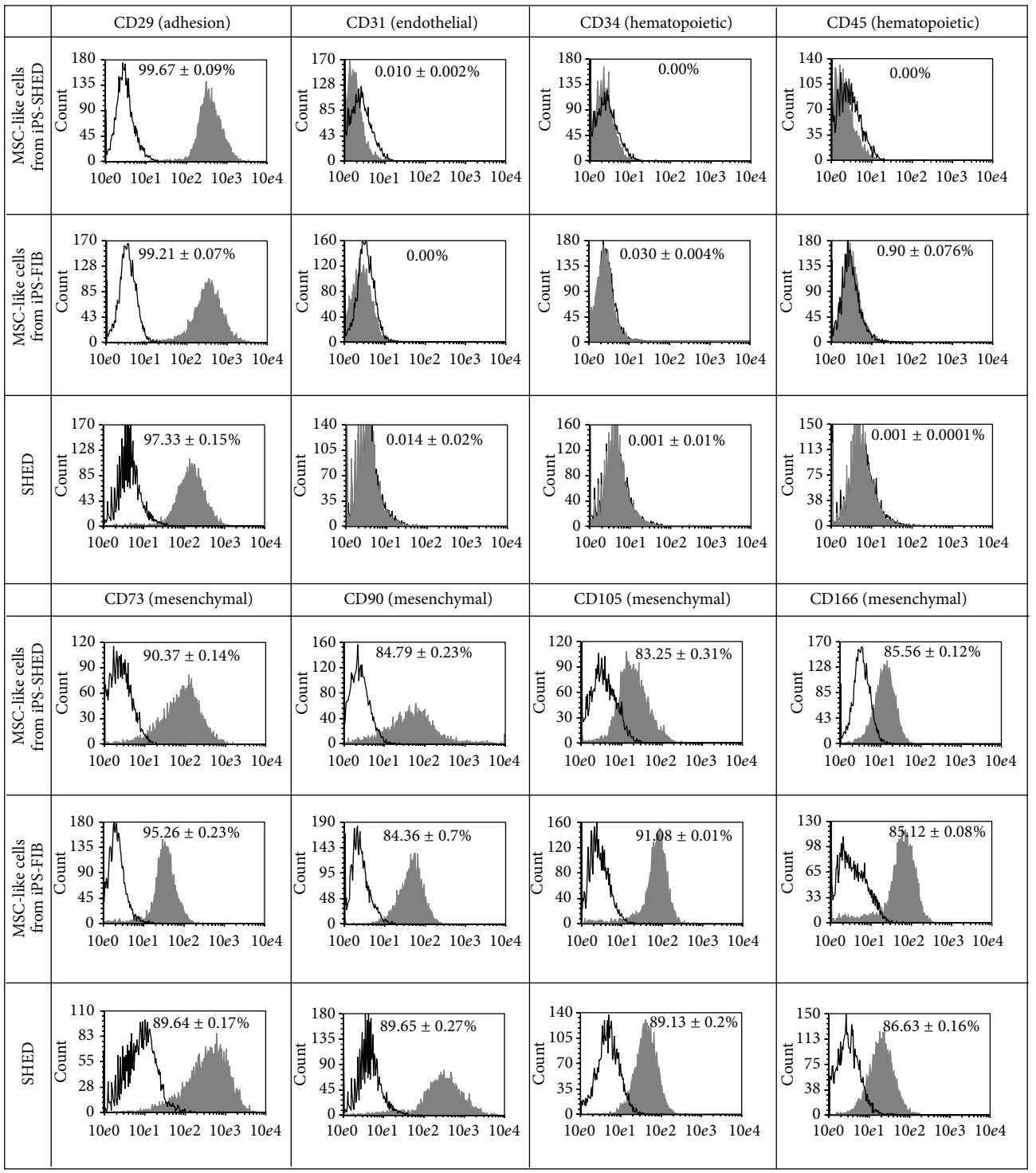

Figure 2: Representative surface antigen profiling of SHED, MSC-like cells from iPS-SHED and from iPS-FIB labeled with antibodies against mesenchymal, endothelial, and hematopoietic antigens. White histograms represent isotype controls and grey histograms represent the fluorescence of conjugated antibodies for each antigen. Mean expression rates are indicated above each graph and displayed as mean +/− SD.

There is an increasing interest in investigating iPSCs for bone regenerative therapies and a series of studies have generated murine iPSCs and assessed their direct differentiation towards osteoblasts [20–23]. From a safety point of view, the use of progenitor cells instead of undifferentiated iPSCs for therapeutic purposes is advantageous since progenitor cells are already primed for a specific differentiation pathway and tumor formation risk is reduced [24]. Moreover, recent

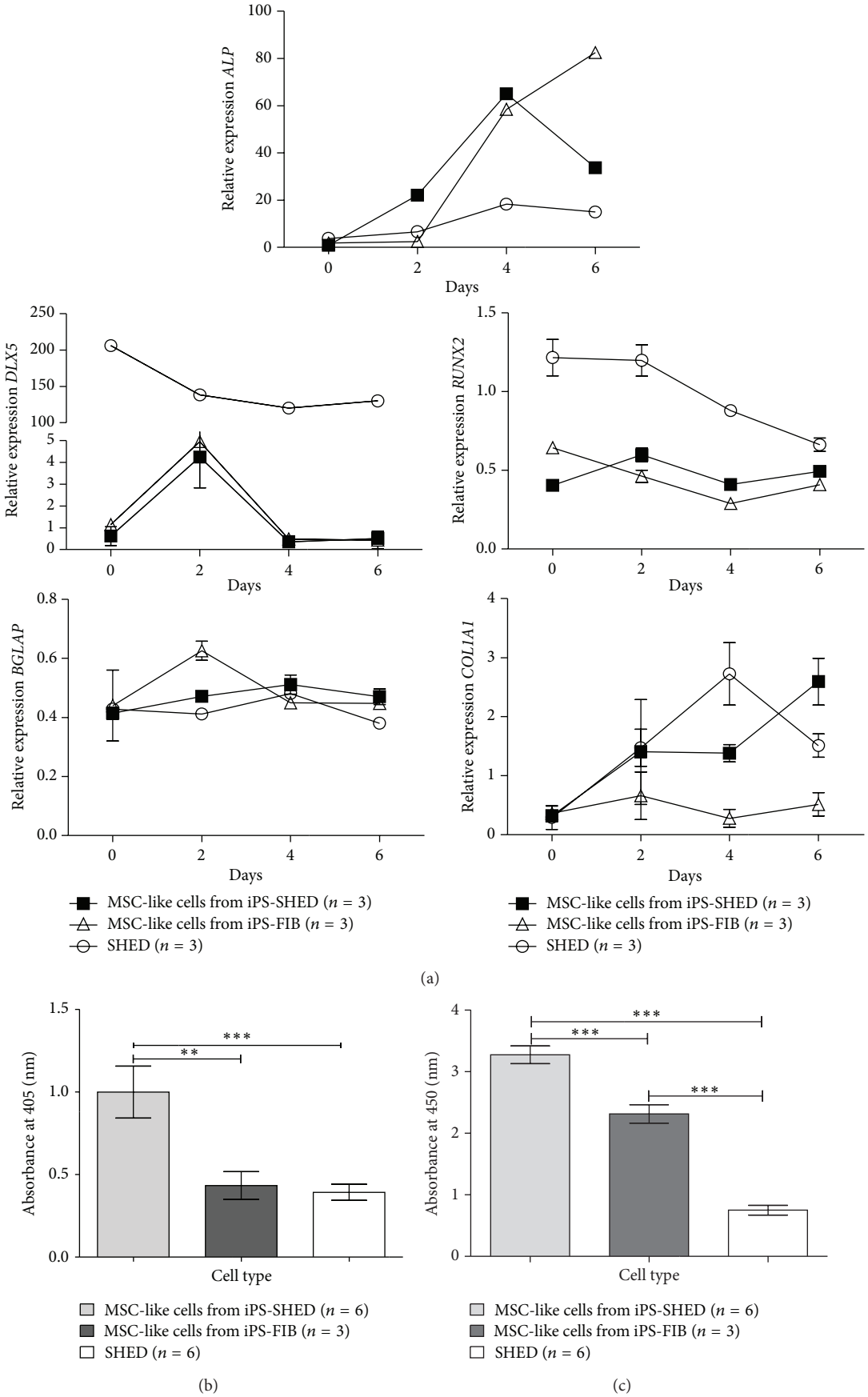

Figure 3: Continued.

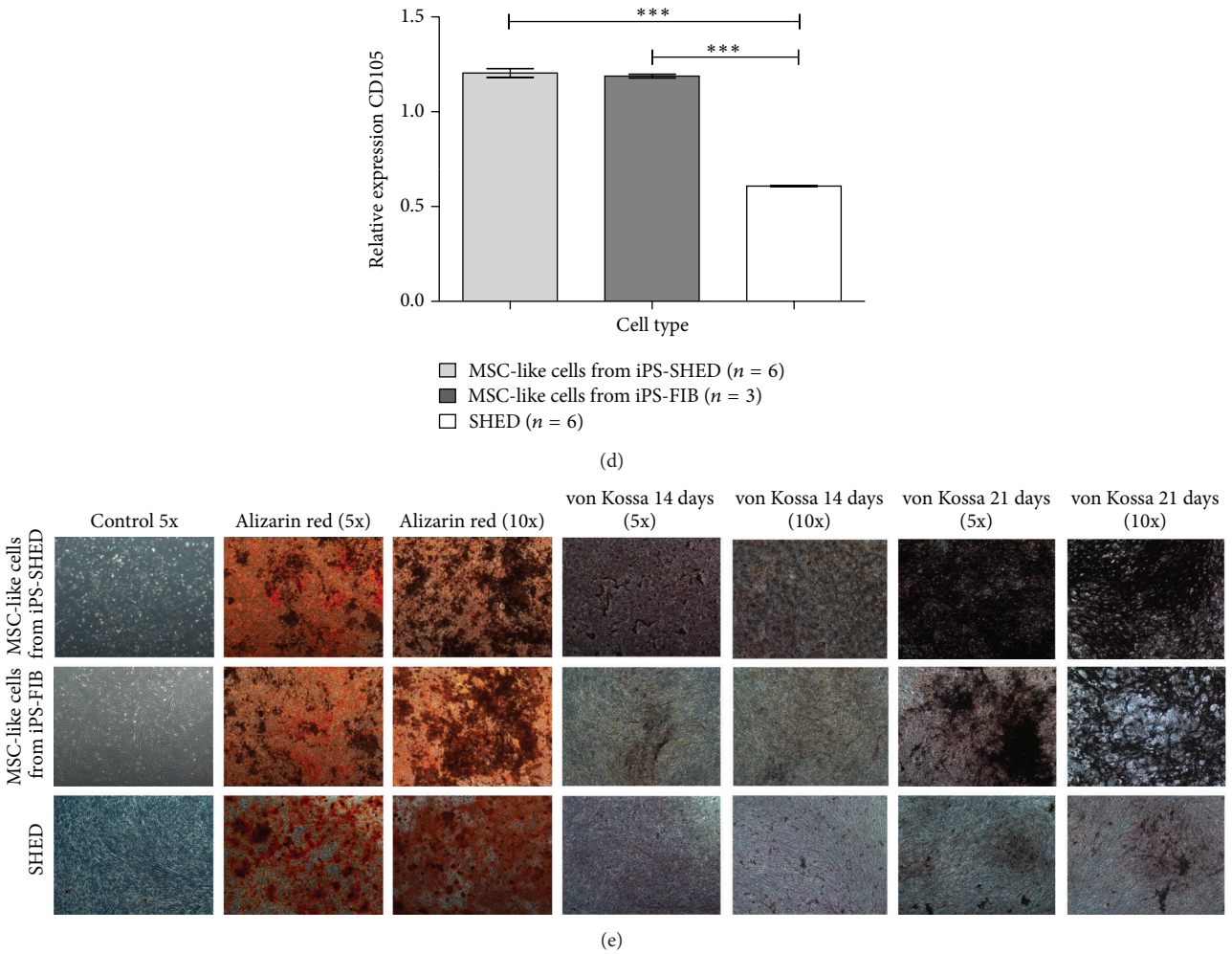

Figure 3: (a) Real-time quantitative PCR analysis of alkaline phosphatase (*ALP*), *DLX5*, *RUNX2*, *BGLAP*, and *COL1A1* in MSC-like cells from iPS-SHED, MSC-like cells from iPS-FIB and SHED. *ACTB*, *TBP*, and *HMBS* were used as endogenous controls. (b) Alkaline phosphatase activity quantification in cells cultured for 9 days in osteogenic medium. Values represent means +/− SD, $P < 0.01$ (**), and $P < 0.001$ (***). (c) Alizarin red S staining quantification in cells cultured for 21 days in osteogenic medium. Values represent means +/− SD, $P < 0.001$ (***). (d) Real-time quantitative PCR analysis of CD105 in undifferentiated SHED and MSCs from iPS-SHED and from iPS-FIB. *ACTB*, *TBP*, and *HMBS* were used as endogenous controls. Values represent means +/− SD, $P < 0.001$ (***). (e) Representative pictures of alizarin red S (after 21 days of *in vitro* osteoinduction, with 5 and 10x magnification) and von Kossa staining (after 14 and 21 of *in vitro* osteogenic induction, with 5 and 10x magnification) of mineralized deposits in MSC-like cells from iPS-SHED, MSC-like cells from iPS-FIB and SHED. Basal growth medium free of osteoinduction factors was used in the control group (with 5x magnification).

reports suggest that some of the reparative effects associated with MSC transplantation are not mediated by cellular differentiation per se but by paracrine factors secreted by them [25]; Fanganiello et al., submitted.

The MSC differentiation from hiPSCs seemed to be successful as both MSC-like cells from iPS-SHED and from iPS-FIB displayed typical mesenchymal cell morphology, downregulation of pluripotency markers and similar cell surface antigen profiles and multipotential when compared with SHED. After *in vitro* osteoinduction, upregulation of osteogenesis markers *DLX5* and *RUNX2* in SHED in comparison with MSC-like cells from iPS-SHED and from iPS-FIB may indicate a previous commitment of this cell population towards the osteogenic lineage. However, in days 4 and 6 of osteoinduction, MSC-like cells from iPS-SHED and from iPS-FIB presented upregulation of *ALP*, a metalloenzyme known as a key early marker of osteogenesis. MSC-like cells from iPS-SHED also had more ALP enzymatic activity when compared with MSC-like cells from iPS-FIB and with SHED in midstage osteogenesis. MSC-like cells from iPS-SHED and from iPS-FIB produced significantly more mineralized extracellular matrix when compared with SHED. Overall, MSC-like cells from iPS-SHED were able to undergo induced *in vitro* osteogenesis in a more efficient fashion than MSCs from iPS-FIB or from the originating SHED populations.

One of the factors that could explain the higher efficiency of the *in vitro* osteogenesis in MSC-like cells from iPS-SHED and iPS-FIB in comparison with SHED might be related to

the presence of a more homogeneous cellular population attributed to the direct plating protocol adopted. We have decided to choose the iPSC direct plating method over the embryoid body (EB) protocol since EBs are known to contain a heterogeneous mixture of cells with different degrees of multipotency that may limit their net osteogenic potential [26–28]. Accordingly, enhanced osteogenic differentiation has been associated with direct plating [29–32], and this method has been proposed to yield uniform batches of osteoprogenitor cells [31].

We also tested if the difference in osteogenic potential between the MSC-like cells from iPS-SHED from iPS-FIB and SHED is related to CD105 expression, as its lower expression has been associated with a higher osteogenic potential in MSCs harvested from human adipose tissue (hASCs) when compared with MSCs with higher CD105 expression [15]. Interestingly we found CD105 expression to be significantly lower in SHED when compared with both MSC-like cells from iPS-SHED and from iPS-FIB. Therefore, the higher osteogenic potential in this case may be due to other factors.

The difference in osteogenic potential here reported between MSC-like cells from iPS-SHED and from-iPS-FIB may possibly be related to a somatic epigenetic memory of the tissue of origin [33]. Derivation of pure populations of functionally differentiated cells from iPSCs is still challenging and different cell types show variable susceptibility to reprogramming. In fact, MSCs derived from iPSC lines from different tissues have been shown to exhibit variability in their differentiation profiles. Hynes et al. 2014 reported that MSC-like cells from iPSCs generated from periodontal ligament displayed higher osteogenic capacity both *in vitro* and *in vivo* when compared to MSC-like cells from iPSCs generated from lung and gingival fibroblasts, which was attributed to epigenetic memory of the donor tissue [34]. In another study, Sanchez-Freire et al. 2014 reported higher cardiac differentiation efficiency in MSC-like cells derived from iPSCs generated from cardiac progenitors in comparison with dermal fibroblasts from the same donor, which was demonstrated to be due to the retention of residual methylation signatures of the tissue of origin [35].

5. Conclusions

Our findings provide an important argument towards the use of iPSCs in tissue bioengineering since MSC-like cells from iPS-SHED and from iPS-FIB displayed higher osteogenic potential than SHED. We also suggest that cellular homogeneity and tissue of origin are important factors to be considered when planning to use iPSCs in bone regenerative medicine. CD105 does not seem to be a main factor involved in these differences. The dissection of the molecular basis of osteogenic differentiation in MSC-like cells from iPSC-derived cells may furnish insights into the clinical usefulness of iPSCs from different sources.

Conflict of Interests

The authors declare that there is no conflict of interests regarding the publication of this paper.

Authors' Contribution

Felipe Augusto Andre Ishiy and Roberto Dalto Fanganiello contributed equally to this work.

Acknowledgments

The authors are grateful to the subjects who participated in this work. They thank Simone Gomes Ferreira and Patricia Semedo Kuriki for technical assistance and Constancia Gotto Urbani for secretarial assistance. This work was supported by grants from the Brazilian Ministry of Health, the Foundation for Research Support of the State of Sao Paulo (FAPESP), and the National Council for Scientific and Technological Development (CNPq).

References

[1] D. Marolt, M. Knezevic, and G. V. Novakovic, "Bone tissue engineering with human stem cells," *Stem Cell Research & Therapy*, vol. 1, no. 2, article 10, 2010.

[2] X. Wang, Y. Wang, W. Gou, Q. Lu, J. Peng, and S. Lu, "Role of mesenchymal stem cells in bone regeneration and fracture repair: a review," *International Orthopaedics*, vol. 37, no. 12, pp. 2491–2498, 2013.

[3] M. Pevsner-Fischer, S. Levin, and D. Zipori, "The origins of mesenchymal stromal cell heterogeneity," *Stem Cell Reviews and Reports*, vol. 7, no. 3, pp. 560–568, 2011.

[4] K. Stenderup, J. Justesen, C. Clausen, and M. Kassem, "Aging is associated with decreased maximal life span and accelerated senescence of bone marrow stromal cells," *Bone*, vol. 33, no. 6, pp. 919–926, 2003.

[5] P. G. Robey, "Cell sources for bone regeneration: the good, the bad, and the ugly (But Promising)," *Tissue Engineering Part B: Reviews*, vol. 17, no. 6, pp. 423–430, 2011.

[6] K. Takahashi, K. Tanabe, M. Ohnuki et al., "Induction of pluripotent stem cells from adult human fibroblasts by defined factors," *Cell*, vol. 131, no. 5, pp. 861–872, 2007.

[7] W. E. Lowry, L. Richter, R. Yachechko et al., "Generation of human induced pluripotent stem cells from dermal fibroblasts," *Proceedings of the National Academy of Sciences of the United States of America*, vol. 105, no. 8, pp. 2883–2888, 2008.

[8] Y. Jung, G. Bauer, and J. A. Nolta, "Concise review: induced pluripotent stem cell-derived mesenchymal stem cells: progress toward safe clinical products," *Stem Cells*, vol. 30, no. 1, pp. 42–47, 2012.

[9] Q. Lian, Y. Zhang, J. Zhang et al., "Functional mesenchymal stem cells derived from human induced pluripotent stem cells attenuate limb ischemia in mice," *Circulation*, vol. 121, no. 9, pp. 1113–1123, 2010.

[10] T. Barberi, L. M. Willis, N. D. Socci, and L. Studer, "Derivation of multipotent mesenchymal precursors from human embryonic stem cells," *PLoS Medicine*, vol. 2, no. 6, article e161, 2005.

[11] L. G. Villa-Diaz, S. E. Brown, Y. Liu et al., "Derivation of mesenchymal stem cells from human induced pluripotent stem

cells cultured on synthetic substrates," *Stem Cells*, vol. 30, no. 6, pp. 1174–1181, 2012.

[12] M. Miura, S. Gronthos, M. Zhao et al., "SHED: Stem cells from human exfoliated deciduous teeth," *Proceedings of the National Academy of Sciences of the United States of America*, vol. 100, no. 10, pp. 5807–5812, 2003.

[13] A. de Mendonça Costa, D. F. Bueno, M. T. Martins et al., "Reconstruction of large cranial defects in nonimmunosuppressed experimental design with human dental pulp stem cells," *Journal of Craniofacial Surgery*, vol. 19, no. 1, pp. 204–210, 2008.

[14] X. Yan, H. Qin, C. Qu, R. S. Tuan, S. Shi, and G. T.-J. Huang, "iPS cells reprogrammed from human mesenchymal-like Stem/Progenitor cells of dental Tissue Origin," *Stem Cells and Development*, vol. 19, no. 4, pp. 469–480, 2010.

[15] B. Levi, D. C. Wan, J. P. Glotzbach et al., "CD105 protein depletion enhances human adipose-derived stromal cell osteogenesis through reduction of transforming growth factor beta1 (TGF-beta1) signaling," *The Journal of Biological Chemistry*, vol. 286, no. 45, pp. 39497–39509, 2011.

[16] T. Aasen and J. C. I. Belmonte, "Isolation and cultivation of human keratinocytes from skin or plucked hair for the generation of induced pluripotent stem cells," *Nature Protocols*, vol. 5, no. 2, pp. 371–382, 2010.

[17] J. Vandesompele, K. de Preter, F. Pattyn et al., "Accurate normalization of real-time quantitative RT-PCR data by geometric averaging of multiple internal control genes," *Genome Biology*, vol. 3, no. 7, Article ID RESEARCH0034, 2002.

[18] M. W. Pfaffl, "A new mathematical model for relative quantification in real-time RT-PCR," *Nucleic Acids Research*, vol. 29, no. 9, article e45, 2001.

[19] I. de Lázaro, A. Yilmazer, and K. Kostarelos, "Induced pluripotent stem (iPS) cells: a new source for cell-based therapeutics?" *Journal of Controlled Release*, vol. 185, no. 1, pp. 37–44, 2014.

[20] H. Egusa, H. Kayashima, J. Miura et al., "Comparative analysis of mouse-induced pluripotent stem cells and mesenchymal stem cells during osteogenic differentiation *in vitro*," *Stem Cells and Development*, vol. 23, no. 18, pp. 2156–2169, 2014.

[21] K. Tashiro, M. Inamura, K. Kawabata et al., "Efficient adipocyte and osteoblast differentiation from mouse induced pluripotent stem cells by adenoviral transduction," *Stem Cells*, vol. 27, no. 8, pp. 1802–1811, 2009.

[22] C.-L. Kao, L.-K. Tai, S.-H. Chiou et al., "Resveratrol promotes osteogenic differentiation and protects against dexamethasone damage in murine induced pluripotent stem cells," *Stem Cells and Development*, vol. 19, no. 2, pp. 247–257, 2010.

[23] T. Hayashi, H. Misawa, H. Nakahara et al., "Transplantation of osteogenically differentiated mouse iPS cells for bone repair," *Cell Transplantation*, vol. 21, no. 2-3, pp. 591–600, 2012.

[24] C. Karlsson, K. Emanuelsson, F. Wessberg et al., "Human embryonic stem cell-derived mesenchymal progenitors—potential in regenerative medicine," *Stem Cell Research*, vol. 3, no. 1, pp. 39–50, 2009.

[25] A. I. Caplan and J. E. Dennis, "Mesenchymal stem cells as trophic mediators," *Journal of Cellular Biochemistry*, vol. 98, no. 5, pp. 1076–1084, 2006.

[26] G. Bilousova, D. H. Jun, K. B. King et al., "Osteoblasts derived from induced pluripotent stem cells form calcified structures in scaffolds both *in vitro* and *in vivo*," *Stem Cells*, vol. 29, no. 2, pp. 206–216, 2011.

[27] J. M. Karp, L. S. Ferreira, A. Khademhosseini, A. H. Kwon, J. Yeh, and R. S. Langer, "Cultivation of human embryonic stem cells without the embryoid body step enhances osteogenesis *in vitro*," *Stem Cells*, vol. 24, no. 4, pp. 835–843, 2006.

[28] A. Nasu, M. Ikeya, T. Yamamoto et al., "Genetically matched human iPS cells reveal that propensity for cartilage and bone differentiation differs with clones, not cell type of origin," *PLoS ONE*, vol. 8, no. 1, Article ID e53771, 2013.

[29] D. A. Shimko, C. A. Burks, K. C. Dee, and E. A. Nauman, "Comparison of *in vitro* mineralization by murine embryonic and adult stem cells cultured in an osteogenic medium," *Tissue Engineering*, vol. 10, no. 9-10, pp. 1386–1398, 2004.

[30] V. Sottile, A. Thomson, and J. McWhir, "*In vitro* osteogenic differentiation of human ES cells," *Cloning and Stem Cells*, vol. 5, no. 2, pp. 149–155, 2003.

[31] Y. Dogaki, S. Y. Lee, T. Niikura et al., "Efficient derivation of osteoprogenitor cells from induced pluripotent stem cells for bone regeneration," *International Orthopaedics*, vol. 38, no. 9, pp. 1779–1785, 2014.

[32] L. Duplomb, M. Dagouassat, P. Jourdon, and D. Heymann, "Differentiation of osteoblasts from mouse embryonic stem cells without generation of embryoid body," *In Vitro Cellular & Developmental Biology—Animal*, vol. 43, no. 1, pp. 21–24, 2007.

[33] K. Kim, A. Doi, B. Wen et al., "Epigenetic memory in induced pluripotent stem cells," *Nature*, vol. 467, no. 7313, pp. 285–290, 2010.

[34] K. Hynes, D. Menicanin, K. Mrozik, S. Gronthos, and P. M. Bartold, "Generation of functional mesenchymal stem cells from different induced pluripotent stem cell lines," *Stem Cells and Development*, vol. 23, no. 10, pp. 1084–1096, 2014.

[35] V. Sanchez-Freire, A. S. Lee, S. Hu et al., "Effect of human donor cell source on differentiation and function of cardiac induced pluripotent stem cells," *Journal of the American College of Cardiology*, vol. 64, no. 5, pp. 436–448, 2014.

Stem Cell Rev and Rep (2015) 11:635–644
DOI 10.1007/s12015-015-9592-x

Increased In Vitro Osteopotential in SHED Associated with Higher *IGF2* Expression When Compared with hASCs

Roberto Dalto Fanganiello[1] · **Felipe Augusto Andre Ishiy**[1] · **Gerson Shigeru Kobayashi**[1] · **Lucas Alvizi**[1] · **Daniele Yumi Sunaga**[1] · **Maria Rita Passos-Bueno**[1]

Published online: 1 May 2015

Abstract Mesenchymal stem cell (MSC) osteogenic differentiation potential varies according to factors such as tissue source and cell population heterogeneity. Pre-selection of cell subpopulations harboring higher osteopotential is a promising strategy to achieve a thorough translation of MSC-based therapies to the clinic. Here, we searched for novel molecular markers predictive of osteopotential by comparing MSC populations from two sources harboring different osteogenic potentials. We show that MSCs from human deciduous teeth (SHED) have an intrinsically higher osteogenic potential when compared with MSCs from human adipose tissue (hASCs) under the same in vitro controlled induction system. Transcriptome profiling revealed *IGF2* to be one of the top upregulated transcripts before and during early in vitro osteogenic differentiation. Further, exogenous IGF2 supplementation enhanced alkaline phosphatase activity and matrix mineralization, and inhibition of IGF2 lessened these parameters in SHED and hASCs, validating *IGF2* as an osteogenic factor in these MSCs. Further, we found *IGF2* to be biallelically expressed in SHED, but not in hASCs. We observed a 4 % methylation increase in the imprinting control region within the *IGF2-H19* locus in SHED, and this is mainly due to 2 specific CpG sites. Thus, we suggest that *IGF2* upregulation in SHED is due to loss of imprinting. This study unravels osteogenic properties in SHED, implying *IGF2* as a potential biomarker of MSCs with higher osteopotential, and unveils *IGF2* loss-of-imprinting in SHED.

Keywords SHED · hASCs · In vitro osteopotential · *IGF2* · Imprinting · Biallelic expression

Introduction

Studies on the use of mesenchymal stem cells (MSCs) for cellular therapies with the ultimate goal of bone regeneration are mainly based on their capacity of self-renewal, direct differentiation toward the osteogenic lineage and the ability to secrete trophic factors that may contribute to bone repair [1, 2]. These characteristics have been firstly explored in bone marrow mesenchymal stem cells (BMSCs) both in the lab and in different clinical scenarios [3–5]. However, BMSCs are scarce, and bone marrow harvesting remains painful and laborious. Therefore, there is an increasing interest in studying osteogenic cells from more convenient tissue sources, such as dental pulp and adipose tissue.

Stem cells from human exfoliated deciduous teeth (SHED), a specific type of dental pulp stem cell (DPSC), are potentially useful due to their differentiation plasticity, noninvasive isolation process, and similarity to osteoprogenitor cells [6–9]. SHED have been used to repair cranial defects in immunocompromised mice [10], to reconstruct trabecular bone in systemic lupus erythematosus-like MRL/lpr mice [8], and to aid critical-size calvarial defect regeneration in Wistar rats [11]. Human adipose tissue-derived stem cells (hASCs) represent another promising MSC type since they can be harvested from the stromal-vascular fraction of adipose tissue in abundant quantities by a simple surgical procedure. Their osteogenic potential has been demonstrated by the use of different culture

Electronic supplementary material The online version of this article (doi:10.1007/s12015-015-9592-x) contains supplementary material, which is available to authorized users.

✉ Roberto Dalto Fanganiello
robertofanganiello@gmail.com

[1] Departamento de Genética e Biologia Evolutiva, Instituto de Biociências, Universidade de São Paulo, Rua do Matao, 277, sala 200, Sao Paulo, SP, Brazil 05508-090

conditions containing osteoinductive factors [12–15] and hASCs were used in clinical trials, however, with a limited number of cases [16, 17].

In spite of these reports, evidence for sound clinical efficacy of the use of MSCs for bone regeneration has been challenging to confirm, and the therapeutic mechanisms supposedly leading to bone formation are incompletely understood and increasingly speculative. In addition, no therapy based on MSCs has yet had FDA approval [18]. Despite many studies examining SHED- and hASC-mediated osteogenesis and bone formation [6, 8–10, 19–23], the molecular rules that govern their osteopotential are still under debate. Variable differentiation potential is seen both in MSCs from different tissue sources and in cellular populations from the same tissue source, the latter being attributed to cell heterogeneity [24], and success of MSC-based bone regenerative medicine could be improved with pre-selection of cells harboring higher osteogenic potential [23, 25–27]. Therefore, this study has three main aims: 1) to compare the in vitro osteopotential of SHED and hASCs under the same induction system; 2) to identify molecular mechanisms governing osteogenic properties in these MSCs; 3) to identify predictive markers of osteogenic potential in these MSCs.

Material and Methods

Ethics and Financial Interest Statement

This study was approved by the Institute of Biosciences'Human Research Ethics Committee (permit number 104.120.09). We certify that no financial support or benefits have been received by any co-author or from any commercial source directly or indirectly related to the work reported in this article.

Isolation of Dental Pulp and Adipose-Tissue Derived Stem Cells

SHED populations were isolated from donated deciduous teeth obtained upon signed informed consent by the subjects'legal guardians. Dental pulps were extracted from normal deciduous teeth of six subjects (aged from 6 to 10 years). Donors were previously evaluated for systemic diseases and oral infections and subjects with these conditions were excluded. Dental pulp fragments were retrieved with a barbed nerve broach instrument and cells were isolated according to the protocol described in Miura et al., 2003 [6].

hASCs were isolated from sub-abdominal adipose tissue obtained after liposuction procedures upon informed consent. Adipose tissue was obtained from six subjects (aged from 24 to 68 years) undergoing elective liposuction procedure. The unprocessed lipoaspirate was washed with equivalent volume of PBS supplemented with 1 % Pen Strep (Life Technologies, CA., USA) and enzymatically dissociated with 0.075 % collagenase type I (Sigma-Aldrich, St. Louis, USA). Enzyme activity was neutralized with DMEM/F12 (Life Technologies, CA., USA) containing 10 % fetal bovine serum (FBS; Life Technologies, CA., USA). Infranatant was centrifuged at 1, 200xg for 5 minutes to pellet cells. Cells were seeded in 6-well culture plates (Corning, N.Y., USA) containing MSC growth medium (DMEM/F12 supplemented with 15 % FBS, 1 % Pen Strep and 1 % MEM non-essential aminoacids (Life Technologies, CA., USA).

After 14 days, SHED and hASCs cultures were washed with 1x PBS, dissociated with TrypLE (Life Technologies, CA, USA) and seeded at a 10 [4] cells/cm [2] concentration onto 25 cm [2] culture flasks (Corning, N.Y., USA). Cells were kept in MSC growth medium at 37 °C in a 5 % CO2 humidified incubator and maintained in semi-confluence to prevent differentiation. Passages were done every 4–5 days and medium was refreshed every 3 days. All experiments were performed between the third and fifth subculture, with n=6 for the SHED and the hASCs groups and samples were not pooled.

Immunophenotyping

Immunophenotype characterization of cultured SHED and hASC populations was done by flow cytometry analysis. Cellular populations were harvested with TrypLe (Invitrogen, CA, USA), washed with 1x PBS and incubated with BSA for 1 hour at 4 °C with the following anti-human antibodies: CD29-PECy5, CD34PerCP, CD31-PE, CD45-FITC, CD90-R-PE, CD73-PE, CD105-PE (Becton, Dickinson and Company, NJ, USA). Matched control samples were incubated with PBS free of antibodies. Cell suspensions were washed with PBS, and 10,000 labeled cells were analyzed using a Guava easyCyte flow cytometer running the Guava ExpressPlus software (Merck Millipore, Darmstadt, Germany). Experiments were done in technical triplicates for each cell sample and for each antibody.

In vitro Osteogenic Differentiation Experiments

Subconfluent cell populations of SHED and hASCs were treated with osteogenic induction medium containing DMEM-Low Glucose (Life Technologies, CA., USA) supplemented with 10 % FBS (Invitrogen, CA., USA), 50μM ascorbate-2-phosphate, 10 mM β-glycerophosphate, 0.1μM dexamethasone (Sigma-Aldrich, St. Louis, USA), 100 U/ml penicillin, 100 g/ml streptomycin (Invitrogen, CA., USA) with media changes every three days. Alkaline phosphatase activity was assessed through a biochemical assay on the 9th day of in vitro osteogenic differentiation (SHED: n=6; hASCs: n=6). Briefly, cells were provided with phosphatase substrate (Sigma-Aldrich, St. Louis, USA) and the resulting p-

nitrophenol was quantified colorimetrically using a Multiskan EX ELISA plate reader (Thermo Scientific, MA., USA) at 405 nm. Calcium matrix production was analyzed after 21 days of in vitro osteogenesis by Alizarin Red-S staining (SHED: n=6; hASCs: n=6). Cells were washed three times with 1xPBS, fixed with a 70 % ethanol solution for 30 minutes at room temperature, followed by three distilled water washes and finally stained with a 0.2 % Alizarin Red-S solution (Sigma-Aldrich, St. Louis, USA) for 30 min at room temperature. Staining was removed with a solution of 20 % methanol / 10 % acetic acid and measured colorimetrically using a Multiskan EX ELISA plate reader at 450 nm. As a negative control for both assays we used the same cells cultivated in regular proliferation medium. Experiments were done in technical triplicates for each time point and for each cell line.

RNA Extraction, Microarray and qRT-PCR Experiments

SHED and hASCs at 80 % confluence seeded in 25 cm [2] cell culture flasks were used for in vitro osteoinduction followed by RNA extraction and microarray / RT-qPCR assays. Total RNA was isolated from osteogenic medium-treated cells and untreated cells using a Nucleospin RNA II kit (Macherey-Nagel, Duren, Germany), following manufacturer's instructions. RNA quality and concentration were measured by 2 % agarose gel electrophoresis and Nanodrop ND-1000 (Thermo Scientific, MA., USA), respectively.

Gene expression microarray assays were performed at three time points of early in vitro osteogenesis: immediately before induction (day 0) and at days 4 and 6 of osteoinduction. cDNA was prepared with Affymetrix GeneChip WT cDNA Synthesis and Amplification Kit (Affymetrix, CA., USA), following manufacturer's instructions. cDNA fragmentation and labeling was performed with Affymetrix GeneChip WT Terminal Labeling Kit (Affymetrix, CA., USA) and 5.5 μg of labeled cDNA target was used to hybridize Affymetrix GeneChip Human Gene 1.0 ST array chips (Affymetrix, CA., USA) for 16 h at 45 °C, following manufacturer's instructions. Chips were washed and stained using an Affymetrix GeneChip Fluidics Station 450 and scanned using an Affymetrix GCS 3000 scan (Affymetrix, CA., USA). Raw microarray data were normalized through Robust Multichip Average preprocessing method [28] and the ComBat method was applied for the batch effect corrections [29]. Only genes showing high expression variance among arrays were retained through the use of interquartile range (IQR=1). Multi-class Significance Analysis of Microarrays (SAM, $p \leq 0.05$ [30],) adjusted by False Discovery Rate [31] was used to detect the differentially expressed genes (DEGs) for each time-point (immediately before induction and at days 4 and 6 of osteoinduction) in each stem cell group (BMSCs, SHED and hASCs). Ingenuity Pathway Analysis (IPA®, QIAGEN Redwood City, www.qiagen.com/ingenuity) software was used for gene interaction analysis and functional classification of differentially expressed genes. Hierarchical clustering was performed with EXPANDER (EXpression Analyzer and DisplayER - http://acgt.cs.tau.ac.il/expander/), under standard parameters.

Gene expression of osteogenic markers (*DLX5*, *RUNX2*, *BGLAP* and *ALP*) and *IGF2* was quantified before (T0) and after one, two and three days (T1, T2 and T3) of in vitro osteogenic induction by qRT-PCR (SHED: n=3; hASCs: n=3). Briefly, one microgram of total RNA extracted from SHED and from hASCs populations (SHED: n=3; hASCs: n=3) was converted into cDNA using Superscript II, according to manufacturer's recommendations. cDNAs from each cell type were pooled and used as a calibrator. qRT-PCR reactions were performed in triplicates with final volume of 25 μL, using 20 ng cDNA, 2X SYBR Green PCR Master Mix, and 50 nM – 200 nM of each primer. Fluorescence was detected using ABI Prism 7500 Sequence Detection System, under standard temperature protocol. Primers were designed with Primer-BLAST (http://www.ncbi.nlm.nih.gov/tools/primer-blast/; see Table S1 for primer sequences). Primers' amplification efficiencies (E) were determined by serial cDNA dilutions expressed in $\log_{10}$ in which $E=10^{-1/slope}$. Expression of target genes was assessed relative to a calibrator cDNA pool (ΔCt). GeNorm v3.4 [32] was used to calculate normalization factors for each sample, considering *GAPDH*, *HPRT1* and *SDHA* endogenous expression. The final expression values were determined based on a previous method [33] dividing $E^{-\Delta Ct}$ by the corresponding normalization factor. Primers and reagents were supplied by Life Technologies.

Western Blotting

SHED and hASCs were plated at a density of 4000 cells/cm [2] in 75 cm [2] flasks and cultured until 80 % confluence in MSC growth medium and serum-starved in DMEM/F12 without FBS for 48 h. Total protein lysates were obtained using RIPA Buffer (1 % NP-40, 0.5 % SDS, 0.5 % Sodium Deoxycholate, 50 mM Tris–HCl, 150 mM NaCl and 1 mM EDTA) containing protease and phosphatase inhibitor cocktails (Sigma-Aldrich, St. Louis, USA). Protein concentration was determined using a bicinchoninic acid assay kit according to manufacturer's instructions (Thermo Fisher Scientific, IL., USA). Total cell lysates (20 μg) were separated by SDS-PAGE and dry-transferred to nitrocellulose membranes with the iBlot system (Life Technologies, CA., USA) according to manufacturer's recommendations. Membranes were blocked in buffer TBS-T (1 M Tris–HCl pH 7.5, 5 M NaCl, 0.1 % Tween-20) 5 % BSA under constant stirring for 1 h at room temperature, washed 4x with TBS-T, and incubated with anti-IGF2 (1:1000 dilution in TBS-T/BSA; SAB1408589 – Sigma-Aldrich, St. Louis, USA) primary antibody overnight at 4 °C. Detection was performed using anti-rabbit IgG, HRP-

linked Antibody (1:2000 dilution in TBS-T/BSA; Cell Signaling) under constant stirring for 1 h at room temperature, ECL Prime substrate (GE Healthcare), and Image Quant LAS 4000 Mini (General Electrics). β-actin was used as a loading control (HRP-linked anti-β-actin, Abcam). The intensity of the bands was determined by densitometry using NIH ImageJ software (http://rsbweb.nih.gov/ij/). IGF2 protein levels were quantified and normalized to the corresponding β-actin levels.

IGF2 and Chromeceptin Treatments

To test the effects of IGF2 supplementation and chromeceptin treatment (C0868 – Sigma-Aldrich, St. Louis, USA) on SHED and hASCs osteogenic potential, we added IGF2 (ProsPec, CYT-265) and chromeceptin (Sigma-Aldrich, St. Louis, USA) to the osteogenic medium at a concentration of 2x10 [2] nM and 0.3 μM respectively, in independent experiments. Alkaline phosphatase activity was assessed after 9 days of in vitro osteogenesis and alizarin red-S staining was performed after 21 days of osteoinduction for both treatments. These experiments were performed in 3 SHED and 3 hASC independent populations.

IGF2 Genotyping

Genotypes of 10 SHED and 10 hASCs populations for potential IGF2 polymorphisms were determined by PCR and Sanger sequencing of genomic DNA and cDNA. Optimal annealing temperatures for each primer pair was determined by PCR on a gradient thermal cycler (Table 1).

Bisulfite Sequencing

Bisulfite treatment was used to convert unmethylated cytosines to uracil. Two micrograms of genomic DNA were bisulfite treated using the Epitect Bisulfite Kit (QIAGen), following manufacturer's recommendations. From 20 μl of eluted converted DNA, 1 μl was used for subsequent PCR. Primers sequences *TGAGATTTTTTTGTAGGGTTTATG* and *AAAA CACCTCATTATTCCCCTAATAT* were used to amplify the *IGF2* converted region, with the following cycling conditions: 95 °C for 5 min followed by 40 cycles of 94 °C for 30 sec, 54 °C for 3 min, 72 °C for 1 min and one cycle of 72 °C for 5 min. PCR products were cloned using the TOPO TA Cloning kit (Life Technologies, CA., USA) and 10 clones per sample were submitted to sequencing reaction using the BigDye® Terminator v3.1 Cycle Sequencing Kit (Life Technologies, CA., USA) and sequenced in the ABI 3730 DNA Analyzer. Finally, CpG methylation levels in each clone were calculated using the BISMA (Bisulfite Sequencing DNA Methylation Analysis) online tool.

Statistical Analysis

Continuous variables were expressed by mean and standard deviation, and groups were compared by Student's *t*-test. A p-value<0.05 was considered statistically significant. Tests were done using the GraphPad InStat software (GraphPad) [34].

Results

After isolation, both SHED and hASCs displayed spindle-shaped fibroblastoid morphology. They showed a similar and homogeneous immunophenotype regarding the panel of cell surface markers: SHED and hASCs expressed similarly high levels of mesenchymal markers (>95 % for CDs 29, 73, 90, 105) and low levels of endothelial (<2 % for CD31) and hematopoietic (<2 % of CDs 34 and 45) markers. Thus, these results attest their mesenchymal origin (figure S1).

Both cell groups showed increased expression of osteogenic markers after three days of in vitro osteogenesis (*RUNX2*, *ALP* and *BGLAP* in SHED and *RUNX2*, *ALP* and *DLX5* in hASCs). Alkaline phosphatase (ALP) activity was higher and mineralized matrix was produced, respectively, after 9 and 21 days of osteoinduction in SHED and hASCs (Fig. 1a-d). Even though SHED and hASCs responded positively to osteoinduction, gene expression of osteogenic markers was generally higher in SHED when compared with hASC populations (Fig. 1a). Additionally, ALP activity after 9 days of osteoinduction and extracellular matrix mineralization after 21 days of in vitro osteogenesis were increased 1.61-fold ($p<0.05$) and 2.24-fold ($p<0.0001$), respectively, in SHED when compared with hASCs (Fig. 1b-d). These results

Table 1 Primers used for real-time quantitative PCR experiments

Gene	NCBI reference sequence code	Forward sequence	Reverse sequence
RUNX2	NM_001024630.3	AGTGGACGAGGCAAGAGTTTC	GTTCCCGAGGTCCATCTACTG
ALP	NM_000478.4	GATACAAGCACTCCCACTTCATCTG	CTGTTCAGCTCGTACTGCATGTC
GAPDH	NM_001256799.1	TGCACCACCAACTGCTTAGC	GGCATGGACTGTGGTCATGA
HPRT1	NM_000194.2	TGACACTGGCAAAACAATGC	GGTCCTTTTCACCAGCAAGCT
SDHA	NM_004168.2	TGGGAACAAGAGGGCATCTG	CCACCACTGCATCAAATTCA

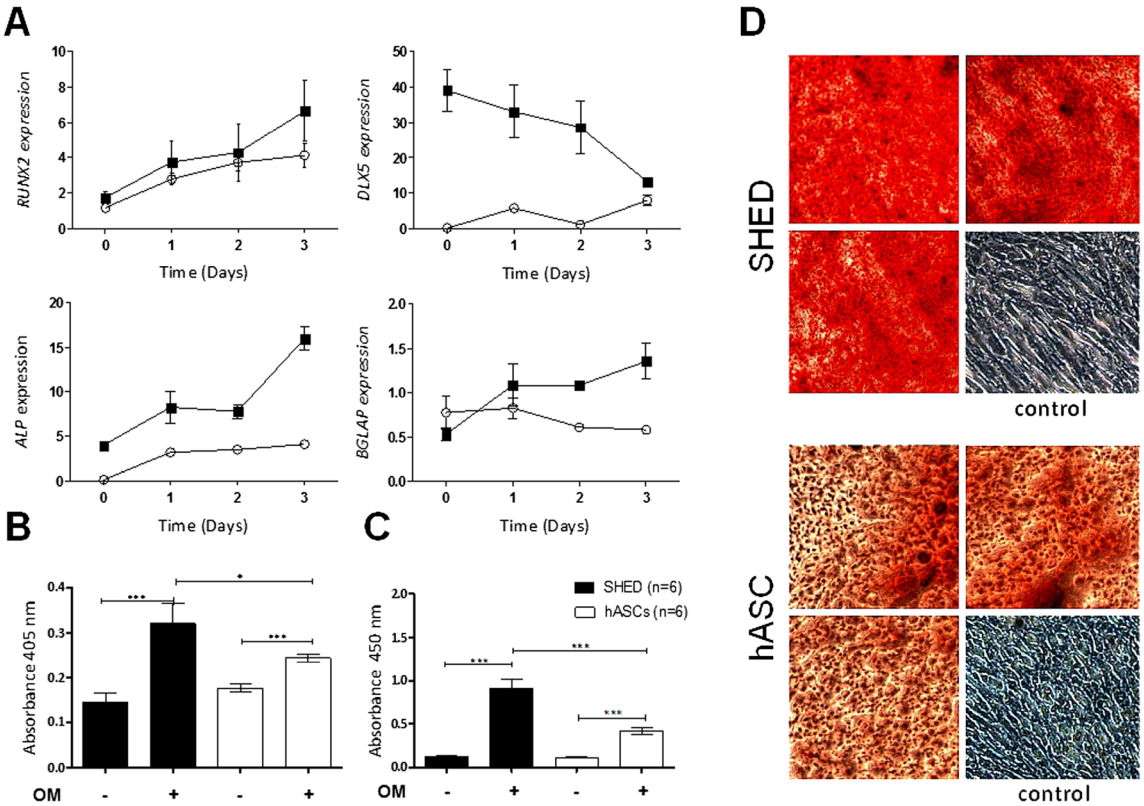

Fig. 1 Analysis of early osteogenesis in SHED and hASCs (n=6 per cell type). **a**) qRT-PCR results for *DLX5*, *RUNX2*, *ALP* and *BGLAP* during the first 3 days of osteoinduction. Quantification of alkaline phosphatase activity (**b**) and alizarin red-S staining (**c**), respectively at the 9th and 21st day of in vitro osteogenic differentiation. **d**) Representative micrographs of the alizarin red-S staining after 21 days of in vitro osteoinduction

suggest that SHED present increased in vitro osteogenic potential as compared to hASCs.

In order to investigate the molecular mechanisms behind the osteogenic differences between SHED and hASCs, we performed global gene expression profiling during three time points of early in vitro osteogenesis: immediately before induction (day 0) and at days 4 and 6 of osteoinduction in SHED and hASCs, using human BMSCs (hBMSCs) as a positive control. By comparing the expression profiles in these three time points for each cell group, we identified 34 differentially expressed genes (DEGs) in SHED, 87 in hASCs and 198 in hBMSCs. We first tested if DEGs exclusively shared by SHED and hBMSCs groups during early osteogenesis contribute to enrichment in pathways associated with osteogenesis. Eleven differentially expressed transcripts were common between hBMSCs and SHED, but they were not identified as DEGs in hASCs; further, through the use of the Ingenuity Pathway Analysis software, we observed that Interleukin 17A (p<6.13 e-4) and RXR/RAR pathways (p<1.85 e-4), both previously associated with osteogenesis, were the most enriched in SHED and hBMSC groups. On the other hand, 43 DEGs were shared exclusively by hBMSCs and hASCs, and using IPA we observed that Serine biosynthesis (p<4.75 e-5) and Superfamily of Serine and Glycine Biosynthesis (p<9.94e-5), none of them involved in osteogenesis, were identified as the most enriched pathways in this group. These data, together with the osteogenic differentiation comparison, show an overall increase in SHED osteopotential when compared with hASCs.

In a second analysis aiming to identify molecular markers predictive of osteodifferentiation capacity, we performed a hierarchical clustering of each cell population grouped per time point. *IGF2* and *ITGA8* were revealed as the top upregulated transcripts in SHED and hBMSCs in comparison with hASCs at day 0 (before osteoinduction), and *IGF2* remained upregulated in these MSCs until day 6 of early osteogenesis (Fig. 2a). Considering the important role played by *IGF2* during bone formation, remodeling and homeostasis [35, 36], and the upregulated pattern of *IGF2* in early osteogenesis in SHED and hBMSCs, we selected *IGF2* for validation of mRNA and protein expression in SHED cultures in comparison with hASCs cultures. Both *IGF2* mRNA upregulation and higher IGF2 protein production were observed in SHED as compared to hASCs before osteoinduction (day 0, average of 32.2-fold upregulation in *IGF2* mRNA, $p \leq 0.01$, n=10 per cell group, and p<0.05, n=11 per cell group for IGF2 protein expression) (Fig. 2b-c). We also validated *IGF2* mRNA upregulation during the first 8 days of in vitro osteogenesis (Fig. 2c).

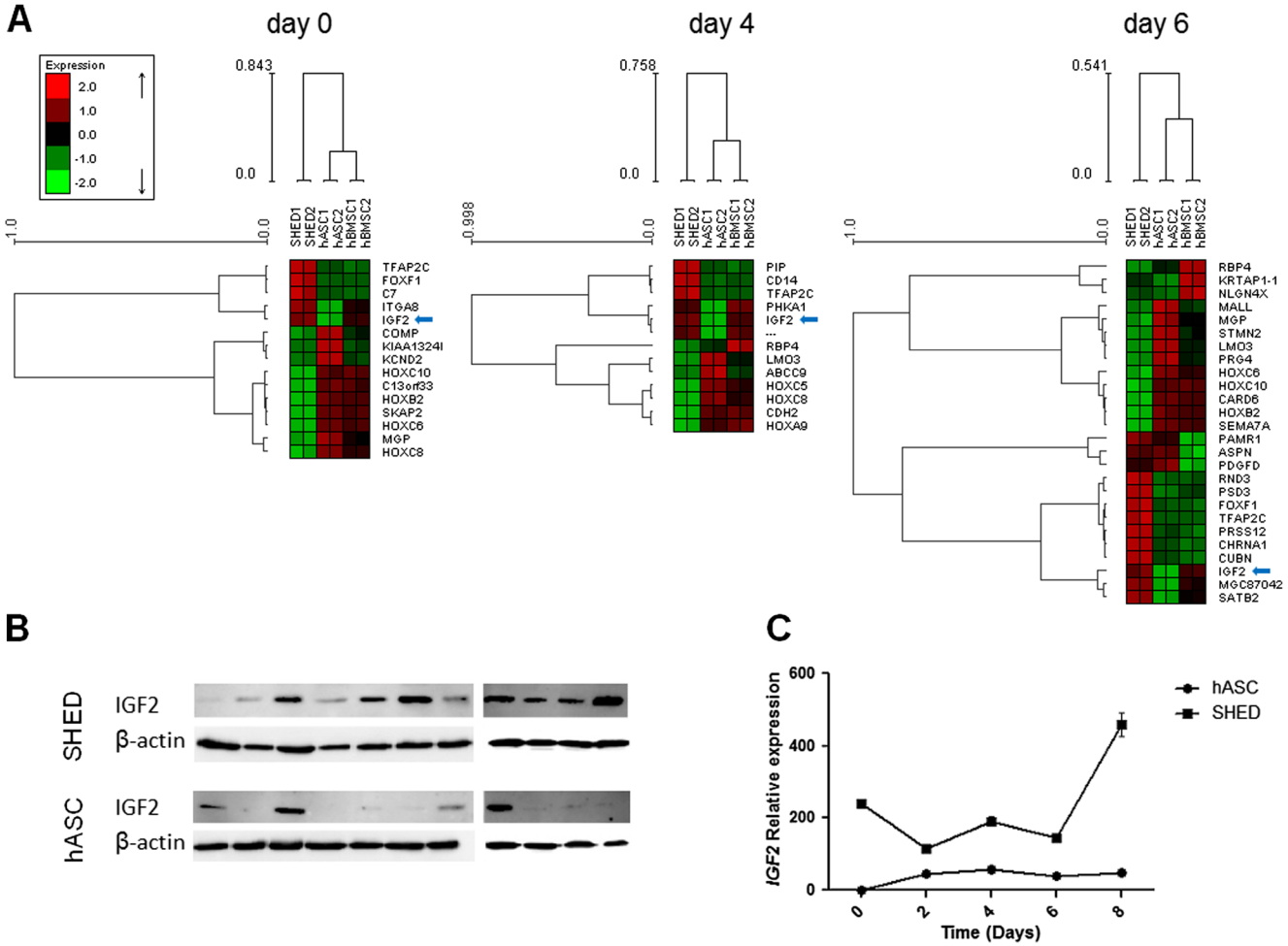

Fig. 2 **a**) Hierarchical clustering analysis showing expression patterns of differentially expressed transcripts during early in vitro osteogenesis in SHED, hASCs and hBMSCs (n=2 per cell type, days 0, 4 and 6). *IGF2* upregulation in SHED and hBMSC is indicated by the *blue arrows*. **b**) Western blotting for IGF2 detection in SHED and hASCs (n=11 for each sample, day 0), anti β-actin antibody was used as loading control. **c**) qRT-PCR of *IGF2* during the first 8 days of in vitro osteoinduction in SHED and hASCs (n=3 per cell type)

To characterize the effect of IGF2 signaling during osteogenesis in SHED and hASCs we added exogenous IGF2 to the osteogenic medium used for in vitro osteoinduction. This treatment intensified osteogenesis both in SHED and in hASC cultures, shown by enhanced ALP activity after 9 days of osteoinduction (1.19 times in SHED, $p<0.01$; 1.30 times in hASCs, $p<0.001$, n=3 per cell group, Fig. 3a) and mineralized matrix production after 21 days of in vitro osteogenesis (3.04 times in SHED, $p<0.05$; 4.41 times in hASCs, $p<0.001$, n=3 per cellular group, Fig. 3a). Next, we administered chromeceptin, an IGF2 inhibitor at both the transcriptional and signaling levels, during in vitro osteoinduction. Chromeceptin treatment led to a significantly lower ALP activity (2.43 times in SHED, $p<0.001$; 2.482 times in hASCs, $p<0.001$, n=3 per cell group, Fig. 3b) and matrix mineralization (1.351 times in SHED, $p<0.01$; 1.572 times in hASCs, $p<0.05$, n=3 per cell group, Fig. 3b) both in SHED and hASCs. These results show a direct correlation between IGF2 pathway activation and in vitro osteogenesis in these MSCs.

We hypothesized that *IGF2* upregulation in SHED may be due to an increase in methylation of the CpG-rich imprinting controlling center within the *IGF2-H19* intergenic region [37, 38] or deviations from the monoallelic expression accounted for this locus. First, we determined the methylation status of 17 CpG sites in the *IGF2-H19* intergenic region (n=10 per cellular population and n=10 clones per sample) by bisulfite sequencing. SHED samples had 50.9 % of methylated CpGs in comparison with 46.9 % in hASCs ($p\leq0.0001$). Since this difference could be due to site-specific increased methylation, we next compared the differences in methylation per site and verified that sites 3 and 16 have significantly higher methylation on SHED samples when compared with hASCs (20.1 % increase, p=0.014 and 18.3 % increase, p=0.023, respectively).

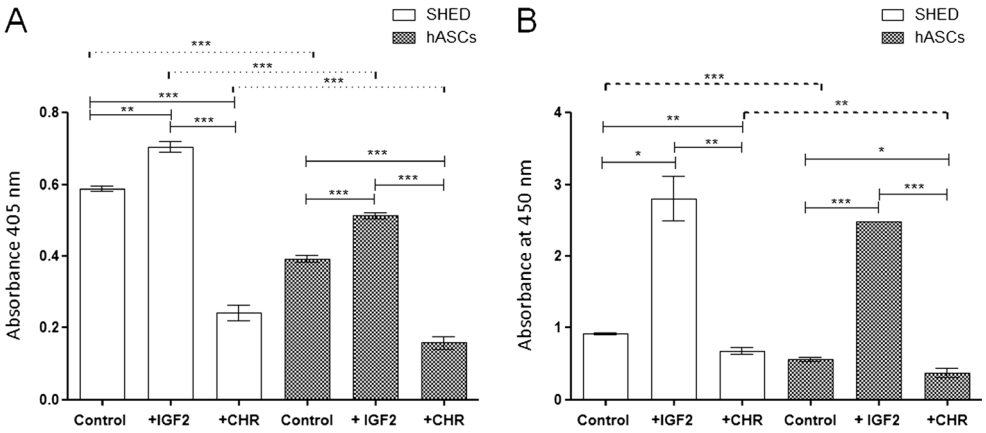

Fig. 3 **a**) Alkaline phosphatase activity and (**b**) alizarin red-S quantification of SHED and hASC in vitro osteogenesis, respectively after 9 and 21 days of osteoinduction with addition of exogenous IGF2 (+IGF2) or chromeceptin (+CHR), an IGF2 inhibitor at the transcriptional and signaling levels (n=3 per cell type)

Additionally, to investigate whether allelic transcriptional imbalances could be leading to the higher *IGF2* expression observed in SHED, we genotyped the *IGF2* polymorphism rs3168310 in SHED and hASCs (n=10 per cell population) by sequencing their genomic DNA as well as cDNA. Four SHED and one hASC population were informative (heterozygous at one or more polymorphisms at the genomic level – Fig. 4). In this group, the hASC population was homozygous at the cDNA level, thus displaying *IGF2* monoallelic expression, as expected. Conversely, the informative SHED populations were heterozygous at the cDNA level, which indicates *IGF2* biallelic expression in these cells. Sequencing of an additional polymorphism (rs2230948) confirmed these results (data not shown).

Discussion

Even though it is well established that SHED and hASCs are capable of undergoing osteogenesis in vitro, we show in this study that SHED have higher osteogenic potential when compared with hASCs under the same in vitro controlled conditions: SHED populations display higher gene expression of four hallmark osteogenesis markers (*RUNX2*, *DLX5*, *ALP* and *BGLAP*) during the first three days of in vitro

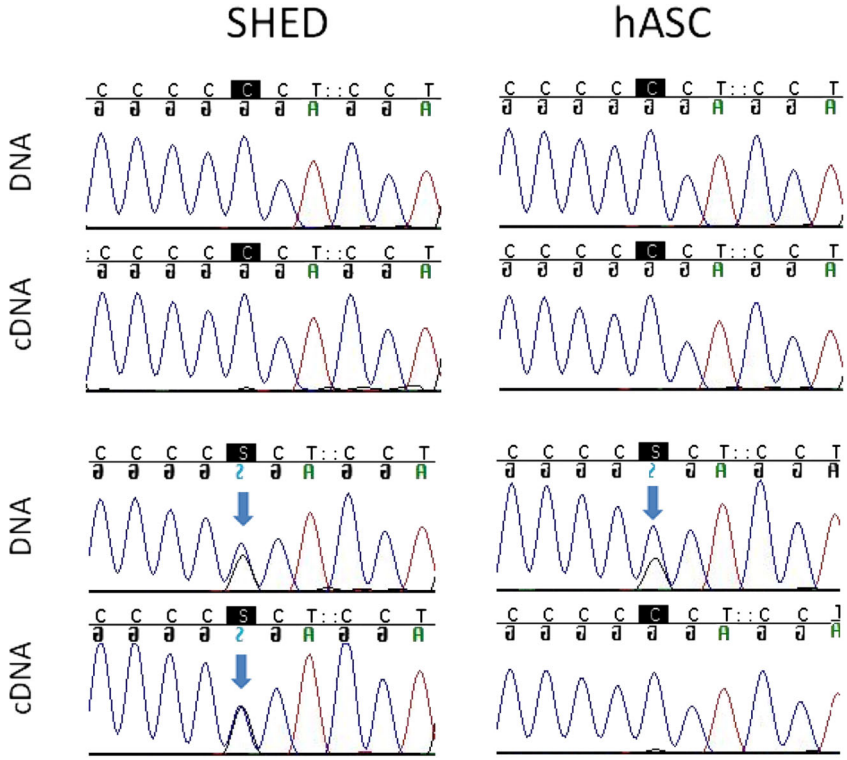

Fig. 4 Electropherograms of DNA and cDNA sequencing of rs3168310 (C/G) *IGF2* polymorphism in SHED and hASC samples (n=10 per cell type). *Blue arrows* indicate heterozygosis

osteodifferentiation, higher alkaline phosphatase (ALP) activity after 9 days of osteoinduction and produce more mineralized matrix after 21 days of in vitro osteogenesis, when compared with hASCs.

To better understand the molecular underpinnings of these variations in osteogenic differentiation efficiency, we performed microarray-based genome-wide expression profiling in three time points spanning early SHED and hASC in vitro osteogenesis. Interleukin-17A (IL-17A) and Retinoid X Receptor / Retinoic Acid Receptor (RXR/RAR) pathways, the most enriched pathways in SHED and hBMSCs during early osteogenesis, are recognized as important mediators of bone metabolism and homeostasis [39–41]. However, no enrichment of osteogenesis pathway was observed in hASCs. These results endorse that enrichment of these pathways during early in vitro osteogenesis of SHED and hBMSCs are in line with the higher in vitro osteogenic potential displayed by them as compared with hASCs.

The comparative transcriptome analysis grouping each cellular population per time point (0, 4 and 6 days of in vitro osteoinduction) led to the identification of *IGF2* as a differentially expressed transcript before and during early osteoinduction in SHED and hBMSCs. We demonstrated that both IGF2 mRNA and protein are upregulated in SHED when compared with hASCs, suggesting that IGF2 plays an important role in the increased in vitro osteogenesis observed in SHED when compared with hASCs.

We validated IGF2 as an osteogenic factor in SHED by verifying that supplementation with exogenous IGF2 enhanced alkaline phosphatase and matrix mineralization both in SHED and hASCs while treatment with chromeceptin efficiently inhibited osteogenesis in both cell types. Moreover, hASCs supplementation with IGF2 during in vitro osteogenesis rescues their osteogenic potential, which becomes very similar to SHED osteopotential. In fact, IGF2 is known to be highly expressed in bone tissue and is recognized to promote bone formation and remodeling [35, 42–44]. It has also been shown that upregulation of IGF2 is implicated in priming MSC differentiation into osteoprogenitor cells, in in vivo osteogenesis and in adult bone remodeling in mice [45].

The finding of endogenous upregulation of *IGF2* before osteoinduction in a MSC population with intrinsically higher osteopotential suggests that this molecule can be a candidate predictive biomarker of bone formation. In this regard, with the purpose of identifying differentiation-stage specific markers defining ex vivo osteoblastic phenotype, Twine et al. 2014 studied the gene expression profile of immortalized hMSC-TERT cells during different time-points of in vitro osteogenesis and identified *IGF2* as a late-stage osteogenic differentiation gene, with peak expression at 9 days of osteoinduction [46]. Even though *IGF2* upregulation was not reported in time points earlier than 9 days of in vitro differentiation, we do not believe this is in discordance with our results since the authors used only one type of MSCs to investigate temporal variations in gene expression during in vitro osteogenesis.

It is possible that the upregulation of *IGF2* in SHED is related to a different pre-differentiation state, to an enrichment of osteolineage progenitor cells or to an altered regulation pattern, which could be linked to the cell source niche. In this manuscript we report a global increase of 4 % in methylation of the *IGF2-H19* intergenic imprinting controlling region (ICR) in SHED, in comparison with hASCs, and these differences were mainly due to significantly higher methylation in two CpG sites in SHED populations, where methylation was increased at least more than 18 % for each site, compared with hASCs. We speculate that this mechanism could be associated with the biallelic *IGF2* expression found in SHED populations but not in hASCs. Although the differences in methylation are not more than two fold, it is well known that the stoichiometry of *IGF2* loss of imprinting leading to a doubling of *IGF2* mRNA abundance does not always occur [47]. Even though *IGF2* is maternally imprinted in most human tissues and transcribed exclusively from the paternally inherited chromosome [48], loss of imprinting has been observed in several situations. For example, *IGF2* overexpression due to dysregulation of *IGF2* imprinting is a hallmark of many human malignant tumors, including osteosarcoma, lung neoplasms, ovarian cancers and Wilms tumor, and it also occurs in Beckwith-Wiedemann Syndrome, a human genetic disease characterized by fetal overgrowth, organomegaly and tumor predisposition [49]. Loss of imprinting of *IGF2* has also been reported in normal human tissues, such as fetal and adult liver [50, 51], brain [52], newborn cord blood [53] and cervical tissue [54].

We suggest that *IGF2* upregulation in SHED is thus related to loss of imprinting. We cannot rule out that the *IGF2* expression differences between SHED and hASCs are due to the age difference of the primary donor tissues; however, in that case we would have observed the opposite, that is, older cells would be more likely to lose *IGF2* imprinting. In line with our findings, there is an increasing body of literature implicating epigenetic regulation as an important modulator of MSC osteogenesis [55–59].

As demonstrated in several studies, mesenchymal stem cells isolated from the dental pulp tissue of adult teeth (DPSCs) harbor a robust osteogenic potential [23, 25–27] and their use in clinical scenarios has commenced [60, 61]. In light of that, the findings outlined in this report help to provide a more solid ground to the use of SHED in stem-cell based tissue engineering and regenerative medicine.

Conclusion

In summary, this study contributes to the elucidation of intrinsic osteogenic properties associated with SHED and hASCs,

indicates *IGF2* as a potential biomarker to pre-select cells with increased osteogenic potential and reveals loss of *IGF2* imprinting in SHED. We expect that our findings will be helpful for a more thorough translation of the stem cell-based bone regeneration technology to the clinic. We also believe that our findings will contribute to the challenging issue of attaining better reproducibility and clinical efficacy in MSC-mediated bone formation.

Acknowledgments We would like to thank Constancia Gotto Urbani for secretarial assistance, Andressa Gois Morales and Simone Gomes Ferreira for technical support. We also thank Erika Yeh, PhD (University of California, San Francisco) and Luciane Portas Capelo, PhD (Federal University of Sao Paulo, Sao Jose dos Campos) for stimulating discussions. This work was supported by grants from the Brazillian Ministry of Health, Fundação de Amparo à Pesquisa do Estado de São Paulo (CEPID/FAPESP), Coordenação de Aperfeiçoamento de Pessoal de Nível Superior (CAPES), and Conselho Nacional de Desenvolvimento Científico e Tecnológico (CNPq).

Disclosure of Potential Conflict of Interest No potential conflict of interest was disclosed.

Author Contributions Roberto Dalto Fanganiello: conception and design, collection and assembly of data, data analysis and interpretation, manuscript writing

Felipe Augusto Andre Ishiy: collection and assembly of data, data analysis and interpretation, manuscript writing

Gerson Shigeru Kobayashi: data analysis and interpretation, manuscript writing

Lucas Alvizi: conception and design, collection and assembly of data, data analysis and interpretation, manuscript writing

Daniele Yumi Sunaga: conception and design, collection and assembly of data, data analysis and interpretation, manuscript writing

Maria Rita Passos-Bueno: conception and design, data analysis and interpretation, manuscript writing, financial support, administrative support

References

1. Caplan, A. I., & Correa, D. (2011). The MSC: an injury drugstore. *Cell Stem Cell, 9*, 11–5.
2. Kean, T. J., Lin, P., Caplan, A. I., & Dennis, J. E. (2013). MSCs: delivery routes and engraftment, cell-targeting strategies, and immune modulation. *Stem Cells International, 2013*, 732742.
3. Krebsbach, P. H., Mankani, M. H., Satomura, K., Kuznetsov, S. A., & Robey, P. G. (1998). Repair of craniotomy defects using bone marrow stromal cells. *Transplantation, 66*, 1272–8.
4. Shayesteh, Y. S., Khojasteh, A., Soleimani, M., Alikhasi, M., Khoshzaban, A., & Ahmadbeigi, N. (2008). Sinus augmentation using human mesenchymal stem cells loaded into a beta-tricalcium phosphate/hydroxyapatite scaffold. *Oral Surgery, Oral Medicine, Oral Pathology, Oral Radiology, and Endodontics, 106*, 203–9.
5. Nolff, M. C., Gellrich, N. C., Hauschild, G., et al. (2009). Comparison of two beta-tricalcium phosphate composite grafts used for reconstruction of mandibular critical size bone defects. *Veterinary and Comparative Orthopaedics and Traumatology, 22*, 96–102.
6. Miura, M., Gronthos, S., Zhao, M., et al. (2003). SHED: stem cells from human exfoliated deciduous teeth. *Proceedings of the National Academy of Sciences of the United States of America, 100*, 5807–12.
7. Graziano, A., d'Aquino, R., Laino, G., et al. (2008). Human CD34+ stem cells produce bone nodules in vivo. *Cell Proliferation, 41*, 1–11.
8. Yamaza, T., Kentaro, A., Chen, C., et al. (2010). Immunomodulatory properties of stem cells from human exfoliated deciduous teeth. *Stem Cell Research & Therapy, 1*, 5.
9. Wang X, Sha XJ, Li GH, et al. Comparative characterization of stem cells from human exfoliated deciduous teeth and dental pulp stem cells. Archives of oral biology 2012.
10. Seo, B. M., Sonoyama, W., Yamaza, T., et al. (2008). SHED repair critical-size calvarial defects in mice. *Oral Diseases, 14*, 428–34.
11. de Mendonca, C. A., Bueno, D. F., Martins, M. T., et al. (2008). Reconstruction of large cranial defects in nonimmunosuppressed experimental design with human dental pulp stem cells. *The Journal of Craniofacial Surgery, 19*, 204–10.
12. Levi, B., & Longaker, M. T. (2011). Concise review: adipose-derived stromal cells for skeletal regenerative medicine. *Stem cells (Dayton, Ohio), 29*, 576–82.
13. Goh, B. C., Thirumala, S., Kilroy, G., Devireddy, R. V., & Gimble, J. M. (2007). Cryopreservation characteristics of adipose-derived stem cells: maintenance of differentiation potential and viability. *Journal of Tissue Engineering and Regenerative Medicine, 1*, 322–4.
14. Dragoo, J. L., Choi, J. Y., Lieberman, J. R., et al. (2003). Bone induction by BMP-2 transduced stem cells derived from human fat. *Journal of Orthopaedic Research, 21*, 622–9.
15. Hattori, H., Sato, M., Masuoka, K., et al. (2004). Osteogenic potential of human adipose tissue-derived stromal cells as an alternative stem cell source. *Cells, Tissues, Organs, 178*, 2–12.
16. Lendeckel, S., Jodicke, A., Christophis, P., et al. (2004). Autologous stem cells (adipose) and fibrin glue used to treat widespread traumatic calvarial defects: case report. *Journal of Cranio-Maxillo-Facial Surgery, 32*, 370–3.
17. Mesimaki, K., Lindroos, B., Tornwall, J., et al. (2009). Novel maxillary reconstruction with ectopic bone formation by GMP adipose stem cells. *International Journal of Oral and Maxillofacial Surgery, 38*, 201–9.
18. Daley, G. Q. (2012). The promise and perils of stem cell therapeutics. *Cell Stem Cell, 10*, 740–9.
19. Levi, B., Peault, B., & James, A. W. (2014). Bone tissue engineering and regeneration. *BioMed research international, 2014*, 137529.
20. Halvorsen, Y. D., Franklin, D., Bond, A. L., et al. (2001). Extracellular matrix mineralization and osteoblast gene expression by human adipose tissue-derived stromal cells. *Tissue Engineering, 7*, 729–41.
21. Zuk, P. A., Zhu, M., Mizuno, H., et al. (2001). Multilineage cells from human adipose tissue: implications for cell-based therapies. *Tissue Engineering, 7*, 211–28.
22. Hattori, H., Masuoka, K., Sato, M., et al. (2006). Bone formation using human adipose tissue-derived stromal cells and a biodegradable scaffold. *Journal of Biomedical Materials Research, Part B: Applied Biomaterials, 76*, 230–9.
23. Laino, G., Graziano, A., d'Aquino, R., et al. (2006). An approachable human adult stem cell source for hard-tissue engineering. *Journal of Cellular Physiology, 206*, 693–701.
24. Anderson, P., Carrillo-Galvez, A. B., Garcia-Perez, A., Cobo, M., & Martin, F. (2013). CD105 (endoglin)-negative murine mesenchymal stromal cells define a new multipotent subpopulation with distinct differentiation and immunomodulatory capacities. *PLoS One, 8*, e76979.
25. Laino, G., d'Aquino, R., Graziano, A., et al. (2005). A new population of human adult dental pulp stem cells: a useful source of living autologous fibrous bone tissue (LAB). *Journal of Bone and Mineral Research, 20*, 1394–402.

26. Papaccio, G., Graziano, A., d'Aquino, R., et al. (2006). Long-term cryopreservation of dental pulp stem cells (SBP-DPSCs) and their differentiated osteoblasts: a cell source for tissue repair. *Journal of Cellular Physiology, 208*, 319–25.
27. d'Aquino, R., Graziano, A., Sampaolesi, M., et al. (2007). Human postnatal dental pulp cells co-differentiate into osteoblasts and endotheliocytes: a pivotal synergy leading to adult bone tissue formation. *Cell Death and Differentiation, 14*, 1162–71.
28. Irizarry, R. A., Hobbs, B., Collin, F., et al. (2003). Exploration, normalization, and summaries of high density oligonucleotide array probe level data. *Biostatistics, 4*, 249–64.
29. Johnson, W. E., Li, C., & Rabinovic, A. (2007). Adjusting batch effects in microarray expression data using empirical Bayes methods. *Biostatistics, 8*, 118–27.
30. Tusher, V. G., Tibshirani, R., & Chu, G. (2001). Significance analysis of microarrays applied to the ionizing radiation response. *Proceedings of the National Academy of Sciences of the United States of America, 98*, 5116–21.
31. Benjamini, Y., Drai, D., Elmer, G., Kafkafi, N., & Golani, I. (2001). Controlling the false discovery rate in behavior genetics research. *Behavioural Brain Research, 125*, 279–84.
32. Vandesompele J, De Preter K, Pattyn F, et al. Accurate normalization of real-time quantitative RT-PCR data by geometric averaging of multiple internal control genes. Genome Biol 2002;3: RESEARCH0034.
33. Pfaffl, M. W. (2001). A new mathematical model for relative quantification in real-time RT-PCR. *Nucleic Acids Research, 29*, e45.
34. Rohde, C., Zhang, Y., Reinhardt, R., & Jeltsch, A. (2010). BISMA–fast and accurate bisulfite sequencing data analysis of individual clones from unique and repetitive sequences. *BMC Bioinformatics, 11*, 230.
35. Langdahl, B. L., Kassem, M., Moller, M. K., & Eriksen, E. F. (1998). The effects of IGF-I and IGF-II on proliferation and differentiation of human osteoblasts and interactions with growth hormone. *European Journal of Clinical Investigation, 28*, 176–83.
36. Boonen, S., Mohan, S., Dequeker, J., et al. (1999). Down-regulation of the serum stimulatory components of the insulin-like growth factor (IGF) system (IGF-I, IGF-II, IGF binding protein [BP]-3, and IGFBP-5) in age-related (type II) femoral neck osteoporosis. *Journal of Bone and Mineral Research, 14*, 2150–8.
37. Ulaner, G. A., Vu, T. H., Li, T., et al. (2003). Loss of imprinting of IGF2 and H19 in osteosarcoma is accompanied by reciprocal methylation changes of a CTCF-binding site. *Human Molecular Genetics, 12*, 535–49.
38. Zhang, H., Niu, B., Hu, J. F., et al. (2011). Interruption of intrachromosomal looping by CCCTC binding factor decoy proteins abrogates genomic imprinting of human insulin-like growth factor II. *The Journal of Cell Biology, 193*, 475–87.
39. van Bezooijen, R. L., Van der Bent, C., Papapoulos, S. E., & Lowik, C. W. (1999). Oestrogenic compounds modulate cytokine-induced nitric oxide production in mouse osteoblast-like cells. *The Journal of Pharmacy and Pharmacology, 51*, 1409–14.
40. Goswami, J., Hernandez-Santos, N., Zuniga, L. A., & Gaffen, S. L. (2009). A bone-protective role for IL-17 receptor signaling in ovariectomy-induced bone loss. *European Journal of Immunology, 39*, 2831–9.
41. Osta, B., Lavocat, F., Eljaafari, A., & Miossec, P. (2014). Effects of interleukin-17A on osteogenic differentiation of isolated human mesenchymal stem cells. *Frontiers in Immunology, 5*, 425.
42. CA, C. (1996). The role of insulin-like growth factors and binding proteins in bone cell biology. In J. B. Bilezikian LGR & G. A. Rodan (Eds.), *Principles of bone biology* (pp. 607–18). San Diego: Academic.
43. Canalis, E. (1993). Insulin like growth factors and the local regulation of bone formation. *Bone, 14*, 273–6.
44. Subburaman Mohan DJB. IGF System Components and Their Role in Bone Metabolism. In: Rosenfeld RG, Roberts, Charles, ed. The IGF System. Contemporary Endocrinology: Humana Press; 1999: 457–96.
45. Hardouin, S. N., Guo, R., Romeo, P. H., Nagy, A., & Aubin, J. E. (2011). Impaired mesenchymal stem cell differentiation and osteoclastogenesis in mice deficient for Igf2-P2 transcripts. *Development, 138*, 203–13.
46. Twine, N. A., Chen, L., Pang, C. N., Wilkins, M. R., & Kassem, M. (2014). Identification of differentiation-stage specific markers that define the ex vivo osteoblastic phenotype. *Bone, 67*, 23–32.
47. Vu, T. H., Nguyen, A. H., & Hoffman, A. R. (2010). Loss of IGF2 imprinting is associated with abrogation of long-range intrachromosomal interactions in human cancer cells. *Human Molecular Genetics, 19*, 901–19.
48. Ohlsson, R., Nystrom, A., Pfeifer-Ohlsson, S., et al. (1993). IGF2 is parentally imprinted during human embryogenesis and in the Beckwith-Wiedemann syndrome. *Nature Genetics, 4*, 94–7.
49. Ping, A. J., Reeve, A. E., Law, D. J., Young, M. R., Boehnke, M., & Feinberg, A. P. (1989). Genetic linkage of Beckwith-Wiedemann syndrome to 11p15. *American Journal of Human Genetics, 44*, 720–3.
50. Davies, S. M. (1994). Developmental regulation of genomic imprinting of the IGF2 gene in human liver. *Cancer Research, 54*, 2560–2.
51. Kalscheuer, V. M., Mariman, E. C., Schepens, M. T., Rehder, H., & Ropers, H. H. (1993). The insulin-like growth factor type-2 receptor gene is imprinted in the mouse but not in humans. *Nature Genetics, 5*, 74–8.
52. Pham, N. V., Nguyen, M. T., Hu, J. F., Vu, T. H., & Hoffman, A. R. (1998). Dissociation of IGF2 and H19 imprinting in human brain. *Brain Research, 810*, 1–8.
53. Dai, Y. M., Hu, Y. L., Wang, Z. Q., & Li, J. (2007). [Loss of imprinting of IGF2 in cord blood of newborns of Chinese Han population]. Zhonghua yi xue yi chuan xue za zhi=Zhonghua yixue yichuanxue zazhi =. *Chinese Journal of Medical Genetics, 24*, 10–4.
54. Douc-Rasy, S., Barrois, M., Fogel, S., et al. (1996). High incidence of loss of heterozygosity and abnormal imprinting of H19 and IGF2 genes in invasive cervical carcinomas. Uncoupling of H19 and IGF2 expression and biallelic hypomethylation of H19. *Oncogene, 12*, 423–30.
55. Eslaminejad, M. B., Fani, N., & Shahhoseini, M. (2013). Epigenetic regulation of osteogenic and chondrogenic differentiation of mesenchymal stem cells in culture. *Cell Journal, 15*, 1–10.
56. Teven, C. M., Liu, X., Hu, N., et al. (2011). Epigenetic regulation of mesenchymal stem cells: a focus on osteogenic and adipogenic differentiation. *Stem Cells International, 2011*, 201371.
57. Im, G. I., & Shin, K. J. (2015). Epigenetic approaches to regeneration of bone and cartilage from stem cells. *Expert Opinion on Biological Therapy, 15*, 181–93.
58. Hemming, S., Cakouros, D., & Isenmann, S. (2014). EZH2 and KDM6A act as an epigenetic switch to regulate mesenchymal stem cell lineage specification. *Stem Cells (Dayton, Ohio), 32*, 802–15.
59. Paino, F., La Noce, M., & Tirino, V. (2014). Histone deacetylase inhibition with valproic acid downregulates osteocalcin gene expression in human dental pulp stem cells and osteoblasts: evidence for HDAC2 involvement. *Stem Cells (Dayton, Ohio), 32*, 279–89.
60. d'Aquino, R., De Rosa, A., Lanza, V., et al. (2009). Human mandible bone defect repair by the grafting of dental pulp stem/progenitor cells and collagen sponge biocomplexes. *European Cells & Materials, 18*, 75–83.
61. Giuliani, A., Manescu, A., Langer, M., et al. (2013). Three years after transplants in human mandibles, histological and in-line holotomography revealed that stem cells regenerated a compact rather than a spongy bone: biological and clinical implications. *Stem Cells Translational Medicine, 2*, 316–24.

Stem Cells in Autism Spectrum Disorders

Maria Rita Passos-Bueno[1], Karina Griesi-Oliveira[1, 2], Andrea Laurato Sertié[2], Gerson Kobayashi[1].

[1]Centro de Estudos sobre o Genoma Humano e Células-Tronco, Departamento de Genética e Biologia Evolutiva, Instituto de Biociências, Universidade de São Paulo, São Paulo, Brazil

[2]Hospital Israelita Albert Einstein

Published in: Stem Cells in Modeling Human Genetic Diseases. Humana Press. eds. Okamoto, OK; Zatz, M. 2015. doi: 10.1007/978-3-319-18314-5

Keywords: disease modeling; TRPC6; mTOR, dental pulp stem cells; IGF-1

Abstract

Autism spectrum disorders (ASD) are a heterogeneous and highly prevalent group of neurodevelopmental disorders. Genome analyses have revealed a large amount of candidate risk variants in ASD patients, of which most are rare and private. Currently available tools and techniques have not been sufficient to pinpoint genuine causative or risk variants for ASD among the multitude of variants discovered in each genome. Moreover, targeted drugs to ameliorate specific symptoms of ASD, such as language impairment, difficulties in social interaction and repetitive behavior, are still unavailable. *In vitro* cellular and molecular analyses of stem cells to study this group of disorders is bringing new insights into this field. Induced pluripotent stem cells (iPSC) have been successfully generated and used to model 6 syndromic, monogenic forms of ASD. The results have been very promising, confirming previous data obtained from studies using mouse models and human brain tissues. Disease modeling with stem cells from nonsyndromic ASD patients, albeit in its early stages, has revealed alterations in expression of cytoskeletal genes, compromised mTOR signaling, and reduced neuronal dendritic arborization in these patients. Finally, investigation of ASD iPSC-derived neurons has consistently suggested IGF-1 as a candidate drug to ameliorate ASD symptoms in some cases. Owing to the use of stem cells, we currently witness an amazing period of discoveries that have revolutionized our knowledge of ASD, with great expectation to deliver a better understanding of ASD pathophysiology.

1. Introduction

Autism spectrum disorders (ASD) are a heterogeneous group of neurodevelopmental disorders characterized by severe developmental defects in social response and communication accompanied by inappropriate repetitive behavior (Ronemus et al., 2014). ASD has an overall prevalence of ~1% (Autism and Developmental Disabilities Monitoring Network Surveillance, 2012). There is a strong male bias, with a ratio of about 4 males to 1 female, particularly among those

with milder ASD forms (Brandler and Sebat, 2015). ASD can be a clinical manifestation of several well characterized monogenic disorders. The ASD penetrance in these disorders varies, and may reach values of ~60% in Fragile X syndrome, tuberous sclerosis and Timothy syndrome (Curatolo et al., 2004; Splawski et al., 2004; Lozano et al., 2014). ASD is also a relevant phenotype in Rett, Rett-like or *CDKL5*-associated syndrome, Angelman and Phelan-McDermid syndromes (Betancur & Buxbaum, 2013; Prilutsky et al., 2014; Liu & Takumi, 2014). The molecular genetic mutational mechanism is very well characterized in all of these conditions. For didactic purposes, we will refer to the group of monogenic disorders frequently associated with ASD as **syndromic ASD** forms, in contrast to **ASD** or nonsyndromic ASD, in which the major clinical manifestation is autism, associated or not with other clinical features, such as epilepsy and hyperactivity, and in which clinical features are not sufficient to define a syndrome.

A high heritability component in ASD has been estimated, varying from 50% to 90% (Brandler and Sebat; 2015; Jeste & Geschwind, 2014). The recurrence risk in families with only one ASD-affected individual is about 10%, and male siblings of ASD individuals have a ~3-fold increase of the risk of being affected by ASD in comparison to female siblings (Brandler and Sebat; 2015; Jeste & Geswhind, 2014). Recurrence risk also increases according to the number of ASD-affected individuals in the family, thus reinforcing the genetic basis of ASD. The disease model seems to be very complex, with a high level of heterogeneity. Based on several worldwide genome-wide association studies (GWAS), there is a consensus that common variants, each with a low predictive risk, play a role in ASD etiology; however, the actual contribution of these variants to ASD heritability is still unclear (Brandler and Sebat, 2015; Jeste & Geswhind, 2014; Gaugler et al., 2014). Genomic studies, in contrast, have revealed that rare CNVs or rare sequencing variants with moderate-to-high penetrance are associated with the etiology of ASD in at least 20% of the cases (Brandler and Sebat, 2015; de Rubeis et al., 2014; Jeste & Geswhind, 2014; Yuen et al., 2015). These studies have revealed a remarkable genetic heterogeneity, as less than 20 of the 100 candidate genes present recurrent putative pathogenic variants. Despite the high heterogeneity of ASD, a growing number of evidence has shown that candidate genes belong to convergent pathways, nowadays represented by regulation of transcription (chromatin remodeling genes and transcription factors), regulation of protein abundance (splicing, translation and ubiquitination genes), synapse (cell adhesion, sodium and calcium channels, N-methyl-D- aspartate (NMDA) receptors, and synaptic scaffold genes) and intracellular signaling factors that regulate cell growth and proliferation (mTOR/PI3K and RAS genes) (Brandler and Sebat, 2015; De Rubeis et al., 2014, Yuen et al.,2015).

The majority of these candidate pathogenic variants have been classified as loss-of-function variants, which occur with a population frequency of about 5% (MacArthur et al. 2012). Therefore, one of the current challenges in the genomic analysis of ASD is pinpointing causative variants; moreover, it is necessary to define the penetrance associated with each one of them and how many pathogenic variants are sufficient for a complete ASD penetrance per individual. Finally, the functional effects of the identified variants must be demonstrated and be translated to the phenotypic effect. One approach to address the above mentioned questions is to

conduct functional studies in order to verify which of these candidate variants are sufficient to cause morphological and functional changes in neurons.

Stem cells have recently emerged as a promising alternative to conduct functional cellular studies, particularly in disorders where the tissue of interest is of limited or nearly no access. This is exactly the case for ASD and several other neurodevelopmental disorders, in which the ideal tissue of interest to conduct cellular and molecular studies is the developing brain. Another drawback is the impossibility to get an accurate diagnosis for these disorders before one year of age. Murine model systems provide genetic homogeneity and allow the study of behavioral phenotypes, but show limited applicability to understand how diseases affect human neocortical regions, and often do not recapitulate the complex human neurodevelopment (Rakic, 2009; Chailangkarn et al., 2012)

Stem cells from human exfoliated deciduous teeth (SHED) are an easily accessible cell type comprised by populations of mesodermal and neuroectodermal origin (Cordero et al., 2011; Janebodin et al., 2011; Komada et al., 2012). The identification of cellular pathways associated with diseases can be successfully achieved by studying SHED, particularly when they share the same embryological origin with cells of the main disease-affected tissue, as in the case of ASD (Bueno et al., 2011; Kobayashi et al., 2013; Griesi-Oliveira et al., 2013, 2014). However, the use of SHED is restricted by their limited potential to be differentiated into functional neurons. These difficulties have been overcome thanks to the possibility of reprogramming somatic cells to a pluripotent state by overexpressing specific transcription factors (Yu et al., 2007; Takahashi et al., 2007). These cells, known as induced pluripotent cells (iPSCs), have opened a new world of possibilities, as they can be differentiated toward multiple cell lines, including neurons; therefore, the generation of disease-specific neurons by reprogramming somatic cells from ASD patients have empowered researchers to functionally characterize genetic alterations and determine how they lead to ASD neuronal phenotypes. In this regard, both glutamatergic and GABAergic neurons as well as astrocytes, which are of interest to study ASD-related phenotypes, can be obtained (Kim et al., 2014). Further, cells from different sources, such as SHED and erythroblasts, in addition to the fibroblasts, which were the first type of cells used to obtain iPSCs, can be reprogrammed by these transcription factors with similar efficiency (Griesi-Oliveira et al., 2014; Hubbard et al., 2014). Even though human embryonic stem cells (hESCs) and neural stem cells (hNSCs) can also be employed to model diseases in a dish, they are in practice, more difficult to be obtained, and their use still represents an ethical issue. Also, the use of these cells is hampered by the impossibility to establish the diagnosis in the early developmental period, particularly for nonsyndromic forms of ASD (Figure 1).

We are currently at the dawn of human stem cell modeling of ASD and ASD-associated monogenic disorders. Although much effort still needs to be gathered to fully understand the etiology of these disorders, the results obtained so far have been encouraging and exciting, as they have unraveled new biological pathways and provided a causal relationship between pathogenic mutations and morphological and functional neuronal alterations. Importantly, in several situations, such findings

recapitulate relevant cellular and/or molecular phenotypes previously reported in murine models or other approaches.

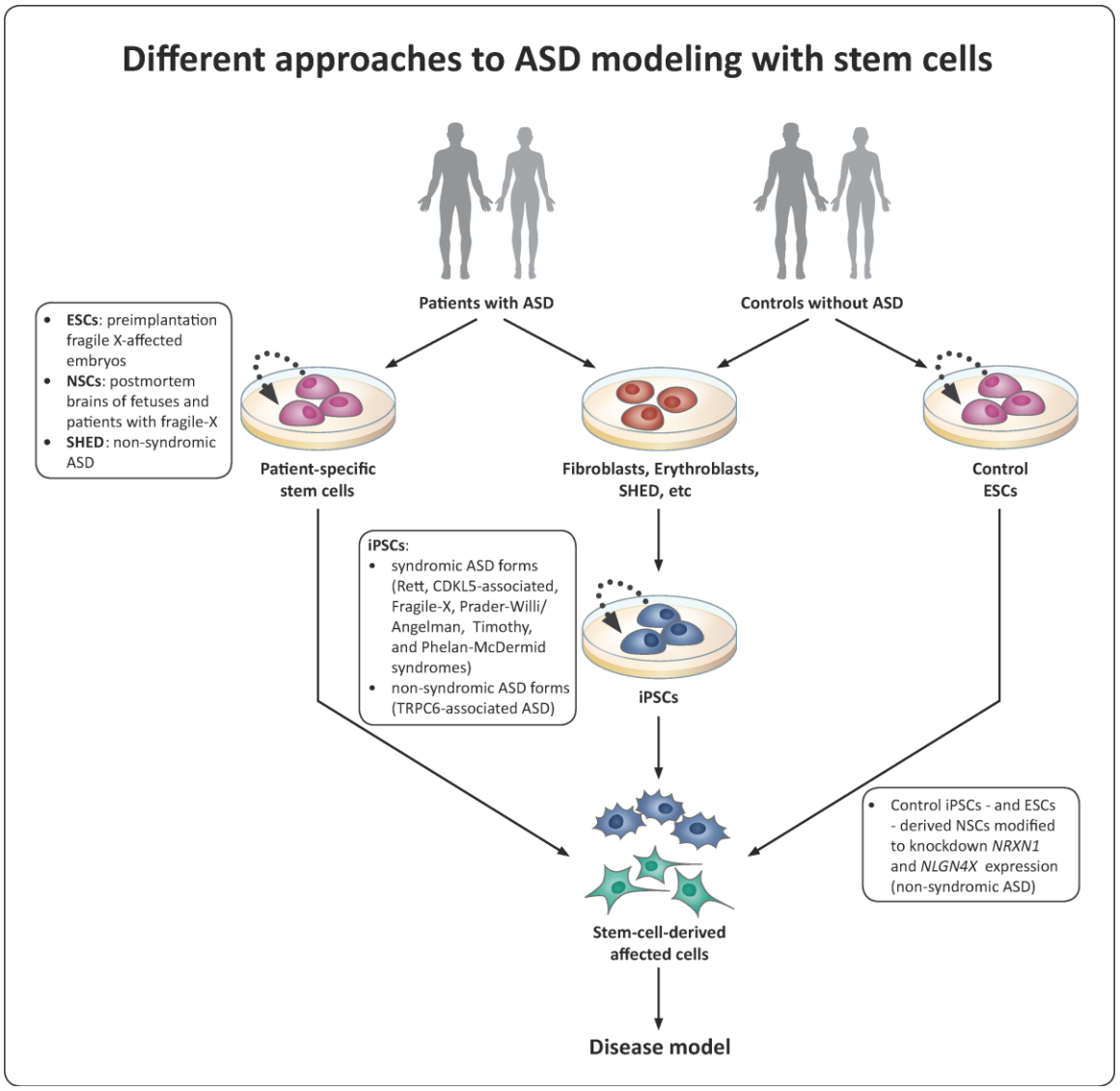

Figure 1 Schematic summary of different approaches to ASD modeling using human stem cells. Patient-derived embryonic stem cells (ESCs) and neural stem cells (NSCs) were used to model the syndromic ASD fragile-X syndrome. Although these patient-derived stem cells have the advantage of do not require any genetic or epigenetic manipulations to be relevant for disease modeling, they are, in practice, difficult to be obtained. Stem cells from human exfoliated deciduous teeth (SHED) represent an accessible source of patient material and have recently been used to model nonsyndromic forms of ASD. Induced pluripotent stem cells (iPSCs) can be generated from adult cells from ASD patients and can be differentiated into the disease-affected cells. At least six monogenic disorders that include ASD features as part of the phenotype have been modeled by the use of iPSC methodology: Rett syndrome, *CDKL5*-associated ASD, Fragile-X syndrome, Prader-Willi/Angelman syndrome, Timothy syndrome, and Phelan-McDermid syndrome. iPSCs have also been used to model nonsyndromic forms of ASD, such as TRPC6-associated ASD. Finally, control-derived stem cells engineered to reduce (knockdown) a particular gene's expression have been used to model the neurodevelopmental impact of *NRXN1* and *Neuroligin 4X NLGN4X* deletions, associated with nonsyndromic ASD and other neurodevelopmental disorders. Figure modified from Sterneckert et al. (2014).

2. Induced pluripotent stem cells (iPSCs): modelling monogenic disorders featuring ASD.

To date, six genetically well-characterized monogenic disorders with ASD features have been modeled with the use of iPSC technology. In the following segment we provide a short background and summarize the most significant findings and current state of the art for each disorder.

Fragile X syndrome (FXS)

FXS is the most commonly inherited form of intellectual disability, which may be accompanied by a characteristic appearance in affected males (large head, long face, prominent forehead and chin, protruding ears), connective tissue defects, and postpubescent macroorchidism (Bowen et al., 1978; Garber et al., 2008). Autistic features may be present in up to 60% of all cases, depending on the clinical criteria adopted (Crawford et al., 2001; Clifford et al., 2007; Harris et al., 2008; McDuffie et al. 2010). FXS is caused by expansions of CGG trinucleotide repeats in the 5' untranslated region of the *FMR1* (fragile X mental retardation 1) gene in the X chromosome. The expansions lead to hypermethylation of the *FMR1* promoter and consequent silencing of FMRP (fragile X mental retardation protein), an RNA binding protein involved in mRNA localization and protein synthesis during synaptic plasticity (Ashley et al., 1993; Sidorov et al., 2013). In hESCs derived from FXS-affected blastocyst-stage embryos, *FMR1* expression is active and gene silencing takes place upon differentiation (Eiges et al., 2007). However, this is not observed in iPSCs derived from FXS patients, in which reprogramming adult cells to a pluripotent state does not reset the epigenetic marks associated with *FMR1* silencing (Urbach et al., 2010). These findings illustrate how iPSCs and ESCs, albeit similar in many aspects, still exhibit differences that might be relevant to the disease under investigation and that should be considered when selecting cell types for disease modelling. In the case of FXS, since *FMR1* is kept silenced during neuronal differentiation, FXS-derived iPSCs remain a suitable model to study neuronal changes caused by the expansion mutations. Additionally, one advantage of FXS-derived iPSCs is the ability to generate cells from clinically well-characterized patients and the possibility of investigating different-sized mutations present in the same individual (a consequence inherent to the dynamic nature of the expansions; Sheridan et al., 2011; Liu et al., 2012). Such approach has shed light on the genotype-phenotype relationship in FXS, showing defective neurite formation and outgrowth occurring prior to synaptogenesis, during neuronal differentiation (Sheridan et al., 2011; Doers et al., 2014). Importantly, a previous study using an *Fmr1*-knockout mouse model and *in vitro* NSCs from postmortem brain of a fragile-X fetus also described reduced neurite outgrowth and branching and altered neuronal differentiation in FMRP-deficient NSCs (Castrén et al., 2005).

Timothy syndrome (TS)

TS is a rare, severe neurodevelopmental disorder accompanied by cardiac defects/arrhythmia and facial dysmorphisms, and one of the most penetrant monogenic forms of ASD. This disorder is caused by mutations in *CACNA1C* (calcium channel, voltage-dependent, L type, alpha 1C subunit), a gene encoding an alpha

subunit of a voltage-dependent calcium channel ($Ca_v1.2$) (Splawski et al., 2004). Neurons derived from TS iPSCs showed action potentials and increased intracellular Ca^{++} concentration indicative of loss of calcium channel inactivation. TS neurons also showed abnormal expression of tyrosine hydroxylase, which could be rescued with the drug roscovitine, a compound that increases the inactivation of L-type calcium channels. Moreover, gene expression studies revealed that iPSC-derived neural progenitor cells and iPSC-derived neurons from TS patients show alterations in expression of genes previously associated with ASD, as well as similarities with gene expression patterns observed in postmortem idiopathic ASD brains (Paşca et al., 2011; Tian et al., 2014). Also in TS-derived iPSCs, Krey et al (2013) observed that depolarization causes dendritic retraction in TS neurons, which occurs independently of the excessive Ca^{++} influx seen in these cells. In fact, their results suggested that the dendritic phenotype was caused by decreased binding between TS $Ca_v1.2$ and the GTPase Gem, leading to ectopic activation of RhoA. These findings directly link $Ca_v1.2$ channels to RhoA signaling in the brain and provide new grounds for studying ASD neuronal phenotypes *in vitro*.

Rett syndrome (RTT)

RTT is a severe progressive neurodevelopmental disorder mainly caused by mutations in the X-linked gene *MECP2* (Methyl CpG-binding protein 2) (Amir et al., 1999; Chahrour and Zoghbi, 2007). RTT individuals undergo apparently normal development until 6-18 months of age, followed by impaired motor function, stagnation and regression of developmental skills, hypotonia, seizures and autistic behavior (Amir et al., 1999; Marchetto et al., 2010). MeCP2, the encoded protein, is involved in transcriptional regulation by binding to methylated CpG dinucleotide and recruiting proteins involved in chromatin remodeling (Chahrour et al., 2008). Marchetto et al (2010) were the first group to model RTT in human cells. By generating iPSCs from RTT patient-derived fibroblasts, they found that deficiency of *MECP2* in RTT neurons resulted in smaller soma, fewer dendritic spines and synapses, and impairment in calcium signaling and in excitatory synaptic transmission, by comparison to control, unaffected neurons. Most of these neuronal phenotypes, such as reduced soma size and dendritic arborization, have been subsequently corroborated by groups employing different techniques to generate *MECP2*-deficient neurons from pluripotent stem cells (Cheung et al., 2011; Li et al., 2013). Li et al (2013) used gene-editing techniques to generate *MECP2*-deficient hESCs, and showed that mutant neurons exhibit global reduction in translation and protein synthesis, and reduced AKT/mTOR activity. Studies in mouse models have suggested a role for astrocytes in RTT pathogenesis, which has been recently confirmed in human cells. Through differentiation of RTT iPSCs to astrocytes and employment of a series of co-culture experiments, Williams et al (2014) showed that *MECP2*-mutated astrocytes lead to reduction in neurite length and in the number of terminal ends of wild-type neurons, and this non-cell-autonomous influence was partially mediated by factors secreted by mutant astrocytes.

Modeling RTT cells in-a-dish has shown that disease-related phenotypes can be rescued *in vitro*. Treatment with insulin-like growth factor-1 (IGF-1) or gentamicin has been shown to improve synaptic density in RTT neurons (Marchetto

et al., 2010), and addition of IGF-1 or BDNF (brain-derived neurotrophic factor) improved protein synthesis through activation of AKT/mTOR pathway. Importantly, these findings provide proof-of-principle evidence for the application of ASD iPSC-derived neurons in drug discovery.

CDKL5-associated syndrome

Dominant-negative mutations in *CDKL5* (cyclin-dependent kinase-like 5), also located in the X chromosome, are responsible for a Rett syndrome-like phenotype (Tao et al., 2004; Weaving et al., 2004), hereinafter referred to as CDKL5-associated syndrome. Patients mainly exhibit early-onset intractable seizures before 6 months of age, severe developmental delay, and autistic features (Tao et al., 2004; Weaving et al., 2004; Archer et al., 2005; Rademacher et al., 2011). *CDKL5* encodes a serine/threonine kinase whose role in brain development is not fully understood. *Cdkl5* silencing in a mouse model has shown the importance of this gene for dendritic spine morphogenesis and maintenance of synaptic contact, which occurs via interaction between the postsynaptic proteins NGL-1 and PSD-95, stabilized through phosphorylation of NGL-1 by *CDKL5* (Ricciardi et al., 2012). The use of patient-derived iPSCs harboring loss-of-function mutations in *CDKL5* further confirmed those findings, as patients' iPSC-derived neurons exhibited a significantly reduced number of synaptic contacts and lacked pre-synaptic terminals (Ricciardi et al., 2012).

Angelman syndrome (AS) and Prader-Willi syndrome (PWS)

AS and PWS were the first imprinting disorders described in humans, in which alterations in the chromosomal region 15q11-q13 lead to different phenotypes depending on which chromosome (paternal or maternal) is affected (Buiting, 2010). AS is characterized by significant intellectual disability, absent speech, frequent seizures, motor impairment and a typical happy demeanor (Williams et al., 2006). PWS is characterized by small stature, neonatal hypotonia, hypogonadism, mild-to-moderate intellectual disability, and compulsive hyperphagia (Cassidy et al., 2009). AS is caused by loss of function of the maternally inherited allele of *UBE3A* (ubiquitin-protein ligase E3A), which undergoes tissue-specific genomic imprinting with silencing of the paternally inherited allele in brain tissues (Rougeulle et al., 1997; Vu et al., 1997). When the paternal chromosome is deleted in the same chromosome region, individuals develop PWS due to loss of a cluster of several species of small nucleolar RNAs (Smith et al., 2009). Although autistic features are reported in AS but not in PWS, the 15q11-q13 region has been systematically associated with ASD (Moreira et al., 2014). Chamberlain et al (2010) were the first to show that iPSCs derived from AS and PWS fibroblasts maintain the genomic imprinting at 15q11-q13 after reprogramming. Moreover, they confirm that expression of the paternally inherited *UBE3A* is repressed upon neuronal differentiation in AS cells, recapitulating the main epigenetic characteristics of AS *in vitro*. Additionally, in neurons differentiated from PWS-derived iPSCs, Cruvinel et al (2014) showed that the zinc-finger protein ZNF274, in association with the histone methyltransferase SETDB1, might protect against methylation of the small nucleolar RNA cluster in the PWS region. Together, the findings obtained through

investigating PWS and AS show that iPSC modeling of alterations at 15q11-q13 is a promising strategy to better understand these disorders and ASD.

Phelan-McDermid syndrome (PMDS)

Another syndrome frequently associated with ASD is PMDS. This syndrome is caused by heterozygous deletions of variable sizes in chromosome 22 (region 22q13.3). Besides ASD, PMDS patients may exhibit hypotonia, normal to accelerated growth and minor dysmorphic features (Phelan and Mcdermid, 2012). Studies attempting to establish a critical region for the syndrome, in combination with analysis of rare ASD-related mutations and functional studies have appointed *SHANK3* to be the most likely candidate responsible for the neurological phenotype in PMDS (Betancur and Buxbaum, 2013). Shcheglovitov et al (2013) produced iPSC-derived neurons from PMDS patients and observed a reduced amplitude and frequency of spontaneous excitatory synaptic events. Such phenotype was caused by impaired AMPA- and NMDA-mediated transmission. Overexpression of *SHANK3* rescued the electrophysiological alterations found, showing that this gene significantly contributes to the neuronal alterations in PMDS. By treating the PMDS neurons with IGF-1, the authors were also able to restore the excitatory synaptic defects. Intriguingly, treatment with IGF-1 decreased the expression of *SHANK3* in control and PMDS neurons. They found that IGF-1 actually increases the number of synapses that lack *SHANK3* but contains PSD-95, which have faster deactivation of excitatory currents, a kinetics that resemble that of neurons appearing later in development.

3. Stem cells to model nonsyndromic ASD

Lymphocytes and fibroblasts have been used in several studies in order to dissect the cellular pathways altered in nonsyndromic forms of ASD (Hu at al., 2009; Chien et al., 2013). However, even though the access of these cells are relatively simple and with minor ethical implications, they present limitations to study neurodevelopmental pathways, as they are mature, post-natal cell types and possess non-neural embryological origins.

Stem cells from human exfoliated deciduous teeth (SHED) are an alternative and interesting source of patient-derived cells to be studied, as they can be non-invasively isolated, they show the same early embryonic origin as neurons, and they express neural progenitor markers (Arthur et al., 2008). Therefore, SHED may bear genetic regulatory networks that resemble those found in neurons. As detailed below, in three recent studies, we show the applicability of SHED in dissecting the genetic regulatory circuitry in nonsyndromic ASD.

Griesi-Oliveira et al (2013) assessed the gene expression profile of SHED from 7 nonsyndromic ASD individuals, with no defined genetic mechanism. By comparing cases and controls, the authors identified 683 differentially expressed genes, of which a significant number is expressed in brain and is involved in mechanisms and molecular pathways previously associated with ASD, such as cytoskeleton regulation, axonal guidance, protein synthesis and cellular adhesion. Among the identified DEGs, one of the upregulated genes was *CHD8*, which has been

found to be mutated in about 0.3% of ASD cases in more than one study (Neale et al., 2012; O'Roak et al, 2012a,b; Sanders et al. 2012; de Rubeis et al., 2014). Interestingly, *CHD8* is a co-regulator of androgen-responsive transcription (Menon et al., 2010) and androgen receptor (AR), as well as a significant number of genes regulated by this receptor, presented overexpression in the studied set of patients. The authors suggested that this might be a possible mechanism through which *CHD8* can contribute to ASD, especially considering the skewed male-to-female prevalence in such disorders.

Suzuki et al. (2015) used SHED to investigate the role of mTOR (mammalian target of rapamycin) signaling pathway in nonsyndromic ASD pathophysiology. mTOR signaling pathway regulates several essential cellular processes including cell growth, proliferation, autophagy, and protein synthesis (Laplante & Sabatini, 2009). In the central nervous system, mTOR signaling is crucial from the early stages of neural development, controlling self-renewal and differentiation of hNSCs and, in neurons, mTOR signaling is involved in synapse formation and plasticity. Dysfunctional mTOR signaling and dysregulated protein synthesis in neuronal cells have been associated with several monogenic syndromes with high prevalence of autism, such as Fragile X syndrome, tuberous sclerosis, and *PTEN*-related syndromes, which are caused by mutations in, respectively, *FMR1*, TSC1/2 and *PTEN*, molecules known to be negative regulators of mTOR pathway (Costa-Mattioli et al., 2013). Functional studies addressing mTOR-signaling activity in patients with nonsyndromic ASD were lacking. To examine this important question, Suzuki et al have made use of cultured SHED derived from 13 patients with nonsyndromic ASD, who were negative for *FRM1*, *TSC1/2* and *PTEN* mutations, and 11 age- and sex-matched controls. They observed that SHED derived from 3 patients (23% of the patient sample) showed dysregulation of mTOR signaling pathway in response to extracellular nutrient availability, enhanced proliferative capacity at higher cell densities, and reduced response to the antiproliferative effect of rapamycin, a specific mTOR inhibitor. Together, the results suggest that dysregulation of mTOR signaling plays an important role in the pathogenesis of a subgroup of nonsyndromic ASD, and that mTOR pathway components might be promising therapeutic targets for these patients. Interestingly, these results were further corroborated by two studies showing altered mTOR signaling in postmortem brain of patients with nonsyndromic ASD (Tang et al., 2014; Oguro-Ando et al., 2014).

Griesi-Oliveira et al (2014), by molecularly characterizing the breakpoints of a balanced translocation between chromosomes 3 and 11 in a patient with nonsyndromic ASD, evidenced disruption of *TRPC6*, a gene that encodes a cation channel. They demonstrated that the transcriptome of SHED from this patient with haploinsufficiency of TRPC6 (TRPC6-mut) is dysregulated as compared to control SHED, with enrichment for genes important for cytoskeleton structure and regulation, such as *SEMA3A*, *EPHA4*, *INA* and *MAP2* (Griesi-Oliveira et al., 2014). Moreover, a significant number of differentially expressed genes between the TRPC6-mut patient's SHED and control SHED are putative targets of CREB, a transcription factor known to be activated via calcium influx through TRPC6 (Tai et al., 2008). Using hyperforin, a specific activator of the channel, the authors also confirmed that part of such genes could in fact be regulated by TRPC6 activation. In

order to evaluate how representative these findings would be in neurons, Griesi-Oliveira et al assessed the phenotype of neuronal cells derived from TRPC6-mut patient iPSC lines obtained from SHED, which represents the first work to evaluate a nonsyndromic case of ASD using such model. Calcium influx upon activation of TRPC6 was reduced in NPCs of TRPC6-mut patient. Paralleling the results found in SHED, activation of TRPC6 in NPCs leads to expression regulation of some of CREB target genes. TRPC-mut neurons have shorter neurites, with a reduction in arborization complexity and lower density of dendritic spines and glutamatergic vesicles compared to control neurons. These results are consistent with previous and authors' findings in rodent models (Tai et al., 2008; Zhou et al., 2008). Moreover, using gain and loss of function models, authors demonstrated that such alterations could indeed be attributed to TRPC6 function. Interestingly, by taking advantage of a pair of isogenic iPSC line of a Rett syndrome patient, one with the mutated copy of MeCP2 inactivated by X-chromosome inactivation, and one with this copy activated, authors showed that MeCP2 is involved in TRPC6 expression regulation, pointing to a shared molecular pathway between a syndromic and nonsyndromic form of ASD. Although using cells in different developmental states, the work points to a mechanism in which haploinsufficiency of TRPC6 leads to reduced calcium influx and consequent dysregulation of the expression of neurodevelopmental genes, at least in part by CREB activity modulation. Such expression dysregulation then would lead to neuronal morphological and functional alterations (Figure 2). Finally, Griesi-Oliveira and colleagues demonstrated that neuronal abnormalities in TRPC6-mut neurons could be rescued with hyperforin or IGF-1 treatment.

The use of control-derived stem cells engineered to reduce (knockdown) a particular gene's expression can also be an approach to *in vitro* model molecular dysfunction associated with nonsyndromic ASD. In two recent studies, the neurodevelopmental impact of *Neurexin 1* (*NRXN1*) and *Neuroligin 4X* (*NLGN4X*) deletions, known to be associated with nonsyndromic ASD and other neurodevelopmental disorders, were investigated using human iPSCs and hESCs as *in vitro* models (Zeng et al., 2013; Shi et al., 2013). *NRXN1* is a presynaptic neuronal adhesion molecule that interacts with postsynaptic neuroligins, such as *NLGN4X*, in excitatory and inhibitory synapses in the brain to form an inter-synaptic complex required for synapse formation and function. Zeng and colleagues (2013) showed that reduction of *NRXN1* expression in both iPSC-derived neural stem cells (hNSCs) and hESC-derived hNSCs leads to alterations in the expression levels of several genes involved in cell adhesion and neuron development during differentiation of the hNSCs into mature neurons. Additionally, NSCs with *NRXN1* knockdown showed reduced astrocyte differentiation potential. These results suggest that *NRXN1* deletion might impair nervous system development and synaptic adhesion and transmission. Using a similar approach, Shi and colleagues (2013) knocked down *NLGN4X* expression in iPSCs-derived NSCs and observed transcriptome alterations as well as morphological changes during differentiation of NSCs into mature neurons over a 6-week period. The authors observed that *NLGN4X* knockdown alters the expression patterns of several biological pathways including nervous system development and neuron differentiation, impairs the differentiation of the

NSCs into neurons, and compromises neurite formation and inter-cell connections. In conclusion, these two studies combined *in vitro* stem cells models and targeted gene silencing to explore molecular, cellular and neurodevelopmental effects of loss-of function mutations in ASD-associated genes.

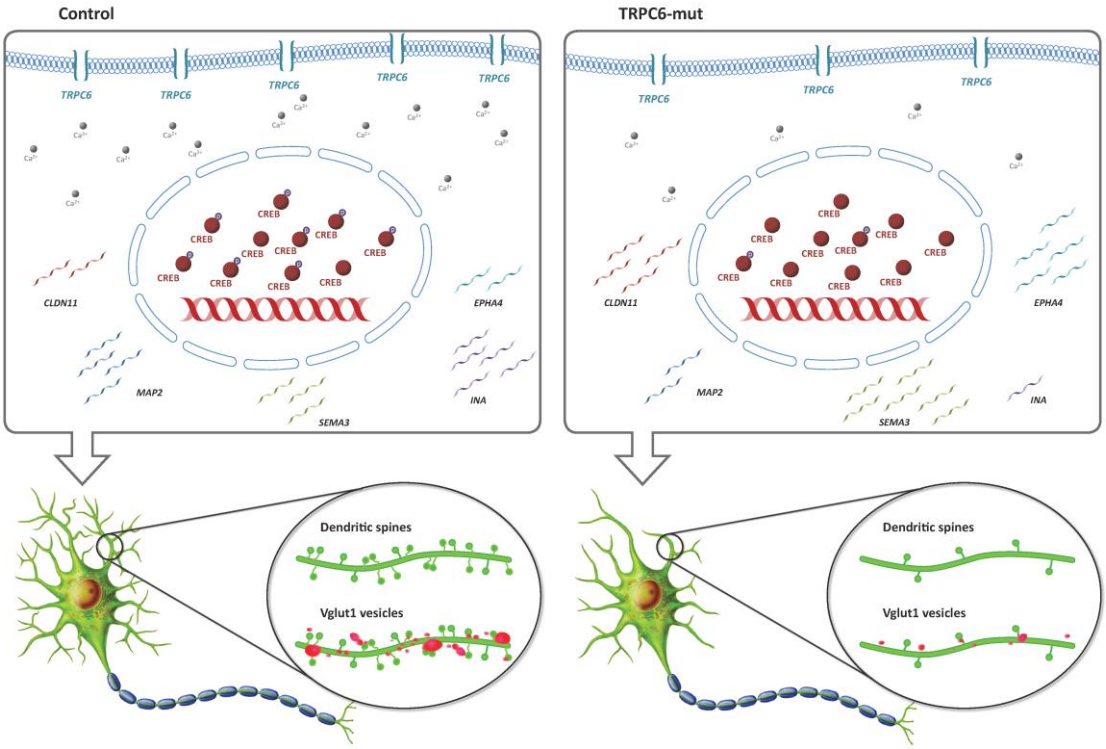

Figure 3 TRPC6 haploinsufficiency consequences in neuronal phenotype: TRPC6 disruption leads to a lower expression of these channels in cell membrane and consequent lower Ca^{++} influx into cells. Calcium signaling through TRPC6 leads to CREB activation, which is consequently diminished in TRPC6-mut cells. This leads to gene expression abnormalities, probably due to dysregulation of CREB activation. A significant number of such dysregulated genes are important for neuronal development and function, especially genes related to cytoskeleton dynamics. Indeed, TRPC6-mut neurons presented less and shorter neurites and a reduction on spine density and glutamatergic vesicles, when compared to controls.

4. Conclusions and perspectives

Disease-modeling in a dish with the use of stem cells has proven to be, so far, a very promising avenue to study ASD, both in its syndromic and nonsyndromic forms. In general, most of the alterations found in iPSC-derived neurons possessing different ASD pathogenic mutations are comparable to data obtained from animal models or brain-derived tissues or cells. This remarkable concordance thus validates disease modelling with iPSCs, which, despite being an *in vitro* biological system, is able to reproduce *in vivo* observations. Nevertheless, in its current state, the use of reprogrammed cells should always be viewed as a complementary approach, as there are still limitations to translating how the morphological, functional or transcriptional changes observed in neural iPSC-derived cells lead to alterations in the human phenotype. In the near future, an extensive cellular characterization of a wide spectrum of ASD variability and mutational mechanisms is anticipated to unveil these relationships.

The monogenic ASD syndromic forms are caused by mutated genes belonging to different but related cellular pathways. The phenotypes can be caused by a variety of mutational mechanisms, including loss-of-function, gain-of-function and dominant- negative mutations, associated with different functional effects at the cellular level. In spite of the genetic heterogeneity associated with the monogenic ASD syndromic forms, in general, the major pathophysiological consequences of the mutations in iPSC-derived neurons apparently are altered dendritic arborization and impaired synaptic function. It is also relevant to mention that comparable neuronal changes have been observed in iPSC-modelling of nonsyndromic ASD. These observations raise some possibilities that deserve our attention: a) impaired dendrite formation can be a feature shared by many neurodevelopmental disorders, as previously suggested (Krey et al., 2013); b) if impaired dendrite formation is such a common f in these disorders, it will be impossible to assign this phenotype to specific neurodevelopmental phenotypes (e.g. ASD or cognitive deficit alone); c) we still need to search for more specific synaptic changes or molecular markers at the cellular and molecular levels in order to establish precise correlations between neuronal phenotypes and clinical phenotypes, as suggested in CDKL5-associated syndrome. In CDKL5-mutated neurons, PSD-95, a protein that plays a significant role in learning and memory, is compromised as a consequence of the dominant-negative effect of the CDKL5 mutations, which would explain the severe mental impairment in these patients.

Mesenchymal stem cells can be easily accessed and manipulated. The few studies conducted on this type of cells have shown promising results. For example, transcriptome analysis conducted on SHED from idiopathic ASD patients and on one patient with haploinsufficiency of TRPC6 revealed cytoskeleton regulation to be one of the most relevant dysregulated pathways (Griesi-Oliveira et al., 2013, 2014). Such dysregulation would predictably result in abnormal dendritic development, which was found in TRPC6-mutated iPSC-derived neurons exhibiting less dendritic arborization and extension (Griesi-Oliveira et al., 2014).

Finally, dysregulation of mTOR signaling has been found in about 25% of ASD patients through analysis of SHED cultures. This is quite an unexpected proportion, as pathogenic variants in mTOR-related genes have been found in a much smaller proportion of ASD patients. Thus, the application of stem cells in the investigation of ASD etiology can not only be useful for dissecting the functional consequences of known mutations, but also for aiding in the identification of common mechanisms involved in different ASD cases, even in those in which genetic alterations have not been identified.

Language impairment, difficulties in social interaction and abnormal behavior with repetitive stereotyped movements are the main clinical hallmarks of ASD patients, and pharmacological treatments have yet to be elected to ameliorate these symptoms. Furthermore, due to the high genetic heterogeneity of nonsyndromic forms of ASD, personalized treatment for each patient has been expected to take place. However, the current studies in iPSC-derived neurons, both from syndromic and nonsyndromic patients, together with mouse models with different mutations, have revealed IGF-1 as a candidate molecule to rescue the phenotype in more than one situation. In this regard, in a first clinical trial using IGF-1 in Phelan-McDermid syndrome, Kolevzon et al (2015) showed that this drug was associated with significant improvement in both social impairment and restrictive behaviors in autistic children. The overall results indicate that IGF-1 might act in neuronal regulation in a very downstream manner, thus compensating any genetic alteration acting upstream. It will be important to investigate this hypothesis further, as further understanding how IGF-1 regulates neuronal morphology and function can aid in finding a more universal drug for ASD treatment.

We stand in a very exciting period with great expectation to move towards a better understanding of ASD etiology and pathophysiology, and it seems that the use of stem cells will certainly change our knowledge in this field.

References

Amir RE, Van den Veyver IB, Wan M, Tran CQ, Francke U, Zoghbi HY: Rett syndrome is caused by mutations in X-linked MECP2, encoding methyl-CpG-binding protein 2. Nat Genet 1999, 23(2):185-188.

Armstrong D, Dunn JK, Antalffy B, Trivedi R. Selective dendritic alterations in the cortex of Rett syndrome. J Neuropathol Exp Neurol. 1995, 54: 195–201.

Arthur A, Rychkov G, Shi S, Koblar SA, Gronthos S. Adult human dental pulp stem cells differentiate toward functionally active neurons under appropriate environmental cues. Stem Cells. 2008;26(7):1787-95.

Ashley CT, Jr., Wilkinson KD, Reines D, Warren ST: FMR1 protein: conserved RNP family domains and selective RNA binding. Science 1993, 262(5133):563-566.

Autism and Developmental Disabilities Monitoring Network Surveillance Year 2008 Principal Investigators; Centers for Disease Control and Prevention. (2012). Prevalence of autism spectrum disorders--Autism and Developmental

Disabilities Monitoring Network, 14 sites, United States, 2008. MMWR Surveill Summ. 30;61(3):1-19

Ballas, N, Lioy, DT, Grunseich, C, and Mandel, G. Non-cell autono- mous influence of MeCP2-deficient glia on neuronal dendritic morphology. Nat. Neurosci. 2009,12, 311–317.

Bauman, ML, Kemper, TL. and Arin, DM. Pervasive neuroanatomic abnormalities of the brain in three cases of Rett's syndrome. Neurology. 1995, 45, 1581–1586.

Belichenko PV, Wright EE, Belichenko NP, Masliah E, Li HH, Mobley WC, Francke U. Widespread changes in dendritic and axonal morphology in Mecp2-mutant mouse models of Rett syndrome: evidence for disruption of neuronal networks. J Comp Neurol. 2009, 514: 240–258.

Betancur C., Buxbaum J.D. SHANK3 haploinsufficiency: a "common" but underdiagnosed highly penetrant monogenic cause of autism spectrum disorders. Review. Mol Autism 4(1):17. 2013

Bowen P, Biederman B, Swallow KA: The X-linked syndrome of macroorchidism and mental retardation: further observations. Am J Med Genet 1978, 2(4):409-414.

Bozdagi O, Sakurai T, Papapetrou D, Wang X, Dickstein DL, Takahashi N, Kajiwara Y, Yang M, Katz AM, Scattoni ML, Harris MJ, Saxena R, Silverman JL, Crawley JN, Zhou Q, Hof PR, Buxbaum JD.vHaploinsufficiency of the autism-associated Shank3 gene leads to deficits in synaptic function, social interaction, and social communication. Mol Autism. 2010, 17;1(1):15.

Brandler WM, Sebat J: From de novo mutations to personalized therapeutic interventions in autism. Annual review of medicine 2015, 66:487-507.

Braun K, Segal M. FMRP involvement in formation of synapses among cultured hippocampal neurons. Cereb Cortex. 2000, 10: 1045–1052.

Bueno DF, Sunaga DY, Kobayashi GS, Aguena M, Raposo-Amaral CE, Masotti C, Cruz LA, Pearson PL, Passos-Bueno MR: Human stem cell cultures from cleft lip/palate patients show enrichment of transcripts involved in extracellular matrix modeling by comparison to controls. Stem Cell Rev 2010, 7(2):446-457.

Buiting K: Prader-Willi syndrome and Angelman syndrome. American journal of medical genetics Part C, Seminars in medical genetics 2010, 154C(3):365-376.

Cassidy SB, Driscoll DJ: Prader-Willi syndrome. European journal of human genetics : EJHG 2009, 17(1):3-13.

Castren M, Tervonen T, Karkkainen V, Heinonen S, Castren E, Larsson K, Bakker CE, Oostra BA, Akerman K: Altered differentiation of neural stem cells in fragile X syndrome. Proc Natl Acad Sci U S A 2005, 102(49):17834-17839.

Castren M. Differentiation of neuronal cells in fragile X syndrome. Cell Cycle. 2006, 5: 1528–1530.

Chahrour M, Jung SY, Shaw C, Zhou X, Wong ST, Qin J, Zoghbi HY: MeCP2, a key contributor to neurological disease, activates and represses transcription. Science 2008, 320(5880):1224-1229.

Chahrour M, Zoghbi HY: The story of Rett syndrome: from clinic to neurobiology. Neuron 2007, 56(3):422-437.

Chailangkarn T, Acab A, Muotri AR: Modeling neurodevelopmental disorders using human neurons. Current opinion in neurobiology 2012, 22(5):785-790.

Chamberlain SJ, Chen PF, Ng KY, Bourgois-Rocha F, Lemtiri-Chlieh F, Levine ES, Lalande M: Induced pluripotent stem cell models of the genomic imprinting disorders Angelman and Prader-Willi syndromes. Proc Natl Acad Sci U S A 2010, 107(41):17668-17673.

Chapleau, CA, Calfa, GD, Lane, MC, Albertson, AJ, Larimore, JL, Kudo, S, Armstrong, DL, Percy, AK, and Pozzo-Miller, L. Dendritic spine pathologies in hippocampal pyramidal neurons from Rett syndrome brain and after expression of Rett-associated MECP2 mutations. Neurobiol. Dis. 2009, 35, 219–233.

Chen RZ, Akbarian S, Tudor M, Jaenisch R. Deficiency of methyl-CpG binding protein-2 in CNS neurons results in a Rett-like phenotype in mice. Nat Genet. 2001, 27: 327–331.

Cheung AY, Horvath LM, Grafodatskaya D, Pasceri P, Weksberg R, Hotta A, Carrel L, Ellis J: Isolation of MECP2-null Rett Syndrome patient hiPS cells and isogenic controls through X-chromosome inactivation. Hum Mol Genet 2011, 20(11):2103-2115.

Chien WH, Gau SS, Chen CH, Tsai WC, Wu YY, Chen PH, Shang CY, Chen CH. Increased gene expression of FOXP1 in patients with autism spectrum disorders. Mol Autism. 2013; 4(1):23.

Clifford S, Dissanayake C, Bui QM, Huggins R, Taylor AK, Loesch DZ: Autism spectrum phenotype in males and females with fragile X full mutation and premutation. Journal of autism and developmental disorders 2007, 37(4):738-747.

Cordero DR, Brugmann S, Chu Y, Bajpai R, Jame M, Helms JA: Cranial neural crest cells on the move: their roles in craniofacial development. Am J Med Genet A 2011, 155A(2):270-279.

Costa-Mattioli M, Monteggia LM. mTOR complexes in neurodevelopmental and neuropsychiatric disorders. Nat Neurosci. 2013; 16(11):1537-43.

Crawford DC, Acuna JM, Sherman SL: FMR1 and the fragile X syndrome: human genome epidemiology review. Genet Med 2001, 3(5):359-371.

Cruvinel E, Budinetz T, Germain N, Chamberlain S, Lalande M, Martins-Taylor K: Reactivation of maternal SNORD116 cluster via SETDB1 knockdown in Prader-Willi syndrome iPSCs. Hum Mol Genet 2014, 23(17):4674-4685.

Curatolo P, Porfirio MC, Manzi B, Seri S: Autism in tuberous sclerosis. European journal of paediatric neurology : EJPN : official journal of the European Paediatric Neurology Society 2004, 8(6):327-332.

De Rubeis S, He X, Goldberg AP, Poultney CS, Samocha K, Cicek AE, Kou Y, Liu L, Fromer M, Walker S et al: Synaptic, transcriptional and chromatin genes disrupted in autism. Nature 2014, 515(7526):209-215.

de Smith AJ, Purmann C, Walters RG, Ellis RJ, Holder SE, Van Haelst MM, Brady AF, Fairbrother UL, Dattani M, Keogh JM et al: A deletion of the HBII-85 class of small nucleolar RNAs (snoRNAs) is associated with hyperphagia, obesity and hypogonadism. Hum Mol Genet 2009, 18(17):3257-3265.

Doers ME, Musser MT, Nichol R, Berndt ER, Baker M, Gomez TM, Zhang SC, Abbeduto L, Bhattacharyya A: iPSC-derived forebrain neurons from FXS individuals show defects in initial neurite outgrowth. Stem cells and development 2014, 23(15):1777-1787.

Eiges R, Urbach A, Malcov M, Frumkin T, Schwartz T, Amit A, Yaron Y, Eden A, Yanuka O, Benvenisty N et al: Developmental study of fragile X syndrome using human embryonic stem cells derived from preimplantation genetically diagnosed embryos. Cell stem cell 2007, 1(5):568-577.

Evans JC, Archer HL, Colley JP, Ravn K, Nielsen JB, Kerr A, Williams E, Christodoulou J, Gecz J, Jardine PE et al: Early onset seizures and Rett-like features associated with mutations in CDKL5. European journal of human genetics : EJHG 2005, 13(10):1113-1120.

Garber KB, Visootsak J, Warren ST: Fragile X syndrome. European journal of human genetics : EJHG 2008, 16(6):666-672.

Gaugler T, Klei L, Sanders SJ, Bodea CA, Goldberg AP, Lee AB, Mahajan M, Manaa D, Pawitan Y, Reichert J et al: Most genetic risk for autism resides with common variation. Nat Genet 2014, 46(8):881-885.

Griesi-Oliveira K, Acab A, Gupta AR, Sunaga DY, Chailangkarn T, Nicol X, Nunez Y, Walker MF, Murdoch JD, Sanders SJ et al: Modeling non-syndromic autism and the impact of TRPC6 disruption in human neurons. Molecular psychiatry 2014.

Griesi-Oliveira K, Sunaga DY, Alvizi L, Vadasz E, Passos-Bueno MR. Stem cells as a good tool to investigate dysregulated biological systems in autism spectrum disorders. Autism Res. 2013; 6(5):354-61.

Harris SW, Hessl D, Goodlin-Jones B, Ferranti J, Bacalman S, Barbato I, Tassone F, Hagerman PJ, Herman H, Hagerman RJ: Autism profiles of males with fragile X syndrome. American journal of mental retardation : AJMR 2008, 113(6):427-438.

Hu VW, Nguyen A, Kim KS, Steinberg ME, Sarachana T, Scully MA, Soldin SJ, Luu T, Lee NH. Gene expression profiling of lymphoblasts from autistic and nonaffected sib pairs: altered pathways in neuronal development and steroid biosynthesis. PLoS One. 2009; 4(6):e5775.

Hubbard JJ, Sullivan SK, Mills JA Hayes BJ, Torok-Storb BJ, Ramakrishnan A. Efficient iPS cell generation from blood using episomes and HDAC inhibitors. J Vis Exp. 2014 Oct 28;(92):e52009. doi: 10.3791/52009.

Janebodin K, Horst OV, Ieronimakis N, Balasundaram G, Reesukumal K, Pratumvinit B, Reyes M: Isolation and characterization of neural crest-derived stem cells from dental pulp of neonatal mice. PLoS One 2011, 6(11):e27526.

Jeste SS, Geschwind DH: Disentangling the heterogeneity of autism spectrum disorder through genetic findings. Nature reviews Neurology 2014, 10(2):74-81.

Kim DS, Ross PJ, Zaslavsky K, Ellis J: Optimizing neuronal differentiation from induced pluripotent stem cells to model ASD. Frontiers in cellular neuroscience 2014, 8:109.

Kishi N, and Macklis JD. MeCP2 functions largely cell-autono- mously, but also non-cell-autonomously, in neuronal maturation and dendritic arborization of cortical pyramidal neurons. Exp. Neurol. 2010,222, 51–58.

Kobayashi GS, Alvizi L, Sunaga DY, Francis-West P, Kuta A, Almada BV, Ferreira SG, de Andrade-Lima LC, Bueno DF, Raposo-Amaral CE et al: Susceptibility to DNA damage as a molecular mechanism for non-syndromic cleft lip and palate. PLoS One 2013, 8(6):e65677.

Kolevzon A, Bush L, Wang AT, Halpern D, Frank Y, Grodberg D, Rapaport R, Tavassoli T, Chaplin W, Soorya L et al: A pilot controlled trial of insulin-like growth factor-1 in children with Phelan-McDermid syndrome. Molecular autism 2014, 5(1):54.

Komada Y, Yamane T, Kadota D, Isono K, Takakura N, Hayashi S, Yamazaki H: Origins and properties of dental, thymic, and bone marrow mesenchymal cells and their stem cells. PLoS One 2012, 7(11):e46436.

Krey JF, Pasca SP, Shcheglovitov A, Yazawa M, Schwemberger R, Rasmusson R, Dolmetsch RE: Timothy syndrome is associated with activity-dependent dendritic retraction in rodent and human neurons. Nature neuroscience 2013, 16(2):201-209.

Laplante M, Sabatini DM. mTOR signaling at a glance. J Cell Sci. 2009; 122(Pt 20):3589-94.

Li Y, Wang H, Muffat J, Cheng AW, Orlando DA, Loven J, Kwok SM, Feldman DA, Bateup HS, Gao Q et al: Global transcriptional and translational repression in human-embryonic-stem-cell-derived Rett syndrome neurons. Cell stem cell 2013, 13(4):446-458.

Liu J, Koscielska KA, Cao Z, Hulsizer S, Grace N, Mitchell G, Nacey C, Githinji J, McGee J, Garcia-Arocena D et al: Signaling defects in iPSC-derived fragile X premutation neurons. Hum Mol Genet 2012, 21(17):3795-3805.

Liu X, Takumi T: Genomic and genetic aspects of autism spectrum disorder. Biochemical and biophysical research communications 2014, 452(2):244-253.

Lozano R, Rosero CA, Hagerman RJ: Fragile X spectrum disorders. Intractable & rare diseases research 2014, 3(4):134-146.

MacArthur DG, Balasubramanian S, Frankish A, Huang N, Morris J, Walter K, Jostins L, Habegger L, Pickrell JK, Montgomery SB et al: A systematic survey of loss-of-function variants in human protein-coding genes. Science 2012, 335(6070):823-828.

Marchetto MC, Carromeu C, Acab A, Yu D, Yeo GW, Mu Y, Chen G, Gage FH, Muotri AR: A model for neural development and treatment of Rett syndrome using human induced pluripotent stem cells. Cell 2010, 143(4):527-539.

McDuffie A, Abbeduto L, Lewis P, Kover S, Kim JS, Weber A, Brown WT: Autism spectrum disorder in children and adolescents with fragile X syndrome: within-syndrome differences and age-related changes. American journal on intellectual and developmental disabilities 2010, 115(4):307-326.

Menon T, Yates JA, Bochar DA. Regulation of androgen-responsive transcription by the chromatin remodeling factorCHD8. Mol Endocrinol. 2010; 24(6):1165-74.

Mironov, S.L., Skorova, E., Hartelt, N., Mironova, L.A., Hasan, M.T., and Kügler, S. Remodelling of the respiratory network in a mouse model of Rett syndrome depends on brain-derived neurotrophic factor regulated slow calcium buffering. J. Physiol. 2009, 587, 2473–2485.

Moreira DP, Griesi-Oliveira K, Bossolani-Martins AL, Lourenco NC, Takahashi VN, da Rocha KM, Moreira ES, Vadasz E, Meira JG, Bertola D et al: Investigation of 15q11-q13, 16p11.2 and 22q13 CNVs in autism spectrum disorder Brazilian individuals with and without epilepsy. PLoS One 2014, 9(9):e107705.

Neale BM, Kou Y, Liu L, Ma'ayan A, Samocha KE, Sabo A, Lin CF, Stevens C, Wang LS, Makarov V, Polak P, Yoon S, Maguire J, Crawford EL, Campbell NG, Geller ET, Valladares O, Schafer C, Liu H, Zhao T, Cai G, Lihm J, Dannenfelser R, Jabado O, Peralta Z, Nagaswamy U, Muzny D, Reid JG, Newsham I, Wu Y, Lewis L, Han Y, Voight BF, Lim E, Rossin E, Kirby A, Flannick J, Fromer M, Shakir K, Fennell T, Garimella K, Banks E, Poplin R, Gabriel S, DePristo M, Wimbish JR, Boone BE, Levy SE, Betancur C, Sunyaev S, Boerwinkle E, Buxbaum JD, Cook EH Jr, Devlin B, Gibbs RA, Roeder K, Schellenberg GD, Sutcliffe JS, Daly MJ. Patterns and rates of exonic de novo mutations in autism spectrum disorders. Nature. 2012; 485(7397):242-5.

Oguro-Ando A, Rosensweig C, Herman E, Nishimura Y, Werling D, Bill BR, Berg JM, Gao F, Coppola G, Abrahams BS, Geschwind DH. Increased CYFIP1 dosage alters cellular and dendritic morphology and dysregulates mTOR. Mol Psychiatry. 2014.

O'Roak BJ, Vives L, Fu W, Egertson JD, Stanaway IB, Phelps IG, Carvill G, Kumar A, Lee C, Ankenman K, Munson J, Hiatt JB, Turner EH, Levy R, O'Day DR, Krumm N, Coe BP, Martin BK, Borenstein E, Nickerson DA, Mefford HC, Doherty D, Akey JM, Bernier R, Eichler EE, Shendure J. Multiplex targeted sequencing identifies recurrently mutated genes in autism spectrum disorders. Science. 2012; 338(6114):1619-22.

O'Roak BJ, Vives L, Girirajan S, Karakoc E, Krumm N, Coe BP, Levy R, Ko A, Lee C, Smith JD, Turner EH, Stanaway IB, Vernot B, Malig M, Baker C, Reilly B, Akey JM, Borenstein E, Rieder MJ, Nickerson DA, Bernier R, Shendure J, Eichler EE. Sporadic autism exomes reveal a highly interconnected protein network of de novo mutations. Nature. 2012; 485(7397):246-50.

Pasca SP, Portmann T, Voineagu I, Yazawa M, Shcheglovitov A, Pasca AM, Cord B, Palmer TD, Chikahisa S, Nishino S et al: Using iPSC-derived neurons to uncover cellular phenotypes associated with Timothy syndrome. Nature medicine 2011, 17(12):1657-1662.

Phelan K, McDermid HE: The 22q13.3 Deletion Syndrome (Phelan-McDermid Syndrome). Molecular syndromology 2012, 2(3-5):186-201.

Prilutsky D, Palmer NP, Smedemark-Margulies N, Schlaeger TM, Margulies DM, Kohane IS: iPSC-derived neurons as a higher-throughput readout for autism: promises and pitfalls. Trends in molecular medicine 2014, 20(2):91-104.

Rademacher N, Hambrock M, Fischer U, Moser B, Ceulemans B, Lieb W, Boor R, Stefanova I, Gillessen-Kaesbach G, Runge C et al: Identification of a novel CDKL5 exon and pathogenic mutations in patients with severe mental

retardation, early-onset seizures and Rett-like features. Neurogenetics 2011, 12(2):165-167.

Rakic P. Evolution of the neocortex: a perspective from developmental biology. Nature reviews. Neuroscience. 2009; 10:724–735.

Ricciardi S, Ungaro F, Hambrock M, Rademacher N, Stefanelli G, Brambilla D, Sessa A, Magagnotti C, Bachi A, Giarda E et al: CDKL5 ensures excitatory synapse stability by reinforcing NGL-1-PSD95 interaction in the postsynaptic compartment and is impaired in patient iPSC-derived neurons. Nature cell biology 2012, 14(9):911-923.

Ronemus M, Iossifov I, Levy D, Wigler M: The role of de novo mutations in the genetics of autism spectrum disorders. Nat Rev Genet 2014, 15(2):133-141.

Rougeulle C, Glatt H, Lalande M: The Angelman syndrome candidate gene, UBE3A/E6-AP, is imprinted in brain. Nat Genet 1997, 17(1):14-15.

Ryan K C Yuen, Bhooma Thiruvahindrapuram, Daniele Merico, Susan Walker et al. Whole-genome sequencing of quartet families with autism spectrum disorder. Nature Medicine 2015.

Sanders SJ, Murtha MT, Gupta AR, Murdoch JD, Raubeson MJ, Willsey AJ, Ercan-Sencicek AG, DiLullo NM, Parikshak NN, Stein JL, Walker MF, Ober GT, Teran NA, Song Y, El-Fishawy P, Murtha RC, Choi M, Overton JD, Bjornson RD, Carriero NJ, Meyer KA, Bilguvar K, Mane SM, Sestan N, Lifton RP, Günel M, Roeder K, Geschwind DH, Devlin B, State MW. De novo mutations revealed by whole-exome sequencing are strongly associated withautism. Nature. 2012; 485(7397):237-41.

Sheridan SD, Theriault KM, Reis SA, Zhou F, Madison JM, Daheron L, Loring JF, Haggarty SJ: Epigenetic characterization of the FMR1 gene and aberrant neurodevelopment in human induced pluripotent stem cell models of fragile X syndrome. PLoS One 2011, 6(10):e26203.

Shi L, Chang X, Zhang P, Coba MP, Lu W, Wang K. The functional genetic link of NLGN4X knockdown and neurodevelopment in neural stem cells. Hum Mol Genet. 2013; 22(18):3749-60.

Sidorov MS, Auerbach BD, Bear MF: Fragile X mental retardation protein and synaptic plasticity. Molecular brain 2013, 6:15.

Splawski I, Timothy KW, Sharpe LM, Decher N, Kumar P, Bloise R, Napolitano C, Schwartz PJ, Joseph RM, Condouris K et al: Ca(V)1.2 calcium channel dysfunction causes a multisystem disorder including arrhythmia and autism. Cell 2004, 119(1):19-31.

Suzuki AM, Griesi-Oliveira K, de Oliveira Freitas Machado C, Vadasz E, Zachi EC, Passos-Bueno MR, Sertie AL. Altered mTORC1 signaling in multipotent stem cells from nearly 25% of patients with nonsyndromic autism spectrum disorders. Mol Psychiatry. 2015.

Tai Y, Feng S, Ge R, Du W, Zhang X, He Z, Wang Y. TRPC6 channels promote dendritic growth via the CaMKIV-CREB pathway. J Cell Sci. 2008; 121(Pt 14):2301-7.

Takahashi K, Tanabe K, Ohnuki M, Narita M, Ichisaka T, Tomoda K, Yamanaka S: Induction of pluripotent stem cells from adult human fibroblasts by defined factors. Cell 2007, 131(5):861-872.

Tang G, Gudsnuk K, Kuo SH, Cotrina ML, Rosoklija G, Sosunov A, Sonders MS, Kanter E, Castagna C, Yamamoto A, Yue Z, Arancio O, Peterson BS, Champagne F, Dwork AJ, Goldman J, Sulzer D. Loss of mTOR-dependent macroautophagy causes autistic-like synaptic pruning deficits. Neuron. 2014; 83(5):1131-43.

Tao J, Van Esch H, Hagedorn-Greiwe M, Hoffmann K, Moser B, Raynaud M, Sperner J, Fryns JP, Schwinger E, Gecz J et al: Mutations in the X-linked cyclin-dependent kinase-like 5 (CDKL5/STK9) gene are associated with severe neurodevelopmental retardation. Am J Hum Genet 2004, 75(6):1149-1154.

Tian Y, Voineagu I, Pasca SP, Won H, Chandran V, Horvath S, Dolmetsch RE, Geschwind DH: Alteration in basal and depolarization induced transcriptional network in iPSC derived neurons from Timothy syndrome. Genome medicine 2014, 6(10):75.

Urbach A, Bar-Nur O, Daley GQ, Benvenisty N: Differential modeling of fragile X syndrome by human embryonic stem cells and induced pluripotent stem cells. Cell stem cell 2010, 6(5):407-411.

Vu TH, Hoffman AR: Imprinting of the Angelman syndrome gene, UBE3A, is restricted to brain. Nat Genet 1997, 17(1):12-13.

Weaving LS, Christodoulou J, Williamson SL, Friend KL, McKenzie OL, Archer H, Evans J, Clarke A, Pelka GJ, Tam PP et al: Mutations of CDKL5 cause a severe neurodevelopmental disorder with infantile spasms and mental retardation. Am J Hum Genet 2004, 75(6):1079-1093.

Williams CA, Beaudet AL, Clayton-Smith J, Knoll JH, Kyllerman M, Laan LA, Magenis RE, Moncla A, Schinzel AA, Summers JA et al: Angelman syndrome 2005: updated consensus for diagnostic criteria. Am J Med Genet A 2006, 140(5):413-418.

Williams EC, Zhong X, Mohamed A, Li R, Liu Y, Dong Q, Ananiev GE, Mok JC, Lin BR, Lu J et al: Mutant astrocytes differentiated from Rett syndrome patients-specific iPSCs have adverse effects on wild-type neurons. Hum Mol Genet 2014, 23(11):2968-2980.

Yazdani M, Deogracias R, Guy J, Poot RA, Bird A, Barde YA. Disease modeling using embryonic stem cells: MeCP2 regulates nuclear size and RNA synthesis in neurons. Stem Cells. 2012, 30:2128–2139.

Yu J, Vodyanik MA, Smuga-Otto K, Antosiewicz-Bourget J, Frane JL, Tian S, Nie J, Jonsdottir GA, Ruotti V, Stewart R et al: Induced pluripotent stem cell lines derived from human somatic cells. Science 2007, 318(5858):1917-1920.

Yuen RK, Thiruvahindrapuram B, Merico D, Walker S, Tammimies K, Hoang N, Chrysler C, Nalpathamkalam T, Pellecchia G, Liu Y et al: Whole-genome sequencing of quartet families with autism spectrum disorder. Nature medicine 2015, 21(2):185-191.

Zeng L, Zhang P, Shi L, Yamamoto V, Lu W, Wang K. Functional impacts of NRXN1 knockdown on neurodevelopment in stem cell models. PLoS One. 2013; 8(3):e59685.

Zhou J, Du W, Zhou K, Tai Y, Yao H, Jia Y, Ding Y, Wang Y. Critical role of TRPC6 channels in the formation of excitatory synapses. Nat Neurosci. 2008; 11(7):741-3.